Design and Assessment of a Laser-Assisted Intradermal Medication

A Prospective Randomised Case-control Clinical Trial

BARBARA HELENA BARCARO MACHADO

PhD Thesis

September 2020

Faculty of Health, Education, Medicine and Social Care

Anglia Ruskin University

United Kingdom

Design and Assessment of a Laser-Assisted Intradermal Medication - A Prospective Randomised Case-control Clinical Trial

A thesis presented by

BARBARA HELENA BARCARO MACHADO

to the Faculty of Health, Education, Medicine and Social Care

in partial fulfilment of the requirements for the degree of Doctor of Philosophy

2020

Anglia Ruskin University

United Kingdom

DECLARATION OF AUTHORSHIP

I, Barbara Helena Barcaro Machado, hereby certify that I had personally carried out the work depicted in the thesis entitled “Design and assessment of a laser-assisted intradermal medication - A Prospective randomized case-control clinical trial”.
No part of this thesis has been submitted for the award of any other degree or diploma prior to this date.

Barbara Helena Barcaro Machado

September 2020

DEDICATION

To God,

to life,

and to Luiz Alberto, Matheus and Sergio.

Hippocratic Oath

“I will remember that there is art to medicine as well as science, and that warmth, sympathy, and understanding may outweigh the surgeon’s knife or the chemist’s drug”.

The Oath of Healer (Louis Weinstein)

“I shall be ever grateful to my teachers who have planted the seeds of knowledge, which I shall nurture forever. I thank them for allowing me to see the importance of learning and realise that lifelong study is critically important to becoming a Healer”.

ACKNOWLEDGEMENTS

The completion of this thesis has involved more than 500 people. It would never have been possible without the support of my family, my team, my patients, my supervisors and my friends, people who have fulfilled my life with joy and significance. My apologies for not mentioning everyone by name.

First of all, I thank God for my existence and for placing so many dear people around me. With the conclusion of this study, I want to honour my parents who gave me life and love, and taught me moral values that have guided my life.

I want to share the happiness of having completed this work with my children, Luiz Alberto and Matheus, and with my husband, Sergio. They have encouraged me and endured my absence for the last four years. Without their love and protection, I would not have reached this point.

I extend my gratitude to Professor Pitanguy (*in memoriam*), my chief for 26 years, from whom I have acquired the knowledge about plastic surgery. Professor Pitanguy was an example of ethics and an inspiration in all ways, but especially to me to keep learning and searching for answers in science.

I want to express my admiration and sincere gratitude to my first supervisor, Dr Mohammad Najlah, who followed every step of this project. His kindness, mentorship and enthusiasm were paramount to the success of my research. Thanks to his encouragement and support, I developed the necessary skills to become an independent researcher.

I would like to thank Professor James Frame, my second supervisor, for his instructions, expertise, and guidance. His insights regarding the methodology used in this research process were essential to its success. Thanks for sharing your precious time.

I thank Dr Rosangela Noe Martins and Dr Jufen Zhang for their support with the statistical analysis involving this thesis. It was a great opportunity to acquire new, different skills under their supervision.

To my dear friend, Joanne Corney, staff member at Anglia Ruskin University, go my thanks for her support and friendship throughout these four years. Without Joanne, my PhD studies in the UK would have remained just a distant dream.

I am thankful to Professor Selim Cellek for the constructive criticism and the wise pieces of advice during my annual reviews. They have stimulated my critical thinking which was vital to overcoming the challenges involved in this research.

Special acknowledgement goes to the examiners Professor Rudolf Schutte and Professor Fahmy Fahmy who have dedicated their time to analysing this thesis. I hope that I have been efficient in putting into words all the novelties and significant findings that I have reached in this study.

I would also like to take this opportunity to thank my staff, as they have been integral in making this journey complete. I would like to acknowledge my assistants Ivy Dantas, Marielisa Carvalho, and Monica Nunes, who have helped me to take care of my patients. Without their support, this endeavour would not have been so joyful.

Special thanks go to Professor Dr João Medeiros, who has encouraged me since the very beginning of this research.

Finally, I would like to express my gratitude to my patients. Their trust in my work transformed this project into a reality.

ABSTRACT

Human skin is a potential route for drug administration. Although some inherent cutaneous pathways assist in transporting drugs into the skin, so effective is the *stratum corneum* that most of the drugs applied do not exhibit the necessary lipophilicity or are too large to permeate this barrier in a significant concentration.

Research aimed at optimising device-assisted transcutaneous medication is a novel paradigm and essential to expanding the drugs suitable for application via the skin. The importance of this research is emphasised by the gap in the literature concerning the use of fractional ablative lasers as physical penetration enhancers to bypass the barrier to drug penetration offered by the *stratum corneum*, allowing for a significant increase in dermal bioavailability of many pharmaceutical agents.

The literature has suggested that drugs can diffuse into the microchannels produced by the lasers and penetrate directly to the dermis but usually do not investigate comparative studies on clinical outcomes. Convincing data has been restricted to the oncology field, and larger, controlled trials are necessary to evaluate the impact on the skin surface and the quantitative and qualitative effectiveness of the method.

Despite the promising results, the lack of standard methodology regarding laser protocols and for analysing the results reinforces the need for comprehensive research to establish laser-assisted medication as a standard therapeutic modality. This is the first study that has validated and employed three-dimensional stereophotogrammetry as a tool to provide accurate quantification of the skin's microtopography before and after laser-assisted medication. The stereophotogrammetry system provided accurate numerical data corresponding to the influence of laser-assisted medication on the surface of wrinkles and scars.

The thesis original contribution to knowledge included the design of a reproducible, active, laser-assisted, intradermal delivery of medication. An *in vivo,* prospective, randomised, double-blind, comparative clinical trial was designed. Consenting patients presenting wrinkles and scars were randomised and subjected to one session of laser skin resurfacing with a 2,940 nm Er:YAG (Erbium dopped Yttrium Aluminium Garnet) fractional ablative laser followed by immediate topical application of the medication. The laser parameters were standardised for all patients.

This is the first robust study that has compared the effect of different substances on the skin surface after laser-resurfacing and on different conditions of skin integrity, scars and wrinkles. A control group received vitamin C immediately after laser skin resurfacing and another study group received vitamin C plus a cosmeceutical containing growth factors. Most patients treated presented an improvement in the skin condition. However, the groups receiving the cosmeceutical containing growth factors exhibited statistically significantly better results compared to the control groups receiving vitamin C only. This finding demonstrates the positive effect of laser-assisted medication on skin surface and that the addition of growth factors to formulae enhances the result of the treatment.

TABLE OF CONTENT

LIST OF FIGURES

Chapter 1
Introduction

Chapter 2
Scientific Validation of Three-Dimensional Stereophotogrammetry for Assessing Skin Facial Wrinkles and Scars in Comparison with a Visual Analogue Clinical Scale

Chapter 4
A Prospective, Randomised, Double-Blind, Comparative Clinical Study on the Outcome of Periorbital Wrinkles Treated with Laser-Assisted Medication

LIST OF TABLES

Chapter 4
A Prospective, Randomised, Double-Blind, Comparative Clinical Study on the Outcome of Periorbital Wrinkles Treated with Laser-Assisted Medication

Chapter 5
A Prospective, Randomised, Double-Blind, Comparative Clinical Study on the Effect of Laser-Assisted Medication (LAM) on Scars

LIST OF ABBREVIATIONS AND ACRONYMS

2D two-dimensional

3D three-dimensional

3D SPM Three-dimensional stereophotogrammetry

đ diffusional path length or membrane thickness

∂ delta

Æ surface area of the *stratum corneum*

AD average depth

AD_R average depth of the wrinkle

AD_{R-C} average depth of the wrinkle treated with Vitamin C

AD_{R-CGF} average depth of the wrinkle treated with Vitamin C plus the cosmeceutical containing growth factors

AFXL ablative fractional laser

AFXLs ablative fractional lasers

AH average height

AH_{DS} average height of the scar

AH_R average height of the skin surrounding the wrinkle

ALA 5-aminolevulinic acid

ARU Anglia Ruskin University

BM basement membrane

CA California

CE European Conformity (Conformité Européene)

CO_2 carbon dioxide

CPE chemical penetration enhancer

CPEs chemical penetration enhancers

CTIMP Clinical Trials of Investigational Medicinal Products

Co concentration gradient

CPE chemical penetration enhancer

CPEs chemical penetration enhancers

D diffusion or permeability coefficient

Da Daltons

DNA Deoxyribonucleic acid

DS Damaged skin group

DS-C Damaged skin group, treated with Vitamin C

DS-CGF Damaged skin group, treated with Vitamin C and the cosmeceutical containing growth factors

ECM extracellular matrix

e.g. *exempli gratia* (for example)

EGF epidermal growth factor

EGFs epidermal growth factors

EMR electromagnetic radiation

Er:YAG Erbium doped Yttrium Aluminium Garnet laser

FDA Food and Drug Administration
FGF fibroblast growth factor
FGFs fibroblast growth factor family
FREP Faculty Research Ethics Panel
GF growth factor
GFs growth factors
Ha alternative hypothesis
HGF hepatocyte growth factor
Ho null hypothesis
IBM International Business Machines Corporation
ICC intraclass correlation coefficient
i.e. *id est* (that is)
IGAIS investigator global aesthetic improvement scale
IGFs insulin-like growth factor family
IGF-1 insulin-like growth factor-1
IQR Interquartile range
J steady-state diffusion flux or flow
KGF keratinocyte growth factor
LAM laser-assisted medication
LASER light amplification by stimulated emission of radiation
LSR laser skin resurfacing
ma1population mean in pre-procedure roughness
ma2 population mean in post-procedure roughness
µm micrometre
mm millimetre
MN microneedling
MTZ microthermal zone
MTZs microthermal zones
MW molecular weight
n number
n/a not applicable
nm nanometre
PDGF platelet-derived growth factor
pH potential for hydrogen
POSAS patient and observer scar assessment scale
PPE physical penetration enhancer
PPEs physical penetration enhancers
PreR: roughness pre-procedure
PosR: roughness post-procedure
PRP platelet-rich plasma
Q1 first quartile
Q3 third quartile

R rejuvenation group

R-C rejuvenation group - treated with Vitamin C

R-CGF rejuvenation group - treated with vitamin C and the cosmeceutical containing growth factors

Rgh roughness

Rgh_{DS-C} roughness of the scar treated with vitamin C

Rgh_{DS-CGF} roughness of the scar treated with vitamin C plus the cosmeceutical containing growth factors

Rgh_{R-C} roughness group R (rejuvenation) treated with vitamin C

Rgh_{R-CGF} roughness group R (rejuvenation) treated with vitamin C plus the cosmeceutical containing growth factors

rhEGF recombinant human epidermal growth factor

RTD residual thermal damage zone

RTDs residual thermal damage zones

SC *stratum corneum*

sddiff standard deviation of the differences

SPM stereophotogrammetry

TGF transforming growth factor

TGF-β transforming growth factor beta

TGF-βs transforming growth factor beta family

TGF-β1 transforming growth factor beta 1

TGF-β2 transforming growth factor beta 2

TGF-β3 transforming growth factor beta 3

TJs tight junctions

USA United States of America

UV ultraviolet

x versus

V_{DS-C} scar volume damaged skin group treated with vitamin C

V_{DS-CGF} scar volume damaged skin group treated with vitamin C plus the cosmeceutical containing growth factors

VEGF vascular endothelial growth factor

VEGFs vascular endothelial growth factors

VSS Vancouver scar scale

Chapter 1

Introduction

1 Introduction

The human skin is a dynamic, hermetic and multitasking organ composed of water (70%), proteins (25%), and lipids (up to 5%). In terms of its surface, this protective cloak extends to an average area of 2 m^2 (21.5 square feet) and weighs around 10 –16% of the total body mass (up to 4,200 g). A cutaneous area of 1 cm^2 contains one linear metre of blood vessels, four linear metres of thin nervous branches and six million cells of mesenchymal and neuroectodermal origin. The average square inch (6.45 cm^2) of skin holds 650 sweat glands, and more than 1,000 nerve endings.

The acid potential for hydrogen (pH < 6) is essential for skin to:

- act as a permeability barrier;`
- have tissue regenerative properties;
- provide an antimicrobial defence;
- promote the synthesis of ceramides;
- regulate local enzymatic activity (hydrolases).

The impressive extension and composition of the skin make it a potential route for drug administration. However, most of the drugs applied do not permeate the cutaneous layers in a significant concentration.

1.1 Skin histology

Histologically, the skin is composed of three nonhomogeneous and distinctive primary layers: the epidermis, the dermis, and the hypodermis.

1.1.1 The epidermis

The epidermis is the outermost layer of the skin and is almost entirely cellular. The epidermis is composed of keratinocytes with neither nerve endings nor blood vessels. The intercellular space is composed of a ground substance that bounds the cells and constitutes less than 2% of skin volume. The ground substance provides strong mechanical integrity and a high cellular attrition rate.

The epithelial cells are interconnected at desmosomes, which are bundles of symmetrically laminated filaments of keratin that form links between cells in one of the several layers of the epidermis, the *stratum spinosum*. The desmosomes are responsible for epidermal structural strength and permeability (Dayan, 2005).

The epidermis gives passage to skin appendages (Figure 1.1).

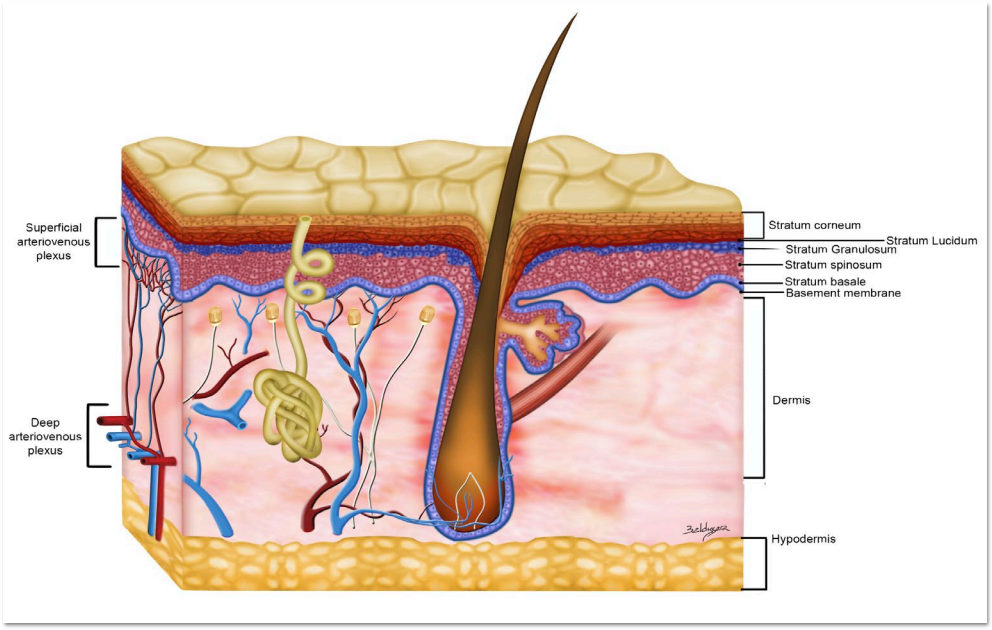

Figure 1.1: Schematic representation of the skin structure. The epidermis is relatively thin (0.1– 0.5mm thick), whereas the dermis is the thickest skin layer, measuring around 3–5 mm.

The epidermis is composed of several layers: *stratum corneum* (SC), *stratum lucidum* (identified only in the palms of the hands and the sole of the feet), *stratum granulosum* or granular layer, *stratum spinosum* or spinous layer and the *stratum basale*, also called *germinativum* or basal layer (Khavkin & Ellis, 2011; Dominguez-Delgado et al., 2010) (Figure 1.2). The epidermal strata are described in Table 1.1.

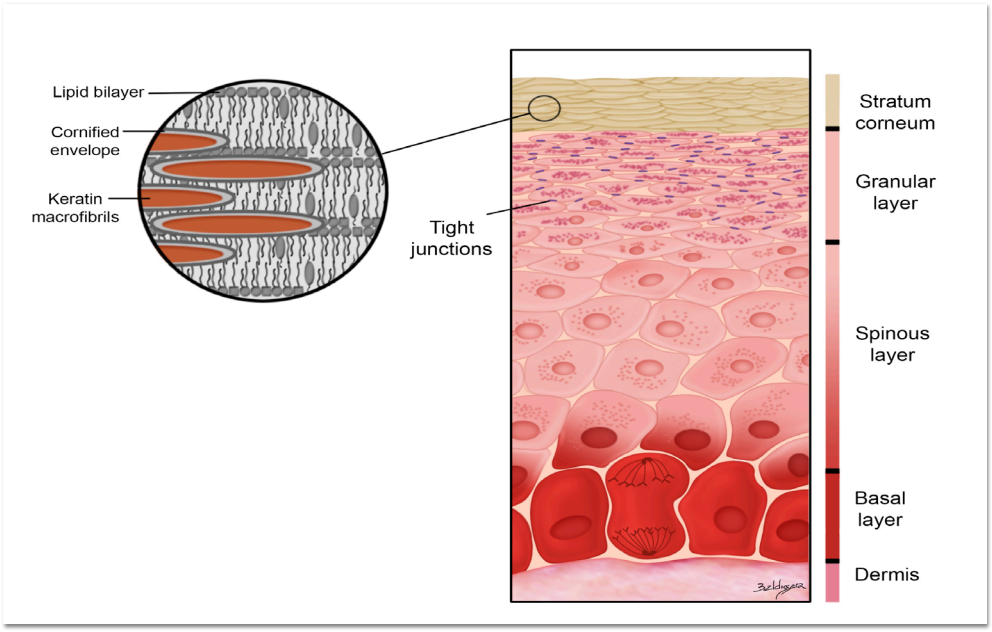

Figure 1.2: Simplified representation of the epidermis showing its layers. The magnified detail displayed on the left shows the arrangement of the lipid lamellar bilayers contained in the *stratum corneum*. Desmosomes can be found in the *stratum spinosum,* whereas tight junctions are located on the granular layer.

Table 1.1 - Representative scheme of the structure and function of each individual epidermal layer

Epidermis	Structure	Function
stratum germinativum (basale)	Single-cell in thickness with columnar-to-oval shaped cells, which rest on the basement membrane, thus binding with the dermis. The cells are actively undergoing mitosis.	Produces the epidermal cells to counterbalance the constant shedding.
stratum spinosum	Multi-layer, metabolically active cells that are tightly joined to each other by desmosomes.	Provides skin strength and flexibility.
stratum granulosum	Up to 5 layers of flattened cells that mark the transition between the deep metabolically active strata and the dead cells of the superficial strata.	Produces granules of keratohyalin and a lipid-rich water-sealant secretion.
stratum lucidum	Translucent layer with up to 5 layers of clear dead cells. This layer is present in the palms of the hands and the soles of the feet.	Keratohyalin dispersion around the keratin fibres.
stratum corneum	The most superficial layer of the skin; up to 30 layers of dead flat keratinocytes that shed continuously in the process of epidermal turnover.	Provides cutaneous structural strength; prevents from water loss and entry of pathogens.

Keratinocytes originate from cells in the *stratum basale* that continuously proliferate. The arrangement of stromal collagen and elastin within the epidermal architecture is responsible for the change in shape as keratinocytes move towards the SC (Dominguez-Delgado et al., 2010; Morgado, 2011; Khavkin & Ellis, 2011). Below the SC, the epidermal layers compose the viable epidermis, with a thickness of 30 – 100 μm. The viable epidermis is nourished by diffusion from the plasma and the interstitial fluid that originates from the capillaries within the dermis (Shashi et al., 2012).

As the keratinocytes move away from their attachment at the basement membrane (BM), they progressively lose water and flatten out, forming the *stratum spinosum* and *stratum granulosum* layers. At the most superficial layer of the *stratum granulosum*, these cells have moved so far from their source of nutritional requirements that they lose cytoplasmic organelles, their nucleus and their ability to divide. The keratinocytes fill with keratin in a process called cornification, or cutaneous keratinisation, which takes up to six weeks to complete. Finally, the keratinocytes reach the *stratum corneum* and are shed through desquamation, being continuously replaced by cells from deeper layers (Morgado, 2011; Dominguez-Delgado et al., 2010). The *stratum corneum* controls the inward and outward movement of chemical substances, biological agents, water and inorganic particles (Shashi et al., 2012; Dominguez-Delgado et al. 2010).

Some epidermal transmembrane proteins, called tight junctions (TJs) (Figure 1.2), form connections between the keratinocytes. The TJs are the primary barrier structure in skin appendages because the SC is absent in these organs. As with the SC, TJs are vital to the integrity of the skin barrier and act as a second line of defence against external pathogens. These adhesions seal or restrict the molecular circulation and flow of fluids into the *stratum granulosum* and may react more promptly than the SC to restore any

breach in barrier integrity. It is hypothesised that impairing the SC's and TJs' barriers may increase the accessibility of a topically administered drug to the deeper cutaneous layers (Basler et al., 2016).

1.1.1.1 The *stratum corneum* (SC)

The SC is a 6 – 10 µm-thick structure composed of approximately 75 – 80% protein, 5 – 15% lipid and 5 – 10% unidentified elements. The SC is structurally assembled like a brick wall, in which flattened dead keratinocytes are organised into layers of parallel plates. The keratinocytes are embedded in a "mortar" consisting of an extracellular lipid matrix (ECM) that contains enzymes and proteins (Lee et al., 2018; Morgado, 2011). The external surface of each keratinocyte is a bi-layered, hydrophobic lipid lamella composed of ceramides, cholesterol, and fatty acids alternating with a hydrophilic region (Morgado, 2011).

The SC was initially regarded as a biologically lifeless impermeable barrier because of its hygroscopic characteristic and the apparent impermeability and metabolic inactivity of the keratinocytes. However, SC is a dynamic, active protective barrier that can be altered for increased dermal bioavailability of pharmaceutical agents.

1.1.1.2 The basement membrane (BM)

The deep, epidermal boundary of human skin is the dermal–epidermal junction or basement membrane (BM). Structurally, the BM presents an extracellular matrix (ECM) synthesised by basal keratinocytes and dermal fibroblasts associated with undulating, rete ridges between the dermis and the epidermis, and provides mechanical support to the epidermis. Anchoring filaments maintain the connection between the BM layers and between the underlying connective tissue-rich dermis and the overlying cellular epidermis (Figure 1.3). With intrinsic skin ageing, the BM becomes significantly thinner and exhibits a flattened appearance and a reduced surface area due to loss of rete ridges. As a result, aged skin is less resistant to shearing forces and more vulnerable to injury (Humbert et al., 2012).

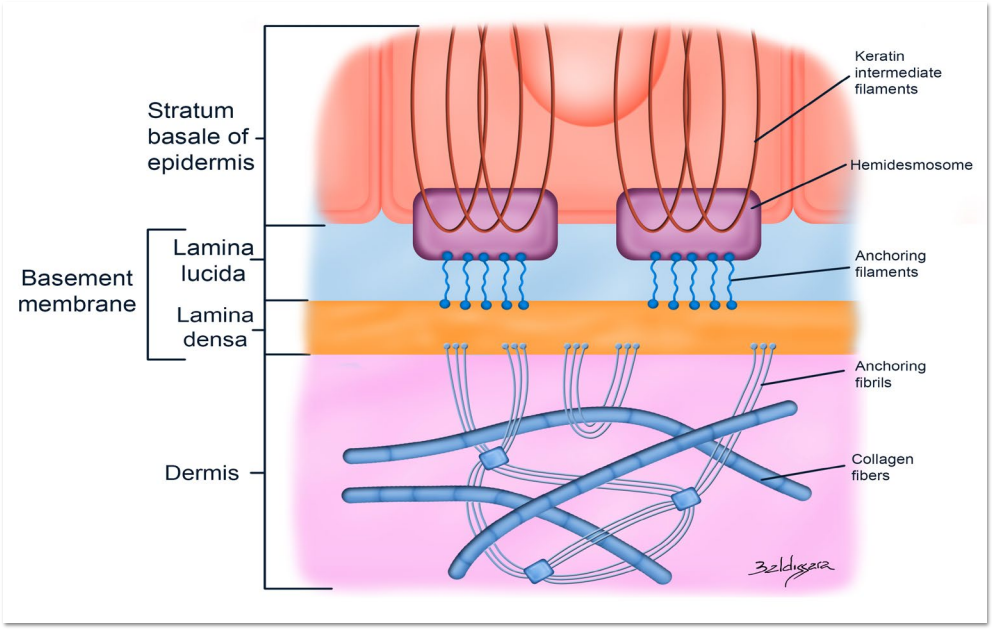

Figure 1.3: Schematic representation of the basement membrane (dermal–epidermal junction) structure. Anchoring filaments maintain the link *lamina densa* and *lamina lucida* and between the BM and the epidermis.

Physiologically, the BM is an active interface acting as a border between the human body and the environment (Kamel et al., 2016). The BM regulates the diffusion of large molecules and also acts as a limiting factor to the invasion of carcinomas in their early stages of malignancy (carcinoma *in situ*) (Dominguez-Delgado et al., 2010; Breitkreutz et al., 2013; Kamel et al., 2016).

The BM is a reservoir for a variety of cytokines and growth factors (GFs) and controls their release. Under inflammation, damage to the BM releases these substances, which are essential for wound healing and angiogenesis (Breitkreutz et al., 2013).

1.1.2 The dermis

The dermis is composed of an extracellular matrix (ECM) and fibroblasts. The fibroblasts are vital for cutaneous structural integrity, skin resilience, and health. They produce collagen and elastic fibres, regulate the ECM, produce substances such as growth factors (GFs) and cytokines. The ECM carries collagen and elastic fibres, blood and lymphatic vessels, sensory nerve endings, the bulb of the hair follicles, and sebaceous and sweat glands (Shashi et al., 2012; Khavkin & Ellis, 2011).

Dermal collagen fibres bind water and provide tensile strength and structural support to the skin. The collagen bundles are loosely arranged around elastin fibres. Dermal blood vessels supply nutrients to the overlying epidermis, remove waste products and help with regulating the body temperature (Kamel et al., 2016).

Biophysical and morphological dermal characteristics vary according to the region of the body, gender and age. The dermis is thicker in men, while the postmenopausal female dermis experiences collagen loss (Dominguez-Delgado et al., 2010).

The dermis is structurally divided into a thinner superficial papillary layer adjacent to the epidermis and the deeper reticular dermis. The papillary dermis lies directly beneath the BM and represents approximately 10% of the dermis. In this layer, conical projections known as dermal papillae project and interdigitate with epidermal ridges. These projections strengthen the dermal-epidermal adhesion.

The thick, reticular dermal layer is composed of ground substance and densely packed connective tissue with a set of irregularly arranged collagen and elastin fibres. The reticular dermis can expand up to 25% by stretching the collagen fibres in many directions. The elastic properties within the elastin network ensure full recovery of tissue shape and architecture after deformation. This layer can also be squeezed due to its capacity to displace the amorphous ground substance.

The dermal microvasculature consists of two linked, horizontally arranged networks originating from vessels in the subcutaneous tissue, themselves originating from larger fascial perforators. The superficial plexus is located in the boundary between the papillary and reticular layers of the dermis and gives rise to vascular loops that ascend to every dermal papilla (Figure 1.4). The deeper plexus lies near the dermal–fat junction.

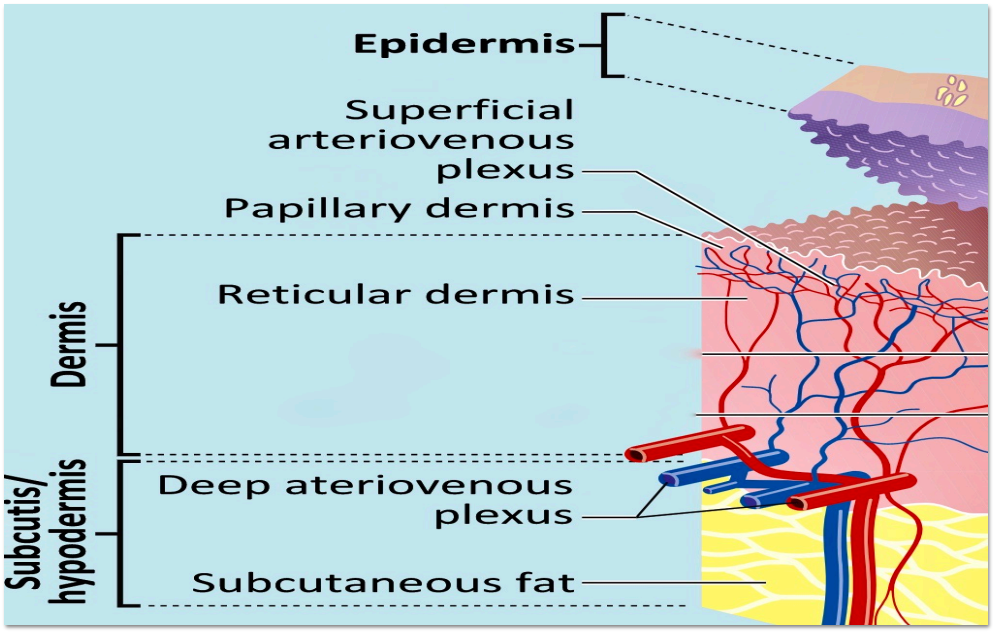

Figure 1.4: Representation of dermal anatomical regions (papillary and reticular dermis) and the superficial and deep arteriovenous plexus (Source: Wikipedia: Skin, on 21 April 2020).

The fibrous network in the papillary dermis protects the vessels and cells against mechanical insults, whereas the permanent tension in the reticular dermis generates the folding of the overlying skin surface (Kamel et al., 2016; Khavkin & Ellis, 2011).
The dermal numerous blood vessels nourish the stratum basale in the overlying epidermis, and help with regulating the body temperature (Kamel et al., 2016). The vascular network removes waste products, and permits skin repair and immune response (Shashi et al., 2012; Dominguez-Delgado et al., 2010).

1.1.3 The hypodermis

The hypodermis, also called subcutis or subcutaneous tissue, is linked to the overlying dermis by interconnecting collagen and elastin fibres. It is composed of fibroblasts, macrophages and adipocytes arranged in lobules, which are separated by connective tissue *septae*. The hypodermic mechanical functions include shock absorption and dispersion of externally applied pressure by allowing the overlying skin to be displaced as a whole, whether horizontally or vertically. The hypodermis contributes to the thermoregulatory property of the skin (Khavkin & Ellis, 2011).

1.1.4 Skin appendages

Skin appendages encompass pilosebaceous follicles, sweat and sebaceous glands, which are embedded within the dermis. Sebaceous glands are present in most areas of the body except for the palms of the hands and soles of the feet, with the highest density of sebaceous glands found on the face. Sebum produced by the sebaceous glands provides emollients for the hair and skin and maintains an acid mantle (pH < 6) on the skin surface and acts as a plasticiser that waxes, protects and lubricates the SC. Its secretion declines by 23% per decade in men and 32% per decade in women (Morgado, 2011).

The epidermal appendages occupy only 0.1% of the skin surface and are open to the external environment via ducts and duct orifices. However, on the face, the skin appendages account for up to10% of the surface area (Morgado, 2011; Dominguez-Delgado et al., 2010; Khavkin & Ellis, 2011).

1.2 Microtopography of human skin

The skin surface is an intrinsic feature of the human skin and depicts the physical, biochemical and physiological relationships between the skin layers. The cutaneous microtopography exists from birth and is not flat. During senescence, there is a progressive loss of elasticity of the dermis, causing effacement of skin microrelief with

dermal thinning and reduced structural support. Fine lines and longer, deeper and wider wrinkles develop.

The cutaneous surface of normal skin has a smooth, velvety feel but varies according to:

- The three-dimensional organisation of supportive dermis and the content of elastic fibres;
- The cohesion of the cells of the superficial cutaneous layers;
- Slightly protruding corneocytes, furrows, follicular orifices and sweat pores;
- The regional variations from one anatomical site to another (Piérard et al., 2003).

Microrelief lines are imprinted in the upper dermis, where the three-dimensional (3D) organisation of coarse collagen bundles defines their geometry. Primary and secondary lines can be observed on the skin surface. These lines are discrete and shallow, reaching up to about 200 μm in depth and creating a criss-cross pattern delineating polygonal plateaus. The microrelief characteristics of the primary lines depend on the structure of the papillary dermis, and their orientation and depth are influenced by ageing.

Delicate, tertiary lines in the skin surface correspond to the thin microrelief determined by the edges of corneocytes, while the quaternary lines are exceedingly thin, forming only discrete blebs and trabecular networks on the corneocyte membrane itself (Piérard et al., 2003).

Microstructures, such as intercellular borders, epidermal grooves, wrinkles, shallow areas, and furrows associated with intersecting lines and follicular and eccrine duct openings result in the genuine three-dimensional cutaneous microtopography called skin roughness, or rugosity (Figure 1.5) (Tchialeva et al., 2010; Ohtsuki et al., 2013; Trojahn et al., 2015; Piérard et al., 2003). Skin roughness is subject to internal influences (chronological age, health, use of medication and lifestyle) and external influences (climatological conditions, sun exposure, and use of topical products). These conditions affect the skin relief by modifying the hydration state of the SC. In older patients, roughness can be augmented by scaling or reduced due to progressive dermal atrophy and reduced skin elasticity (Piérard et al., 2003; Trojahn et al., 2015). The presence of scars or other skin abnormalities also modifies roughness. Roughness is used in clinical studies to characterise skin irritation and to investigate scaling, tumours, scars, and skin ageing. Notably, an objective measurement of roughness is also used to evaluate the efficacy of preventive or anti-ageing treatments such as laser remodelling (Trojahn et al., 2015).

Figure 1.5: Image exhibiting the criss-cross pattern of primary to tertiary lines. The delimited, polygonal plateaus result in a three-dimensional skin surface pattern called skin roughness.

1.3 Major skin alterations: ageing process and scars

1.3.1 Skin ageing

Senescence of human skin is characterised by loss of elasticity and tensile strength. The epidermis becomes thinner, and its turnover decelerates, and there is a reduction in cellular desquamation in the *stratum corneum* (SC), coupled with a reduced capacity to retain water. In addition, dramatic quantitative and qualitative histological changes are seen in the dermis. Collagen synthesis by fibroblasts decreases and an increase in collagen degradation takes place. These structural alterations result from two biological processes, which may occur concurrently:

1. A methodical and progressively slow, chronological phenomenon including selective apoptosis. The consequences of this intrinsic ageing event are a decrease in dermal strength and a reduction of volume within the cutaneous layers. Morphologically, the passage of time causes a reduced activity of fibroblasts at a cellular level, which leads to a disruption of collagen fibres within the ECM. Epidermal flattening occurs as a consequence of the loss of interdigitation with capillary-rich dermal papillae, and the visual impact from a reduced capillary flow within a collapsing skin results in a pale, thin, fragile epidermis (Tobin, 2017).

2. A degenerative phenomenon which results from environmental influences. The most important external factor influencing how skin appears during the skin ageing process is chronic UV irradiation accruing from sun exposure. The functional alteration caused by UV exposure is called photoageing or actinic damage (Tobin,

2017). UV radiation induces the production of free radicals and reactive oxygen species, which cause irreversible defects in the dermal matrix turnover, leading to degradation of elastic fibres and a reduction in the renewal of elastin and type I collagen fibres. Consequently, the thickness of the dermis is reduced by up to 20% and skin resilience changes. The actinic damage also leads to elastosis, i.e. the synthesis of amorphous, non-functional elastic material in the upper and mid dermis (Humbert et al., 2012; Aldag et al., 2016).

1.3.2 Scars

Trauma arising from physical agents (e.g. car accident, surgeries) or thermal damage (burn injuries) can compromise skin integrity. The injured dermis immediately triggers a universal well-orchestrated response called wound healing. There are three phases to wound healing: hemostasis and inflammation, proliferation (new tissue formation), and tissue remodelling (contraction) (Boateng et al., 2008; Gauglitz et al., 2011; Amini-Nik et al., 2018). These synchronised phenomena illustrated in Figure 1.6 involve physiological interactions between the epidermis and the dermis and are coordinated by the secretion of signalling proteins, namely GFs and cytokines (Park et al., 2017; Aldag et al. 2016; Behm et al., 2012).

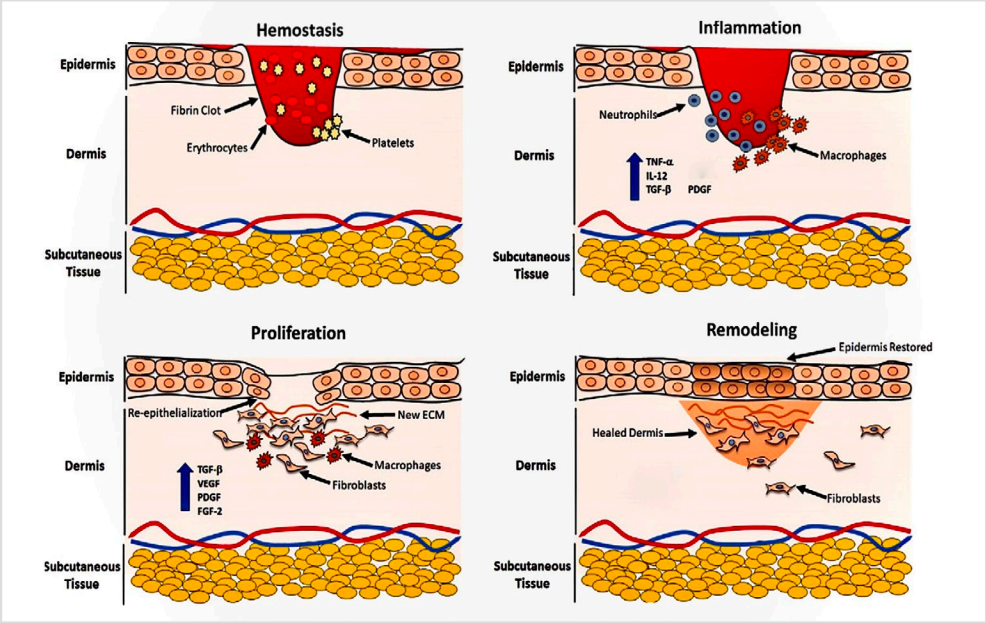

Figure 1.6: Schematic illustration of cell types and GFs involved in the phases of wound healing. The classical blood clot serves as a provisional matrix for further cell migration. The platelets release granules and the cells involved in wound healing secrete several GFs and proteolytic enzymes. Extracted from Amini-Nik et al., 2018.

During wound healing phases, the fibroblasts replace the initial ECM under the influence of GFs, producing type III collagen, and adult/mature type I collagen in the scar. Type IV collagen is produced at the dermal-epidermal junction. Re-epithelialisation occurs by

keratinocyte mitosis and cell proliferation above the ingrowing BM as the wound size naturally contracts (Amini-Nik et al., 2018). This process depends on the presence of oxygen, vitamin C, and ferrous iron (Qing, 2017).

The remodelling phase is also a GFs-dependent process characterised by controlled proteolysis of the newly synthesised ECM. Capillary ingrowth into the injured area ceases, and the metabolic activity diminishes as the initial vascular granulation tissue fades and matures into a relatively soft and less vascular scar composed of inactive fibroblasts, fragments of elastic tissue, dense collagen and other components of the ECM (Amini-Nik et al., 2018; Park et al., 2017).

After complete wound healing, the visual appearance of the end-scars following injury varies dramatically among individuals. The expression "scarring" refers to abnormality in colour, contour (bulging or indentation), roughness (rugosity or smoothness) or texture (softness or hardness) arising during the skin healing process (Metcalfe & Ferguson, 2007). Scars are clinically and histopathologically classified as normotrophic, atrophic, hypertrophic, and keloid (Verhaegen et al., 2009) (Figure 1.7). Each type may require a different approach.

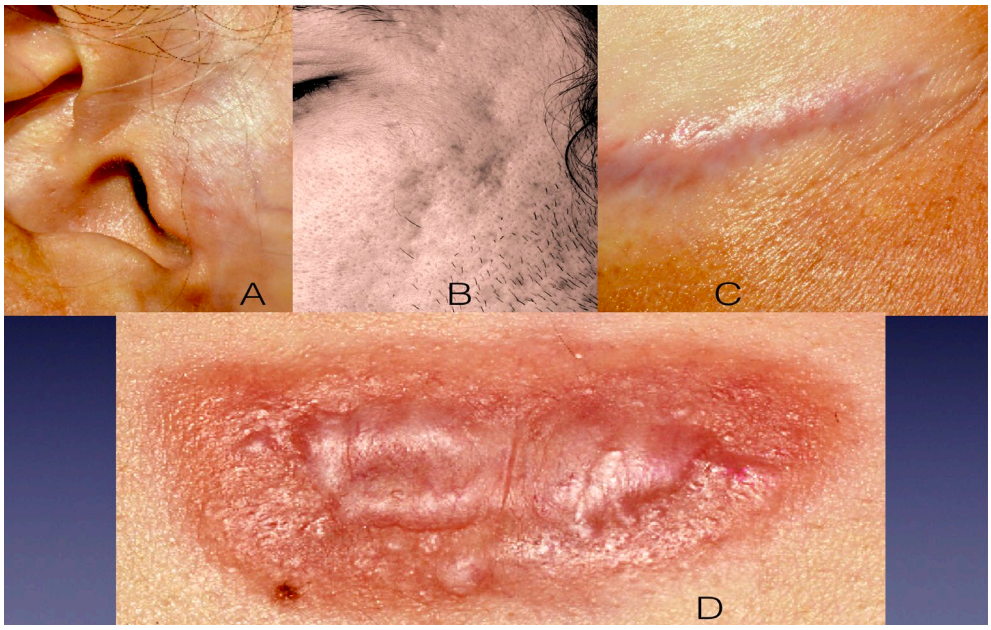

Figure 1.7: Examples of (A) a normotrophic pre-auricular scar, (B) an atrophic scar consequent to acne, (C) a post-mammoplasty hypertrophic scar, and a keloid (D) that spontaneously developed in the pre-sternal region resulting from an acne lesion.

The longer the wound healing process and the deeper the wound, the higher the possibility of developing hypertrophic scars or keloids.

Although normotrophic scars present a skin relief distinct from the normal adjacent skin and are witness to the presence of a wound, their appearance is flat and aesthetically acceptable (Figure 1.7 A).

Atrophic scars exhibit thin and discoloured valleys or depressions on the skin surface due to tissue loss and collagen destruction or deficiency (Figure 1.7 B). Some of them can be deeper and punctiform, as seen with icepick acne scars (Metcalfe & Ferguson, 2007).

Hypertrophic scars are flushed, itchy, firm, erythematous raised tissue (Figure 1.7 C). They exhibit numerous fibroblasts, increased vascularity and collagen synthesis or reduced collagenase expression during the remodelling phase.

Hypertrophic scars commonly occur in areas that exhibit slow wound healing or in pressure-dependent or movement-dependent regions. Their aetiology has been linked to (i) skin tension, (ii) wound infection, (iii) prolonged inflammatory response, (iv) genetic and (v) environmental causes (Bloemen et al., 2011; Edwards, 2011; Gauglitz et al., 2011).

The first description of abnormal scar formation in the form of keloids was made in approximately 1700 BC. The word keloid, meaning "crab claw", illustrates the lateral expansion of the scar beyond the boundaries of the original wound, i.e. invading the normal skin tissue (Figure 1.7 D).

Keloids are unique to humans and there is no suitable animal model for research (Metcalfe & Ferguson, 2007). These exuberant, inflammatory scars are related to significant morbidity, functional restrictions, stigma, psychological distress, cosmetic disfigurement, local pain and pruritus (Edwards, 2011; Verhaegen et al., 2009; Gauglitz et al., 2011).

The main differences between hypertrophic scars and keloids are summarised in Table 1.2.

Table 1.2 - Main differences between hypertrophic scars and keloids

Characteristic	Hypertrophic scar	Keloid
Genetic connection	Less familial incidence. Autosomal inheritance.	Familial predilection. Possible auto-immune phenomenon.
Ethnicity	Less ethnicity-related.	Blacks more than Caucasians.
Sex ratio	Equal sex ratio.	Females more than males.
Age	Commonly observed in patients under 20 years old.	Most common in 10 to 30 years-old.
Wound borders	Confined to the boundary of the original injury.	Overgrows the boundaries of the original injury.
Anatomical preferences	Locations with high tension, such as shoulders, neck, pre-sternum, knees and ankles.	High predilection for the face, anterior chest, shoulders, earlobes, and upper arms.
Time of development	Related to tension and timing of wound closure; Develops soon after injury and subsides with time.	Develops months after injury and rarely subsides; Aspect does not improve over time.
Signs and symptoms	Pinkish, elevated scar that may be related to pruritus.	Elevated surface, increased volume; Pruritus, tenderness and hyperesthesia.
Involution	Typically regresses one year after injury.	Can grow indefinitely.

1.3.3 Molecular biology related to ageing skin and scars

The regeneration of any corporal tissue is a complex process characterised by dynamic interactions between cells, the ECM, and dependent on the abundance of several substances, namely vitamin C, GFs and inflammatory cytokines (Qing, 2017).

1.3.3.1 Growth factors

The terms growth factors and cytokines have been used interchangeably as research has demonstrated that both initiate signalling pathways. GFs bind to their specific receptors on the cell surface (Figure 1.8) and this interaction activates several molecular events that are essential for wound healing and tissue repair (Aldag et al., 2016; Husein el Hadmed & Castillo, 2016; Demidova-Rice et al., 2012). The major growth-factor families involved in these processes are the epidermal growth factor (EGF), keratinocyte growth factor (KGF), fibroblast growth factor (FGF), platelet-derived growth factor (PDGF), TGF-βs (transforming growth factor beta), heparin-binding growth factor (HGF), and vascular endothelial growth factor (VEGF). These GF families (i) regulate the growth, differentiation, proliferation, and cellular influx of fibroblasts and monocytes, (ii) affect collagen and ECM biosynthesis, and (iii) promote neoangiogenesis (Aldag et al. 2016; Amini-Nik et al., 2018; Park et al., 2017; Qing, 2017).

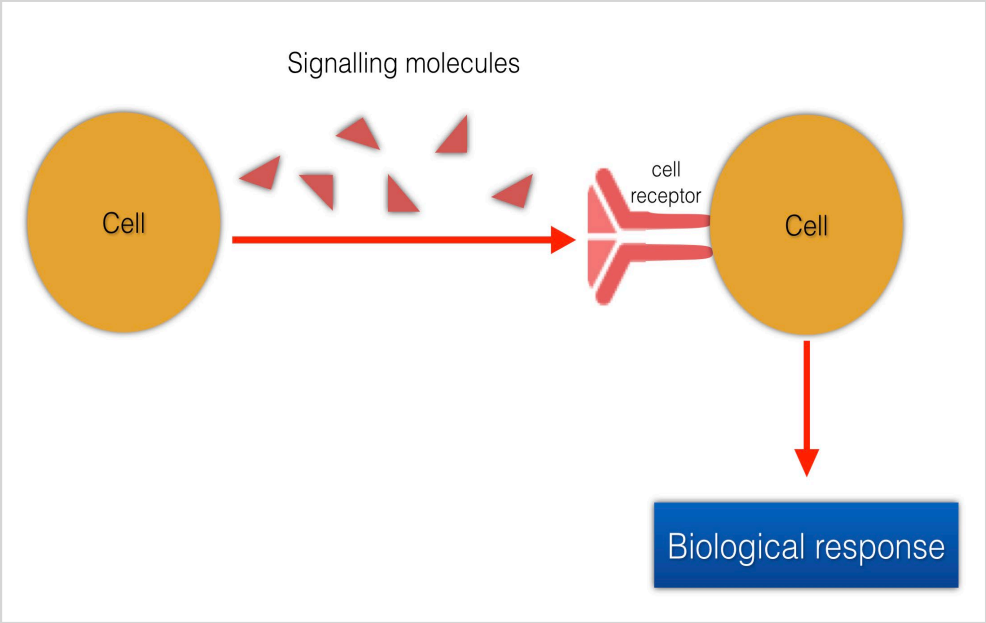

Figure 1.8: Mechanism of action of growth factors. The GF-cell binding results in the activation of signalling molecules, which in turn can either activate proteins present in the cytoplasm or induce transcription of new proteins.

Transforming growth factors beta (TGF-βs)

TGF-βs comprise the multifunctional regulators TGF-β1, TGF-β2, and TGF-β3 secreted by fibroblasts and macrophages, platelets, and keratinocytes. TGF-βs are essential for cutaneous wound healing as they mediate the cutaneous immune response, and the crosstalk between the dermis and epidermis (Amini-Nik et al., 2018; Qu et al., 2012). TGF-βs (i) increase the synthesis of ECM proteins, (ii) enhance granulation tissue formation, (iii) improve the tensile strength of the dermis, and (iv) regulate the pathogenesis of scars and other fibrotic conditions (Demidova-Rice et al., 2012; Qu et al., 2012). TGF-βs can also be used in clinical practice to treat intrinsically and extrinsically aged skin.

Burn injuries and other severe cutaneous traumas activate dermal fibroblasts that produce a large amount of TGF-β1, which is profibrotic. Inordinate TGF-β1 activity leads to excessive myofibroblast activation, stretching of the scar tissue and increased tissue tension. These undesirable effects increase the likelihood of hypertrophic scar formation (Amini-Nik et al., 2018). Similarly, TGF-β2 increases scar tissue formation whereas depletion of fibroblast-specific TGF-β2 receptor results in reduced granulation tissue formation and decreased scar size. As a counterpoint, TGF-β3 accelerates wound healing, and its intradermal injection has been reported to improve scar appearance (Amini-Nik et al., 2018).

Vascular endothelial growth factors (VEGFs)

VEGFs are produced by endothelial cells, keratinocytes, fibroblasts, platelets, neutrophils and macrophages. VEGFs are unique in their effects on multiple components of the wound-healing cascade as they (i) regulate angiogenesis and vascular permeability, (ii) stimulate cell survival, proliferation and migration, and (iii) stimulate granulation tissue formation.

VEGFs are associated with the closure of chronic wounds exhibiting hypoxia and compromised vascularity (Barrientos et al., 2008; Metcalfe & Ferguson, 2007). However, deregulation of VEGFs has been associated with tumours, intraocular neovascular disorders, and nonhealing wounds (Bao et al., 2009; Demidova-Rice et al., 2012).

Epidermal growth factors (EGFs)

Platelets, macrophages and fibroblasts produce EGFs. These GFs stimulate keratinocyte proliferation and migration, differentiation and re-epithelialisation. EGFs also increase the number of fibroblasts in the wound and augment the expression of keratins involved in the proliferative signalling pathway.

Research has demonstrated that dose-dependent, repeated treatment with EGF increased the epithelial cell proliferation and accelerated the wound-healing process (Kwon et al., 2006; Barrientos et al., 2008). In addition, EGF has the potential to improve acne scars, brown spotting, skin texture, pore size, red spotting, stretch marks and wrinkles (Seidel & Moy, 2015; Aldag et al., 2016; Disphanurat et al., 2020).

Platelet-derived growth factors (PDGFs)

Platelet-derived growth factors (PDGFs) are mitogenic proteins produced by macrophages, epithelial and endothelial cells, and platelets. PDGFs stimulate macrophages to secrete GFs, such as TGF-βs. They are essential for fibroblast proliferation, production of ECM, wound healing and angiogenesis. Abnormal regulation and production of PDGFs may cause tumours and fibrotic disease.

Fibroblast growth factors (FGFs)

FGF-α and -β, also known as acidic and basic FGF, respectively, are pluripotent proteins produced by inflammatory cells, vascular endothelial cells, fibroblasts, and keratinocytes.

FGFs are angiogenic factors involved in morphological (embryonic) processes, keratinocyte organisation and wound healing (granulation tissue formation, matrix remodelling and re-epithelialisation) (Demidova-Rice et al., 2012). FGF-7, or

keratinocyte growth factor (KGF), is singular among the FGFs for its highly specific action on keratinocytes (Behm et al., 2012).

Insulin-like growth factors (IGFs)

The IGFs are produced by fibroblasts, macrophages, neutrophils and hepatocytes. IGFs (i) stimulate both cellular hypertrophy (increase in cell size) and hyperplasia (increase in cell number), (ii) stimulate wound re-epithelialisation and fibroblast proliferation, and (iii) can induce neuron survival.

Hepatocyte growth factor (HGF)

HGF is secreted by mesenchymal cells. HGF regulates cell growth, cell motility, wound healing and morphogenesis (embryonic organ development and adult organ regeneration). Its ability to stimulate mitogenesis and matrix invasion gives it a central role in angiogenesis and tumorigenesis.

1.3.3.2 Vitamins

Although there is a need for further data concerning the use of other vitamins such as vitamins A and D to treat skin conditions (Amini-Nik et al., 2018), water-soluble vitamin C has proven effective in skin treatments. Vitamin C is the most abundant antioxidant in humans and is a vital cofactor in several reactions of hydroxylation of proline and lysine in procollagen, which is converted into collagen (Ganceviciene et al., 2012; Humbert et al., 2012).

Vitamin C increases the density of the dermal papillae, due to the angiogenesis and stimulation of dermal fibroblasts (Qing, 2017). The topical application of vitamin C (ascorbic acid) has demonstrated a positive effect on skin rejuvenation because the antioxidant nature of vitamins controls the changes observed in ageing skin, namely skin dryness, pigmentary mottling, elastosis and degraded collagen that underlies the wrinkles.

The ingestion of ascorbic acid enhances the immune function during wound repair because it promotes an increase in the motility of neutrophils and stimulates lymphocyte transformation (Anderson, 1981; Amini-Nik et al., 2018). Additionally, vitamin C reduces the production of free radicals and reactive oxygen species that delay cicatrisation. Vitamin C has been applied to managing hypertrophic scars (Masaki, 2010; Ganceviciene et al., 2012; Humbert et al., 2012; Al-Niaimi & Chiang, 2017). Furthermore, ascorbyl derivates inhibit the oxidative damage to the skin that eventually may be induced by laser irradiation (Fujimoto et al., 2017).

Although ascorbic acid is widely applied to the skin, its poor skin penetration and instability in formulations reduce its clinical efficacy. The instability can be counterbalanced by combining it with alpha-tocopherol (vitamin E) to retard vitamin C oxidation and to potentiate the action of ascorbic acid. Vitamin E is a general term for tocopherols, major lipophilic antioxidants of the skin.

Vitamin E (i) stabilises cell membranes, (ii) modulates cellular responses, (iii) inhibits lipid peroxidation, (iv) prevents effects in oxidative stress conditions and (v) relieve free radical damage caused by neutrophils in the inflammatory phase of wound healing (Masaki, 2010). The application of vitamin E in scar treatment is controversial. While some authors reported that topical application of vitamin E can be related to scar worsening and an inhibitory effect on collagen synthesis and wound repair (Amini-Nik et al., 2018), other publications have reported an improvement in hypertrophic scars and keloids that were treated with vitamin E added to silicone sheets (Sinno et al., 2011).

1.4 The skin as a via for drug administration

1.4.1 The genesis of transcutaneous medication

For thousands of years, people have placed chemical substances and physical agents on the skin surface to treat or rejuvenate it. In ancient times, Turks used fire to scorch the skin to induce exfoliation. Records of Babylonian and Egyptian medicine make references to the use of ointments, sour milk, oils, salt and alabaster to improve the skin aesthetically. These historical landmarks reinforce the importance of the skin as the corporal frame, associated with health, apart from physical attractiveness (Prausnitz & Langer, 2008).

The extent and exposure of this vital organ in supporting the systems of the body linked with homeostasis, immunological defence and for maintaining biological equilibrium make it an important pathway for drug administration (Kamel et al., 2016; Tobin, 2017; Shashi et al., 2012). From the genesis of transcutaneous medication, based on the use of topical ointments relying on natural drug diffusion, to sophisticated transdermal drug delivery systems, the growing demand for patient-friendly therapies has emphasised the advantages of transdermal medication over conventional drug delivery methods.

1.4.2 Skin kinetics

The process of uptake, distribution, and elimination of drugs is called pharmacokinetics. As the skin receives approximately one-third of the entire blood volume, in spite of presenting a thickness of a few millimetres, after dermal penetration, the rich dermal vascular network system controls the availability of drugs. Due to the *stratum corneum*'s

hydrophobic, lipophilic characteristics, most drugs do not permeate the skin at a relevant concentration because either they are too large in molecular size or they lack the necessary lipophilic properties. On the other hand, a variable amount of topically applied substances can be absorbed into the circulation with possible detrimental effects. This uncertainty of absorption has restrained regulatory approval of several medications. Consequently, the biggest hindrance to transcutaneous medication is the limited number of drugs that are amenable to administration by this route.

Besides, the catabolic activity within the epidermis is complex and substantial, and becomes higher with increasing age. The skin contains all the major enzymes produced in the liver and other detoxifying tissues (e.g. esterases, monooxygenase, alcohol dehydrogenase, carboxylesterases, cytochromes, hydrolases, among others). Whereas cytochromes are the largest group of metabolizing enzymes in skin, some enzymes, namely 5-α reductase, are only found in specific regions of the body, and may present gender-specific expression.

Although the action of cutaneous enzymes is less intense when compared to hepatic enzymes, the bioavailability and pharmacological activity of any topically applied drug can be significantly reduced due to biotransformation during skin penetration (Mbah & Uzor, 2011). The catalytic breakdown may result in helpful or harmful toxicological side effects (Shashi et al., 2012).

The highest enzyme activity (hydrolysis) is observed in the viable epidermis. There is limited knowledge on how to bypass or synergistically use the skin enzymes for improved transdermal medication. However, the epidermal enzymes undergo substantial loss of activity when heated above 40°C (Pyo & Maibach, 2019).

1.4.3 Transcutaneous drug permeation and penetration pathways

The percutaneous transport of chemicals is a complex process that involves different phenomena and can be divided into:

- Penetration: the entry of a substance into a particular layer or structure such as the *stratum corneum*;
- (ii) Permeation: the penetration through one layer into another that is both functionally and structurally different from the first layer.

The former describes the passage of an agent into the skin to the intended cutaneous layer. The latter depicts the complete transdermal passage of a compound which can reach into the circulatory system. A compound traversing the SC can undergo both penetration and permeation. In this case, the compound absorbs into the underlying

epidermal environment and diffuse into the dermis and the circulation via lymphatics and dermal blood vessels.

The rate of molecular transport through the SC is slow and highly constrained, i.e. between only 1–5% of the substance applied to the skin may be absorbed (Shashi et al., 2012; Wiedersberg & Guy, 2014). In an intact SC, a permeant applied to the skin has three possible routes of entry through the epidermis:

- Intercellular absorption: the molecule is transported through the sinuous pathway around the corneocytes, into the lipid-rich intercellular domains;
- Transcellular route: chemical substances are transported through the corneocytes and the intervening lipids by partitioning into and out of the cell membrane;
- Transappendageal or shunt route: absorption occurs via the skin appendages.

The relative contributions of the routes to the chemical flux (Figure 1.9) are usually regulated by the physicochemical properties of the permeating molecule. Most compounds applied to the skin will permeate through more than one route simultaneously depending on the compound's characteristics and the vehicle employed (Dayan, 2005; Shashi et al., 2012; Zorec et al., 2013). The intercellular and transcellular routes are the most expressive pathways for transcutaneous drug permeation. The intercellular route is the major route for small, uncharged molecules, and both lipid and polar molecules can be transported through this pathway (Mbah & Uzor, 2011; Tsakovska et al., 2017; Dayan, 2005; Shashi et al., 2012).

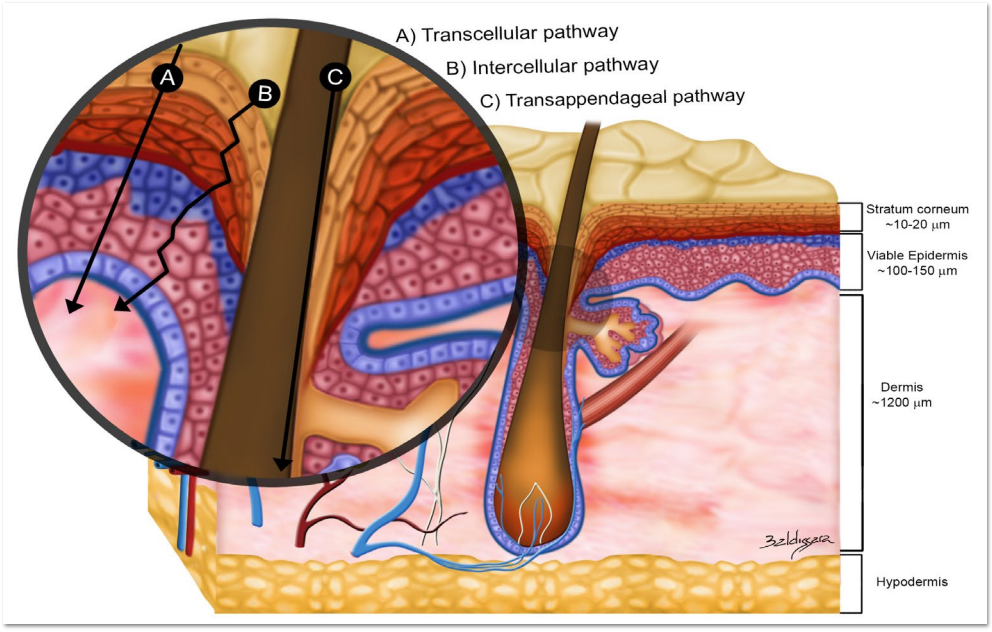

Figure 1.9: Schematic representation of transcutaneous drug pathways. (A) represents the intercellular absorption, (B) is the transcellular route and (C) is the shunt, transappendageal route.

The skin appendages occupy a small fractional area of the skin surface area, yet may have a major role in transcutaneous delivery of drugs. However, it is difficult to study the cutaneous penetration of drugs via follicles experimentally because of the lack of suitable animal models (Dayan, 2005). Although Mbah & Uzor (2011) and Dominguez-Delgado et al. (2010) considered the transport of drugs through the shunt routes as negligible, other authors maintain that cutaneous appendages acting as diffusional shunts can bypass the relatively poor diffusivity at the SC (Tsakovska et al., 2017; Shashi et al., 2012). The follicular pathway has also proven to play a significant role in laser-assisted permeation of medications such as Imiquimod and 5-aminolevulinic acid (ALA) (Lee et al., 2014). This is probably due to the laser interference with the TJs, which are the primary barrier structure in skin appendages.

1.4.4 Transdermal, intradermal and topical drug administration

The terms topical, intradermal and transdermal administration of medications define the use of the transcutaneous route for the application of drugs. As these terms are applied for specific purposes, their definitions are provided in Table 1.3 (Wilbur, 2019).

Table 1.3 - Transcutaneous medication: definition and examples

Application	Definition / aim	Example
Topical	Topical medications are those meant to remain and exert their effect on the skin surface only	Sunscreens
Transdermal	Transdermal medications passively diffuse and penetrate through an intact epidermis to target the deeper cutaneous layer or be absorbed into the systemic circulation	Transdermal patches such as estradiol, nicotine, and scopolamine for motion sickness
Intradermal	Intradermal delivery of medication specifically defines the direct introduction, usually through injection or infusion, of a medicine or fluid into the dermal layer	Vaccines; triamcinolone acetonide; 5-Fluorouracil

A drug delivery system is a pharmacological expression used to define an organised and controlled process for incorporating a chemical substance into the body (Wiedersberg & Guy, 2014). The main intention of drug delivery system is to facilitate the pharmacokinetics, maximise the therapeutic effect and reduce local and systemic adverse events (Münch et al., 2017; Amini-Nik et al., 2018; Lee et al., 2018). Transdermal drug delivery systems are usually occlusive and designed to be applied to the skin for prolonged periods, a situation that can cause skin sensitisation and adverse effects intrinsic to the drug or at the site of application.

Laser-assisted drug delivery is described as a procedure that creates a temporary change in the surface of the epidermis that is used as an opportunity for intradermal and

transdermal drug delivery (Watkinson, 2013; Wenande et al., 2019; Wiedersberg & Guy, 2014). As the effects of a substance applied after laser skin resurfacing and eventual post-laser drug absorption have not been elucidated nor controlled, the use of the expression “drug delivery system” may be inappropriate. Therefore, the term “laser-assisted medication” (LAM) has been used in this study that designs a protocol for LAM and investigates the impact of applying different medications on the skin surface immediately after laser skin resurfacing.

1.4.5 Benefits of the transcutaneous route

The ideal route of medication to achieve the best pharmacokinetics is dictated by factors such as the clinical condition of the patient, the target, the physical and chemical properties of the drug and the rate of absorption of the drug (Mbah & Uzor, 2011).

The main challenge of percutaneous absorption is achieving consistent therapeutic concentrations of active drugs that may be variably lipophilic or hydrophilic. The transcutaneous route is a shortcut that presents several benefits (Table 1.4) and can enhance drug bioavailability (Münch et al., 2017; Fujimoto et al., 2017). Despite several benefits and decades of research, transcutaneous drug delivery is still sporadic, and any commercial formulae are restricted to low molecular weight, lipophilic drugs (Münch et al., 2017; Wiedersberg & Guy 2014).

Table 1.4 - Possible benefits of transcutaneous medication

Less toxicity and reduction of side effects
Requires a lower dosage of drugs than oral administration
Easier compliance with the treatment
Constant serum concentrations
Circumvents the absorption through the gastrointestinal tract
A shorter route to the bloodstream than via the gastrointestinal tract
Bypasses the hepatic metabolism

1.5 Skin penetration enhancers

Permeation modifiers can reduce or overcome potential enzymatic inactivation, shorten the diffusional path and, in the final instance, improve the bioabsorption of a drug (Mbah & Uzor, 2011; Haedersdal et al., 2016; Münch et al., 2017; Prausnitz & Langer, 2008). These skin penetration enhancers give hydrophilic molecules, and those with a large

molecular weight (> 500 Dalton) access into the deeper cutaneous layers or help the drug penetrate to the circulatory system (Dayan 2005; Prausnitz & Langer, 2008).

The skin penetration enhancers can be classified into active, physical or passive, chemical enhancers according to their mechanism of action (Figure 1.10). Chemical penetration enhancers (CPEs), also called 'sorption promoters' or 'accelerants', are pharmacologically inactive agents that alter the barrier properties of the *stratum corneum*, and increase skin permeability in a temporary, reversible manner (Münch et al., 2017; Lee et al., 2018). Physical penetration enhancers (PPEs) are mechanical stressors that intentionally produce micron-scale defects in the SC by applying electrical, mechanical or thermal energy to superficial tissues.

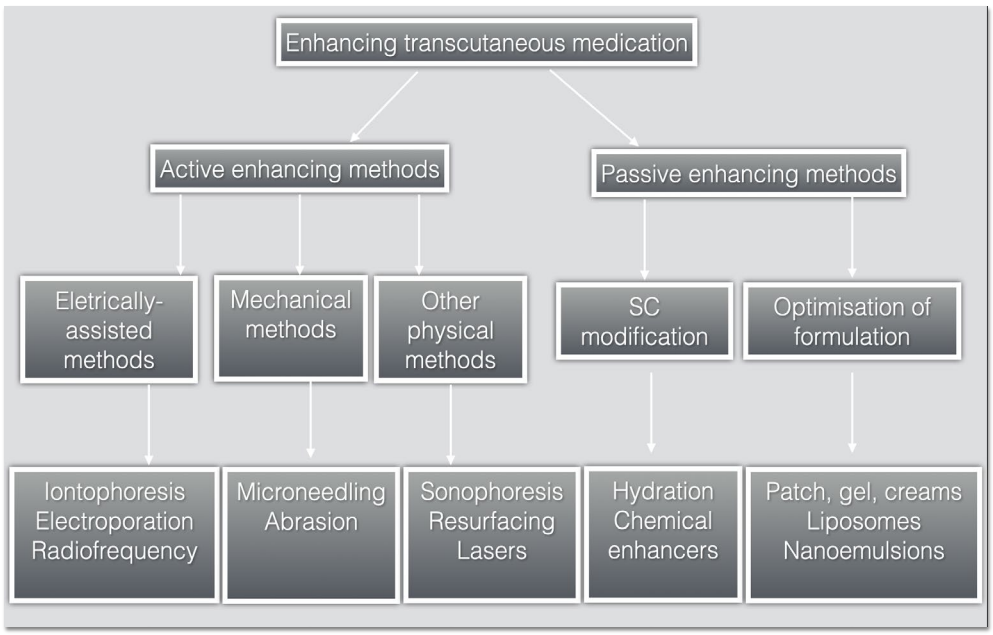

Figure 1.10: Schematic representation of active (physical) and passive (chemical) methods available to enhance transcutaneous drug penetration.

CPEs diffuse and partition into the skin and cause substantial perturbance of the intercellular lipid bilayers through the development of pores or channels. CPEs affect intercellular, desmosomal connections and diminish the diffusional resistance of the SC. Nonetheless, no CPE has yet been shown capable of causing a significant increase in drug permeation or the absorption of hydrophilic drugs and macromolecules (Münch et al., 2017; Lee et al., 2018). Furthermore, the effects of CPEs on the *stratum corneum* can cause skin irritation, erythema, scaling, contact urticaria, stinging, burning, dryness or most significantly, toxicity to living cells. These reactions have constrained their application in clinical practice (Dayan, 2005; Prausnitz & Langer, 2008). A comprehensive discussion concerning CPEs is not within the scope of this thesis.

PPEs are either energy-based devices using iontophoresis, electroporation, radiofrequency, laser, plasma radiation or ultrasound, or mechanical-based devices using microneedles or abrasion (Münch et al. 2017; Lee et al., 2018). Actual disruption of the epidermis by PPEs broadens the available surface area and range of drugs that can be delivered through the skin (Lee et al., 2018; Prausnitz & Langer 2008). Hence, PPEs promote the penetration and permeation of therapeutic agents containing macromolecules exceeding 20,000 Da (3,321077842 x 10^{-20} grams). This includes vaccines and hydrophilic molecules, namely peptides and proteins. Figure 1.11 shows some examples of PPEs. These approaches are medically acceptable and safe since the interference is constrained to the SC, while deeper tissues are spared (Shashi et al., 2012; Haedersdal et al., 2016; Prausnitz & Langer, 2008).

Figure 1.11: Physical penetration enhancers. (A) CO_2 laser, (B) Er:YAG laser, (C) microneedling and (D) mechanical dermabrasion.

Fractional ablative lasers (AFXLs) create vertical, uniform, open channels on the skin surface consisting of a central, ablated zone, surrounded by a cuff of coagulated tissue (Figures 1.11A and B) (Bay et al., 2017; Münch et al., 2017). Microneedling (MN) are devices composed of an array of microneedles that fabricate micron-scale pathways into upper skin layers (Figure 11C) (Prausnitz & Langer 2008; Münch et al., 2017; Lee et al., 2018; Kalil et al., 2015). Penetration depths can be similar after microneedling and lasers, reaching the superficial dermis (median of 125 μm) (Bay et al., 2017). However, it is difficult to be precise regarding the depth placement of the needling. The heat produced during laser treatment can enhance drug solubility and increase its bioavailability by reducing the activity of enzymes (Pyo & Maibach, 2019). Conversely, the microchannels produced by microneedling do not present a surrounding coagulation

zone and can be filled with a serosanguinous collection, and this obstructs drug penetration.

Dermabrasion (Figure 1.11D) disrupts the SC with ablative control of depth. However, cell spray produced by the procedure creates a potential infection transmission risk, and there is a risk of skin hypopigmentation.

1.5.1 Selecting a physical penetration enhancer (PPE)

The characteristics of the most commonly used PPEs are briefly described in Table 1.5.

Table 1.5 - The main physical penetration enhancers

Method	Definition, advantages, disadvantages, clinical use, and research
Mechanical dermabrasion	• Surgical procedure that involves a small, portable, low-cost, hand-held device. Removes the superficial layers of the skin. No thermal effect is involved. Risk of hypopigmentation and scarring, infections, and facial herpes virus reactivation. Requires anaesthesia. • Clinical use: to improve acne scars, perioral wrinkles, and to increase the uptake of substances namely lidocaine and 5-fluorouracil.
Microneedling (microporation)	• Array of microneedles of 10–200 μm in height and 10–80 μm in base diameter that fabricate micron-scale pathways into upper skin layers. • Low-cost. The damage is constrained to the epidermis. • Risk of infection; the holes created can fill with a serosanguineous collection, which prevents from drug penetration. • Clinical use: improvement of acne scars and skin rejuvenation.
Electroporation	• Application of intense and pulsating electrical fields to the skin surface to fabricate transient transmembrane pores and disrupt the cellular membranes. • High level of energy causes irreversible cellular damage with consequent apoptosis. • Clinical use: delivery of macromolecules (insulin and vaccines).
Iontophoresis	• Application of a low-density electrical current that repels the substance and forces it into the skin. • Application time cannot exceed 20 minutes due to the risk of skin damage. • Clinical use: topical delivery of anaesthetics during dermal surgery and to treat palmoplantar hyperhidrosis.
Sonophoresis (ultrasound)	• Application of transient cavitation in intercellular lipid-bilayer. • Cavitational ultrasound is not believed to contribute a significant driving force for drug transport. The equipment is expensive. • Clinical use: transcutaneous delivery of insulin, heparin and vaccines.
Microjets	• Device delivers macromolecules across the superficial layers of the skin through pulsed microjets. • Unpredictable drug penetration. • Clinical use: transcutaneous delivery of corticosteroids.
Laser	• Fractional lasers remove the SC and produce microscopic channels to the dermis. • The equipment is expensive. • Clinical use: increases the transdermal uptake of corticosteroids, immunotherapy agents and photosensitisers.
Plasma	• Heat source based on gas ionisation that results in a mixture of free electrons, positively charged ions and unionised gas. • Few available publications. • Clinical use: treatment of hypertrophic scars, and to accelerate the healing of burn wounds.

The selection of PPE type depends on user intent and the advantages, disadvantages and availability of equipment. For instance, the benefit of sonophoresis and iontophoresis

is the preservation of skin tissue. However, skin permeability is only available at the nanometre scale and therefore these techniques may not be broadly applicable for delivery of compounds with high MW (Prausnitz & Langer, 2008).

1.5.2 Lasers

1.5.2.1 Physics: The fundamentals of laser operation

The acronym “laser” (light amplification by stimulated emission of radiation) refers to a device that emits light through a process of optical amplification.

Laser light is a self-propagating wave resulting from the action of electromagnetic radiation (EMR). The elementary unit of EMR is the photon. Laser devices emit electromagnetic radiation (EMR) between 150 nm and 11,000 nm, from the UV up to the far-infrared spectrum (Figure 1.12).

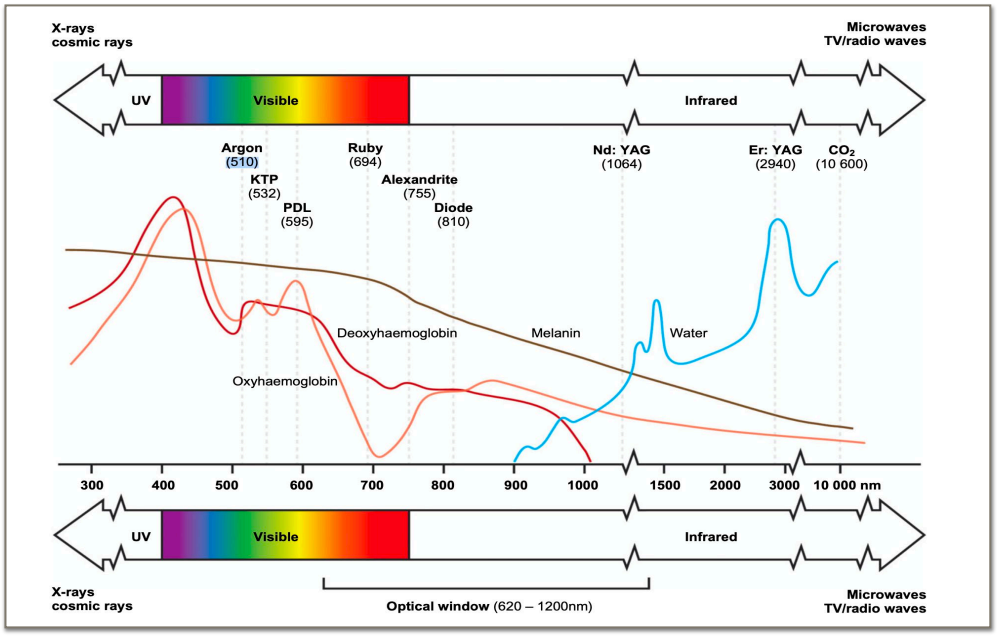

Figure 1.12: Effective range of lasers according to the electromagnetic spectrum (Extracted from Stewart et al., 2013. Lasers and laser-like devices: Part one. Australasian Journal of Dermatology 54, page 177).

Laser action relies on the atomic nature of matter according to the quantum theory proposed by Einstein in 1917.

A laser is composed of an optical resonator cavity, which contains the laser-active medium, an external power source (also called pumping) and two mirrors (Figure 1.13). One mirror contained within the laser cavity is fully reflective. The other is partially reflective and has a central hole by which the generated laser is channelled to form a beam that is delivered through this output aperture (Stewart et al., 2013).

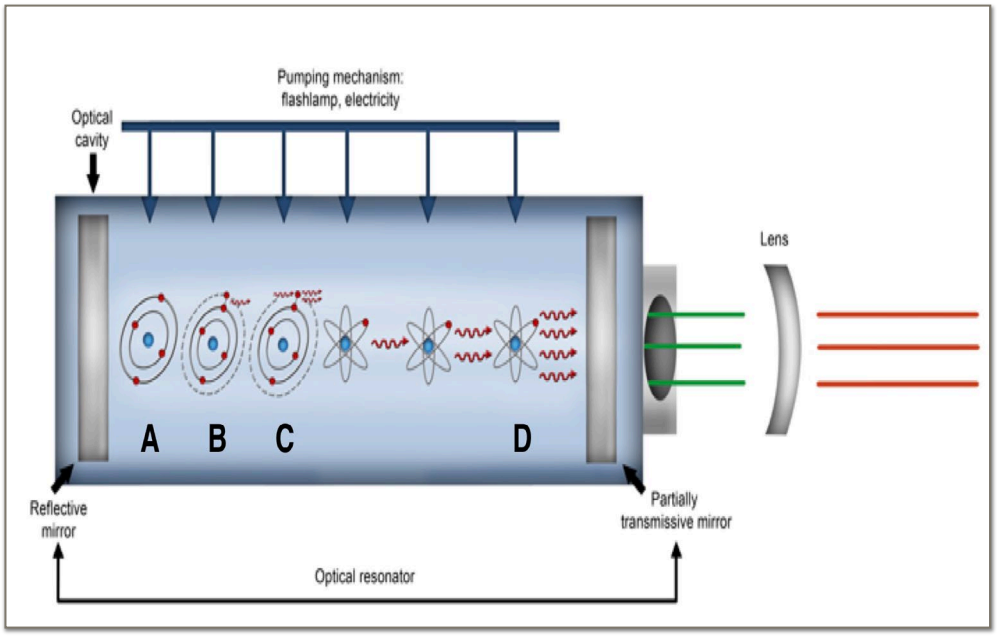

Figure 1.13: Schematic representation of the atomic reaction that produces the laser light inside the resonator cavity.

The laser medium is the active environment inside an optical cavity where the stimulated emission of radiation occurs and can be a gas, a solid or a liquid. Inside this laser medium are atoms in the ground state, i.e. consisting of the usual configuration of one central nucleus surrounded by a stable, low-energy level cloud of electrons at thermal equilibrium (Figure 1.13 A). The atomic ground state is modified by the emission or absorption of a photon, i.e. a particle of light (Figure 1.13 B). The electron cloud absorbs the light and achieves an excited, higher energy level. The excited atom tends to return to its stable state, which requires that this atom is prompted into emission of a "twin" new photon that presents the same wavelength as the photon that was initially generated (Figure 1.13 C). Therefore, the photons generated from an external energy source are joined by new photons emitted spontaneously by neighbouring atoms. This junction triggers the amplification of radiation (Figure 1.13 D), a cascade effect in which these photons excite adjacent atoms (Catorze, 2009). When pumped, the spontaneous photon emission travels back and forth and is amplified at a frequency determined by the optical characteristics of the laser medium.

1.5.2.2 Characteristics of the light emitted by lasers

Sunlight and incandescent light emit incoherent radiation, meaning that the light wave propagates in all directions. Lasers generate a beam of intense light with characteristics of:

- Monochromaticity: the light produced by the laser presents a single wavelength;

- Coherence: all the photons emitted are in the same phase as each other. The coherence allows a laser to be focused to a tight spot, a paramount characteristic that directs the laser beam to the desired target (Catorze, 2009);
- Collimation: the laser beam stays narrow, concentrated on a minimal area and maintains high beam intensities over great distances (e.g. laser pointers).

1.5.2.3 Selective photothermolysis and laser-tissue interaction

Lasers perform selective photothermolysis, i.e. part of the emitted light is selectively absorbed by specific targets called chromophores. This concept has been described in the 1980's (Haak et al., 2017; Stewart et al., 2013). Chromophores are usually groups of atoms that make up a particle, a tissue or pigments contained in biological tissues, namely haemoglobin, tattoo pigments and melanin.

In selective photothermolysis, the laser-tissue interaction is based on the laser action on chromophores and there is minimal diffusion of the thermal energy to the surrounding structures. Part of the light energy emitted by these lasers is reflected or scattered, while a substantial part of the radiation is absorbed by the target particle (Figure 1.14).

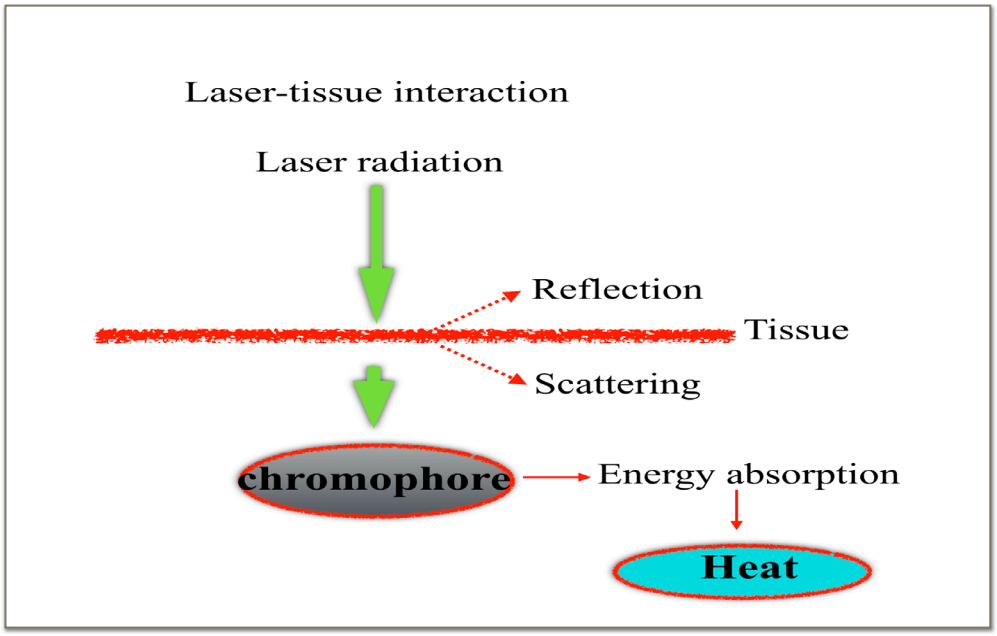

Figure 1.14: Diagram illustrating the laser-tissue interaction. The light emitted by the laser is absorbed by the chromophore and transformed into heat.

The chromophores are heated at high temperatures (50 – 100ºC) and boil. In the case of skin treatment, the high temperature promotes vaporisation (ablation) of the targeted tissue, and the result is the precise peeling characterised by instantaneous vaporisation of the SC followed by immediate, heat-induced collagen shrinkage. The mild after-lasing heat transference to underlying and surrounding cutaneous tissues causes denaturation

of collagen fibres and cytoplasmic proteins (Stewart et al., 2013; Haedersdal et al., 2016, Haak et al., 2012, Sklar et al., 2014). The protein denaturation gives rise to beneficial effects such as long-term neocollagenesis, and remodelling of the collagen and elastin fibres contained in the dermis with consequent skin tightening, improvement of the skin tone, texture, and appearance (Ganceviciene et al., 2012; Preissig et al., 2012; Amini-Nik et al., 2018).

1.5.2.4 Laser hazard risks

Lasers are categorised into four, general hazard classes based on the level of risk of injury. As the laser can travel over great distances as an intense, nearly parallel, collimated beam, the light can be concentrated enough to damage the retina or evaporate human tissue and metal. Lasers of classes 1 and 2 are eye-safe, whereas classes 3 and 4 lasers can cause irreversible ocular damage with just one glance into a direct or reflected laser beam, even at relatively low power levels. These lasers require the use of specific safety glasses for all personnel in the operating room.

Laser light can be reflected by mirrors, reflective glass, metal surfaces. Surgical instruments must have an anti-reflective surface (bare metal) or be made of plastic. The skin must be cleaned before treatment with saline solution because alcoholic solutions are volatile and present a risk of fire. In addition, antimicrobial solutions can be toxic when vaporised.

Lasers treating biological tissues produce smoke consisting of noxious gases, bioaerosol, steam and cell debris. Human papillomavirus, and particles of the HIV and hepatitis C virus were found in the smoke caused by CO_2 laser vaporisation. However, the Erbium:yttrim-aluminum-garnet (Er:YAG) laser is safer since the presence of viral deoxyribonucleic acid (DNA) was not detected in smoke resulting from the vaporisation of human viral warts treated with this laser (Kauvar & Hruza, 2005).

1.5.2.5 Lasers performing skin resurfacing

Laser skin resurfacing (LSR) is a procedure that involves the use of a laser device to treat the skin surface whether to improve skin alterations (e.g. scars and warts) or to promote skin rejuvenation. LSR reduces skin laxity and produces amelioration of facial wrinkles, atrophic acne scars, and hypertrophic scarring (Preissig et al., 2012; Murphy & Carmichael, 2000).

The carbon dioxide (CO_2) and Er:YAG lasers are commonly used to perform skin resurfacing. CO_2 lasers emit long-wavelength laser light (10,600 nm), while Er:YAG lasers emit mid-infrared light at a wavelength of 2,940 nm (2,94 μm). Both wavelengths

are highly absorbed by biological water-containing soft tissues using water as the chromophore (Catorze, 2009).

The laser energy emitted by the erbium wavelength is approximately 20 times more absorbed by water than that of CO_2 wavelength (Stewart et al., 2013). Consequently, treatments with Er:YAG lasers result in 95% tissue coagulation, and only 5% thermal injury (photomechanical effect), while CO_2 lasers induce mostly thermal coagulation (around 80%) as a photothermal effect (Alexiades-Armenakas et al., 2012).

Traditional ablative lasers were developed in the 1990s. The main feature of these lasers was the laser beam which was evenly delivered to the skin to disrupt the entire SC layer. Depending on the energy output and the number of passes, the ablation caused by these devices could reach the dermal reticular layer, which made them effective in reducing rhytides, photoageing, and acne scarring. However, traditional ablative lasers were associated with severe complications, namely scarring, temporary hyperpigmentation and permanent skin hypochromia (Disphanurat et al., 2020; Preissig et al., 2012). The procedure was extremely painful and required intravenous sedation or general anaesthesia. All patients underwent post-procedure oozing, bleeding, crusting, and prolonged downtime due to healing. These devices were substituted by fractional technology.

Fractional lasers deliver a laser beam divided into thousands of microscopic treatment zones that target a fraction of the skin at a time, analogous to a photographic image which is composed pixel by pixel. Fractional lasers are subdivided into ablative and nonablative. Fractional nonablative lasers produce microcolumns of thermal injury and protein coagulation in the dermis without epidermal ablation or vaporisation of the SC (Genina et al., 2013). Despite recent reports on the impact of nonablative lasers to the structures and barrier functions of epidermis (including SC), dermal-epidermal junction, and dermis (Lee et al., 2016 a), their use in drug delivery is controversial (Alexiades-Armenakas et al., 2012).

Fractional ablative lasers (AFXLs) produce controlled fractioned microperforations through the epidermis and towards the dermis. The microchannels are interspersed with untreated skin areas. The intact skin bridges between the microcolumns of ablated skin remain as the source of nutritional elements, viable tissue stem cells, keratinocytes and fibroblasts, which migrate to the traumatised area to facilitate the re-epithelisation (Ali & Al-Niaimi, 2016; Preissig et al., 2012; Stewart et al., 2013). Although the underlying molecular changes induced by LSR have not been completely elucidated, studies have shown that the laser action induces the production of heat shock proteins, growth factors,

hyaluronic acid, and dermal collagen and elastic fibres that are important in the development of tighter and better-quality skin (Ganceviciene et al., 2012; Manstein et al., 2004).

1.5.2.6 Fractional ablative laser parameters

Fractional Er:YAG and CO_2 lasers deliver predictable, non-ionising radiation that is transformed to thermal energy on the skin surface. AFXLs produce 3D microchannel matrixes that are surrounded by zones of coagulated protein and cutaneous tissue which are called residual thermal damage zones (RTDs) (Preissig et al., 2012; Haak et al., 2012):

- The residual thermal damage zone (RTD) and each microchannel constitute a unit called the microthermal zone (MTZ);
- The microthermal zones (MTZs) reach up to 100 – 400 μm in diameter and the depth of 50 – 120 μm, depending on the choice of laser device and settings (Preissig et al., 2012; Haak et al., 2012; Banzhaf et al., 2019);
- Laterally, the RTD usually does not exceed 50 μm (Taudorf et al., 2014; Alexiades-Armenakas et al., 2012; Preissig et al., 2012).
- AFXLs are associated with fast healing and reduced risk of post-inflammatory hyperpigmentation because of constraining the RTDs.

AFXLs still retain some risk of acneiform eruption, cutaneous infection, herpes simplex virus exacerbations, temporary hyperpigmentation, scarring and discolouration (Taudorf et al., 2014; Alexiades-Armenakas et al., 2012; Preissig et al., 2012). The CO_2 fractional laser is also linked to increased thermal injury with the potential for more significant collateral fibrosis and scarring compared to the Er:YAG laser (Sklar et al., 2014). The Er:YAG laser was selected to treat patients as safely as possible with as little depth of skin injury as required for an effective laser-assisted medication (LAM) (Amini-Nik et al., 2018).

The energy output and ablative penetration depth are directly proportional to each other. Usually, a small microspot diameter results in deeper ablation because the energy output is more concentrated. Targeting larger diameter results in more superficial epidermal removal, which is appropriate for the treatment of photodamage, superficial wrinkles, melasma, or superficial scarring. In addition:

- Short pulse durations and high fluence produce greater ablation reaching deeper dermal layers, before significant heat diffusion to the surrounding tissues, which is ideal for treating scarring (Alegre-Sanchez et al., 2018).

- Long pulse durations and low fluences emphasise coagulation and cause a greater thermal effect on the surrounding tissue before ablation takes place (Badawi & Osman, 2018).
- The density is the number of MTZs produced by the laser per unit area (cm^2) (Figure 1.15). The density and the output energy are device-dependent and can be selected according to the intended depth of perforation and the severity of the deformity. The total density depends on both the number of channels, the size of the laser beam and the number of laser passages over the skin.

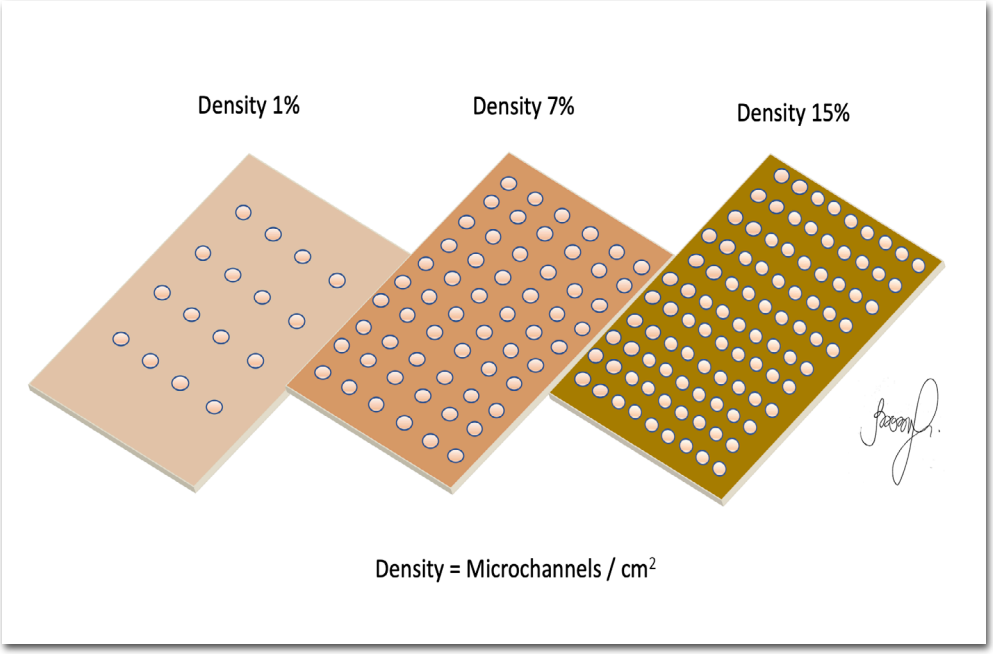

Figure 1.15: Diagram illustrating the treatment density (number of microperforations per cm^2) caused on the skin surface by fractional lasers.

1.5.2.7 The fundamentals of laser-assisted medication

In an intact SC, only small molecules and lipophilic drugs succeed in diffusing through the lipid-rich SC layer. The influence of AFLXs on skin permeability results from some theoretical mechanisms related to molecular diffusion. Diffusion (or molecular diffusion) is the transport of molecules from a region of higher concentration to a region of lower concentration by random molecular motion (Ali & Al-Niaimi, 2016; Mbah & Uzor, 2011). Laws that govern the molecular diffusion were established in 1855 by the physiologist Adolf Fick. Fick's first law of molecular diffusion is the chemical basis of LAM.

Mathematically, the three-dimensional, passive diffusion of a drug across the MTZ is established by Fick's first law using the formula: $J = \frac{-D \times Co \times Æ}{đ}$

- **J** = the steady-state diffusion flux or flow (particles per m^2/sec) across the *stratum corneum*,

- **D** = diffusion or permeability coefficient of the drug in the SC (cm^2/s) (the number of molecules available for diffusion across a membrane);
- **Co** = the concentration gradient of a drug across the SC (g/cm^3); it is assumed to be constant.
- **Æ** = the surface area of *stratum corneum* (cm^2)
- **ð** = the diffusional path length or membrane thickness (*stratum corneum*) in cm.

The concentration gradient (**Co**) is the thermodynamic potential or driving force for diffusion. The diffusion is directly proportional to the drug concentration in the formulation and the exposed surface area of the skin. After sufficient accumulation in the SC, the permeant diffuses into deeper strata along a concentration gradient (Lee et al., 2018). As there is a low concentration on the receiver side due to the uninterrupted dermal bloodstream, the donor side always has a higher drug concentration compared to the receptor (Shashi et al., 2012).

The diffusion coefficient (**D**) is directly influenced by the characteristics of the drug, the constitution of the transfer vehicle, the skin temperature and local pH. The higher the molecular weight, the greater the frictional resistance to its movement, which decreases the inherent diffusibility of a molecule across the membrane (Preissig et al., 2012).

The disruption of the SC's ultrastructure by the photoacoustic wave caused by AFLXs is theorised to improve drug diffusivity by expanding the lacunar space within the intercellular lipid bilayers (Wenande et al., 2019). As any drug penetration is inversely proportional to the thickness of the skin (**ð**), AFXLs decrease the diffusion path length and so augment the permeability into the SC, thereby modifying the transdermal flux of the drug (Shashi, 2012; Haedersdal et al., 2016; Lee et al., 2014; Banzaf et al., 2019;).

The removal of the SC by the LSR is not the only mechanism influencing a drug's permeability into the skin. The tissular heat generated by the laser results in accentuated molecular motion and consequent transcutaneous permeation of topically applied medication towards the MTZs (Lee et al., 2014; Münch et al., 2017; Bay et al., 2017). This explains the efficiency of AFXLs in enhancing drug penetration over other physical penetration enhancers (Alegre-Sanchez et al., 2018; Ibrahim et al., 2018).

The MTZs increase the diffusion area (**Æ**) by allowing the permeant to spread into deeper strata and penetrate laterally towards the RTD (Figure 1.16) (Mbah & Uzor, 2011). The RTDs produced by AFXLs temporarily cause a disparity between the uptake and clearance of hydrophobic and hydrophilic drugs inside the viable epidermis.

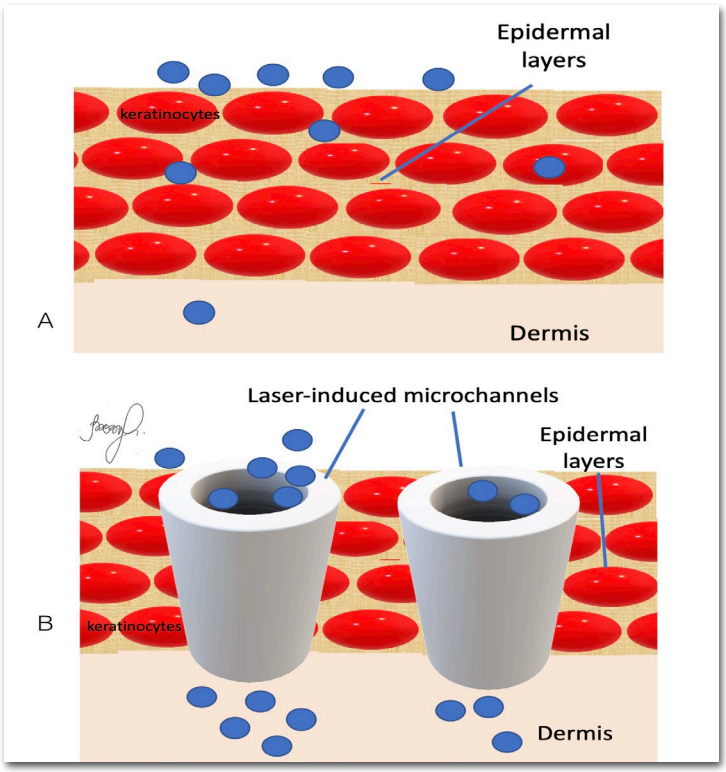

Figure 1.16: Scheme showing the planar drug diffusion in an intact SC (A) and the transcutaneous medication via fractional laser-induced microchannels (B). The blue circles represent the drug applied on the skin surface and the white cylinders represent the RTD surrounding the microchannels produced by fractional lasers.

Low molecular weight and hydrophilic permeants are more rapidly cleared from the skin by the dermal vasculature and penetrate deeper aqueous skin layers through the laser-induced MTZs. Conversely, the after-laser topical delivery of highly lipophilic compounds is modest (Banzhaf et al., 2019; Alegre-Sanchez et al., 2018; Ibrahim et al., 2018). Although lipophilic compounds undergo rapid diffusion in microchannels without RTD, they remain longer in the skin (Wenande el al. 2019).

1.6 Investigation of transcutaneous drug penetration

The interest in topical application of chemicals has generated significant research to measure, model and predict the rate of transcutaneous penetration.

Techniques and complex equations used to analyse pharmacokinetics and predict the bioavailability of drugs can be expensive, exceedingly laborious, inaccurate and demonstrate limited success especially if the cutaneous barrier's morphology and absorption characteristics are modified (Mbah & Uzor, 2011; Anissimov & Roberts, 2011). Even if the sophisticated models predict that blood/lymphatic transport into deep tissues may dominate over dermal diffusion (Anissimov & Roberts, 2011), it is challenging to determine cutaneous drug penetration and permeation based on molecular properties when there are other confounding factors such as:

- the dermal blood flow;

- the geometry of the microchannels and the RTD caused by the laser-tissue interaction (Basler et al., 2016; Haedersdal et al., 2016; Wenande et al., 2019);
- the channel dimensions which vary even employing the same laser settings because of the differences in skin thickness among individuals.

Wenande et al. (2019) presented a guide to experimental methodology related to LAM. Apart from the skin source and the nature of the study (*in* or *ex vivo*; human or experimental), they explored the analytical techniques that can be used to determine the bioavailability of drug inside the skin layers:

- Mass spectrometry and high-performance liquid chromatography are sensitive and selective analytical techniques (Hendel et al., 2019). However, both methods require sample extraction, intensive analysis and expensive equipment;
- Fluorescence spectroscopy is based on the use of fluorescent analytes, and provides information on superficial biodistribution only;
- Pharmacodynamic analysis is a technique that involves the indirect assessment of drug delivery based on the enhanced biological activity of the medication. This method is not necessarily an indicator of drug delivery (Wenande et al., 2019);
- Laser scanning confocal microscopy and optical coherence tomography are optical imaging technologies that provide visualization of biodistribution of fluorescent molecules in the skin and information on the morphology of the laser-induced microchannels and laser-drug-tissue interaction. Despite the capability of these systems to prove drug absorption, their use is limited to fluorescent agents and the resolution of optical coherence tomography is approximately 5 – 10 μm.

Recent research involving sophisticated morphology-based computational models has supported pharmacists by anticipating the permeant-barrier interaction. The computational modellings are based on real pharmacokinetic phenomena and mimic skin absorption, cutaneous physiological variability, and clarify the fate of absorbed compounds in the skin layers or biological media such as plasma and urine (Dominguez-Delgado et al., 2010; Basler et al., 2016; Tsakovska et al., 2017).

Limitations in using mathematical models stem from the datasets, which are regularly derived from aqueous vehicles, and may present restricted quality and high variability to support the development of quantitative structure-permeability relationship models (Tsakovska et al., 2017). In addition, these models will have to be adapted to take into account the three-dimensional architecture of the microchannels and the RTD caused by the laser (Haedersdal et al., 2016; Wenande et al., 2019).

Finally, the mere demonstration of drug absorption after laser skin resurfacing does not imply a positive clinical effect on the skin.

1.7 Rationale for the research

1.7.1 Laser-assisted medication

Laser-assisted medication (LAM) refers to transcutaneous, active delivery of chemicals and drugs after laser resurfacing of skin as an adjunct to treatment. Investigation on laser-assisted medication started in 1987 when Jacques et al. first reported an *in vitro* human experiment which consisted of the controlled removal of about a micrometre of human stratum corneum by an excimer laser (193 nm wavelength, 14 ns pulse width) to enhance the skin permeability to substances. They found that the gentlest laser ablation produced a 124-fold enhancement of the permeability constant. Higher radiant exposures lead to a 45-fold enhancement of transcutaneous drug transport (Jacques et al., 1987).

After years of research, lasers are still one of the best alternatives aiming at the transcutaneous delivery of molecules (Haedersdal el al., 2016; Wenande et al., 2019). This option is based on the following reasons:

- Fractional laser technology is efficient and safe and can promote microperforations up to 1500 µm in depth (Genina et al., 2013);
- Treatments with AFXLs have the advantage of inducing customisable and highly controllable laser-tissue interaction;
- Lasers can act as physical penetration enhancers that permit for increasing the molecular weight range of drugs suitable for the transcutaneous medication (Haedersdal et al., 2016; Sklar et al., 2014);
- The high temperatures created by AFXLs allow increased molecular motion and skin penetration of the drug;
- The combination of this physical agent and the drug is expected to improve skin quality and enhance the outcome of scars, chronic wounds and mycosis fungoides (Sklar et al., 2014; Ibrahim et al., 2018; Haedersdal et al., 2016).

Despite a profound interest in this field, LAM is yet to be considered as a standard or feasible therapy and delivery system. Although promising results have been obtained in several studies on animal models, human studies are scarce and usually restricted to preclinical trials. Convincing evidence is mostly linked to the oncology field (Sklar et al., 2014). The few available studies present different medications and assorted laser equipment and settings, which impedes the achievement of uniform responses regarding

the unknown factors involving this technique (Lee et al., 2016 b; Kohl et al., 2014; Martin et al., 2014).

The sparsity of data on this topic confirms that larger controlled trials are necessary to:

- analyse the effects of laser-tissue-drug interaction;
- quantify the interference of LAM on the skin surface;
- vouch for LAM's efficiency and safety;
- establish treatment protocols.

1.7.2 The hiatus concerning the ideal methodology to investigate LAM

Medical journals have published a plethora of papers related to procedures directed at improving scar management and promoting skin rejuvenation. However, only a few authors have validated the methodologies that they have employed in their studies. Biopsies have been frequently used. Limitations to using such method include freezing artefacts and cross-section misalignment. The clinical result may be under-represented because skin shrinkage and tissue distortion can accrue from the material preparation and impair the measurement of skin improvement (Wenande et al., 2019). Finally, it can be difficult to quantify tenuous changes in collagen fibres.

Traditionally, direct anthropometry through two-dimensional (2D) photogrammetry was the primary evaluation tool in dermatology and plastic surgery procedures. However, 2D photographs can introduce considerable bias depending on the angle at which the photo is obtained and the subjective evaluation of the researcher (Ardehali et al., 2007). Further potential error when relying upon a 2D photographic image includes the absence of objective data on pre- and post-treatment changes in volume and depth of the tissue being investigated.

Clinical scales such as the Vancouver Scar Scale (VSS) and the Patient and Observer Scar Assessment Scale (POSAS) have also been used, but they are subjective and cause a critical bias. In addition, scar severity, scar-related symptomatology and the age of the scar lead to varied individual perception of the deformity (Lee et al., 2016 b).

As the outcome from some treatments may be subtle, a more objective tool is necessary to accurately quantify changes in skin surface after treatment and allow the clinician to form a more effective management plan and post-treatment outcome assessment (Martin et al., 2014; Nedelec et al., 2000). Three-dimensional stereophotogrammetric systems are now available in clinical and research setting with this goal. Their unparalleled advantage is the ability to perform accurate volumetric quantification comparisons and to measure skin relief alterations (Honeybrook et al., 2018). However,

robust studies on three-dimensional stereophotogrammetry (3D SPM) efficacy to assess skin changes after treatment regimens such as LAM therapy are not available (Kohl et al., 2014; Ud-Din et al., 2015).

1.8 Working hypotheses

The working hypotheses for this thesis are:

- Three-dimensional stereophotogrammetry is a reliable method to quantify after-treatment skin changes;
- Skin medication with a cosmeceutical containing growth factors (GFs) as part of laser-assisted medication enhances the result of the skin treatment.

1.9 Thesis objectives and research questions

It is of paramount importance to quantify the LAM impact on the skin surface as opposed to the plain demonstration of enhanced delivery of substances (Haak et al., 2012; Banzhaf et al., 2019; Lee et al., 2016 b; Kohl et al., 2014). Furthermore, it is necessary to focus research on the establishment of ideal laser parameters that can be correlated among the different AFXLs irrespective of the drug being applied after laser treatment. The rationale for this assignment was to perform the first prospective, comparative, controlled, randomised trial in order to:

- establish 3D SPM as a valid and accurate method to measure the impact of laser-assisted intradermal medication on skin regeneration and scar improvement;
- evaluate the efficiency of using growth factors (GFs) contained in cosmeceuticals as part of LAM for improved skin relief alteration.

As secondary objectives, the study should:

- determine if the intact skin and scar tissue present a similar response to the treatment;
- establish a protocol comprising laser settings that could serve as a ground for additional studies involving the application of different medications while aiming to treat wounds, cutaneous diseases or to reach the bloodstream to treat remote pathologies.

The research questions posed were:

1. Is 3D stereophotogrammetry sufficient and efficient as a tool to quantify superficial skin changes after treatment?
2. What is the impact of using medication such as vitamin C in conjunction with growth factors contained within a cosmeceutical, on skin primarily treated with laser resurfacing?

The information provided by this research has set a baseline for future investigation and clarified some critical issues related to the use of LAM in clinical practice.

1.10 Study design

This thesis encompassed an *in vivo* three-phase clinical trial involving LAM. Figure 1.17 represents the conceptual framework of the research.

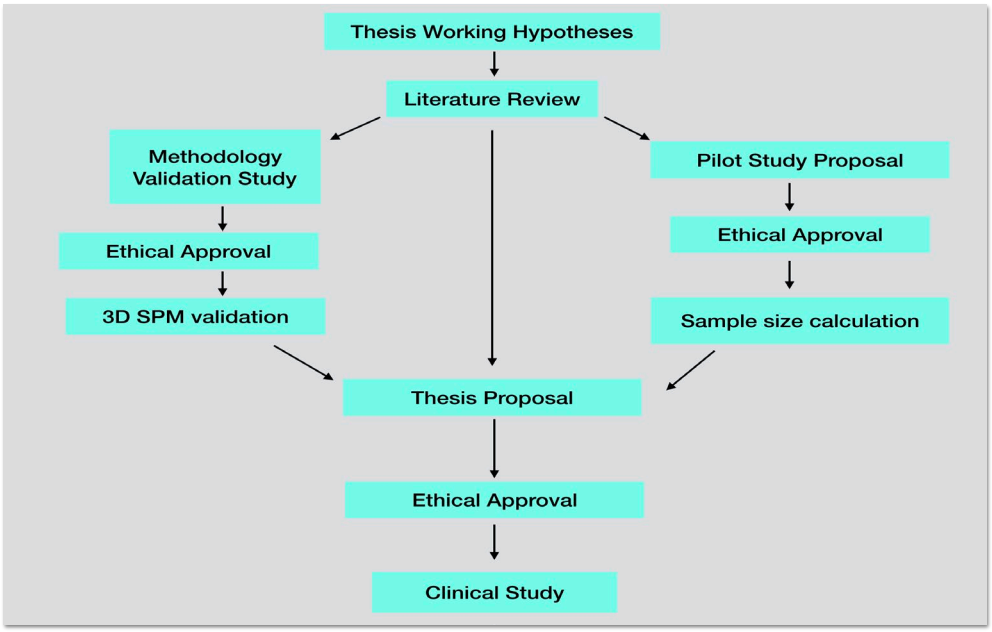

Figure 1.17: Conceptual map of the research.

Each phase consisted of two study groups of consenting patients:

- Patients of both genders, between 40 and 70 years old with Fitzpatrick skin type I–IV, seeking periorbital wrinkle improvement constituted group R (rejuvenation).
- Patients of both genders, between 18 and 70 years old with Fitzpatrick skin type I–IV, seeking scar improvement constituted group DS (damaged skin).

On the day of the treatment, patients signed the consent form, and the 3D system documented the skin surface pre-procedure. In phase 3, patients were randomised.

The patients were followed up at three months after the treatment when the 3D system documented the skin surface post-procedure. The Dermapix® software analysed the photographs and provided data regarding skin relief, and the software package SPSS (SPSS 24 and SPSS 2.6, IBM) was used to perform the statistical analysis.

In all three phases, an FDA-approved fractional Er:YAG laser (Starlux® 500, Palomar, USA) breached the skin surface to facilitate drug penetration. The three-dimensional stereophotogrammetry system, LifeViz™ Micro (QuantifiCare, Valbonne, France) was used to quantify any skin amelioration. Both are non-contact approaches and therefore prevented mechanical skin deformation from interfering with the laser's action or with the 3D SPM readouts.

Phase 1: Methodology validation study design

The qualitative and quantitative prospective study, described in Chapter 2, evaluated the therapeutic response of 48 patients (26 presenting wrinkles and 22 exhibiting scars) treated with one session of laser with topical vitamin C (LAM). Its objective was to standardise the tools for use in phases 2 and 3 of the study. The 3D SPM camera system was compared to a scale-based peer evaluation for visually assessing and quantifying changes in skin microrelief. The secondary objectives were to design a protocol concerning the laser parameters and establish the anthropometric landmarks related to the 3D SPM documentation to set a precedent for the next steps.

Phase 2: Pilot study

The prospective pilot study, described in Chapter 3, assessed the impact of the LAM with vitamin C of 59 periorbital wrinkles and 74 scars. The goal was to perform a feasibility study and to calculate the sample size for the clinical study (phase 3). A total of 95 patients seeking improvement of periorbital wrinkles (Group R) and patients seeking scar improvement (group DS) were recruited, screened and treated. The protocols were the same as those used in the validation methodology study. Twenty patients from group R and twenty-three from group DS were followed-up three months after the treatment.

Phase 3: Clinical study

Phase 3 was a prospective randomised, double-blind, comparative controlled trial comparing the effect of one session of Er:YAG fractional ablative LSR in patients seeking improvement of periorbital wrinkles and patients seeking scar improvement.

In phase 3, a total of 149 patients presenting periorbital wrinkles and 132 patients complaining of scars were treated. As randomised, controlled clinical trials are routinely analysed according to the intention-to-treat principle (Groenwold et al., 2014), every patient who was admitted to this research was systematically followed up and analysed in terms of outcomes defined by the randomisation study protocol at its conclusion.

Both the researcher and the patient were unaware of the treatment given (double-blind study). The research assistant randomised patients into two further groups, C and CGF. All patients received laser treatment immediately followed the topical application of 200mg of vitamin C (ascorbic acid, liquid for injectable use, Vitasantisa®) in group C. Patients treated with vitamin C composed the control groups.

Patients in group CGF received the same treatment combined with the topical application of a cosmeceutical (serum) containing a solution with a high concentration (93.6%) of patented, human, growth factor blend obtained from cultured neonatal foreskin

fibroblasts (TNS Recovery Complex®, SkinMedica). The cosmeceutical was chosen at the request of the Faculty Research Ethics Panel (FREP) because it is commercialised for topical use and duly licensed in the Conformité Européene (CE).

According to the fabricants, the fibroblasts grow and proliferate on artificial matrix, they generate extracellular substances such as naturally produced collagen, cytokines and over 380 growth factors. This information may be found in Chapter 8 – Appendices (document 8.1.1 and 8.1.2).

1.10.1 Study procedures

The studies comprising the different stages of this research were submitted for ethical approval to the Brazilian Ethics Committee of the Association Congregation Santa Catarina Casa de Saúde São José, Rio de Janeiro, Brazil and FREP at Anglia Ruskin University. The three phases of the research (Figure 1.18) were registered on the virtual database Plataforma Brasil. They received the reference numbers:

- CAAE:71398617.7.0000.5664: methodology validation study;
- CAAE:63710716.2.0000.5664: pilot study and clinical study.

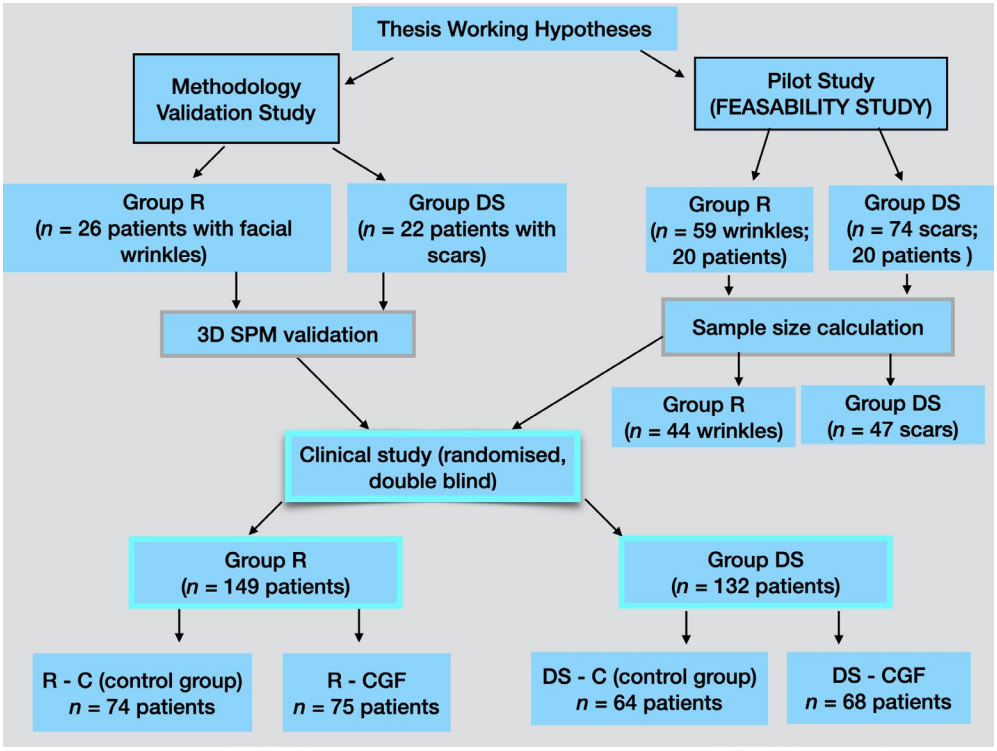

Figure 1.18: Flowchart displaying the number of patients investigated in each phase of the research.

All required documents, including the form related to Clinical Trials of Investigational Medicinal Products (CTIMP), were presented to the Ethics Committees. Data related to the storage, stability and handling of the vitamin C (VITASANTISA C® Ascorbic acid) and the cosmeceutical TNS Recovery Complex® (SkinMedica) were provided.

All patients received a participant information sheet that explained each phase of the study and a consent form. They read the information sheets and had the opportunity to discuss the study further with a research assistant. Patients signed the consent form and consented to the use of clinical photography and its inclusion for investigation and publication. Patient confidentiality was safeguarded, and personal data was not included, other than patient initials, study number, sex and age.

On the day of the treatment and before entering the treatment room, each patient picked a paper from a container for the randomisation process. The paper contained a description of the treatment to be delivered by the research assistant. After the laser treatment, the assistant applied the chemical substances according to the branch of the study.

The clinical trial ended three months after the date of the treatment. Patients were followed-up between 90 and 107 days after the treatment. The spread was largely due to the logistics of travel for the patient. Two patients from group DS-C (Figure 1.18) were observed with some days of delay (118 days after the procedure), and the collected data were used to preserve the benefit of randomisation. This strategy allowed a balanced distribution of prognostic factors in the compared groups, and the observed effect could actually be attributed to the designated treatment (Groenwold et al., 2014).

1.10.2 Risk assessment and potential benefits for patients

Some experimental studies have already demonstrated that laser pre-treatment can enhance the transcutaneous delivery of vitamin C by 15 to 102 times depending on its chemical composition and the type of laser (Sobhi et al., 2018; Huang et al., 2013). Therefore, clinical benefit was expected to all patients.

The low complexity outpatient procedure (LAM) performed in this research did not involve risk of life, and medications under investigation have no component involving potential toxicity. Although facial allergic granulomatous reaction has been associated with a serum containing vitamin C applied prior to microneedling (Soltani-Arabshahi et al., 2014), the vitamin C applied on the skin is currently marketed for intravenous use and has shown an excellent safety profile (Al-Niaimi & Chiang, 2017).

The cosmeceutical composed of a blend of growth factors and cytokines is regularly registered in the CE and distributed worldwide. Investigation on cosmeceuticals containing GFs has demonstrated no significant morphological alteration in the proliferation of normal human fibroblasts and the cultured human melanoma (Dieamant et al., 2012).

Potential benefits of LAM in this study included:

- A general improvement of the skin quality;
- A smoothing of superficial lines and creases in the ageing face;
- A reduction in scar volume.

1.10.3 Statistical considerations

Data generated by this research were submitted for statistical analysis using SPSS 24 and SPSS 26 IBM software. The statistical analysis investigated outcomes using GFs versus control treatments for scars and for ageing wrinkles around the eyes. The primary endpoint was the after-treatment skin surface change and was reached after completion of all 3D photographs obtained 90 days after LAM.

1.11 Thesis outline

The present study evaluates LAM impact on the skin surface of ageing individuals and patients with scars. The role of the 3D SPM camera system was investigated and used to objectively measure for improvement in outcomes.

Chapter 1 is an overview of the skin as a potential conduit for drug delivery and medication. It contains an introduction to skin histology, functions of the skin and the role of the *stratum corneum* as a shield to chemical, biological and physical penetrating agents. The gaps in our understanding and knowledge of the potential use of medical lasers to enhance the absorption is reflected by the paucity within the literature.

Chapter 2 reports the methodology used in validating the 3D SPM system as a sufficient and efficient method to quantify the impact of laser-assisted intradermal medication on wrinkle and scar improvement. This branch of the thesis compared the quantitative 3D SPM system with the traditional qualitative method using a clinical scale based on peer reviews. The findings endorsed the use of a research model containing a photographic protocol and a set of laser parameters, suitable for treating both skin regeneration and scar treatment groups.

Chapter 3 describes the pilot study investigating the treatment of patients with scars (group DS) and patients desiring facial skin rejuvenation (group R). This feasibility study permitted a calculation for the sample size needed in the next phase of the study.

Chapters 4 and 5 outline an extensive clinical study comparing the effects of LAM and the topical application of different chemical agents (vitamin C and the cosmeceutical containing GFs) on ageing skin and scars. Both chapters contain a critical analysis of

the hypothesis within the thesis and discuss the significance of the results in light of the literature review.

Chapter 4 shows the clinical study investigating the effect of LAM on facial wrinkles (group R) and further discusses aspects related to laser parameters and laser-assisted medication.

Chapter 5 is the clinical study that analyses the use of LAM on patients presenting with scars (group DS) and describes the role of GFs in the scarring process and tissue regeneration.

Chapter 6 summarises and makes conclusions from the findings of the overall research and proposes future work. Chapter 7 contains bibliographic references, and Chapter 8 displays the appendices to this thesis.

Chapter 2

Scientific Validation of Three-Dimensional Stereophotogrammetry for Assessing Skin Facial Wrinkles and Scars in Comparison with a Visual Analogue Clinical Scale

2.1 Introduction

A statistical analysis of outcomes from any treatment regimen involving skin is a necessary step to elucidate possible benefits to the patients and assist professionals in the decision-making process. The design of quantitative technologies to objectively analyse human skin remains a challenging task. Currently, more than half of the clinical trials investigating improved skin appearance following a treatment protocol rely on ordinal scales and statistical significance based on data generated from patient satisfaction scores and two-dimensional photographs assessed by experienced clinicians (Martin et al. 2014).

Skin is neither a linear nor a bi-planar structure, and therefore, 2D imagery is insufficient as a precise assessment tool (Rkein et al., 2014). Notwithstanding the high quality and flexibility of modern devices, two-dimensional photograph-based analyses are open to peer criticism when the magnification, background, photographing angle and posture are inconsistent. In addition, 2D photography may introduce a considerable bias depending on the subjective evaluation of clinical observers (Ardehali et al. 2007; Rkein et al., 2014).

Validated methods and bioengineering technologies used in the evaluation of skin morphology include visual analogue scales, skin tattooing, skin impressions, skin biopsy, and three-dimensional stereophotogrammetry. Most are inadequate or inaccurate at quantifying changes in skin texture and volume. As an example, the clinical analysis based on skin tattooing may vary according to mimics and facial movement. Biopsies can demonstrate the improvement of the histological composition of the skin layers, but the analysis of the skin relief is frequently impaired because of the material preparation.

Although several scales have been validated as objective methods, the individual perception of a skin condition does create bias and observer error (Levy et al., 2004; Lee et al., 2016 b; Dobos et al., 2015). Furthermore, difficulties in rating subtle results are frequently reported (Ardehali et al., 2007; Cavallini & Papagni, 2016). Several sophisticated, more accurate quantitative surface assessments utilise three-dimensional images created in a standard, reproducible setting (Plooij et al., 2009). The three-dimensional technology extracts information on the three measures of width, height and depth of skin surface topography. Table 2.1 provides a summary of the most commonly employed methods to assess scars and skin surface morphology.

Table 2.1- Methods used to assess scars and skin surface morphology

Method	Objective	Method limitations	References
Scales	To assess the skin surface characteristics and the evolution of skin conditions such as scars and wrinkles.	Subjective analysis of the results may lead to discrepant inter-assessor variation.	Lee et al., 2016 b; Ardehali et al., 2007; Dobos et al., 2015; Nedelec et al., 2000; Valet et al., 2009; Levy et al., 2004; Cavallini & Papagni, 2016; Rhee & McMullin, 2008; Rkein et al., 2014.
Skin tattooing	To measure facial wrinkles and skin roughness reduction after laser resurfacing.	Subjective peer-review analysis using a clinical scale can cause a bias.	Manstein et al., 2004.
Skin replicas or negative impression	Replication of wound bed and skin surface based on negative impression employing elastomer putty, clay modelling, plasters or callipers.	Time-consuming; lack of precision; direct contact with the lesion or skin may cause patient discomfort or introduce artefacts that distort the surface of the replica.	Ardehali et al., 2007; Nedelec et al., 2000; Lee et al., 2016 b; Stockton et al., 2015.
Skin biopsy	To investigate collagen remodelling.	The method does not deliver numerical data.	Skvara et al., 2013.
Three-dimensional skin scanners	To exhibit detailed skin surface information.	High cost; low availability; some devices require contact with skin.	Zapletalova et al., 2017; Ohtsuki et al., 2013; Jacobi et al., 2004; Kottner et al., 2013.
Three-dimensional stereophotogrammetry (3D SPM)	To study volumetric changes and monitor the effect of different treatments (for instance, acute burn oedema, lymphoedema, wound surface, acne scars, wrinkles, tumours, hypertrophic scars and keloids, cleft lip, hand rejuvenation and cutaneous carcinomas).	High cost; some devices permit for the registration of small areas making it challenging to document more extensive deformities.	Ardehali et al., 2007; Hameeteman et al., 2016; Hermans et al., 2014; Honeybrook et al., 2018; Kohl et al., 2014; Lee et al., 2016 b; Plooij et al., 2009; Skvara et al., 2013; Stekelenburg et al., 2015; Stockton et al., 2015; Tzou et al., 2014; Van der Loon et al., 2010; Ghoddousi et al., 2007; Ud-din et al., 2015; Disphanurat et al., 2020 ; Rijsbergen et al., 2019.

Photogrammetry is a science that uses photographs as the input to computer-generated measurements and is essential in the development of 3D models of real objects or scenes. By combining photogrammetry with three-dimensional information, it is possible to measure changes in textures and surfaces of a structure or an object (Tchialeva et al., 2010).

The three-dimensional stereophotogrammetry imaging system relies on areal topography, a method that incorporates the fundamentals of the stereoscopic binocular human vision. Figure 2.1 is a schematic illustration of areal topography. Point x is a specific point situated on the surface of an object that will be captured by two lenses (y1 and y2). The green lines in Figure 2.1 (A) depict the lines of sight, which intersect at point x. Figure 2.1 (B) is a diagram representing the stereoscopic vision, where y1 and y2 represent the vision captured by each eye and x illustrates the cerebral interpretation that accrues from the fusion of both images.

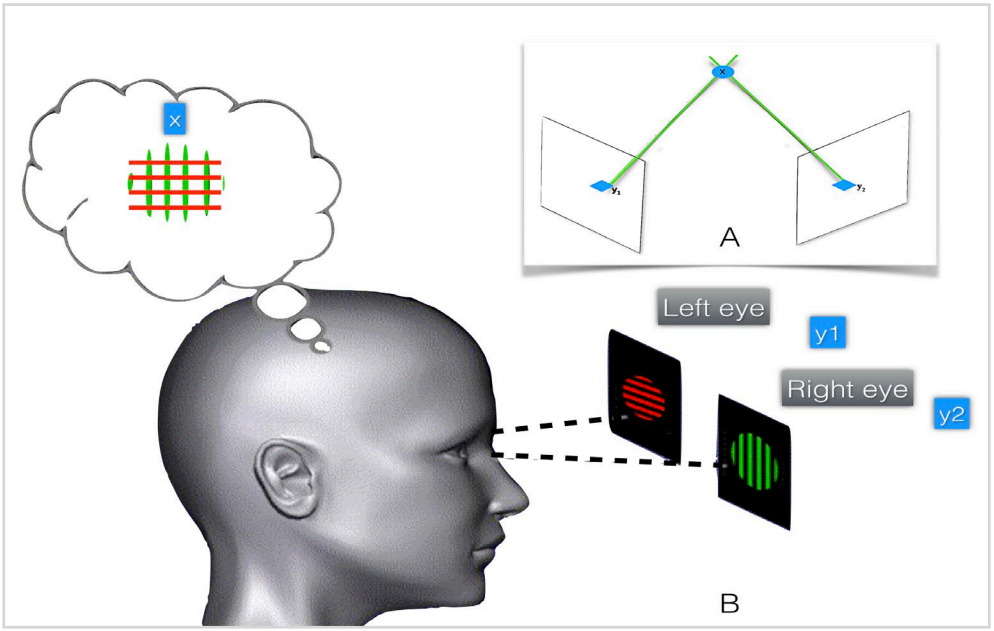

Figure 2.1: (A) Schematic representation of the triangulation of the lines of sight, which is the basis of areal topography. (B) Diagram representing the stereoscopic vision. Slightly different images (y1 and y2) are captured by each eye and interpreted in the brain as a combination of them.

Similar to human vision, which results from the capture of a different image by each eye, stereophotogrammetry uses a pair of two-dimensional pictures obtained from two different camera angles. The focal distance is constant, and the lens cannot be adjusted when taking the photographs. The point of shared focal convergence from two cameras or lenses in relation to a reference point on the surface of the object creates the 3D image, i.e. the visual topography of an object is derived from the convergence of these two slightly different images (Tzou et al., 2014). This system was first described by Thalmann-Degen in 1944 and improved by Deacon et al. in 1999, who appended digitalised images and software analysis to the method (Miranda et al., 2018; p. 573). The three-dimensional stereophotogrammetry imaging system associates the stereoscopic images with advanced technology software specifically programmed for soft tissue analysis.

Three-dimensional stereophotogrammetric (3D SPM) devices can be active or passive according to the source of light. Active SPM involves the active projection of light on to the object's surface, whereas passive SPM uses the natural ambient light.

The images are uploaded to specific software that performs a spatial analysis based on the intersection of ray bundles deriving from the pairing of differently aligned photographs at the same focal point. Mathematical algorithms embedded in the software permit for precise reconstruction and the extraction of consistent information from an object's surface. As for the analysis of the cutaneous microrelief, the software linked to three-

dimensional stereophotogrammetry detects and quantifies differences in skin surface height, depth, width and texture (Honeybrook et al., 2018; Tchialeva et al., 2010).

In a literature review, three-dimensional stereophotogrammetry (3D SPM) has been described as one of the most precise, practical, harmless, non-invasive, surface and volumetric measuring systems (Cavallini & Papagni, 2016; Hameeteman et al., 2016). This method has been reported to monitor a number of skin surface irregularities including cutaneous tumours, scars and wrinkles and to compare pre and post-procedure outcomes to treatment (Skvara et al., 2013; Disphanurat et al., 2020).

As an additional advantage, the fast image acquisition time (less than two milliseconds) is ideal for imaging children and facial structures (Hermans et al., 2014; Kohl et al., 2014) and minimises errors accruing from motion artefacts.

As the 3D SPM technology is supposed to detect minimal surface alteration, the changes in object position or even a small angulation or movement can impair an accurate analysis. Therefore, it is paramount to establish standards to capture images when pre and post-procedures photographs must be compared.

The parameters investigated by 3D SPM are usually related to the skin microtopography, as described in Chapter 1 (section 1.2 Microtopography of human skin). Apart from the skin roughness, skin alterations can be measured by perimeter, area, volume, heights and depths.

Some 3D SPM devices work as skin scanners and require a slight skin pressure for obtaining data concerning the skin surface. Usually, contactless 3D SPM systems are preferred when patients present open wounds or when subtle alterations are to be analysed.

Table 2.2 presents a summary of papers containing important contributions related to this new technology.

Table 2.2 - Summary of the literature review related to 3D stereophotogrammetry

Authors	Study	Conclusion
Ardehali et al., 2007	Assessment of keloid scars with 3D SPM imaging system (Vectra, Canfield, Fairfield, N.J.) to quantify the response to intralesional steroid therapy	3D SPM is a rapid and non-invasive method to monitor the surface of abnormal scars and has considerable value in evaluating new therapeutic strategies
Bloemen et al., 2011	Comparison of the performance of a 3D SPM system (PRIMOS, Germany) and the analysis of three observers who assessed burn scars in 60 patients using a subjective scale (POSAS - Patient and Observer Scar Assessment Scale)	The 3D SPM system analysed three roughness parameters and showed good intraobserver and interobserver reliability. The system was considered as a valid and reliable tool for objective evaluation of skin roughness
Ghoddousi et al., 2007	Comparison of nose measurements obtained through three methods of facial measurement (3D SPM, manual anthropometry, and 2D photography)	The accuracy of the 3D SPM was satisfactory. The variability of the 3D measurements was less significant than the manual and 2D measurements
Hameeteman et al., 2016	Volume measurement through water displacement to analyse upper extremity lymphoedema with 3D SPM (3dMD Cranial, Atlanta, USA)	3D SPM is an accurate method for measuring upper extremity volume in patients with lymphoedema and gives a lower variance value compared to that of the water displacement measurements
Hermans et al., 2104	A pilot study to evaluate the usability and clinical relevance of 3D SPM in the volume measurement of infantile haemangioma (3dMDface System, 3dMD Ltd., Atlanta, GA)	The authors concluded that 3D SPM is a fast, accurate and non-invasive way to determine and compare volumetric changes in infantile haemangiomas in time
Hoevenaren et al., 2015	Three-dimensional hand photographs were analysed to investigate the reproducibility of the 3D SPM system (3dMD Ltd., Atlanta, GA)	3D SPM provided realistic images of the hand. Advantages included no harmful side effects and reliability for soft tissue analysis (volume)
Honeybrook et al., 2018	Non-randomized, prospective analysis of 14 patients who underwent treatment with submental cryolipolysis with a 3D SPM system (Vectra, Canfield Imaging Systems, Fairfield, N.J.)	Considered the 3D SPM benefits over conventional 2D photographs, such as accurate, objective volumetric quantification comparisons. Pre and post-procedure comparisons were easily obtainable. This study involved a small sample size and no controls to allow for accurate comparisons of the 3D measurements
Kohl et al., 2014	Antera D3, a 3D SPM system and a clinical scale were used to investigate the result of three sessions of CO_2 laser to reduce facial wrinkle depth reduction and skin roughness	3D SPM was a valid tool to confirm treatment's efficacy. The study did not involve LAM
Kohl et al., 2015	Used 3D SPM and query regarding patient's satisfaction to investigate laser treatment for wrinkles	Evaluated if the 3D SPM measurement was correlated with patient-reported outcomes
Kottner et al., 2013	Performed measurements on the volar forearm skin in 12 healthy, young subjects with different three-dimensional imaging systems (SELS and PRIMOS 3D)	Both technologies provide reliable skin roughness measurements

Table 2.2 - Summary of the literature review related to 3D stereophotogrammetry

Lee et al., 2016 [(b)]	Systematic literature review comprising 157 articles related to objective burn scar measurement systems or tools	3D SPM devices provide effective objective measurement related to scar roughness and volume.
Plooij et al., 2009	Evaluated the reproducibility and reliability of soft tissue landmarks with 3D SPM images	Soft tissue analysis based on 3D photographs allows accurate and realistic documentation. It is important to use a rigid reference frame to enable individual matching of data
Puviani et al., 2015	Prospective study to evaluate actinic keratosis through 3D SPM system (Antera 3D)	3D image objectively assessed actinic keratosis area and the haemoglobin content via spectral analysis
Skvara et al., 2013	Volumetric analysis of 3D SPM images related to basal cell carcinomas under topical therapy (LifeViz, Quantificare, France).	3D SPM documented skin surface in a micrometre range. The method was validated as an accurate tool in the oncology field
Stekelenburg et al., 2015	Evaluated the reliability and validity of 3D SPM for measuring scar volume. No treatment was performed (LifeViz, Quantificare, France)	To assess the reliability of the camera, the scars were photographed by two observers, who independently performed a volume measurement of the photograph. 3D SPM was validated as a reliable and valid measurement instrument in the research field
Stockton et al., 2015	Evaluated the volume of acute burn wounds in paediatric patients	3D SPM is a valuable outcome measure throughout the scar continuum of care
Tzou et al., 2014	Analysed 3D surface-imaging systems fabricated by five different companies (3dMD, Canfield, Crisalix and Dimensional Imaging Di3D)	3D surface-imaging systems are taking surgeons to a new level of communication with patients, surgical planning and outcome evaluation
Ud-Din et al., 2015	Analysed data from acute wound-healing in healthy volunteers using non-invasive 3D SPM devices (LifeViz, QuantifiCare, France and Eykona, Eykona Technologies, Oxford, United Kingdom)	The study showed the usefulness of 3D SPM in monitoring the process of wound healing, which has been further evidenced by immunohistochemical analysis. This may contribute to the development of prognostic parameters for assessment of response to wound therapy
Van der Loon et al., 2010	Evaluated 3D SPM performance in documenting volumetric changes of the nose in patients with cleft lip or cleft lip and palate after secondary open rhinoplasty (3dMDface System, 3dMD LLC, Atlanta, USA)	3D SPM is a sensitive, quick, non-invasive method for evaluating facial morphology and volumetric changes
Zapletalova et al., 2017	Measured the skin roughness based on 3D scanning of silicone replicas and 3D imaging system.	This study focused on the development of a methodology for objective measurement of skin roughness using 3D scanning
Rijsbergen et al., 2019	Validated the 3D SPM system used in this research (LifeViz) to quantify human papillomavirus-induced lesions	3D SPM is an accurate and precise method for the clinical visualization and quantification of human papillomavirus-induced skin lesions
Miranda et al., 2018	Systematic literature review comprising publications investigating 3D SPM	Emphasised the lack of studies presenting good quality

2.2 Purpose of study

This prospective, qualitative and quantitative study was designed to analyse the accuracy of a 3D SPM system in assessing the therapeutic response in patients with facial wrinkles or scars treated with one session of laser-assisted medication (LAM), using topical vitamin C. The quantitative data delivered by the software linked to the 3D SPM system was compared to a visual analogue scale assessment made by experts, plastic surgeons recognised as experts in the field. The study intended to establish if objective differences relating to the use of LAM could be detected using the 3D SPM system and whether they correlated with the perceptions of the three clinical assessors using photographs derived from 2D and 3D imagery. The objective accuracy of each assessment tool was subjected to statistical analysis and directly compared.

The contactless 3D SPM system (LifeViz^{TM} Micro, QuantifiCare, Valbonne, France) was selected to be used in the pilot study described in Chapter 3 and the comparative clinical studies described in Chapters 4 and 5. The precision of the camera was evaluated for absolute 3D measurements through validation tests that were corrected for systematic bias (Chapter 8, Appendices, document 8.1.3). The experiments were based on a physical phantom manufactured by a metrology institute (National Physical Laboratory, Teddington, UK). Boiled water was injected into the phantom, and volume variations were compared. The camera was reported to reliably evaluate the depth of a paper sheet of 0.1 mm (100 µm). The AD precision was of 0.008 mm (8 µm), and AD error was 0.066 mm (66 µm) for a measurement surface of 178 mm (Skvara et al., 2013).

2.3 Material and methods

This research was approved by the Association Congregation Santa Catarina Casa de Saúde São José (Ethics Committee), Plataforma Brasil, Rio de Janeiro, Brazil (registration number CAAE: 71398617.7.0000.5664), and the FREP at Anglia Ruskin University. The clinical study took place in Rio de Janeiro and complied with the principles of the World Medical Association Declaration of Helsinki (2013). All patients signed a consent form.

A bibliographic review was conducted, encompassing digital libraries (PubMed, Medline, LILACS, SciELO, Elsevier and Wiley Online) which were accessed through an Anglia Ruskin University subscription.

The 3D SPM system (LifeViz^{TM} Micro) was used to photograph and measure the therapeutic response of 26 facial wrinkles and 22 scars located on the face, torso or limbs (total 48 patients). All patients were treated with one session of laser skin resurfacing immediately followed by the surface application of vitamin C. The

photographs were uploaded to the software Dermapix® which converted the photographs into three-dimensional images. The software delivered information on change of skin relief after LAM treatment.

A single, blind, negative control was included to observe the scoring behaviour of the raters and to test the accuracy of the system in quantifying skin microrelief intervention. All two-dimensional and three-dimensional pre and post-procedure photographs were rearranged in a slide presentation that was presented to three experienced plastic surgeons. The area of skin or scar selected for assessment on each patient was highlighted with a black marker in all cases so that the same area could be analysed by both the software and the observers.

The observers assessed the photographs and independently scored skin changes within the selected area using the visual analogue Investigator Global Aesthetic Improvement Scale (IGAIS) (Ko et al., 2017; Dobos et al., 2015; Valet et al., 2009; Levy et al., 2004). The 3D SPM results were compared with those obtained from the observer scoring system (IGAIS).

2.3.1 Subject selection

Consenting participants were recruited between September and November 2017. Patients selected for the study were between 49 and 70 years of age and had requested treatment for facial skin wrinkles. These patients were included in the wrinkle group (R). A separate scar reduction group (DS) consisted of patients between 23 and 70 years of age seeking improvement in appearance and volume of surface scars. Patients with recent treatment (180 days) involving the same cutaneous area and/or presence of pathologies that could impair the skin surface assessment were excluded. Follow-up assessments were at three months for all patients.

2.3.2 Photograph protocol and set of digital images

Before the photographic documentation, the patients were instructed to remove make-up from the area to be treated and apply the topical anaesthetic ointment composed of lidocaine 7% and tetracaine 7%.

The 3D SPM device LifeViz^{TM} Micro consists of a customized camera with enclosed dual flash system and a bifurcated lens beam splitter protected by a solid plastic block. The device was used to obtain pre and post-procedure photographs (three months after the procedure). Each shot captured a pair of two-dimensional pictures from different angles.

Environment conditions emulated daylight luminosity in order to obtain standard photographs. Patients were placed on a printed protractor scale laid on the floor, and the camera was positioned perpendicular to the skin.

As skin topography is unique in every patient, the centre of the picture and anatomical reference points on each patient were individually determined by a laser tape measure (Figure 2.2). Landmark-based, two-dimensional pictures of up to 5.25 cm x 7 cm were obtained so that pre- and post-procedure images could present the same central axis, angle and focus. The digital pictures were transferred to the software Dermapix®.

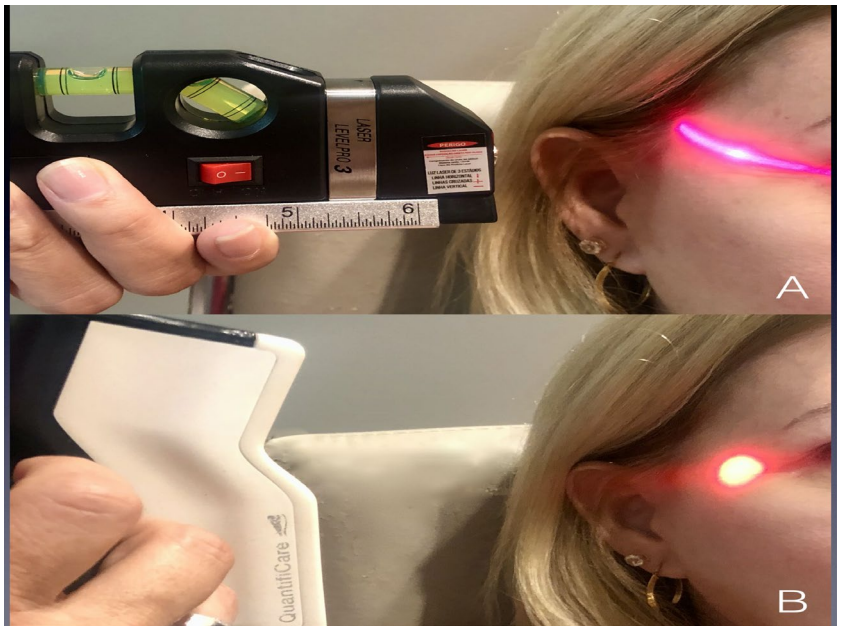

Figure 2.2: A laser tape measure provided landmarks for each photographed area. The camera was provided with two light beams that converged to one spot to ensure standard image acquisition with a focal distance of 20 cm.

2.3.3 Treatment protocol

The treatment consisted of one session of a 2,940nm Er:YAG ablative laser skin resurfacing (Starlux® 500, Palomar Inc., Burlington, MA). The same laser protocol was applied to facial wrinkles (group R) and scars (group DS). A blue optic 6x6 mm handpiece was employed, and the energy output was measured in fluence (Joule/cm^2). The dual pulse mode was used to induce skin contraction. The short pulse, which targets cutaneous ablation was set to 9 mJ/µb, and its duration was pre-set in 250 µs (0.25 ms). The energy of the long pulse, which promotes tissue coagulation was set to 8 mJ/µb with a duration of 5 ms. Four passes were conducted to achieve homogeneous tissue ablation so that the distribution of microspots was similar in all patients. After the laser treatment, 200 mg of vitamin C (ascorbic acid - Vitasantisa®; registered by ANVISA under the number 1.0186.0031.0001-7, Health Ministry, Brazil) was applied to the skin surface and kept under occlusion to be protected from light exposure for 30 minutes. The anatomical

sites being evaluated were clearly documented. Wide or large scars, present on various parts of the body, had their centre and extremities photographed. Patients were followed up three months after the procedure.

2.3.4 Assessment of the outcomes

2.3.4.1 Three-dimensional stereophotogrammetry measurement of skin surface microtopography

The photographs were uploaded to the computer and rearranged in individual files in Dermapix® software. To ensure symmetrical analysis, the pre- and post-procedure images were overlapped to match the same position and angle in a process called synchronisation. Any images that did not present the same angle were discarded.

The areas selected for analysis in group R were assessed pre-treatment as having thin to prominent, visible wrinkles (grade 1– 3 of Fitzpatrick wrinkle Classification) and in group DS comprised patients exhibiting significant surface irregularity with obvious elevations and/or depressions associated with hypertrophic scars.

The drawing tools in the software were used to map out the area to be investigated with reproducible accuracy in both pre- and post-LAM treatment groups. The contour design was adapted to allow for the normal distortion of the skin seen after laser treatment (e.g. skin shrinkage and/or skin tightening).

For three-dimensional reconstruction, the software determined a sampling section of the photographed region called the “closing surface area”. The three-dimensional image was then displayed on the computer screen, and a coefficient called “sigma” was automatically generated. Sigma is the software’s primary feature and is used to analyse the surface characteristics of the skin being investigated and contained inside the enclosed area. In other words, sigma works as a surface reference from which elevations (positive volumes) or depressions (negative volumes) can be detected and quantified numerically. Sigma values vary from 1 to 99, and its value can be constrained according to the goal of the researcher. A smaller sigma number provides an accurately measured value on the variability of the skin surface, whereas a higher sigma value detects more significant surface alterations (Figure 2.3).

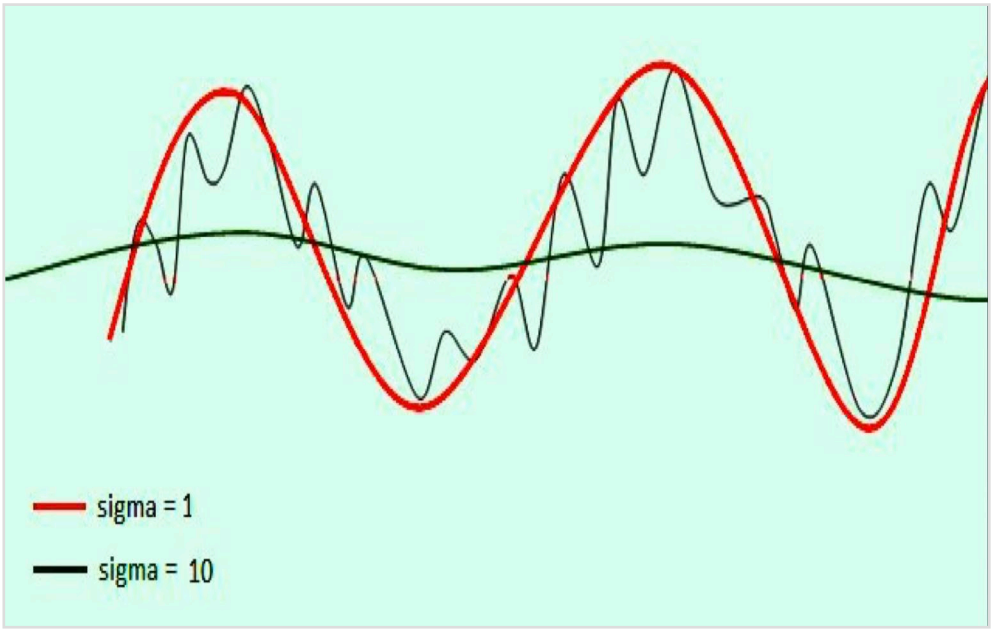

Figure 2.3: Sigma is a reference plane that allows an accurate evaluation and quantification of any skin surface variability. The red line represents sigma 1, and the black line illustrates a sigma 10. The green line represents sigma zero. (Obtained from QuantifiCare's LifeViz^{TM} Micro: A new breakthrough in 3D devices. Printed on 10 June 2009 by QuantifiCare S.A).

The sigma value was set to 10 to analyse all cases. After sigma selection, the same contour design was reproduced using the 3D photographic image, and the integrated software automatically displayed information concerning the volume, roughness, average height and average depth of the selected scar or wrinkle on the right of the computer screen.

The software can provide graphics representing the roughness, heights and depths concerning the topographical relief inside the enclosed area. It is possible to explore some parameters delivered by the 3D SPM system and to contrast them with the results obtained from the clinical observation and based on the scores of the visual analogue scale.

Table 2.3 provides an overview of the publications related to clinical applications of 3D SPM systems and the concepts of some parameters delivered by the related software. As described in Chapter 1 (section 1.3), the configurations of fine grooves and shallow areas result in a cutaneous surface characteristic called roughness, or rugosity (Tchialeva et al., 2010; Ohtsuki et al., 2013; Trojahn et al., 2015). Roughness is specified by the International Organization for Standardization (ISO 3274:'96 and ISO 4287:'97) and is defined as the arithmetical mean of peak-to-valley height skin characteristics (Tchialeva et al., 2010; Ohtsuki et al., 2013; Kottner et al., 2013). The higher the roughness, the greater the skin unevenness.

Table 2.3 - Parameters delivered by 3D SPM - description, calculation and utility

Parameter	Calculation	Utility	Authors
Surface (mm^2)	Surface area is the amount of space covering the outside of a 3D object.	Surface is used by the software to calculate other parameters.	Ghoddousi et al., 2007; Stekelenburg et al., 2015.
Skin roughness (rugosity)	Roughness is equal to the absolute positive volume plus the absolute negative volume divided by the surface.	Roughness depicts the uniformity of the skin surface or detects the lack thereof. It is utilised to analyse the efficacy of skin surface interventions for different cutaneous alterations, such as cutaneous diseases, scars and wrinkles.	Lee et al., 2016 b; Skvara et al., 2013; Tchialeva et al., 2010; Ohtsuki et al., 2013; Manstein et al., 2004; Kottner et al., 2013; Zapletalova et al., 2017; Bloemen et al., 2011; Trojahn et al., 2015.
Volume (mm^3)	Volume is calculated by the multiplication of each dimension: length, width and height (depth) of the designed area containing the deformity.	Useful to control wound healing, to assess cutaneous neoplasias and to calculate the after-treatment reduction of hypertrophic scars or keloids.	Skvara et al., 2013; Stekelenburg et al., 2015; Stockton et al., 2015; Ud-din et al., 2015; Bloemen et al., 2011; Honeybrook et al., 2018.
Average height (mm)	The average height is equal to the positive volume (elevations and peaks) divided by the surface in an area delimited by a designed contour.	It is efficient in quantifying hypertrophic scars and keloids elevation in relation to the reference skin plane (sigma) and the elevation surrounding the wrinkle's depth.	Skvara et al., 2013.
Average depth (mm)	The average depth is equal to the negative volume (depressions) divided by the surface in an area delimited by a designed contour.	It is useful to quantify the depth of wrinkles, nasolabial folds and atrophic scars.	Kohl et al., 2014.

Roughness (Rgh) is equal to the absolute positive volume, plus the absolute negative volume divided by the surface. Although the origin of the measurement is in mm, roughness is unitless.

$$Rgh = \frac{\text{ABSOLUTE POSITIVE VOLUME } (mm^3) + \text{ABSOLUTE NEGATIVE VOLUME } (mm^3)}{\text{SURFACE (area in } mm^2)}$$

The change in skin roughness is linked to the ageing process, scars, skin manipulation, and some pathological conditions. Skin roughness is the parameter most frequently investigated in scientific reports to document any cutaneous elevation or flattening after skin treatments (Table 2.3). Based on these publications, roughness was chosen for assessment in both DS and R groups to detect the post-treatment skin flattening, wrinkle reduction or scar improvement (Skvara et al., 2013; Lee et al., 2016 b; Trojahn et al., 2015).

The perimeter, measured in mm, represents the continuous line forming the boundaries of a closed geometric area, i.e. the analysed area, and is not often used in clinical trials. Volume, an endpoint used to evaluate tumours, and other cutaneous alterations was a useful parameter to evaluate the scar evolution in group DS. Volume is given in mm^3 and represents the total volume of the designed area containing the scar. Negative and

positive volumes are the areas located in a level lower or higher than the closing surface, respectively.

The average height (AH) and the average depth (AD) of a surface are stable parameters that can be selected to investigate specific skin alterations. The average depth of a wrinkle (AD) was one parameter chosen for the pre- and post-LAM procedure (Kohl et al., 2015).

2.3.4.2 Peer review - photographic grading scale

Digital images pre and post- LAM procedure of the 48 patients were arranged into a slide presentation. The presentation was delivered to each of the three experienced raters for an independent clinical evaluation. Based on clear and simple guidelines, they employed the Investigator Global Aesthetic Improvement Scale (IGAIS) to rate the post-procedure skin interference (Table 2.4).

Table 2.4 - IGAIS scale: score and percentage of skin improvement

Score	Skin alteration	Percentage of skin improvement
0	null or minimal change	0-25%
1	mild improvement	25-50%
2	moderate improvement	50-75%
3	significant improvement	>75%

Any pre- and post-treatment alterations in skin roughness, wrinkle depth or volume of scar were scored by the observers based on their interpretation of outcomes shown in 2D photographs and 3D images. Observers recorded the scores in a spreadsheet. They were also requested to estimate a percentage of skin interference based on 3D photographs. Blank spaces were available for additional comments. Finally, they answered two questions: a) Is the scale satisfactory to quantify the volumetric change or the skin relief alteration after the procedure? b) Do the 3D images improve the ability to use the scale to quantify the skin alteration after the procedure?

2.3.5 Statistical methodology

The primary endpoint was the obtention of quantitative data provided by the 3D stereophotogrammetric analysis of skin surface changes, this being compared to IGAIS scores. The secondary endpoint was an evaluation of the consistency using the clinical scale (IGAIS) and the accuracy and specificity of 3D SPM system using standard statistical analyses.

The statistical study comprised a qualitative analysis (based on the ordinal classification provided by the IGAIS) and a quantitative evaluation obtained from (i) the 3D SPM and (ii) the percentage of improvement provided by the observers. Numerical data were distributed according to the central tendency and dispersion measures, and categorical data were expressed by frequency and percentage. Statistical evaluation was performed using SPSS version 24 IBM software (Chicago, USA) and comprised several analyses:

- The first statistical analysis considered the response to the treatment based on the 3D SPM results. The Shapiro-Wilk test and histograms verified that the variables' distribution was not normal. The Wilcoxon signed-rank test was run for inferential analysis and verified the variation between two moments (pre and post-procedure). The criterion to determine significance was a level of 5% (alpha level 0.05 and 95% confidence interval). The hypothesis test was considered statistically significant with a *p*-value < 0.05, and very significant with *p*-values < 0.01.
- As a second analysis, the Mann-Whitney test was employed to assess the data obtained with the 3D SPM system and the percentage of wrinkle/scar improvement provided by the observers. This test evaluated if the difference of percentages of improvement in both study groups was statistically significant.
- The third statistical study consisted of the Spearman correlation coefficient to test quantitative data concerning the correlation between both the estimated percentage of skin improvement provided by the observers and the 3D SPM data.
- The inter-observer agreement to confirm the reliability of IGAIS was assessed by intraclass correlation coefficient (ICC) with a two-way model. The agreement calculation was based on the absence of an interaction effect among the observers and the 3D SPM.
- The Kappa coefficient was processed to evaluate the inter-rater ordinal agreement between both the clinical scale and the 3D SPM related to the total sample. Kappa calculation took into account the IGAIS scores provided by the observers (Landis & Koch, 1977). The original 3D SPM values (continuous variables) were transformed into ordinal variables, based on the same IGAIS interval (Table 2.4). The Spearman correlation coefficient was run to analyse the scores (ordinal data) to ratify the Kappa analysis;
- Bland-Altman graphs analysed the dispersion of the differences in the estimated percentage of modification provided by each observer in relation to the 3D SPM ∂ (delta) reduction against their respective average. The formula for ∂ reduction calculation is described ahead, in item 2.4.2.

2.4 Results

2.4.1 Patients' demographics

Patients in groups R and DS were assessed between days 90 up to the 103 post-procedure (mean 91.9 days ± 4.6 SD). All participants were female. The patients in the scar group (DS) comprised 45.8% of the cases, and the group R constituted 54.2% of the cases. The majority of the subjects presented Fitzpatrick skin type II (34%) and III (39.6%). The mean age of patients in group DS was 43.9 years old ±13.3 (SD). The mean age of participants in group R was 61.8 years old ± 6.1. For the total sample, the mean age was 53.6 years old ± 13.46.

Patients in Group DS had hypertrophic scars on the abdomen (7 patients), on the face (8 patients) and limbs (7 patients). In Group R, the severity of the wrinkles varied from thin (Fitzpatrick grade 1, visible wrinkle and clear indentation less than 1 mm in depth) to prominent, deep furrow appearing to measure more than 3 mm in depth (grade 3 of Fitzpatrick wrinkle Classification).

2.4.2 Statistical analysis

Patients in group R were significantly older ($p < 0.01$ according to Mann-Whitney test) than those in group DS. The median ages were 59 and 43 years old, respectively. An overall positive skin change was observed in 45 patients, which represented 93.8% of the cases. In 2 patients (4.1% of the patients) the scars worsened (negative outcome). One patient was randomly selected to be a blind negative, control (2.1%).

Data provided by the 3D SPM permitted for analysing the variation of the parameters. A positive change was expressed by a reduction of the post-procedure measurement, whereas an increased measurement represented a negative response to the treatment. The variation was also calculated as a percentage of modification (also called ∂ reduction) based on the equation:

$$\text{Percentage of parameter modification } (\partial \text{ reduction}) = \left(\frac{\text{pre} - \text{post-measure}}{\text{pre-measure}} \right) \times 100$$

The calculation of ∂ reduction computed the three-dimensional difference between the pre- and post-procedure skin surface measurements, i.e. skin roughness in both groups, scar volume in group DS and the average depth of the wrinkles in group R. Additionally, the simultaneous computation of the ∂ reduction concerning both parameters measured in each group was performed (∂ reduction of Rgh_R + ∂ reduction of AD_R in group R and the ∂ reduction of Rgh_{DS} + ∂ reduction of V_{DS} in group DS).

The data did not present a normal distribution. The results were analysed according to the median and interquartile range (IQR), i.e. the interval between the first (Q1) and the third quartiles (Q3). Mean and standard deviation (SD) were also calculated. A Wilcoxon rank test analysed the 3D SPM readouts regarding the roughness variation in both study groups. The test confirmed very significant variation (reduction) in roughness measurements in groups R and DS and the total sample ($p < 0.01$) (Figure 2.4).

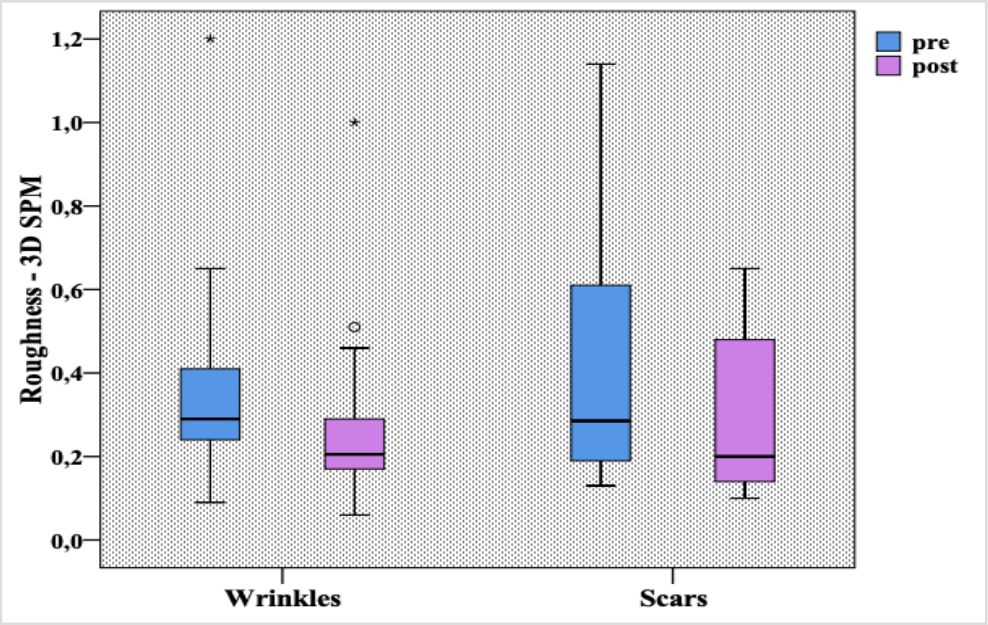

Figure 2.4: Boxplot demonstrating the roughness variation in Group R and Group DS based on the 3D SPM findings. Roughness variation was statistically significant in both study groups ($p < 0.01$). The circle and asterisks represent outliers, values that lie outside most of other values in the set of data concerning the wrinkles roughness.

There was a significant reduction in the average depth measurement in group R ($p < 0.01$) (Table 2.5). In group DS, the scar volume reduced in most patients; however, this variation was not statistically significant ($p = 0.37$). Two patients presented scar volume augmentation, which was detected by the 3D SPM system.

Table 2.5 – Pre- and post-procedure quantitative measurements provided by three-dimensional stereophotogrammetry (Wilcoxon signed-rank test)

Sample	Variable	Moment	Mean	SD	Median	IQR (25^{th} – 75^{th} percentiles)	*p*-value
All cases *n* = 48	Roughness (Rgh)	pre	0.37	0.24	0.29	0.19 – 0.46	< 0.01
		post	0.27	0.19	0.20	0.15 – 0.31	
Group R *n* = 26	Roughness (Rgh_R)	pre	0.34	0.22	0.29	0.24 – 0.42	< 0.01
		post	0.26	0.19	0.21	0.17 – 0.29	
	Av depth (AD_R)	pre	-0.22	-0.17	-0.23	-0.33 – -0.08	< 0.01
		post	-0.14	-0.12	-0.14	-0.19 – -0.03	
Group DS *n* = 22	Roughness (Rgh_{DS})	pre	0.40	0.27	0.29	0.19 – 0.62	< 0.01
		post	0.29	0.19	0.20	0.14 – 0.50	
	Volume (V_{DS})	pre	34.6	76.40	25.00	-6.50 – 70.0	0.37
		post	31.20	62.10	13.10	-3.80 – 76.0	

* SD: Standard Deviation; IQR: Interquartile range (Q1- Q3). Volume was expressed in mm^3 and average depth in mm. Group R= wrinkle group; Group DS = scar group

Table 2.6 exhibits the Mann-Whitney test applied to the median of the estimated percentage of skin improvement provided by each observer and the objective data provided by three-dimensional stereophotogrammetry. According to the test, the observers provided a higher percentage for skin modification in group R compared to scar alteration in group DS. Although this finding may suggest that it is more difficult for the observers to visually detect some restructuration of the impaired skin architecture in scars than to observe an overall improvement of the skin quality during the ageing process, this finding was statistically significant for observers A and C (p = 0.01) only. The 3D SPM data did not detect a statistically significant difference between both study groups.

Table 2.6 - Mann-Whitney test comparing the estimated percentage of skin improvement provided by the observers and 3D SPM system to each group

Variable	Wrinkle Group (*n* = 26)		Scar Group (*n* = 22)		
	Median	IQR (25^{th} – 75^{th} percentiles)	Median	IQR (25^{th} – 75^{th} percentiles)	*p*-value
Observer A % of improvement	90.0	58.8 – 100	67.5	36.3 – 80.0	**0.01**
Observer B % of improvement	60.0	48.8 – 75.8	57.5	25.8 – 71.3	0.28
Observer C % of improvement	80.0	63.8 – 85.0	57.5	35.0 – 80.0	**0.01**
3D SPM - volume ∂ reduction	n/a	n/a	26.2	10.0 – 39.3	n/a
3D SPM - average depth ∂ reduction	33.3	22.1 – 54.0	n/a	n/a	n/a
3D SPM - roughness ∂ reduction	28.4	19.1 – 33.3	28.8	10.8 – 42.7	0.75
3D SPM - highest ∂ reduction	39.8	28.7 – 54.0	40.2	25 – 56.0	0.91
3D SPM - simultaneous analysis of both parameters	62.6	46.1 – 87.5	48.0	33.1 – 74.4	0.10

IQR: interquartile range (Q1- Q3); n/a: not applicable

The percentage of skin improvement provided by the observers was compared to that of the others and to:

- The skin roughness ∂ reduction;
- The highest 3D SPM parameter ∂ reduction;
- The simultaneous analysis of both parameters involved in the skin condition. As mentioned before, for group DS, this comparison resulted from the Rgh_{DS} ∂ reduction and the V_{DS} ∂ reduction. For group R, the comparison consisted of analysing the Rgh_{R} ∂ reduction and the AD_{R} ∂ reduction.

Figure 2.5 illustrates the percentage of skin modification (∂ reduction) in the total sample according to the three observers and the 3D SPM system. The negative values representing worsening of the skin condition were detected by the software but were not adequately reported by the observers.

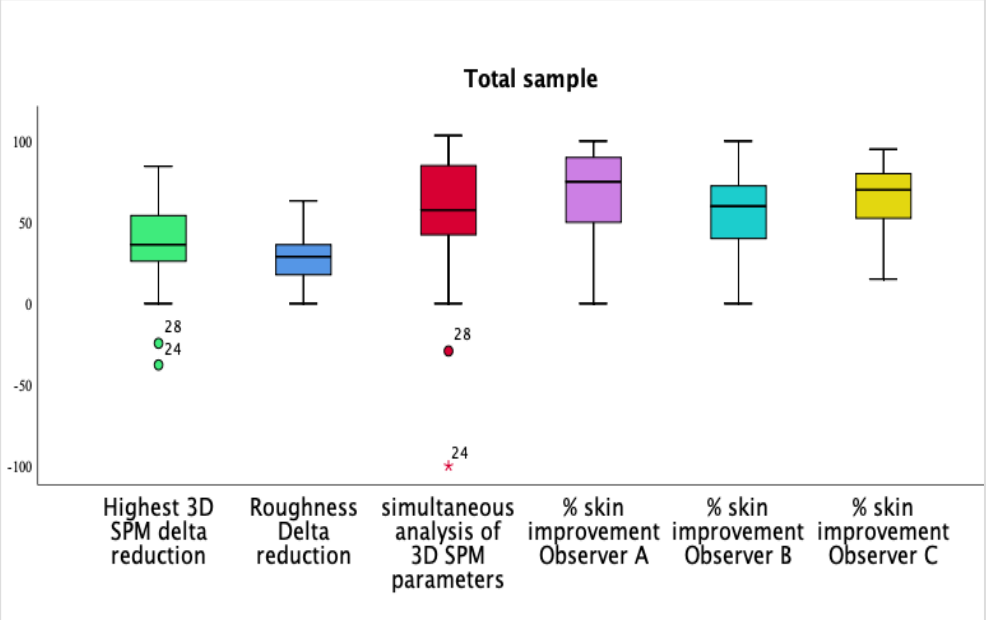

Figure 2.5: Graphic illustrating the percentage of skin modification (∂ reduction) in the total sample according to each observer and the 3D SPM readouts. The circles and asterisk represent clinical cases numbered as 24 and 28 in which scar worsening was verified.

2.4.2.1 Scale consistency

Due to the inherent subjectivity of clinical scales, IGAIS was investigated for internal consistency (homogeneity). ICC < 0.4 means poor agreement, values between 0.4 and 0.75 corresponds to a satisfactory agreement, and an ICC ≥ 0.75 signifies an excellent agreement. The agreement among the three observers was excellent and statistically significant (p < 0.01) and the ICC (two-way model) was higher when the observers evaluated the 3D photographs (Table 2.7).

Table 2.7 - Intraclass correlation coefficient for consistency and the descriptive level (p-value) of skin improvement among the observers

Agreement	ICC	95% CI	*p*-value
2D images (total sample *n* = 48)			
Observer A x Observer B	0.72	0.50 – 0.84	< 0.01
Observer A x Observer C	0.62	0.27 – 0.79	< 0.01
Observer B x Observer C	0.78	0.61 – 0.88	< 0.01
A x B x C	0.79	0.65 – 0.87	< 0.01
3D images (total sample *n* = 48)			
Observer A x Observer B	0.85	0.74 – 0.92	< 0.01
Observer A x Observer C	0.78	-0.52 – 0.89	< 0.01
Observer B x Observer C	0.83	0.60 – 0.92	< 0.01
A x B x C	0.88	0.78 – 0.93	< 0.01

2.4.2.2 Agreement between the observers and the 3D SPM measurements

The ordinal data related to the total sample delivered by the observers using IGAIS scores were correlated to the data delivered by the 3D SPM. The agreement calculations did not use the average of the scores delivered by the observers, because this average would represent the creation of a fourth observer, which could lead to misinterpretation of the data (Bartko & Carpenter, 1976).

The roughness ∂ reduction, the highest 3D SPM parameter ∂ reduction and the simultaneous analysis of both parameters analysed in each group (Rgh_{DS} + V_{DS} ∂ reduction in group DS; Rgh_R + AD_R ∂ reduction in group R) were converted into ordinal data based on IGAIS scale.

The agreement of the ordinal (qualitative) data was calculated by crossing the results delivered by each pair of observers, and each observer versus the 3D SPM system. Spearman's *rho* measured the association of ordinal data between both methods, and the Kappa coefficient measured the inter-rater agreement. Both tests established whether the skin alteration received an equivalent relative ranking (scores) by both methods. The closer Spearman's *rho* or Kappa is to one (1), the stronger is the agreement.

Spearman's *rho* and Kappa coefficient confirmed that the agreement between observer A and the 3D SPM system was high, whether by comparing the scores representing the highest ∂ reduction (*rho* = 1 and Kappa = 1; $p < 0.01$) detected by the software or by

comparing the scores related to the simultaneous computation of both ∂ reduction parameters, according to the study group (*rho* = 0.99 and Kappa 0.97; $p < 0.01$).

Overall, the correlation increased when the observers analysed the 3D images. Table 2.8 displays the results. Most findings were statistically significant. The correlation between each observer and the roughness ∂ reduction was weaker and not statistically significant.

Table 2.8 - Spearman's *rho* correlation coefficient, the Kappa statistics and the descriptive level (*p*-value) based on the ordinal data (scores) *n* = 48 cases

Observers and 3DSPM	Observers' scores on 2D images				Observers' scores on 3D images			
Comparison	**Spearman's *rho***	***p*-value**	**Kappa**	***p*-value**	**Spearman's *rho***	***p* - value**	**Kappa**	***p*-value**
A x B	0.52	< 0.01	0.41	< 0.01	0.75	< 0.01	0.46	< 0.01
A x C	0.54	< 0.01	0.16	0.59	0.67	< 0.01	0.97	< 0.01
A x 3D SPM roughness ∂ reduction	0.19	0.20	0.06	0.13	0.51	< 0.01	0.13	0.03
A x 3D SPM highest ∂ reduction	0.45	< 0.01	0.18	0.03	1.0	< 0.01	1.0	< 0.01
A x 3D SPM simultaneous analysis of both parameters	0.47	< 0.01	0.18	0.35	0.99	< 0.01	0.97	< 0.01
B x C	0.67	< 0.01	0.38	<0.01	0.74	< 0.01	0.49	< 0.01
B x 3D SPM roughness ∂ reduction	0.37	< 0.01	0.10	0.04	0.47	0.01	-0.01	0.82
B x 3D SPM highest ∂ reduction	0.48	< 0.01	0.18	0.03	0.75	< 0.01	0.46	< 0.01
B x 3D SPM simultaneous analysis of both parameters	0.48	< 0.01	0.25	< 0.01	0.79	< 0.01	0.46	< 0.01
C x 3D SPM roughness ∂ reduction	0.61	< 0.01	0.13	0.82	0.52	< 0.01	0.01	0.98
C x 3D SPM highest ∂ reduction	0.70	< 0.01	0.41	< 0.01	0.67	< 0.01	0.36	< 0.01
C x 3D SPM simultaneous analysis of both parameters	0.70	< 0.01	0.43	< 0.01	0.69	< 0.01	0.36	< 0.01

Standard error: asymptotic standard error (Kappa); x = versus

Finally, the Spearman correlation concerning quantitative data was calculated. The percentage provided by the observers, based on the 3D images, was compared between

each observer and also between each observer and the 3D system (Table 2.9). All findings were statistically significant with $p < 0.01$ and the best agreement was between observers A and C (rho = 0.843 and $p < 0.01$). Spearman's *rho* was higher when the simultaneous computation of Rgh_{DS} + V_{DS} ∂ reduction in group DS and Rgh_R + AD_R ∂ reduction in group R were compared to the percentage provided by each observer.

Table 2.9 - Spearman's rho correlation coefficient and the descriptive level (p-value) of skin improvement based on the percentages provided by the observers and 3D SPM

Observer	*rho*	*p*-value
Observer A x observer B	0.754	< 0.01
Observer A x observer C	0.843	< 0.01
Observer A x 3D SPM roughness ∂ reduction	0.493	< 0.01
Observer A x 3D SPM highest ∂ reduction	0.620	< 0.01
Observer A x 3D SPM simultaneous analysis of both parameters	0.652	< 0.01
Observer B x observer C	0.781	<0.01
Observer B x 3D SPM roughness ∂ reduction	0.430	<0.01
Observer B x 3D SPM highest ∂ reduction	0.654	<0.01
Observer B x 3D SPM simultaneous analysis of both parameters	0.682	< 0.01
Observer C x 3D SPM roughness ∂ reduction	0.361	0.002
Observer C x 3D SPM highest ∂ reduction	0.621	< 0.01
Observer C x 3D SPM simultaneous analysis of both parameters	0.699	< 0.01

n = 48 cases

2.4.2.3 Dispersion graphics

Bland-Altman plots were applied to the numerical data to further investigate the agreement reliability between both methods.

Figure 2.6 displays the graphs representing the dispersion of the differences in the estimated percentage of modification provided by each observer in relation to the 3D SPM ∂ reduction readouts against their respective average. Column 1 refers to the highest delta reduction, and column 2 corresponds to the simultaneous computation of the two parameters analysed in each group. Column 3 represents the roughness ∂ reduction. The letters correspond to observers A, B and C. From the amplitude of the agreement intervals, the quality of agreement could be analysed. Relatively wide intervals express weak agreement, whereas narrow intervals confirm good agreement among observers and the 3D SPM system. Additionally, biases can be detected. Despite the moderately wide intervals, Figure 2.6 shows a random distribution of differences over

the mean values, which confirms the absence of systematic behaviour. The few points outside the limits of agreement confirmed the concordance among observers and the 3D SPM system. The agreement was higher among the observers and the highest ∂ reduction (column 1) followed by the simultaneous computation of the two parameters analysed in each group.

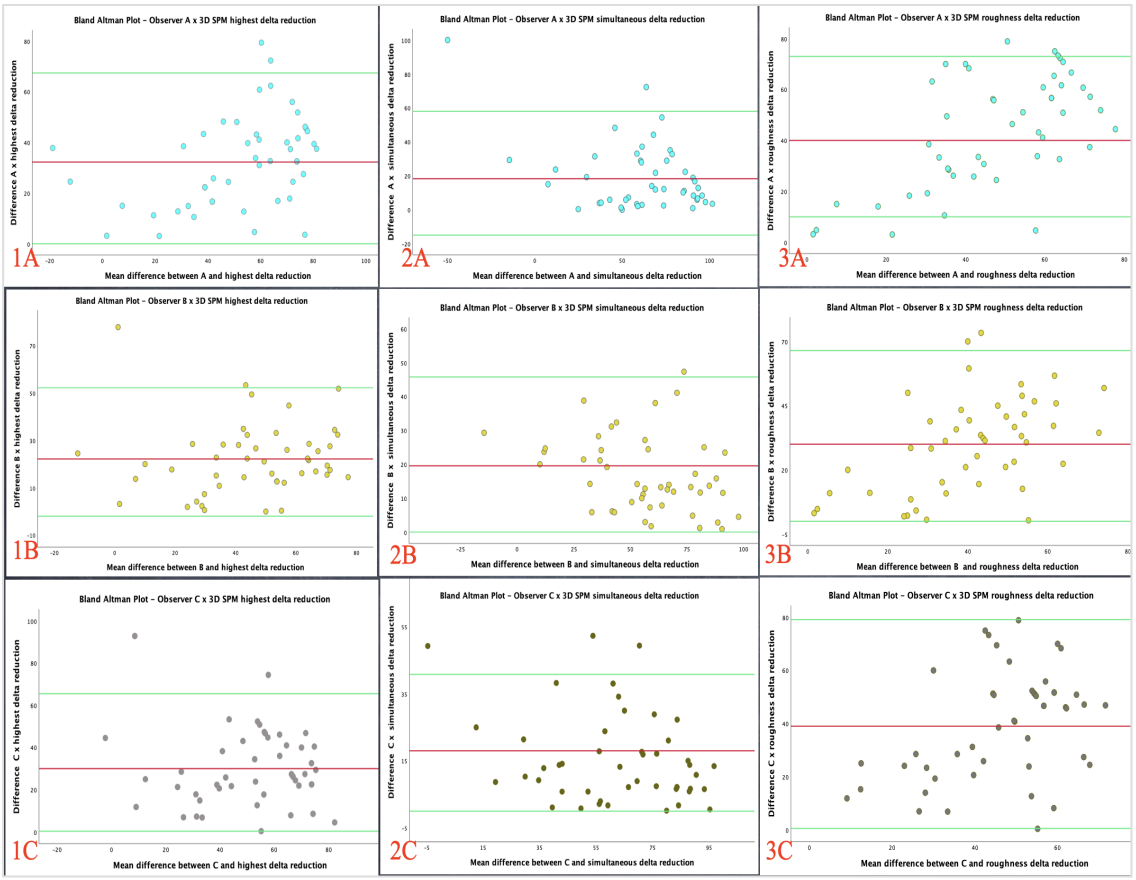

Figure 2.6: Bland-Altman plots representing the differences in the estimated percentage of modification provided by each observer in relation to 3D SPM ∂ reduction readouts against their respective average. Column 1 refers to the highest delta reduction, and column 2 corresponds to the simultaneous computation of the two parameters analysed in each group. Column 3 represents the roughness ∂ reduction. The letters correspond to observers A, B and C.

Figure 2.7 illustrates the relationship between the 3D SPM readouts and the estimated percentage of skin modification provided by the three raters, based on the 3D images. Column 1 refers to the highest ∂ reduction, and column 2 corresponds to the simultaneous computation of the two parameters analysed in each group. Column 3 represents the roughness ∂ reduction. The letters correspond to observers A, B and C. The data dispersion showed a positive agreement between IGAIS and 3D SPM and confirmed that both methods reproduced each other (Figure 2.7 1A-C and 2A-C). Nonetheless, the graphics show more significant data dispersion when roughness ∂ reduction and the percentage of skin improvement provided by the observers are crossed (Figure 2.7 3A-3C), which confirms the weaker agreement between them.

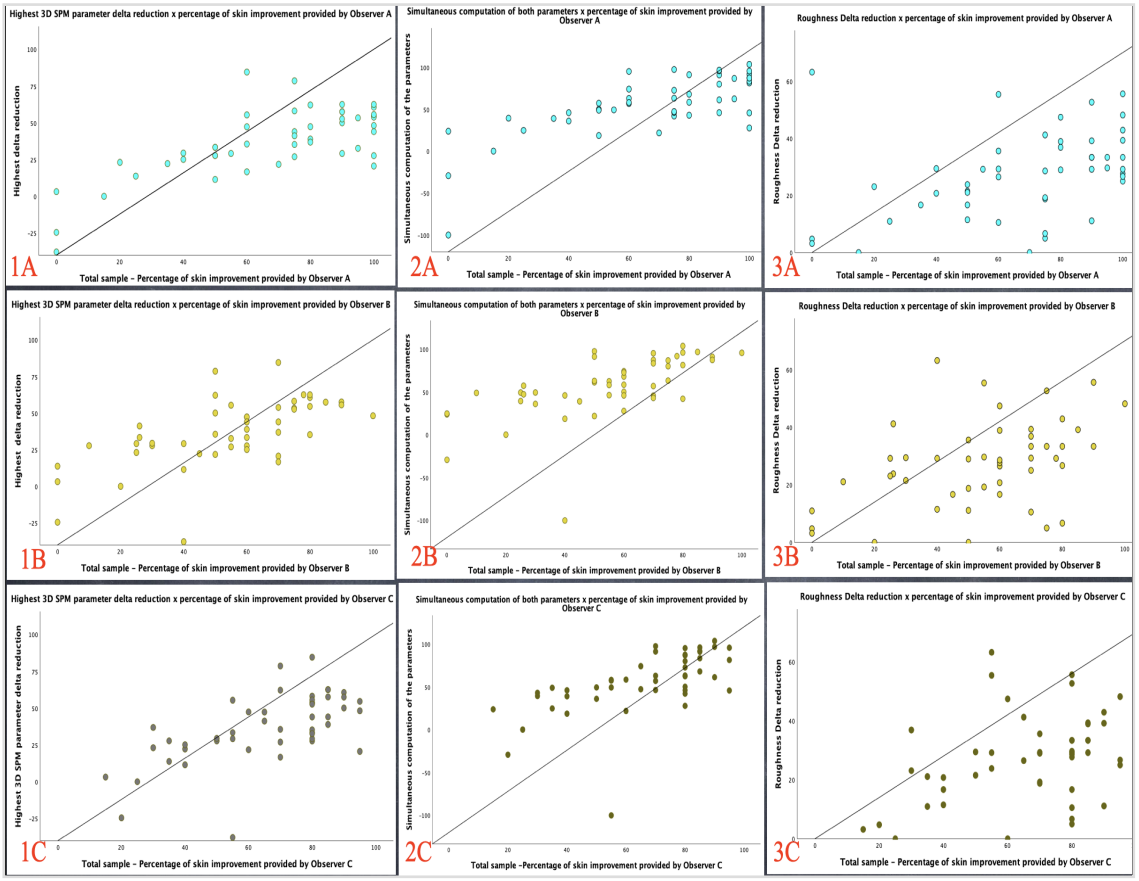

Figure 2.7: Scatterplots illustrating the concordance between data delivered by the 3D SPM software and each observer. Column 1 refers to the highest ∂ reduction, and column 2 corresponds to the simultaneous computation of the two parameters analysed in each group. Column 3 represents the roughness ∂ reduction. The letters correspond to observers A, B and C.

By analysing the scatterplots in Figure 2.7, it is possible to conclude that the observers tended to overestimate the skin improvement. The overrating was confirmed by crossing the data concerning the blind negative control (Figure 2.8). The raters estimated an average of 20% of improvement inside the designed area. In contrast, the 3D SPM confirmed that the roughness remained at 0.46 and that the average depth of the wrinkles remained at -0.01 mm. On the other hand, Figure 2.9 is an example in which the raters could not report worsening of the scar condition with scores. They provided a score of 0 and estimated an improvement of 20%, 0% and 12%. Conversely, 3D SPM detected a volume increase of 24.53% and an augmentation of 4.76% in scar roughness (Rgh_{DS}), which corresponds to the scar worsening.

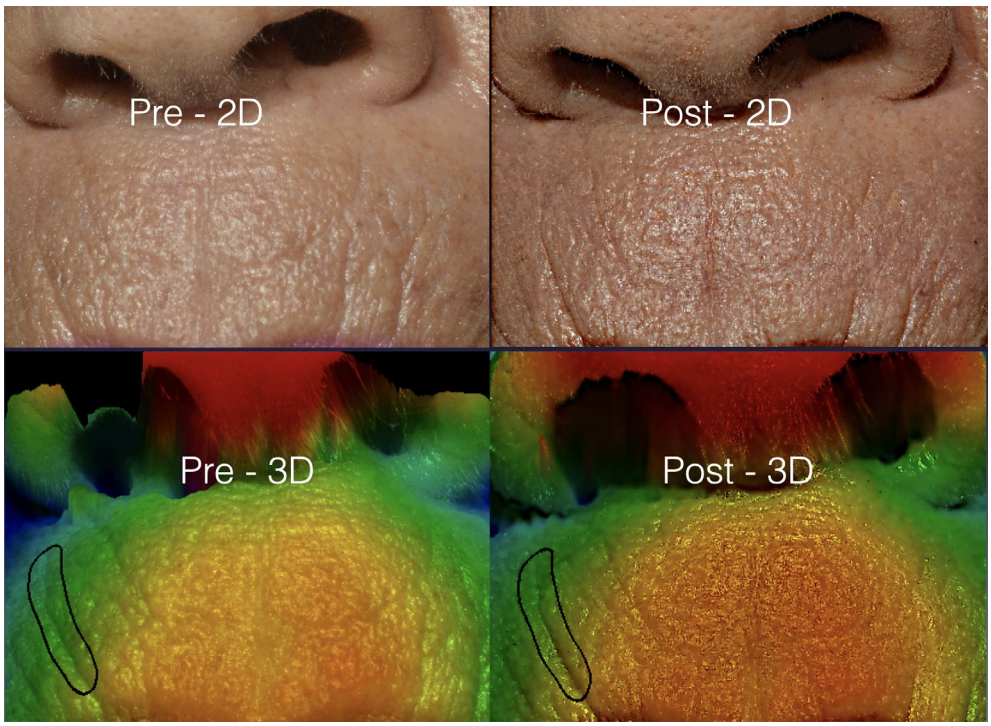

Figure 2.8: (A) A 67-year-old patient with perioral wrinkles. (B) The image on the right represented the post-procedure photograph. This patient was the negative control. The scores given by the observers were 1/0/0. The score given by the stereophotogrammetry was 0.

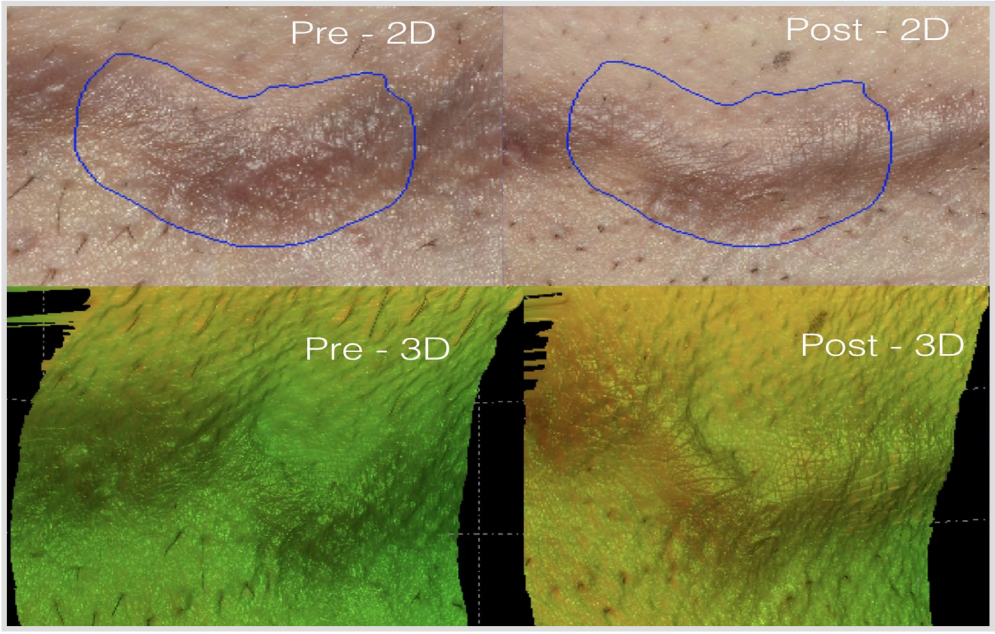

Figure 2.9: A 37-year-old patient with an abdominal scar. The scale did not permit for the raters to provide information on the scar worsening. The stereophotogrammetry detected a scar volume and roughness increase.

Figure 2.10 displays a 67-year-old patient with perioral wrinkles. Regarding the wrinkle's improvement, the raters were unanimous in providing a score of 1, whether by observing 2D or 3D photographs. They estimated skin improvement of 40%. The 3D SPM detected that Rgh decreased from 1.2 to 1 (a reduction by 16.67%) and wrinkle AD decreased

from -0.18 to -0.14 mm (a decrease of 22.22%). The simultaneous computation of both parameters totalled 38.89%, which confirms the agreement between the two methods.

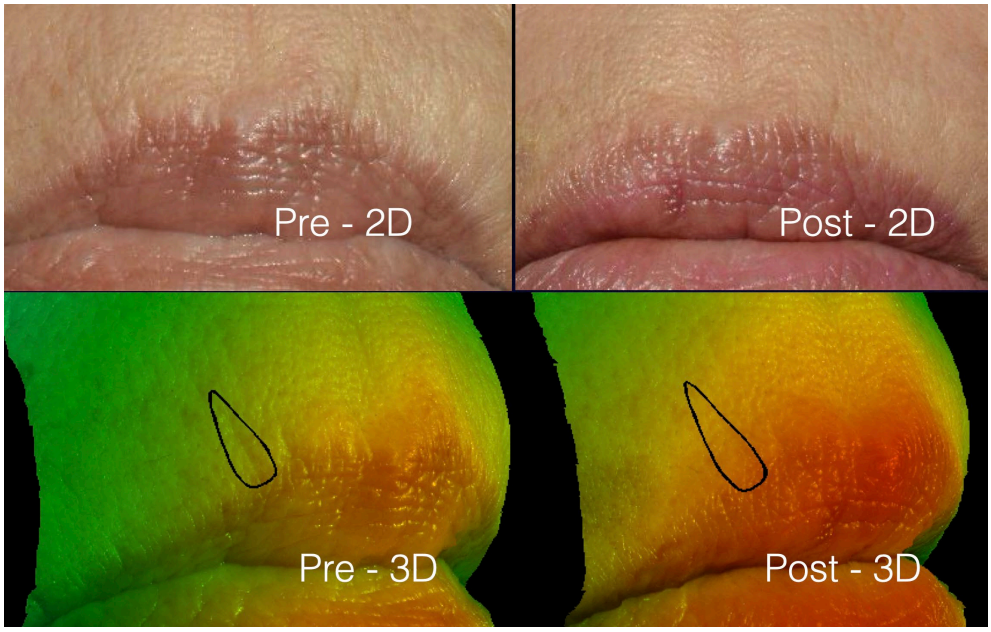

Figure 2.10: A 67-year-old patient with perioral wrinkles. On the left, the pre-treatment images. On the right, the result of the treatment. The black contour specified for the wrinkle to be analysed by the observers and by 3D SPM. The clinical observers estimated the wrinkle improvement by 40%, and the 3D SPM system confirmed that both parameters modified by 38.89%.

An in-depth analysis of the cases involving subtle skin alteration confirmed that observers diverged from each other. However, stereophotogrammetry was precise in measuring the slight changes. Figure 2.11 exemplifies this situation. The raters estimated skin improvement of up to 70% and provided scores that varied from 1 to 3. The 3D SPM software measured Rgh_R reduction from 0.24 to 0.17 (∂ reduction of 29.16%) and AD_R ∂ reduction of 16.67% (from -0.03 to -0.025). This finding demonstrates the difficulty of the observers in judging minor cutaneous interferences based solely on photographs and reinforces the necessity for accurate methods to evaluate skin surface changes.

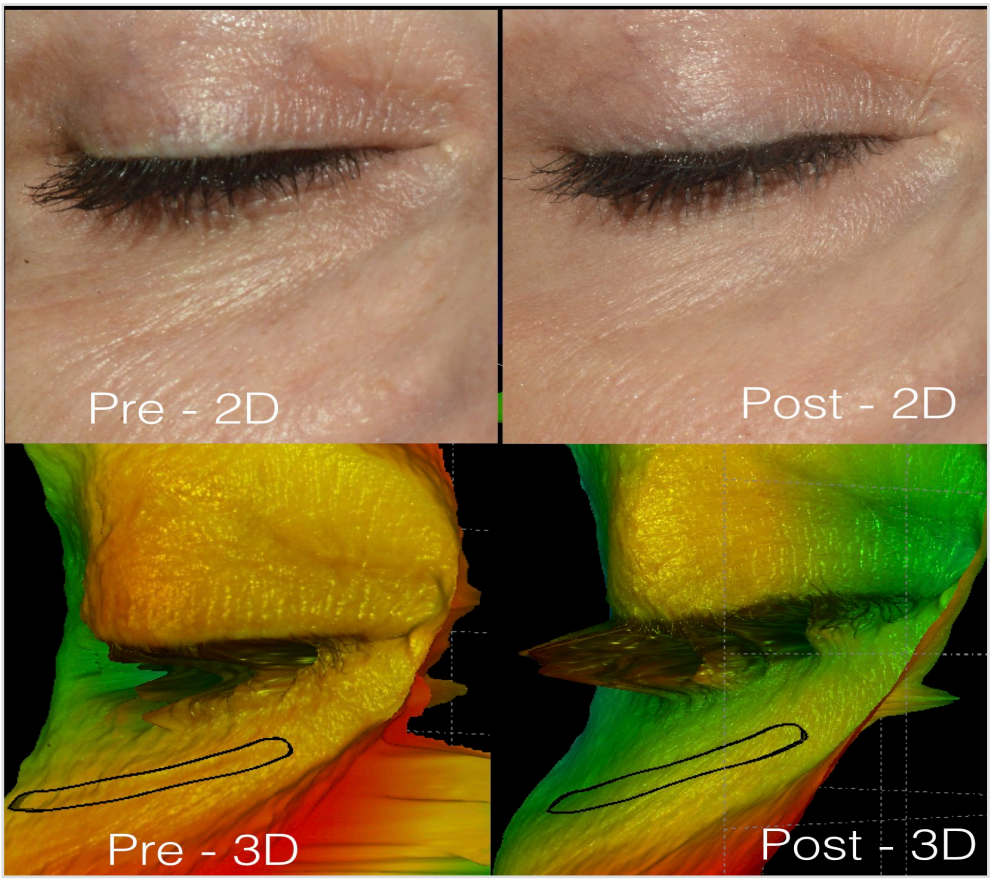

Figure 2.11: A 56-year-old patient complaining of delicate periorbital wrinkles (Fitzpatrick grade 1.5: visible wrinkle and clear indentation less than 1 mm in depth). Pre-procedure images are on the left. On the right, the post-treatment aspect. Roughness reduced from 0.24 to 0.17 post-procedure and the wrinkle average depth reduced from -0.03 pre-procedure to -0.025 mm post-procedure.

2.5 Discussion

Validated instruments designed to measure clinical outcomes for wound healing, scar and facial wrinkling are divided into two categories: either patient-reported or objective measures. The latter can be based on independent, observer-orientated, visual analogue scales or automation systems such as the three-dimensional stereophotogrammetry. Nevertheless, these subcategories are different in their strengths, biases, availability and interpretation (Valet et al., 2009; Levy et al., 2004; Dobos et al., 2015).

The first standardised scale was published by Daniell in 1971 to measure crow's feet wrinkles. Most contemporary, clinical scales such as the Fitzpatrick, Glogau and Carruthers wrinkling scales have been developed to analyse specific facial areas only. Other clinical scales, namely Manchester and Vancouver (VSS), were designed to evaluate scars (Rkein et al., 2014). The Investigator Global Aesthetic Improvement Scale (IGAIS) used in the present study is a scientifically recognised, reliable tool used in clinical trials as an instrument to measure the aesthetic improvement of skin surface post-procedure, regardless of the nature of the intervention (surgical or clinical) and

independent of the anatomical region (Sasaki et al., 2017; Jabbour et al., 2017; Ko et al., 2017). Therefore, evaluating the degree of post-laser alteration with IGAIS worked for both study groups, wrinkles and scars.

In 2015, Dobos et al. performed a systematic review of 111 clinical observation scales. They concluded that there is limited scientific evidence supporting their usage. Important criticism of the scales includes the assessors' innate subjectivity, a bias toward improvement (Qu et al., 2012), and the difficulty in rating minor changes based on photographic imagery (Flynn et al., 2012; Valet et al., 2009; Levy et al., 2004; Rkein et al., 2014). Despite the critics, scales have been useful and the most commonly employed tool to measure the results of clinical investigations in dermatology and plastic surgery.

This is one of the few studies that has used 3D SPM to evaluate the mean difference in the pre and post-treatment outcomes from LAM and correlates this against an assessment of 2D and 3D photographic images by a group of experts based on the IGAIS scores. As part of the methodology of this study, specific and identical areas were marked on the 2D and 3D, pre- and post-procedure patient photographs, and presented to the observers for scoring. The attention of the observers was restricted to the anatomically marked area of visible wrinkles or the cicatricial area with more significant surface alterations. Other areas of facial and corporal topography were ignored because analysing any more extensive areas could distract the experts or impair their accuracy, especially in the presence of subtle alterations (Dobos et al., 2015; Valet et al., 2009; Flynn et al., 2012).

Statistical tests were applied to confirm the consistency of the clinical scale. The high ICC indicated that the judgement of the observers was coherent, although the scores could seem arbitrary. Answering the original question posed by this study, the observers considered that the 3D images, rather than conventional 2D images, improved their capacity to use the scale to quantify post-treatment volumetric changes. This statement was also verified by statistical analysis. The higher ICC found after evaluation of the high-quality 3D photographic images confirmed that the observers experienced greater perception of depth and height of the deformity. The three-dimensional images enhanced the raters' ability to provide a consistent and more accurate assessment of the skin changes. Nonetheless, the observers complained that the clinical scale offered no provision for negative scores. They were unable to express through the scale that the outcome was unfavourable.

Several papers investigating the 3D SPM system have been published to determine the best use of the information provided by this recently developed technology. This study

has explored useful parameters delivered by the software, according to the skin condition. Roughness (Rgh_{DS}) and volume (V_{DS}) were analysed in group DS and roughness (Rgh_R), and the average depth of the analysed wrinkle (AD_R) were the parameters evaluated in group R. These readouts were compared to the report provided by the observers.

Overall, the percentage improvement given by the raters matched the 3D SPM findings. The inter-rater agreement measured by correlation tests (Spearman's *rho*) was higher when the ratings provided by each observer based on 3D images were compared to (i) the highest ∂ reduction or (ii) the simultaneous computation of the two parameters analysed in each group (Rgh_{DS} + V_{DS} ∂ reduction in group DS and Rgh_R + AD_R ∂ reduction in group R). This can be explained by the fact that in several cases (i) the scar volume decreased more significantly than the scar roughness or (ii) the depth of the wrinkle improved more than the skin roughness. This situation was detected and registered by the observers and by V_{DS} ∂ reduction in group DS or AD_R ∂ reduction in group R, while the correlation between the observer and the roughness ∂ reduction became weaker.

When the software readouts were transformed into ordinal data, Spearman correlation and Kappa agreement tests confirmed that the agreement between observer A and the 3D SPM system was high when comparing the observer's score to the score related to the highest ∂ reduction detected by the software (*rho* = 1; Kappa 1.0; $p < 0.01$) or that related to the simultaneous analysis of both parameters (*rho* = 0.99; Kappa 0.97; $p < 0.01$).

The statistical tests confirmed that the human eye perceived meaningful skin surface alteration, which was also detected by the software. However, adverse outcomes and cases involving subtle results were better, if not solely, registered by the software. Divergent results were the negative control and adverse outcomes. Despite the freedom to provide any percentage of skin modification, the observers restricted their evaluation to zero or positive values which reduced the correlation in cases of adverse outcomes because the software could detect and quantify the worsening of the skin condition.

The scores provided by raters for the negative control and the adverse outcomes confirmed that people, whether laypeople or professional, perceive the severity of the deformities differently. As in this study, the tendency of observers to overrate the skin alteration was verified by Kohl et al. (2015). In their report, they compared three-dimensional photographs to the clinical observation using a 5-point satisfaction scale to rate skin pigmentation and wrinkle improvement after a CO_2 laser treatment.

Including a negative control, blinded to the observers, created a standard score for no improvement and reduced the source of bias. The negative control was blinded to the 3D SPM system and the observers. If the observers had been warned about the non-treated patient, they could have been unduly influenced and downrate any skin alterations. The resultant scoring would reinforce the efficiency of 3D SPM and reduce the accuracy of the observers, thus causing a critical bias.

The camera and the 3D software have minor limitations (Table 2.10) including delay with uploading multiple pictures to the computer at the same time.

Table 2.10 - Advantages and disadvantages of the 3D SPM system

Advantages	Disadvantages
Compact and portable camera	High cost
Equipment easily stored	Need for calibration and prevention from shock hazard
Supportive team to instruct about the camera and software	Learning curve to optimise the handling of the camera and software analysis
Accurate 3D graphic representation	Hair strands and dark holes cause 3D image distortion
Close up images of smaller areas permit for a thorough examination of skin surface	Analysed area is restricted to around 50 X 70 cm
Direct data exportation to spreadsheet	Software does not work in IOS systems
High-quality image (12.3 megapixels). Fast image acquisition time. Optics accurate up to 8 µm.	Need to set a template that guides the obtention of a post-procedure photograph at exactly the same position to enable pre- and post- procedure subject comparison

The software is unable to interpret data without error for deep or dark holes (e.g. nostrils) or with any 3D distortion such as is seen when imaging skin containing hair strands (Figure 2.12).

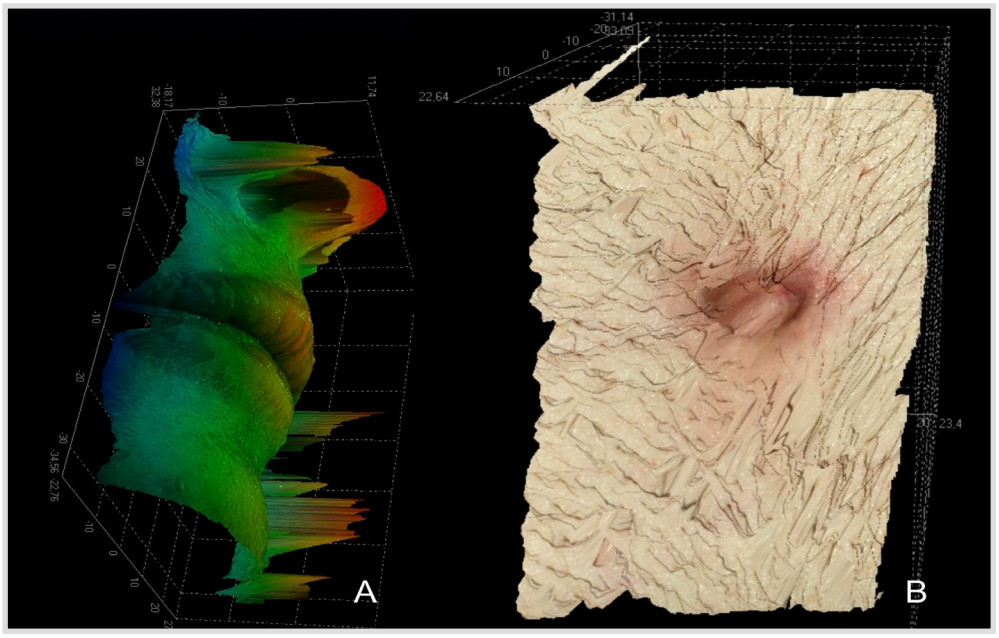

Figure 2.12: The 3D reconstruction of the pictures can present distortion of the image in areas containing anatomical elements such as nostrils (A) and hair strands (B).

The biggest challenge and the main limitation of this study were to ensure consistency in identifying the central axis of the area of skin or scar being photographed and to optimise the use of the information collected from the images.

The incident angle of the camera image to the skin had to be consistent to ensure a precise overlap between pre- and post-treatment photographs (Lee et al. 2016; Plooij et al., 2009). Training and practice were needed to establish the proper angles, and to optimise the use of the information obtained from the images.

As any error involving the 3D reconstruction process and skin marking could cause loss of matched and meaningful data (Plooij et al., 2009), the camera was operated by the researcher only to ensure that the photographic protocol was followed. There was no need to test the inter-operator reliability, and neither was it required to establish the coefficient of variation in the use of the equipment.

Despite the perfect agreement between the scores provided by observer A and the 3D SPM system, the use of this four-point visual analogue scale might have reduced the statistical agreement between the ordinal data provided by both methods because of the broad range (25% skin alteration) between each score. While no five-point scale was found to match the needs of this particular research, IGAIS made it possible to provide scores for wrinkle and scars improvement based on the same scores, which facilitated the observers' rating.

In concordance with other authors, this study has confirmed that computerised software processing of data created by this 3D SPM system, has brought consistent, precise and meaningful information (Kohl et al., 2014; Skvara et al., 2013; Stockton et al., 2015). The software objectively analysed treatment-related morphologic changes and enabled a comparison of outcomes for the subjects. As part of the methodology, roughness proved adequate to analyse skin surface related to wrinkles and scars. Volume was appropriate to quantify scar improvement. The average depth was suitable for wrinkle analysis.

The layers of the SC are usually around 10–15 μm thin, whereas in a hydrated state the corneocytes absorb water and the thickness of the SC can increase up to 40 μm (Pio & Maibach, 2019). In the present study, the anaesthetic ointment was applied for thirty minutes and removed 10 minutes before the treatment so that skin could recover its texture. As skin hydration can reduce pre-treatment roughness readouts, the topical anaesthetic ointment was applied only after photographic documentation in the next phases of the research.

2.6 Conclusion

It is hard to achieve an ideal mathematical model to analyse outcomes of skin surface modification. This is the first research that correlates the performance of the Investigator Global Aesthetic Improvement Scale (IGAIS) with a three-dimensional imaging system to investigate the changes in skin microtopography after laser-assisted, topical vitamin C medication. The former method involves input from clinical specialists, and the latter is an objective method of computing skin alterations.

This study confirmed the importance of providing numerical data that correlate to the visual perception of skin relief alterations. Three-dimensional stereophotogrammetry delivered accurate information by objectively measuring geometric and volumetric changes in response to surface skin treatment.

Bland-Altman plots, dispersion graphics and statistical tests confirmed the capability of the three-dimensional information to report surface demotions such as roughness, the average depth when evaluating wrinkles and the elevations when evaluating scars. The agreement between the observers and 3D SPM system was higher when comparing the 3D images and by comparing scores (ordinal data) rather than percentages (quantitative data).

The 3D system was consistent as an analytical tool, even in the presence of minimal change. The reliability of the stereophotogrammetry was also confirmed by the blind

negative control. The non-treated patient misguided the raters, while the numerical data provided by stereophotogrammetry were consistent with the absence of intervention.

Skin pigmentation, wrinkle depth or scar characteristics did not affect the capability of the observers and the software in providing readouts about the skin surface. If researchers opt to use clinical scales, the observers should be blinded and independent to reduce the potential for bias. In contrast, stereophotogrammetry can eliminate any trend towards favourable or inconsistent analysis by the observers.

Chapter 3

Assessing Morphological Change in Scar and Wrinkle Surface Using 3D Stereophotogrammetry Imaging After Surface Laser Treatment and Application of Vitamin C

3.1 Introduction

Three-dimensional stereophotogrammetry (3D SPM) and laser-assisted medication (LAM) are novel areas for research. The main criticisms of previously published research on these subjects are directed at a lack of statistical power or clinical significance in findings, small sample population and/or inconsistent methodology (Miranda et al., 2018; Haedersdal et al., 2016). Furthermore, some papers that involve human subjects are not actually related to a targeted treatment regime (Haak et al., 2012; Haedersdal et al., 2016).

In evidence-based medicine, the sample size calculation defines the number of subjects required to statistically answer the research question and provide an accurate interpretation of results. The sample size is calculated using a mathematical formula that, by convention, establishes an alpha error of 0.05 and a power of 0.80 (Noordzij et al., 2010). This calculation relies on the population variance of a given outcome variable and is estimated through the standard deviation (SD). In general, the greater the standard deviation, the larger the sample size. Because the variance is usually an unknown quantity, investigators often use information from previously published data or the estimates obtained from a pilot study (Noordzij et al., 2010).

This chapter describes the feasibility study, which was designed to assess the practicality of the research proposed by this thesis. The goal was to (i) objectively and rationally uncover the strengths and weaknesses of the study project, (ii) confirm the variables to be evaluated as part of the methodology, (iii) calculate the population required, and ultimately (iv) the prospects for success. It also anticipated project completion in terms of a timeline, and the regulatory and ethical challenges.

As a secondary outcome, this study calculates the sample size that is required to achieve clinical significance in further, prospective, comparative clinical trials involving LAM treatment of wrinkles (Chapter 4) and scars (Chapter 5). LAM treatment in this preliminary study involved a single application of a fractional ablative Er:YAG laser to selected areas of wrinkled face skin or obvious areas of scar hypertrophy, followed immediately by the topical application of vitamin C to the treated area. Response to LAM treatment was investigated using the 3D photometric assessment tool previously described, in Chapter 2.

3.2 Material and methods

The protocol for one session of laser-assisted medication (LAM) followed by topical application of vitamin C has been described in Chapter 2 (section 2.3.3). Response to treatment was assessed using digital camera images and appropriate software for data

analysis (LifeViz™ Micro) on photographed patients before and three months after LAM treatment. This pilot study was approved by the Brazilian Ethics Committee and was registered on the website Plataforma Brasil under the number CAAE:71398617.7.0000.5664 (Association Congregation Santa Catarina Casa de Saúde São José). The study was also approved by the FREP at Anglia Ruskin University and followed the principles of the World Medical Association Declaration of Helsinki (2013).

3.2.1 Patients' demographics

Patients requesting periorbital skin rejuvenation or scar improvement were eligible for inclusion in the study. The patients were allocated to two study groups, labelled group R and group DS:

- Group R: Patients aged between 40 and 70 years, seeking treatment for facial wrinkle with Fitzpatrick skin type I to IV;
- Group DS: Patients aged between 18 and 70 years, seeking scar improvement, regardless of the scar origin (accidents or surgeries). Scars must have been present for two or more months, and their width had to fit the measuring frame of the camera, regardless of their length.

The following patients were excluded:

- patients who were not available for the follow-up visits.
- patients with unrealistic expectations;
- patients taking any other drug known to interfere with the healing processes;
- patients subjected to dermabrasion or chemical peeling up to 6 months in the area to be treated within 6 months before the study;
- patients with a history of recent cutaneous allergies, chronic dermatitis or other cutaneous pathology.

The recruitment of participants took place between September and November 2017. In total, 95 patients met the inclusion criteria and were included in this study. Participants were fully informed about the study and given a comprehensive information sheet prior to consent being given in writing to participate in the research. Thirty-nine patients spontaneously seeking improvement in the appearance of facial wrinkles were included in group R, and 56 patients seeking scar improvement were included in group DS. Enrolled patients were screened and treated. Follow-up visits occurred between 6 December 2017 and 1 February 2018.

3.2.2 Study design

The 3D digital camera (LifeViz^{TM} Micro) was used to photograph patients before and three months after the laser skin resurfacing followed immediately by the topical application of vitamin C.

Landmarks and laser tape measurements were used to standardise the area of treatments under investigation. For group R, a landmark-based photograph for both sides of the periorbital region was designed. It consisted of a vertical line directed from the eyebrow tail down towards the jaw with a perpendicular line leading from the eyebrow tail and directed towards the temporal hairline. A horizontal line parting from the ipsilateral nostril to the tragus defined the area of the face under investigation. Since scars are unique in every patient and occurred at different anatomical sites, landmarks were determined individually in group DS. A laser tape measure was used to establish relevant landmarks and measure the width and margins of the scars.

3.2.2.1 Procedure

After 3D SPM documentation, an anaesthetic ointment composed of lidocaine 7% and tetracaine 7% was applied to the targeted area for 30 minutes. Immediately before the procedure, 20 mg of oral prednisolone and 10 mg of ketorolac tromethamine were given to the patients. The eyes were protected with moist gauze and laser protection glasses.

The patients were subjected to one session of class II 2.940nm fractional Er:YAG laser treatment (Starlux® 500 Palomar Inc., Burlington, USA). The laser was employed to cause a controlled, superficial disruption to the epidermal skin barrier, enabling direct intradermal delivery of topical vitamin C.

Standardised laser parameters were used on all patients in both groups, regardless of the depth of the rhytids or elevation of the scar. A blue optics handpiece (6x6 mm) and a speed of up to 3 Hz were used to perform the resurfacing. The laser protocol was presented in Chapter 2 (section 2.3.3) and is summarised in Table 3.1. The energy of the long pulse promotes tissue coagulation and, ultimately, tissue contraction whereas the short pulse instigates tissue ablation (Mattos et al., 2009). Four passes were accomplished to achieve homogeneous tissue ablation. No intentional laser overlapping was performed. The laser treatment was applied to the areas containing the scars in group DS. In group R, each patient received a full-face treatment.

Table 3.1 - Fractional Er:YAG laser parameters' protocol used in this research

Handpiece / Optics	Energy short pulse (250 µs or 0.25 ms)***	Energy Long Pulse (5 ms)	Density of microbeams (µb/cm²)	Number of passes	Microbeam size
2940 nm, Blue optic 6x6 mm	9 mJ*/µb**	8 mJ/µb	469	4	120-140 µm

*mJ = milijoules (1 mJ =0.001 Watt-sec); ** µb = microbeams (structure of optical spots through which light radiation is emitted); *** ms = miliseconds; µs = microseconds

Although laser application was well-tolerated, all patients classified the pain level as intense, especially in the perioral and periorbital zones. After laser application, small scattered bleeding spots were noticed (Figure 3.1). Patients initially described a burning sensation that became less intense after the topical application of 200mg of vitamin C (Vitasantisa® registered by ANVISA under the number 1.0186.0031.0001-7 Health Ministry - Brazil). The vitamin C skin occlusion was kept on the lasered skin surface for 30 minutes. The occlusion was supposed to protect the vitamin C from photodegradation.

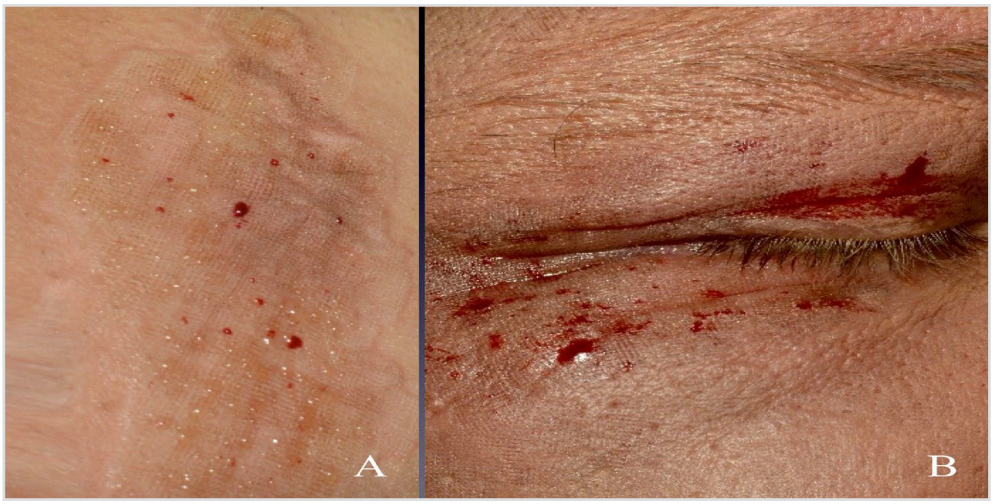

Figure 3.1: After laser treatment, swelling, exudation and bleeding spots were observed on the cicatricial area (A) and the periorbital region (B).

3.2.2.2 Post-treatment regime

Patients were discharged and instructed to clean the treated area with a saline solution once a day and to avoid the use of cosmetics until the third month to avoid interference with intrinsic cutaneous hydration. They were advised to apply topical dexpanthenol (Bepantol® - Bayer) to cover the treated area four times a day until the cutaneous debris had entirely disappeared. Dexpanthenol has the function of reducing transepidermal water loss, which is important during the phase of skin recovery. Patients were monitored for adverse events up to one week after the treatment. For patients in group R, fexofenadine was prescribed for five days, and 10 mg of ketorolac tromethamine was administered every eight hours in case of pain. Anti-viral prophylaxis against herpes

simplex using valaciclovir was prescribed for up to seven days after treatment in twelve patients with a previous history of herpes infection.

3.2.2.3 Photographic records

Three months after the treatment, digital photographs were taken based on the pre-procedure landmarks. The photos were transferred to the software Dermapix®, described in Chapter 2 (section 2.3.4.1). Synchronisation between pre and post-procedure images, using the software, was performed by establishing landmarks on these images so that the same area could be compared. An area comprising the scar (Figure 3.2) or periorbital wrinkles (Figure 3.3) was highlighted so that *in vivo* quantitative measurements of skin topography could be achieved, and a 3D reproduction of the skin surface was constructed (Figure 3.4).

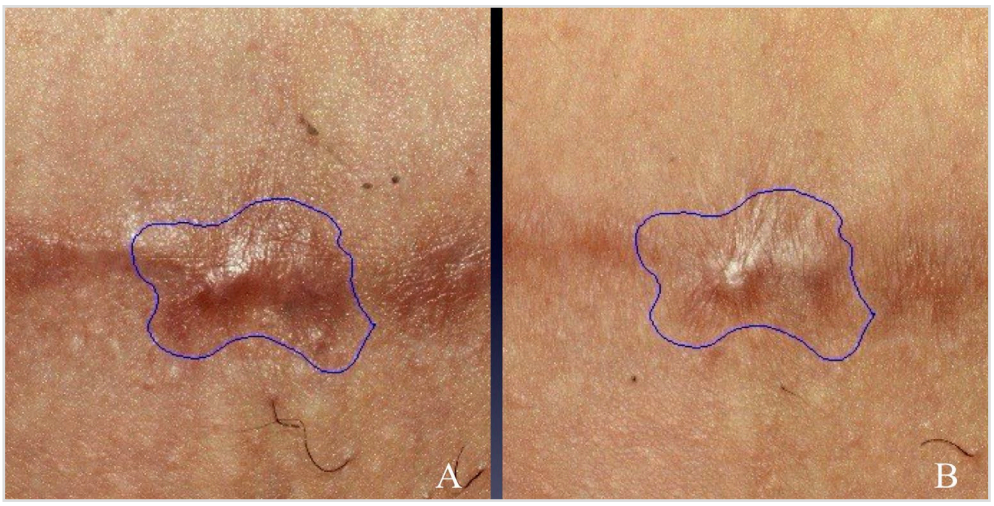

Figure 3.2: Pre (A) and post-procedure (B) photographs were synchronised. The contour (in blue) encompassing the central and elevated area of an abdominal scar was designed in the pre-procedure photograph and then replicated to the post-procedure image.

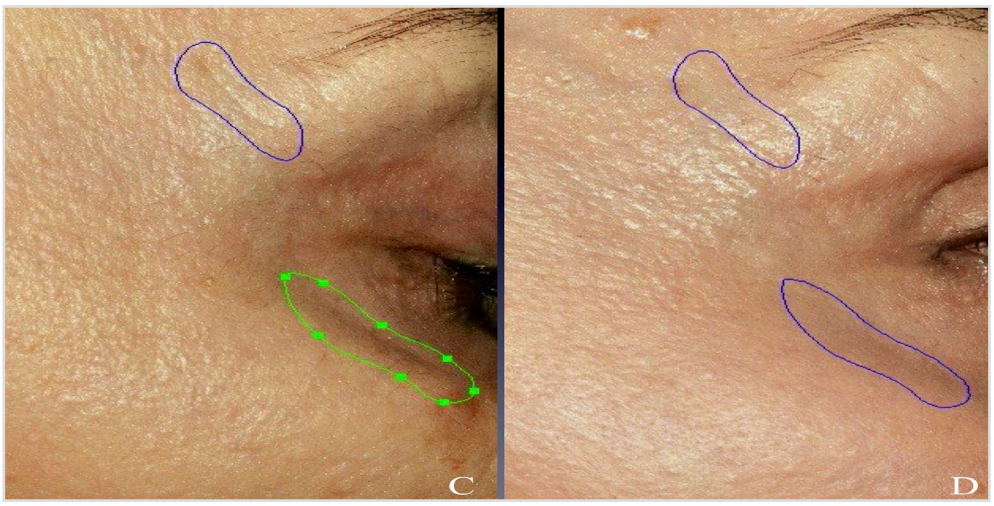

Figure 3.3: (A) The pre-procedure photograph with a design contour (in blue) including a periorbital wrinkle. The green contour is an example of the area that the investigator includes, which is then saved and re-drawn to the post-laser photograph (B) in exactly the same area of anatomy. The software can analyse the area or volume within each contour.

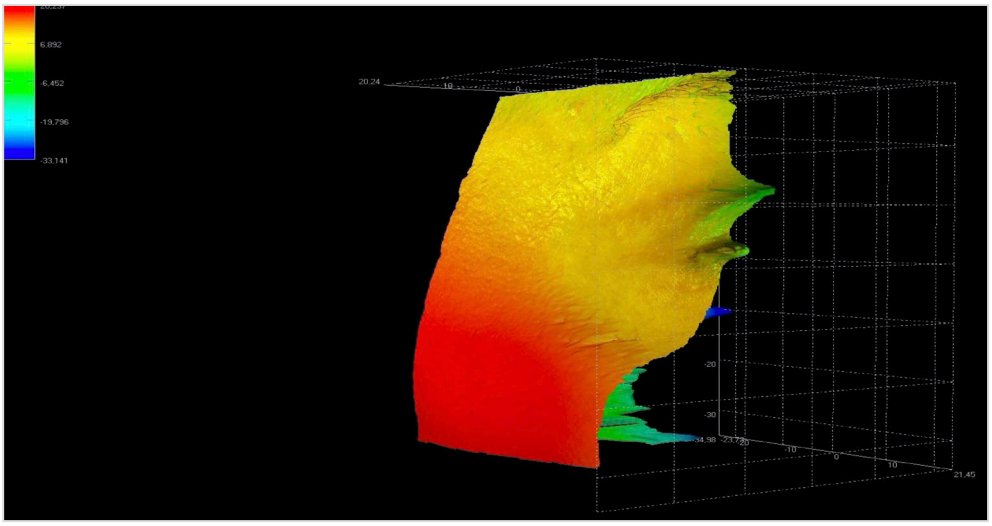

Figure 3.4: Three-dimensional reconstruction of the periorbital area by Dermapix® software. The software allows image rotation so that the area can be viewed from different angles.

3.2.2.4 Data generation

When the designed contour was transposed to the 3D photo, the reference, sigma, was automatically displayed. Sigma has been described in Chapter 2, section 2.3.4.1 (Figure 3.5).

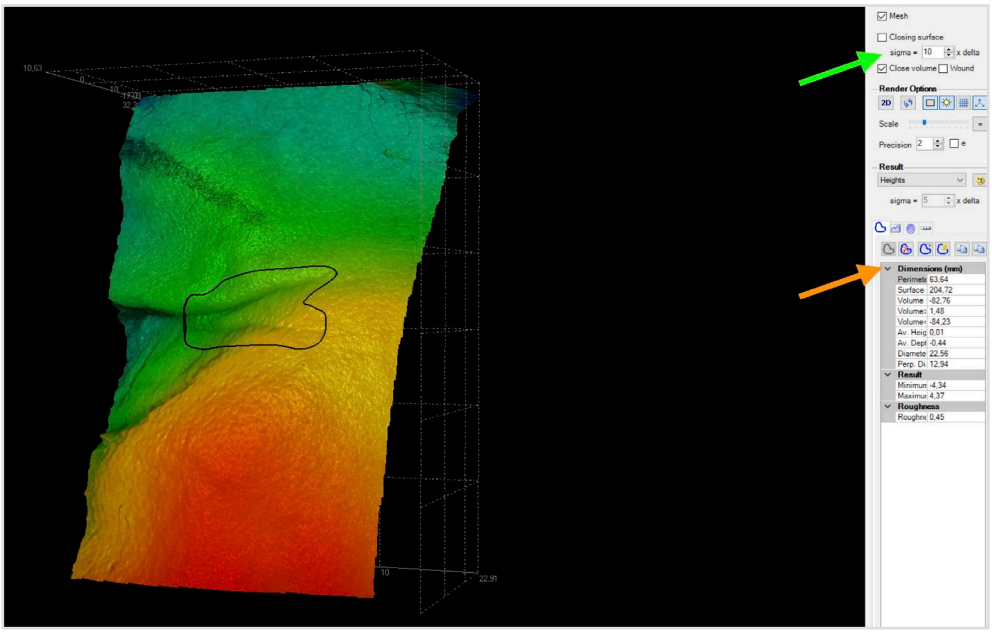

Figure 3.5: Three-dimensional representation of a periorbital area. On the right, the data (parameters) provided by the software (orange arrow). The green arrow shows the blank space to select the sigma value.

After constraining the sigma value to 10 in all patients, a pop-up window was accessed, and the software automatically calculated the surface alteration inside the drawn contour. Measurements related to scar volume, skin/scar roughness, and wrinkle/scar average height and depth, were displayed on the right of the computer screen. The software can also measure the width of selected wrinkles or scars.

3.2.3 Statistical analysis

Data obtained via the Dermapix® software were analysed by the program SPSS IBM (Version 24.0 IBM Corp© for Mac, Armonk, New York, USA). Tests were applied to compare and correlate pre- and post-procedure skin roughness, skin average height, scar volume and wrinkle average depth measurements. The software Stata (Version 13 StataCorp LP, College Station, Texas, USA) was used for the sample size calculation (power analysis for a two-sample, paired-means test).

Medians, means, standard deviations, and histograms linked to each parameter were established. The numerical variables under study did not present as a normal distribution, according to the Shapiro-Wilk test of normality at the level of 5%. Data were summarised by quartiles. The interquartile range (IQR or Q1 - Q3) is a measure of dispersion that contains 50% of the observations between the limits between the 1st quartile (Q1 or 25th percentile) and the 3rd quartile (Q3 or 75th percentile).

The non-parametric Wilcoxon signed-rank test (with a corresponding 95% prediction interval and alpha error set to 0.05) evaluated the difference between the pre- and post-procedure data to measure the parameter variability. Findings were considered statistically significant with *p*-values < 0.05 and very significant with *p*-values < 0.01. Additionally, Spearman's *rho* was used for correlation between each pair of the analysed parameters in each study group.

3.3 Results and discussion

After scrutiny and evaluation of the data obtained through the 3D imaging system, three variables, *i.e*. three parameters related to cutaneous alteration, were analysed in each study group (Table 3.2).

Table 3.2 - The selected parameters by groups and their abbreviations

Study group	Parameter	Abbreviation
Group DS	Average height of the scar (mm)	AH_{DS}
	Roughness	Rgh_{DS}
	Volume (mm^3)	V_{DS}
Group R	Average height of the skin surrounding the wrinkle (mm)	AH_R
	Roughness	Rgh_R
	Average depth of the wrinkle (mm)	AD_R

In both study groups, the skin roughness, and the average height were evaluated (Tchialeva et al., 2010). The average height of the skin surrounding the wrinkle was abbreviated as AH_R, while the average height of the scars was referred to as AH_{DS}. In group R, the objective was to obtain a more uniform skin relief by reducing the wrinkle depth; hence the selected wrinkles were analysed based on their average depth (AD_R). Volume variation, an endpoint used frequently in clinical studies, was selected to evaluate scars in group DS (Hermans et al., 2014; Skvara et al., 2013; Stockton et al., 2015).

3.3.1 Group R

Of the 39 patients enrolled in group R, only twenty were adequately followed up, and a total of 59 different periorbital wrinkles were analysed. Nineteen patients were females and the age range of patients included was 48 to 70 years old (mean 59.75 ± 6.47).

Crusting duration was around five days. Considerable periorbital swelling was revealed in all but one patient. However, obvious oedema usually spontaneously subsided on the third post-procedure day.

In all patients, some degree of erythema was observed on the seventh day post-procedure and disappeared within 18 days. One patient experienced an acneiform eruption after excessive use of dexpanthenol ointment. Complications such as post-procedure hypochromia and herpes eruption were not seen.

Most wrinkles became less perceptible post-procedure. Clinically, an overall skin texture improvement associated with a decrease of pigmentary changes, particularly of the solar lentigines, was observed. However, the melanin variation was not measured in this study.

Around 74.5% of the periorbital wrinkles presented a decline in the skin roughness. Pre-procedure, the Rgh_R the median was 0.3 mm (IQR 0.21 – 0.45 mm) compared to median 0.24 mm post-procedure (IQR 0.16 – 0.38 mm).

A 62.7% decrease in the AD_R was observed. The median of AD_R was -0.19 mm (IQR -0.35 – -0.10mm) pre-procedure, whereas the post-procedure measurements showed a median of -0.12 mm and IQR of -0.24 – -0.04 mm (Table 3.3).

Finally, 55.93 % of the wrinkles exhibited average height reduction in the area surrounding their profundity.

Figure 3.6 shows an example of wrinkle alteration. The AD_R inside the contour decreased from -0.12mm to -0.08mm (AD_R ∂ reduction by 33.3%). Rgh_R decreased from 0.16 to 0.14 (Rgh_R ∂ reduction of 12.5%).

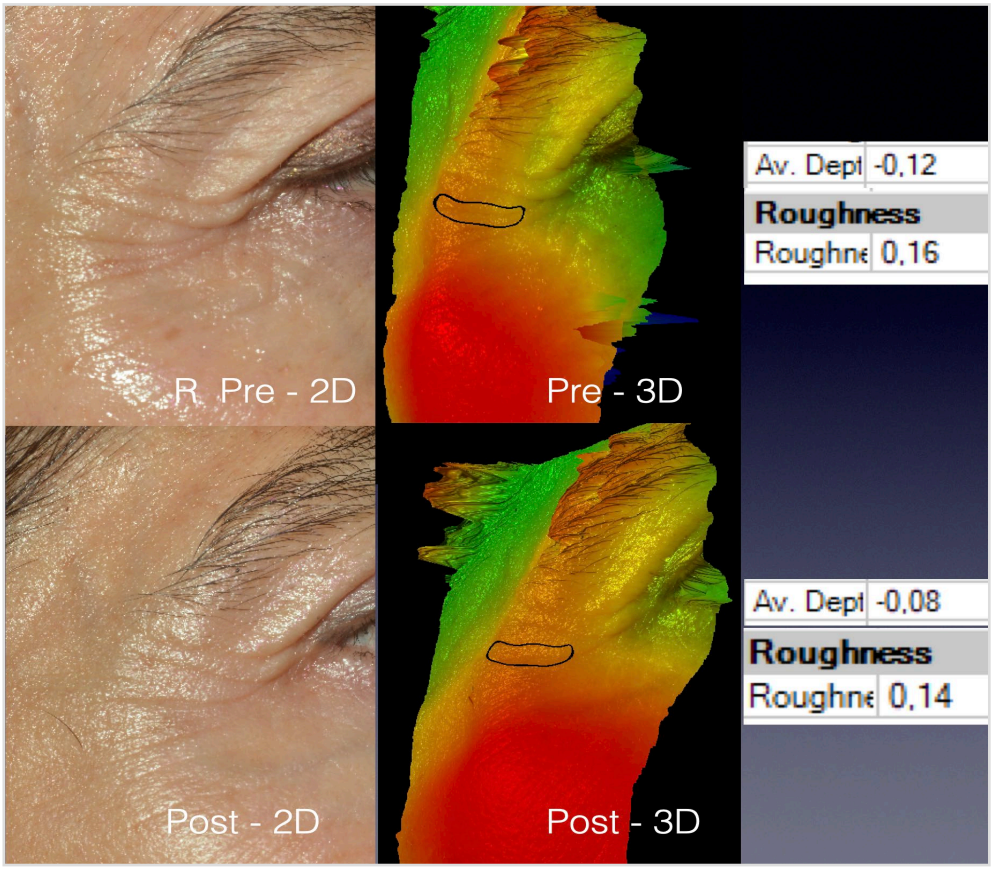

Figure 3.6: Two and three-dimensional pictures of periocular wrinkles in a 53-year-old patient subjected to LAM with vitamin C. The result observed on the 94th day after the procedure shows a reduction of Rgh_R and AD_R.

The three parameters measured did not present as a normal distribution, as confirmed by analysis of skewness and kurtosis and Shapiro-Wilk and D'Agostino & Pearson omnibus normality tests. The non-parametric Wilcoxon signed-rank test with a corresponding 95% prediction interval and alpha error set to 0.05 permitted for establishing the parameter variability and the *p*-value.

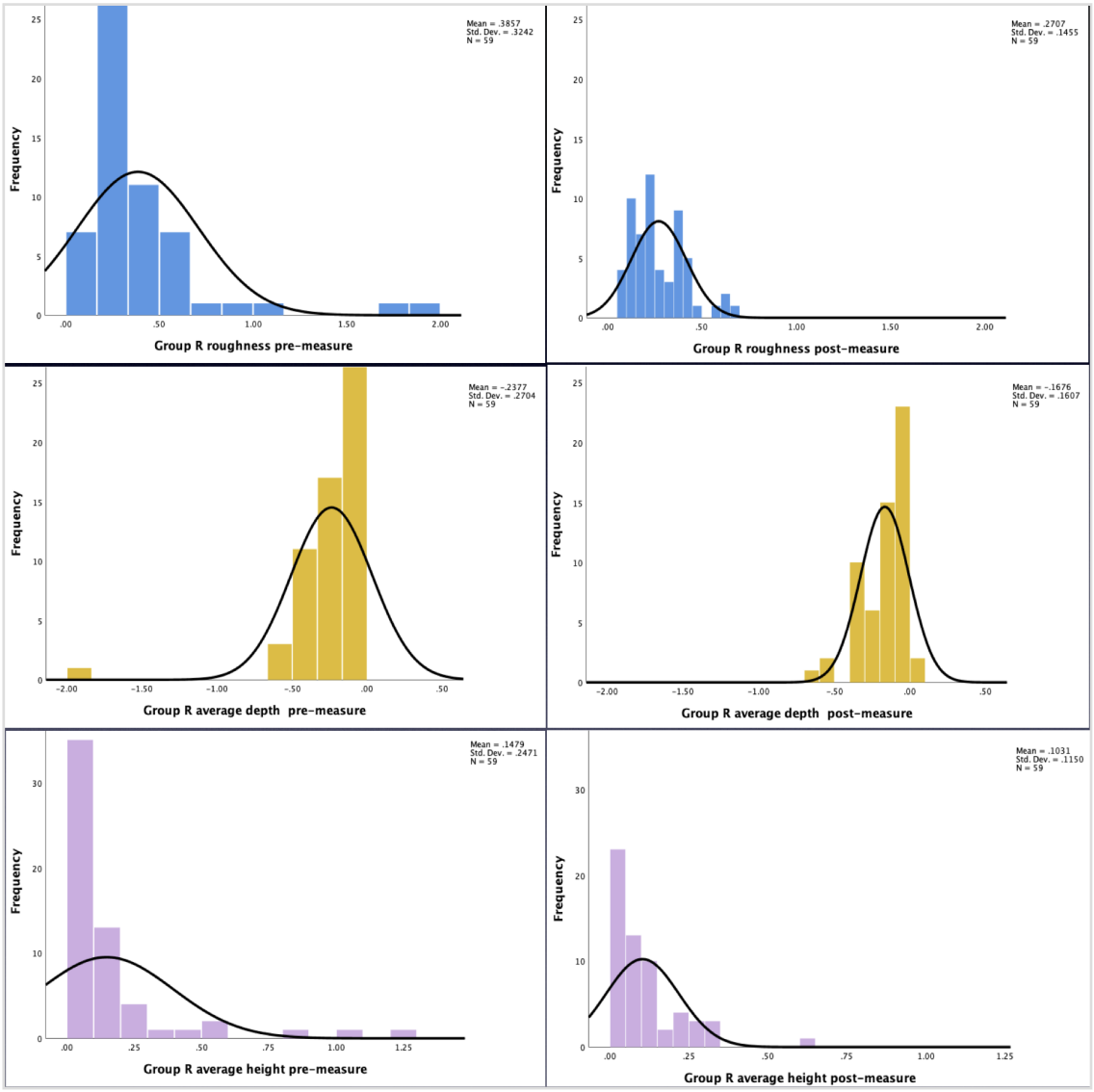

Figure 3.7: Histograms representing the population distribution in group R before and after the treatment. In blue, roughness, in ochre the average depth of the wrinkle and in lilac the representation of the wrinkle average height. The variation of roughness and wrinkle average depth parameters presented statistical significance ($p < 0.01$) according to Wilcoxon signed-rank test.

The individual percentage of parameter modification (∂ reduction) established the variation between the pre- and post-measurements and was calculated by the formula presented in Chapter 2, section 2.4.2:

$$\text{Percentage of parameter modification } (\partial \text{ reduction}) = \frac{(\text{pre - post measure})}{\text{pre-measure}} \times 100$$

Using the non-parametric Wilcoxon signed-rank test with a corresponding 95% prediction interval and alpha error set to 0.05, the mean difference in the pre- and post-procedure data showed statistical significance ($p < 0.01$) for Rgh_R ($p = 0.0001$) and the AD_R ($p = 0.002$) whereas the AH_R variation did not ($p = 0.421$).

Spearman coefficient (Sig 2-tailed) was used to calculate the correlation among skin roughness, AD_R and AH_R of the skin surrounding the wrinkles. A positive correlation

between the AD_R and the AH_R was verified (pre-procedure: *rho* = 0.639; $p < 0.01$; post-procedure: *rho* = 0.643; $p < 0.01$) (Figure 3.8).

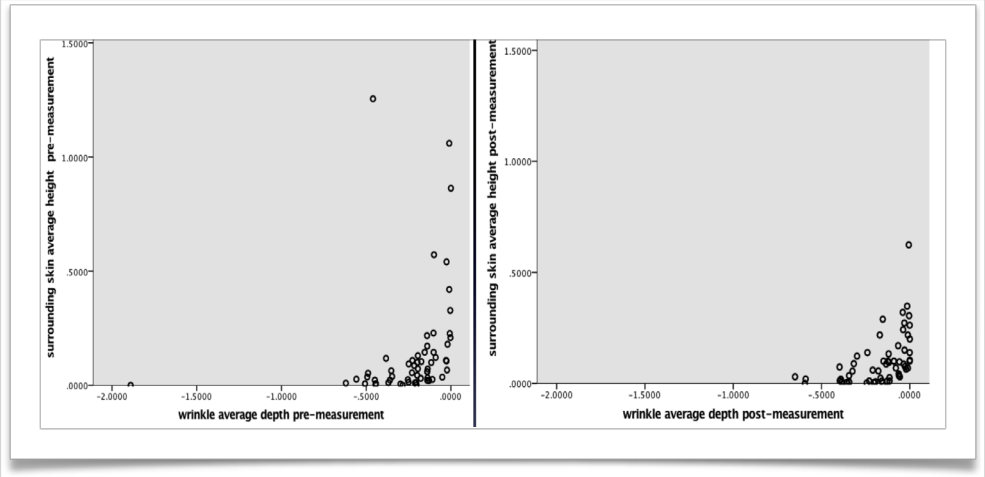

Figure 3.8: Scattergrams showing the correlation between the AD_R and the AH_R of the skin surrounding the wrinkle and demonstrating the post-procedure tendency to skin levelling. *Rho* was 0.639 and $p < 0.01$ pre-procedure. *Rho* increased to 0.643 post-procedure ($p < 0.01$).

The parameters Rgh_R and the AD_R (negative value) decreased, which showed that the treatment was capable of modifying the skin relief towards a flatter surface (Figure 3.9). Spearman *rho* confirmed the negative correlation between Rgh_R and AD_R. *Rho* was -0.495 pre-procedure ($p < 0.01$) became -0.610 ($p < 0.01$).

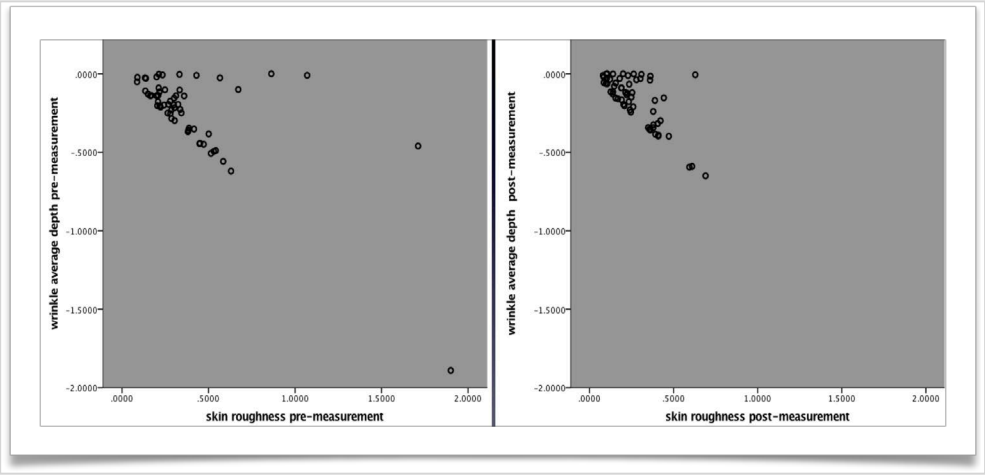

Figure 3.9: The scatterplots demonstrate the correlation between the AD_R and Rgh_R. Rho was -0.495 pre-procedure and became -0.610 post-procedure ($p < 0.01$).

The pre-procedure negative values related to the AD_R lean towards reduction, which shows the tendency to skin flattening. Conversely, the correlation between Rgh_R and AH_R was not significant (Figure 3.10) (pre-procedure: *rho* = 0.118; $p = 0.374$; post-procedure: *rho* = 0.086; $p = 0.516$).

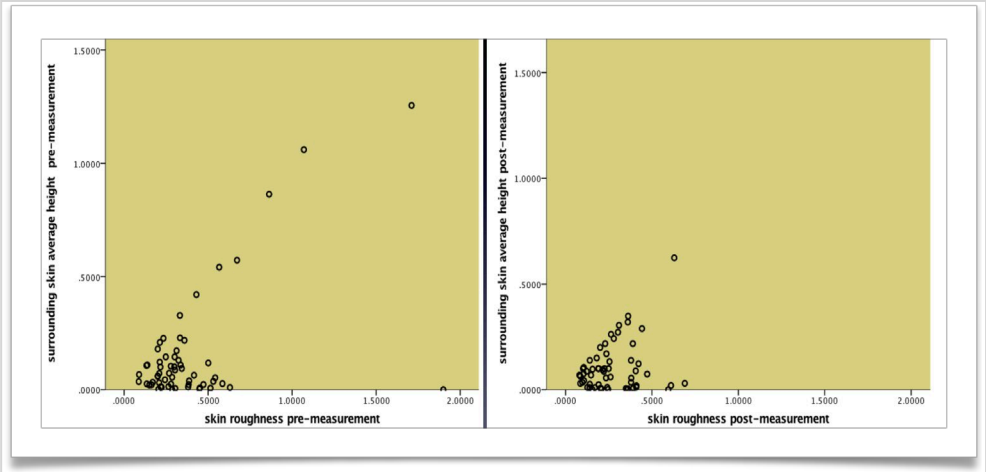

Figure 3.10: Correlation between Rgh_R and AH_R. Pre-procedure, Spearman *rho* was 0.118 and $p = 0.374$. Post-procedure *rho* became 0.086 and $p = 0.516$.

3.3.2 Group DS

From the 56 patients enrolled in group DS, a total of 23 patients presented for the post-procedure follow-up three months after the treatment. Three patients were rejected because the 3D reconstruction was distorted due to the presence of hair strands interfering with the 3D imagery in the area selected for analysis. It was possible to include multiple scars on the same individuals because selected scars were at varying stages of maturation. The study included 74 scars at different sites on the body in 20 patients aged between 18 and 60 years old (mean 41.3 ± 13.2). Eighteen patients were female. As skin appendages are absent in the scarring tissue, the duration of crusting following LAM was longer compared to the patients in group R and lasted around 15 days. After that, the debris spontaneously detached from the underlying skin.

Three patients from group DS had a history of hypertrophic scars and were admitted to the study with immature scars of three months. They did not exhibit improvement at the post-procedure review. These participants were reviewed at six months when an impressive improvement in the scars was observed. This implies that the benefits of LAM on scar improvement might have been delayed because the spontaneous improvement in the scar can be observed up to 12 months after the trauma. However, a longer follow-up would be necessary to confirm this finding.

Clinically, most scars were clearly less noticeable with a perceivable reduction of the Rgh_{DS} and V_{DS} . Patient in Figure 3.11 presented Rgh_{DS} ∂ reduction of 47% (from 0.98 to 0.52 post-LAM) and V_{DS} ∂ reduction of 36.5% (from 38.9 to 24.7 mm^3 post-LAM).

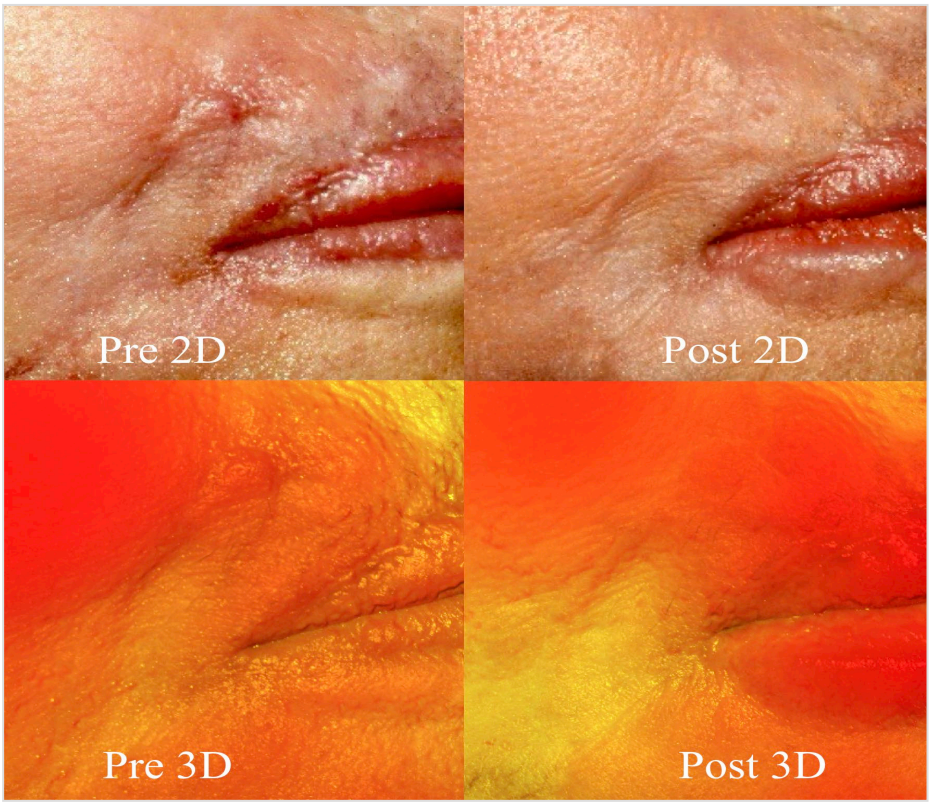

Figure 3.11: Two- and three-dimensional photographs of a patient with perioral scars (eight months old). The post-procedure images exhibit a noticeable improvement of the scars after one session of LAM with vitamin C.

Scars on the abdomen (33.78% of the scars) and the face (32.43%) were more commonly treated (Figure 3.12).

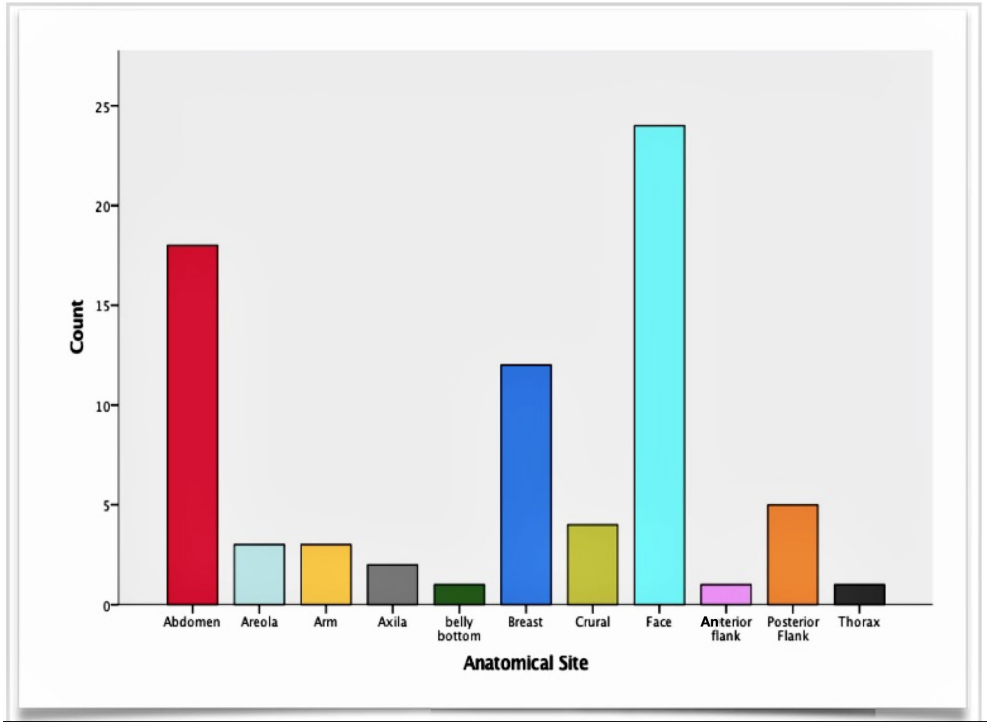

Figure 3.12: Graphic demonstrating the distribution of the analysed scars by location.

A total of 92.3% of the scars located on the face showed a reduction of the three evaluated parameters following LAM treatment. However, only 50% of scars located on the breasts showed simultaneous improvement of the three parameters. The difference in the results between anatomical locations could be an important scope of future investigation.

Statistical analysis compared the pre- and post-procedure 3D SPM data concerning the scar Rgh_{DS}, V_{DS} and AH_{DS} (Table 3.4).

Table 3.4 - Parameters related to group DS (*n* = 74 scars; missing = 0)

Parameter	Mean ± SD	Median	IQR (25^{th} – 75th percentiles)	Min	Max	Skewness (SD error: 0.28)	Kurtosis (SD error: 0.55)
Rgh_{DS} pre	1.56 ± 2.14	0.49	0.27 – 2.20	0.05	10.65	2.05	4.45
Rgh_{DS} post	0.99 ± 1.24	0.37	0.19 – 1.39	0.05	5.03	1.69	2.02
V_{DS} pre (mm^3)	562.78 ± 1025.94	108.56	1.70 – 730.30	-262.44	4507.20	2.28	5.02
V_{DS} post (mm^3)	245.03 ± 529.54	38.39	-18.03 – 273.19	-380.10	2433.10	2.14	4.52
AH_{DS} pre (mm)	1.43 ± 2.12	0.35	0.11 – 1.99	0	10.15	1.98	3.97
AH_{DS} post (mm)	0.76 ± 1.17	0.24	0.47 – 0.76	0	5.03	2.15	4.14

IQR = interquartile range (Q1-Q3); Min = minimum; Max = maximum; SD: standard deviation

Table 3.4 shows the median, IQR (25^{th} – 75th percentiles), mean and SD of skin roughness (Rgh_{DS}), the scar volume (V_{DS}) and the average height of the scar (AH_{DS}). Pre-procedure, the median of Rgh_{DS} was 0.49 (IQR 0.27 – 2.20), and the median Rgh_{DS} post-procedure was 0.55 (IQR 0.19 – 1.39).

Scar volume (V_{DS}) showed large variation pre-procedure. V_{DS} presented a median of 108.56 mm^3 pre-procedure (IQR 1.7 – 730.3 mm^3), whereas the V_{DS} post-procedure median was 38.09 mm^3 (IQR -18.03 – 273.2 mm^3).

The pre-procedure AH_{DS} was 0.35 mm (IQR 0.11 – 1.99 mm), whereas the post-procedure measurements decreased to 0.24 mm (IQR 0.47 – 0.76 mm). The AH_{DS} decreased by 77%, while scar volume decreased by 70.3%.

Rgh_{DS} decreased by 74.3%. Pre-procedure scar roughness was 1.56 ± 2.14 compared to 0.99 ± 1.24 post-procedure.

Using the non-parametric Wilcoxon signed-rank test with a corresponding 95% prediction interval and alpha error set to 0.05, the mean difference in the pre- and post-procedure data showed statistical significance ($p < 0.01$) for the three parameters.

Histograms (Figure 3.13), Shapiro Wilk and D'Agostino & Pearson omnibus normality tests demonstrated that the population did not have a normal distribution.

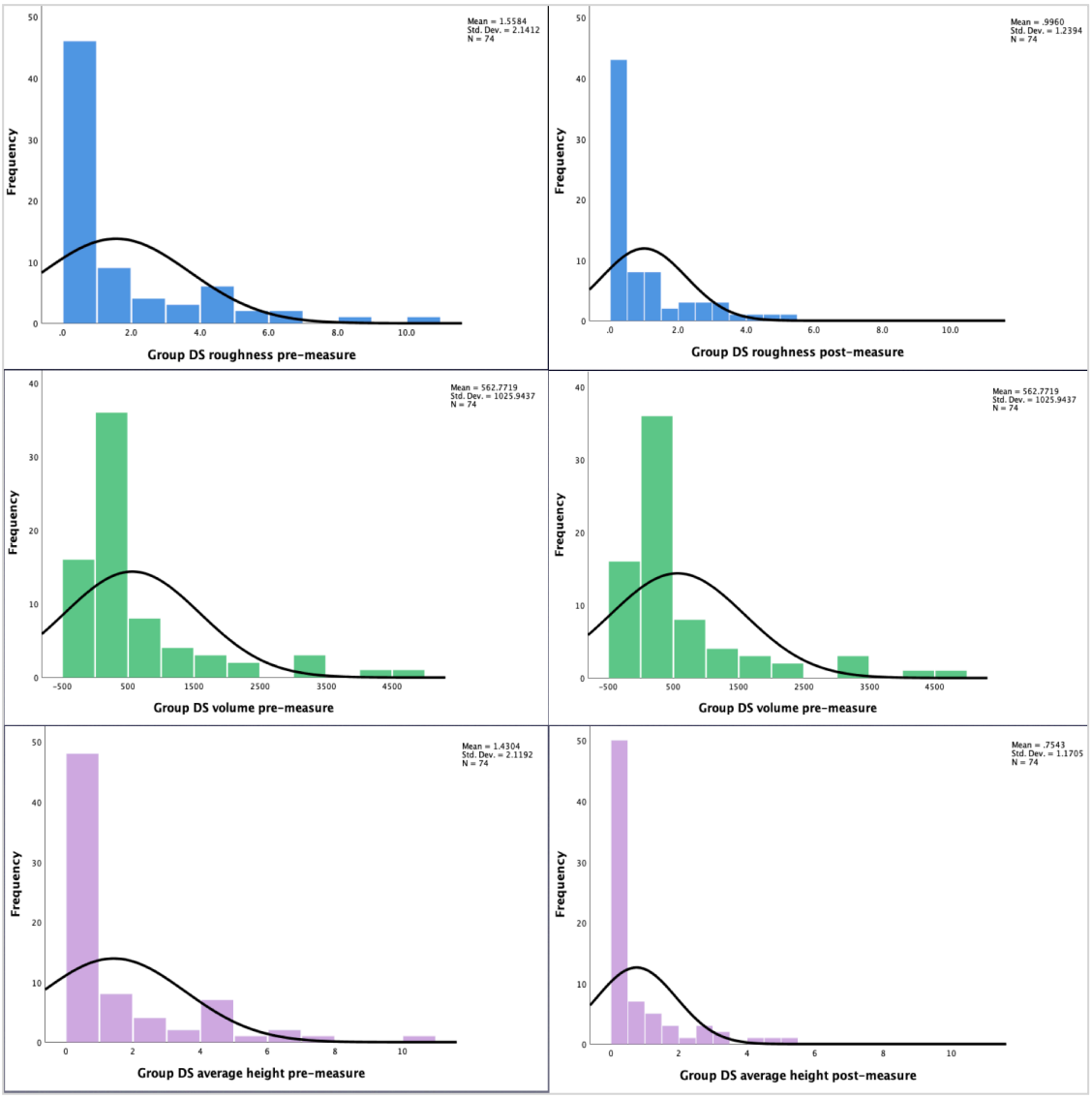

Figure 3.13: Histograms representing the population distribution in group DS before and after the treatment. In blue, scar roughness, in green, the scar volume, and in lilac, the representation of the scar average height. Data variation was statistically significant for the three parameters ($p < 0.01$) according to Wilcoxon signed-rank test.

The Spearman correlation coefficient (Sig 2-tailed) demonstrated an excellent correlation among the parameters established a significant correlation ($p < 0.01$) between scar roughness, volume and AH_{DS}, thus demonstrating that the scar tissue tended to be less prominent. Figures 3.14 - 3.16 illustrate the correlation between the parameters pre and post-procedure.

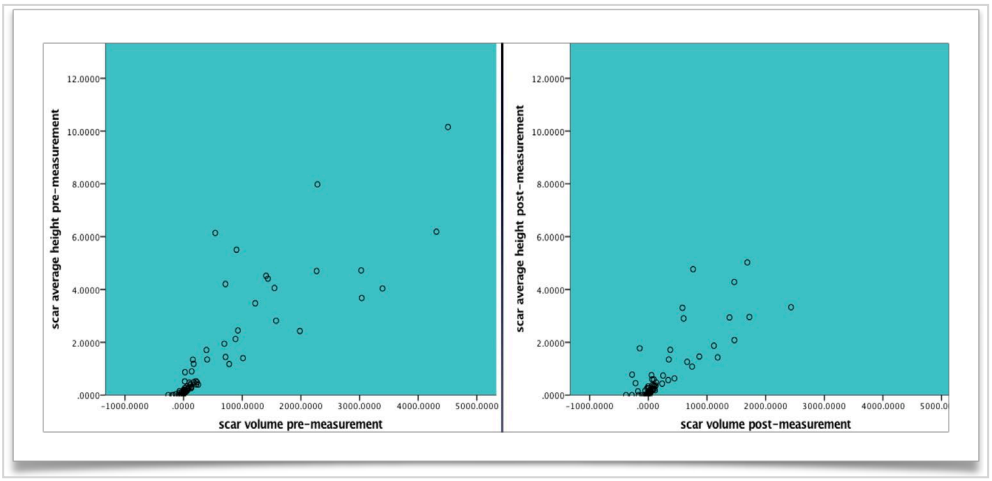

Figure 3.14: The graphics demonstrate that the correlation between the V_{DS} and AH_{DS} became stronger post-procedure (*rho* = 0.946 and $p < 0.01$).

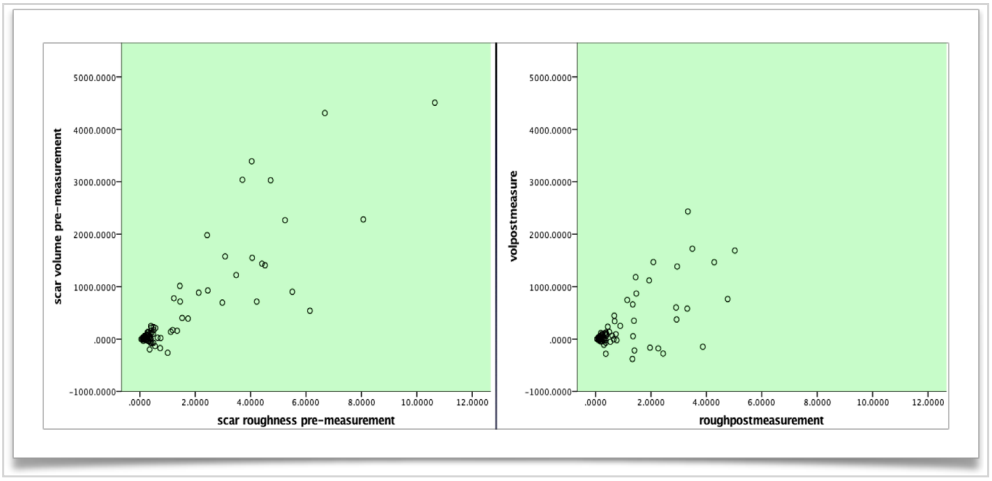

Figure 3.15: Scatterplots showing a satisfactory correlation between the V_{DS} and Rgh_{DS} (*rho* = 0.735 and $p < 0.01$). As the V_{DS} decreases, the scar surface tends to flatten.

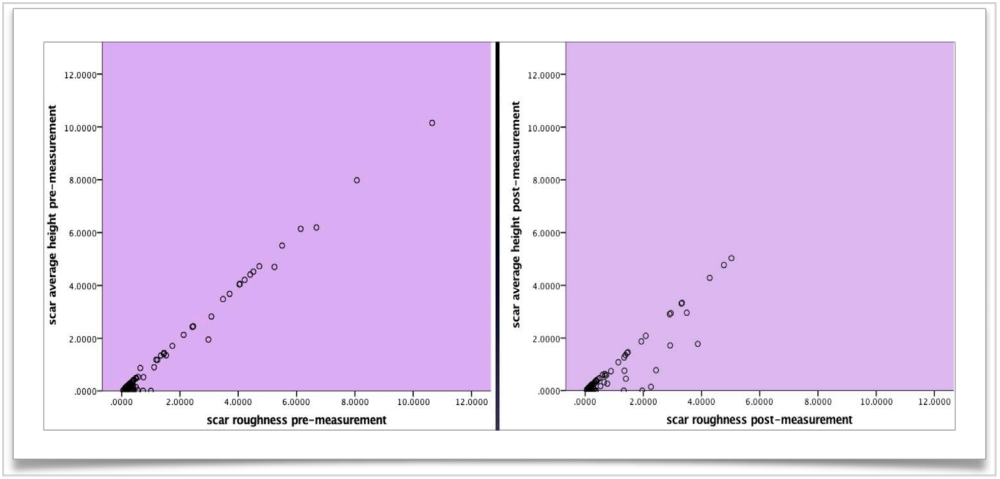

Figure 3.16: The graph illustrates the strong correlation between the AH_{DS} and the scar roughness (*rho* = 0.839 and $p < 0.01$).

3.3.3 Sample size calculation

Skin roughness data was used to build a framework for the clinical study that involved both study groups. This variable has already been validated as a scientific reference parameter in evaluating skin change (Lee et al., 2016 b; Skvara et al., 2013; Bloemen et al., 2011). The sample size calculation took into account the population variance of the outcome variable roughness, which was estimated by using the standard deviation (SD). The sample size calculation was performed for each group separately. Data related to the AD_R, AH_R, AH_{DS} and scar volume were collected for exploratory analysis. The questions related to these parameters were considered as being of secondary interest.

Calculations were performed for a two-sided hypothesis. This test is commonly used to analyse before and after measurements on the same individual. By default, the alpha significance level was set to 0.05, and the beta probability of type II error was 0.2 or 20%. These settings adjusted the computation of the sample size to 95% confidence interval and 0.8 power. The description of the data required by the software Stata (StataCorp. 2013, TX) to perform the calculation is shown as:

- SD: standard deviation; represents the population variance
- sddiff : standard deviation of the differences (difference between the pre- and post-procedure SD)
- *n*: the sample analysed in each group of the pilot study.
- degrees of freedom = *n* - 1
- PreR: the roughness pre-procedure
- PosR: the roughness post-procedure
- ma1 = sample population mean in pre-procedure roughness
- ma2 = sample population mean in post-procedure roughness
- delta = ma1 – ma2: the difference between the sample population post-procedure mean (ma2) and sample population pre-procedure mean (ma1) related to this study.
- null hypothesis: Ho= ma1 - ma2 = 0
- alternative hypothesis: Ha = ma1 > ma2 or Ha = ma1 - ma2 > 0

3.3.3.1 Sample size calculation - group R

The sample size calculation for the group of patients seeking wrinkle improvement considered the mean difference of Rgh_R (0.1149) and the SD of the differences (0.2634). The scheme of the iteration concerning the two-sided paired *t*-test performed by Stata software is detailed in the text box. The *n* (number) for the clinical study was 44 periorbital wrinkles for each subgroup of group R.

```
Variable |     n       Mean    Std. Err.   Std. Dev.   [95% Conf. Interval]
---------+--------------------------------------------------------------------
    preR |     59    .385661    .042203    .3241676    .3011825    .4701396
    posR |     59   .2707288   .0189344    .145438    .2328275    .3086302
---------+--------------------------------------------------------------------
    diff |     59   .1149322   .0343039    .2634934    .0462655    .1835989
------------------------------------------------------------------------------
 mean(diff) = mean(preR - posR)                                t =   3.3504
 Ho: mean(diff) = 0       Ha: mean(diff) > 0       degrees of freedom = 58
 Pr(T < t) = 0.9993       Pr(|T| > |t|) = 0.0014       Pr(T > t) = 0.0007
power paired means .385661 .2707288, sddiff (.2634934)

Paired t test  -  Performing iteration ...
Estimated sample size for a two-sample paired-means test:    Paired t test
Ho: d = d0  versus  Ha: d != d0
Study parameters:     sddiff =    0.2635
alpha =    0.0500         ma1 =    0.3857
power =    0.8000         ma2 =    0.2707
delta =   -0.4362
d0 =    0.0000
da =   -0.1149
Estimated sample size:    n =  44
```

3.3.3.2 Sample size calculation - Group DS

The sample size calculation for the group seeking scar improvement was based on the mean difference of Rgh_{DS} (0.5623) and the SD of the differences (1.3352). The *n* (number) calculated as required for the clinical study was 47 scars for each subgroup of group DS. The iteration performed by the software is detailed below.

```
Variable |     n       Mean    Std. Err.   Std. Dev.   [95% Conf. Interval]
---------+--------------------------------------------------------------------
     pre |     74   1.558397   .2489091    2.141197    1.062322    2.054472
     pos |     74   .9960162   .1440774    1.239401    .7088704    1.283162
---------+--------------------------------------------------------------------
    diff |     74   .5623811   .1552187    1.335242    .2530306    .8717316
------------------------------------------------------------------------------
mean(diff) = mean(pre - pos)   t =   3.6232
Ho: mean(diff) = 0      Ha: mean(diff) > 0       degrees of freedom = 73
Pr(T < t) = 0.9997       Pr(|T| > |t|) = 0.0005       Pr(T > t) = 0.0003
power paired means 1.558397 .9960162, sddiff(1.335242)

Paired t test - Performing iteration ...
Estimated sample size for a two-sample paired-means test:  Paired t test
Ho: d = d0  versus  Ha: d != d0
Study parameters: sddiff =    1.3352
alpha =    0.0500         ma1 =    1.5584
power =    0.8000         ma2 =    0.9960
delta =   -0.4212
d0 =    0.0000
da =   -0.5624
Estimated sample size:    n = 47
```

3.4 Conclusion

This robust feasibility study was an important phase of this research. This was a necessary step because this thesis aimed to perform the first *in vivo* evaluation of LAM treatment on the surface of scars and wrinkles with objective measurements obtained through 3D stereophotogrammetry. The study's primary objectives were met, confirming its feasibility, and provided a realistic alignment in terms of study design and timelines. As a primary outcome, a synergistic beneficial effect to the treatment of wrinkles and scars using superficial skin laser resurfacing followed by the topical application of vitamin C was confirmed. Overall, the periorbital wrinkles were reduced, and scar appearance was improved. Vitamin C, as a component of LAM, has proved to be safe because it did not add any more complications to those already linked to fractional laser treatments.

As a secondary outcome, the feasibility study provided the data necessary for the sample size calculation for the next phases of the research. Identifying the correct sample size when designing a study is a crucial step that requires statistical confirmation because it increases the likelihood of achieving the goal of the research. If the sample size is too small, the researcher may fail in detecting statistical significance. Conversely, excessively large sample sizes may be a waste of time, money and resources. After analysing the parameters provided by the 3D SPM system, roughness was selected to assess the response to LAM treatment and to calculate the sample because:

- Roughness is the parameter used in most scientific publications concerning skin surface alterations;
- Roughness was a parameter that provided adequate data concerning both study groups;
- The parameter average height presented a larger SD and the findings were not statistically significant in group R; its use could lead to inconsistent data;
- The average depth of the wrinkles is relevant to the rejuvenation group. While this parameter cannot be representative in group DS, volume proved a useful parameter to evaluate hypertrophic scars and keloids.

The sample size calculation for the clinical study demonstrated that the *n* is 44 for periorbital wrinkles in each sub-category within group R, and *n* is 47 scars for each sub-category in group DS. Finally, this pilot study with validation of the methodology (described in Chapter 2), established the basis and a rigid protocol that guided the comparative clinical study described within the next two chapters.

Chapter 4

A Prospective, Randomised, Double-Blind, Comparative Clinical Study on the Outcome of Periorbital Wrinkles Treated with Laser-Assisted Medication

4.1 Introduction

As age increases, wrinkles appear as coarser lines on almost all the visible parts of the body. These skin depressions correspond to marked biological and structural changes in all skin layers. Histologically, the SC overlying the wrinkle is thickened by an accumulation of corneocytes, and the *stratum spinosum* becomes thinner. The extent and depth of wrinkles are linked to the degree of atrophy of dermal collagen and the hypodermis. In addition, there is fading and depletion of the papillary dermal layer compared to the epidermis **(**Humbert et al., 2012; Kamel et., al, 2016; Tobin, 2017).

Wrinkles have been successfully treated with laser skin resurfacing (LSR). Apart from reproducibility and precision, the laser action has the advantage of conforming to irregular skin surfaces, whether convex or concave. This permits the laser to uniformly fabricate microchannels towards the dermis, irrespective of the cutaneous conditions. In addition, AFLXs can provide drug penetration at a sufficiently large depth with a low area of skin damage, which reduces the risk of infection (Genina et al., 2013). As a general principle though, the deeper the dermal injury with laser therapy, the more risk of depigmentation and scar formation.

Several studies substantiate that lasers disrupt skin protective layers (e.g. the SC outside-in barrier, and the TJs inside-out barrier), deliver drugs directly into the dermis (Sklar et al., 2014), and facilitate the bioavailability of macromolecules whether lipophilic or hydrophilic via MTZs (Basler et al., 2016; Ali & Al-Niaimi, 2016; Badawi & Osman, 2018; Wenande et al., 2018). However, there is an indication that the diffusion of hydrophilic substances is more dependent on laser microchannel delivery compared to lipophilic compounds and undergo greater relative enhancement *in vitro*. Nonetheless, the laser-assisted delivery of hydrophilic drugs may be more sensitive to differences in tissue responses *in vitro* than *in vivo* (Wenande et al., 2019).

The rise in the temperature on the lasered cutaneous surface not only can increase drug permeability, but also can reduce the activity of epidermal enzymes (Pyo & Maibach, 2019). All these factors reinforce the necessity for clinical trials to investigating the laser-tissue interaction and possible benefits of LAM. However, most publications rely on *in vitro* experiments, animal experiments or cadaver skin. In addition, it is often hard to compare studies, as only a few authors have validated or thoroughly explained the methodologies that they have employed. Consequently, after decades of research, LAM is not yet considered standard therapy and the commercialisation of suitable formulae for transcutaneous drug delivery is limited to only a few products on the market (Münch et al., 2017; Wiedersberg & Guy 2014; Watkinson, 2013).

The present *in vivo* human study investigates the impact of applying different substances on the skin surface immediately after laser skin resurfacing. The substances investigated in this thesis are subject to dietary influences or endogenous production, which could cause a bias in pharmacokinetics studies. In addition, most analytical techniques described in Chapter 1 section 1.7 prove the enhanced delivery of substance after LAM but not the clinical effect of this combination. Biopsies only show the enhancement of neocollagenesis. Based on these facts and also because no biological material could be transported from Brazil to the United Kingdom, alternatives to analysing LAM treatment results ranged from visual non-invasive assessment to optical imaging systems. The three-dimensional stereophotogrammetry system employed has been standardised and validated in a comparative study described in Chapter 2.

4.2 Study objectives

The present clinical trial has involved human subjects to answer one of the research questions: What is the impact of using medications, such as growth factors contained within a cosmeceutical associated with vitamin C or compared to vitamin C alone, on skin primarily treated with laser resurfacing?

The vitamin C (Vitasantisa®) used in all patients is fabricated for intravenous use and is registered under the number 1.0186.0031.0001-7 in the Health Ministry, Brazil. The cosmeceutical TNS Recovery Complex® (SkinMedica, Carlsbad, CA, USA) contains growth factors as active ingredients.

4.3 Materials and methods

This prospective, double-blind, randomised clinical study was approved by the Brazilian Ethics Committee and the FREP at Anglia Ruskin University and has followed the principles of the World Medical Association Declaration of Helsinki (2013).

- Fitzpatrick skin type I to IV female patients, 40 to 70 years old, spontaneously seeking facial treatment for periorbital wrinkles were recruited to compose group R. The following patients were excluded:
- patients who are not available for the follow-up visits;
- patients with unrealistic expectations;
- patients taking anti-inflammatories or any other drug known to interfere with the healing processes;
- patients subjected to laser treatment, dermabrasion or chemical peeling within six months before the treatment in the area to be treated;
- patients subjected to the injection of botulinum toxin at the periorbital area within the last four months;

- patients with a history of recent cutaneous allergies, chronic dermatitis or other cutaneous pathology on the face.

The recruitment of participants took place between September 2018 and September 2019. In total, 149 patients met the inclusion criteria and were included in this study. The primary endpoint was the change in the surface of wrinkles between baseline and three months after the procedure. This analysis was based on readouts provided by a three-dimensional stereophotogrammetry system. The secondary endpoints included the visual facial skin alteration and the alteration in skin thickness. The efficacy of each treatment regimen was statistically analysed and compared to confirm if there was a significant difference in the skin roughness and the average depth of the wrinkles between the two groups.

4.3.1 Study design

On the day of the treatment, the patients enrolled were screened and randomised after having signed the consent form. Pre-treatment photographs were obtained. As mentioned in Chapter 1 (section 1.10.1), before entering the treatment room, each patient picked a paper from a container indicating the description of the treatment to be delivered by the researcher's assistant. The assistant applied the chemical substances according to the arm of the study. Both the researcher and the patient were unaware of the randomised treatment given (double-blind study).

A digital camera was used to photograph patients before and three months after the treatment. The photographic documentation followed the protocol described in Chapter 2, section 2.3.2. A laser tape measure guided the design of a vertical line leading from the eyebrow tail towards the jaw and a perpendicular line leading from the eyebrow tail towards the temporal hairline. A horizontal line leading from the ipsilateral nostril to the tragus completed the area delimitation. Both periorbital regions were photographed.

After photographic documentation, an anaesthetic ointment composed of lidocaine 7% and tetracaine 7% was applied to the targeted areas for 30 minutes. Immediately before the procedure, 20 mg of oral prednisolone and 10 mg of ketorolac tromethamine were given to the patients. The eyes were protected with moist gauze and laser protection glasses. All patients were subjected to a single session of fractional ablative laser treatment by the researcher (Starlux® 500 Palomar Inc., Burlington, MA). Standardised laser parameters were used for all patients, as summarised in Table 3.1 (Chapter 3 section 3.2.2.1). Each patient received a full-face treatment.

After laser application, small scattered bleeding spots were noticed. The skin was cleaned to remove the blood clots, and the researcher's assistant applied the chemical substances according to the branch of the study. Group R-C was the control and received topical application of 200mg of Vitamin C, whereas group R-CGF underwent topical application of vitamin C plus the cosmeceutical containing GFs. Both the researcher and the patient were unaware of the treatment given (double-blind study). The skin was occluded with the medication for 30 minutes.

Patients were discharged and instructed to clean the treated area with a saline solution once a day. Patients were directed to cover the treated area with dexpanthenol (Bepantol® - Bayer) four times a day until the cutaneous debris had entirely disappeared. Fexofenadine was prescribed for five days, and 10 mg of ketorolac tromethamine was administered every eight hours in case of pain. A valaciclovir prescription was restricted to patients with a previous history of herpes simplex.

Patients were monitored for adverse events and instructed not to apply cosmeceuticals and other topical medications to the face until after the follow-up visits, which occurred three months after the treatment, between January 2019 and January 2020.

Of the 149 patients included in the study and randomised according to the protocol, 74 patients were followed up in group R-C (control group) and 75 were followed up in group R-CGF. The doses applied were 200 mg of vitamin C in patients from group R-C, in the form of a 2 ml aqueous, sterile solution plus 1 ml of the cosmeceutical containing growth factors (serum solution) in patients from group R-CGF.

Skin crusting lasted from five to eight days, early moderate periorbital swelling was revealed in all patients and spontaneously resolved on the third day post-procedure. Post-laser erythema started on the seventh day after the procedure and subsided on the twentieth day. Hypochromia and herpes eruptions were not detected.

Following the same procedure described in Chapter 2 (section 2.3.2), photographs of the same pre-laser treated area of skin being investigated were taken using the pre-procedure landmarks, uploaded to the computer and transferred to the software. The pre- and post-procedure images were synchronised for comparison. Sigma 10 was selected, and a contour comprising periorbital wrinkles was designed. The pop-up window was accessed, and the measurements related to skin roughness and wrinkle average depth were displayed.

4.3.2 Statistical analysis

Data obtained via the Dermapix® software were analysed by the program SPSS IBM (Version 26.0 IBM Corp© for Mac, Armonk, New York, USA). The descriptive analysis presented the data in the form of tables and illustrative graphics.

Tests were applied to compare and correlate skin roughness (Rgh_R) and wrinkle average depth (AD_R) measurements, pre and post-procedure. The objectives were to verify the efficacy of the treatment regimen and to confirm if there was a significant difference in the Rgh_R and AD_R measurements between the two groups: R-C and R-CGF. The criterion for determining significance was set at 5%; findings were considered significant with a *p*-value < 0.05 and very significant with a *p*-value < 0.01.

The Shapiro-Wilk test and histograms verified the normality of the variables. Data included median, IQR, mean and SD of the numerical variables under study. Since the variables had a non-Gaussian distribution in at least one group, data were summarised by quartiles. The interquartile range (IQR) contains 50% of the observations between the limits that correspond to the first quartile (25^{th} percentile) and the third quartile (75^{th} percentile) (Q1 - Q3). This interval is given as a measure of central tendency and adequate dispersion that follows the median, as the standard deviation follows the mean.

The inferential analysis involved related sample tests (Wilcoxon signed-rank test) and independent sample tests (Mann-Whitney U test). Additionally, Spearman *rho* was used to establish a correlation between wrinkle average depth (AD_R) and skin roughness (Rgh_R) improvement.

4.4 Results

In both groups, crusting lasted around 5 days, and no complication nor adverse reaction related to cutaneous use of vitamin C, GFs and the cosmeceutical medium used in this research was documented.

4.4.1 Group R-C

The age of the patients varied between 43 and 70 years old (mean 57.1 years ± 6.7 SD; median 57 with an IQR of 52.0 – 62.3 years).

The histograms and statistical tests for normality (Shapiro-Wilk and Kolmogorov-Smirnov) demonstrated that the population related to pre- and post-procedure variables roughness and average depth was not within a normal distribution (Figure 4.1). Wilcoxon signed-rank tests (Sig. 2-tailed test) showed that the reduction of $Rgh_{R\text{-}C}$ and the $AD_{R\text{-}C}$

was very significant with a $p < 0.01$. Pre-procedure, the median of Rgh_{R-C} was 0.16 (IQR 0.10 – 0.22) compared to 0.13 (IQR 0.08 – 0.17) post-procedure. The AD_{R-C} presented a median of -0.11 mm pre-procedure (IQR -0.19 – -0.05 mm), whereas the post-procedure measurements showed a median of -0.07 mm with an IQR of -0.13 mm – -0.07mm.

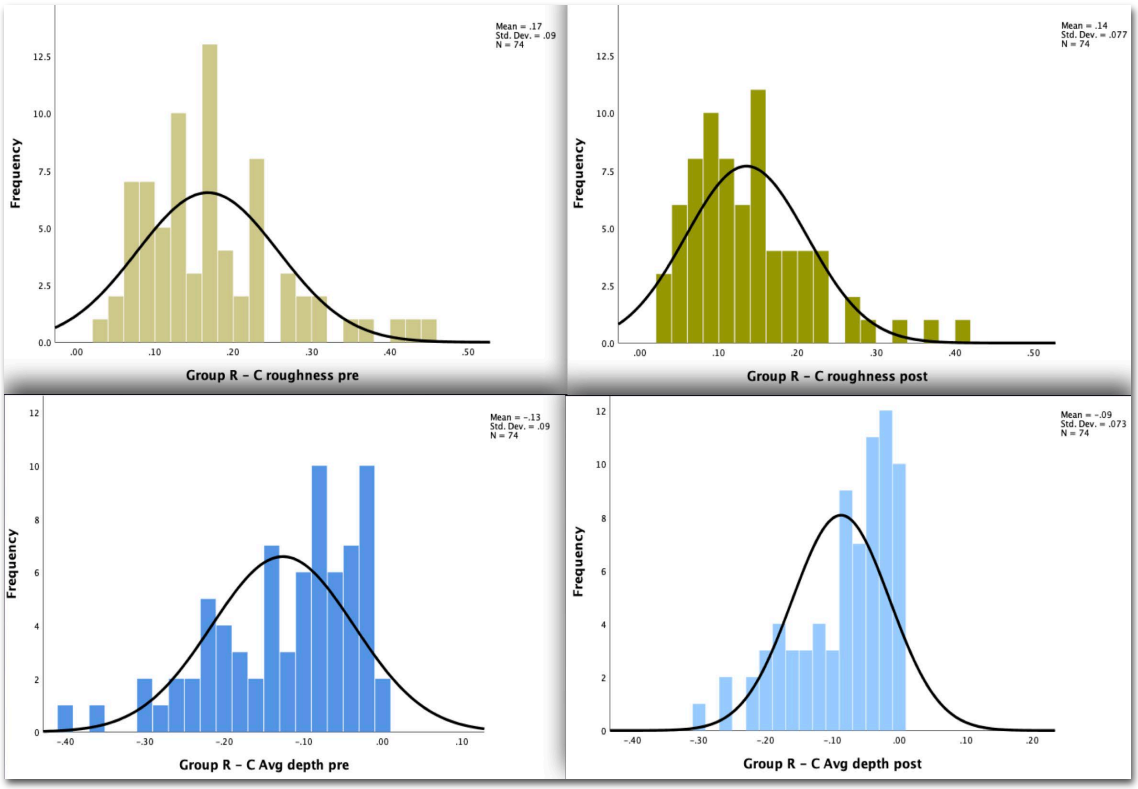

Figure 4.1: Histograms representing the population distribution related to the wrinkle average depth (blue) and skin roughness (ochre) of group R-C. Data distribution were not normal and non-parametric tests were applied.

The percentage of parameter modification (∂ reduction) established the variation between the pre- and post-measurements of a given parameter and was calculated by the formula presented in Chapter 2, section 2.4.2:

$$\text{Percentage of parameter modification } (\partial \text{ reduction}) = \frac{(\text{pre - post measure})}{\text{pre-measure}} \times 100$$

The simultaneous computation of the parameters (Table 4.1) corresponded to the sum of the ∂ reduction of Rgh_R and AD_R, as described in Chapter 2 (section 2.4.2).

Table 4.1 - Descriptive analysis of the variables roughness ($Rgh_{R\text{-}CGF}$) and average depth ($AD_{R\text{-}CGF}$) in group R-C (n= 74)

	Pre-procedure					Post-procedure					WRT
Variable	**Mean ±SD**	**Median**	**IQR**	**Min**	**Max**	**Mean ±SD**	**Median**	**IQR**	**Min**	**Max**	***p*-value**
Age (years)	57.1 ± 6.7	57.0	52.0 – 62.3	43.0	70.0	n/a	n/a	n/a	n/a	n/a	n/a
Rgh	0.17 ± 0.09	0.16	0.10 – 0.22	0.03	0.44	0.14 ± 0.08	0.13	0.08 – 0.17	0.03	0.41	**<0.01**
AD	-0.13 ± 0.09	-0.11	-0.19 – -0.05	-0.4	-0.01	-0.09 ± 0.07	-0.07	-0.13 – -0.03	-0.3	-0.01	**<0.01**
Rgh ∂ reduction						19.0 ±15.5	18.8	7.5 – 29.1	-27.3	59.5	n/a
AD ∂ reduction						30.5 ± 30.7	33.3	8.5 – 50.0	-66.7	83.3	n/a
Simultaneous computation of AD and Rgh ∂ reduction						49.5 ± 35.7	50.1	18.8 – 72.3	-31.3	132	n/a

IQR: interquartile range (25th - 75th percentile); Min: Minimum: Max: Maximum; n/a : not applicable; WRT: Wilcoxon rank test; ∂ reduction is in percentage; AD is measured in mm

4.4.2 Group R-CGF

Of the 149 randomised participants, 75 patients composing group R-CGF were followed-up at three months. Participants were aged from 43 to 70 years old (58.1 ± 6.8 years). Shapiro-Wilk and Kolmogorov-Smirnov tests for normality demonstrated that the data distribution related to pre- and post-procedure variables were not normal, as represented by the histograms in Figure 4.2.

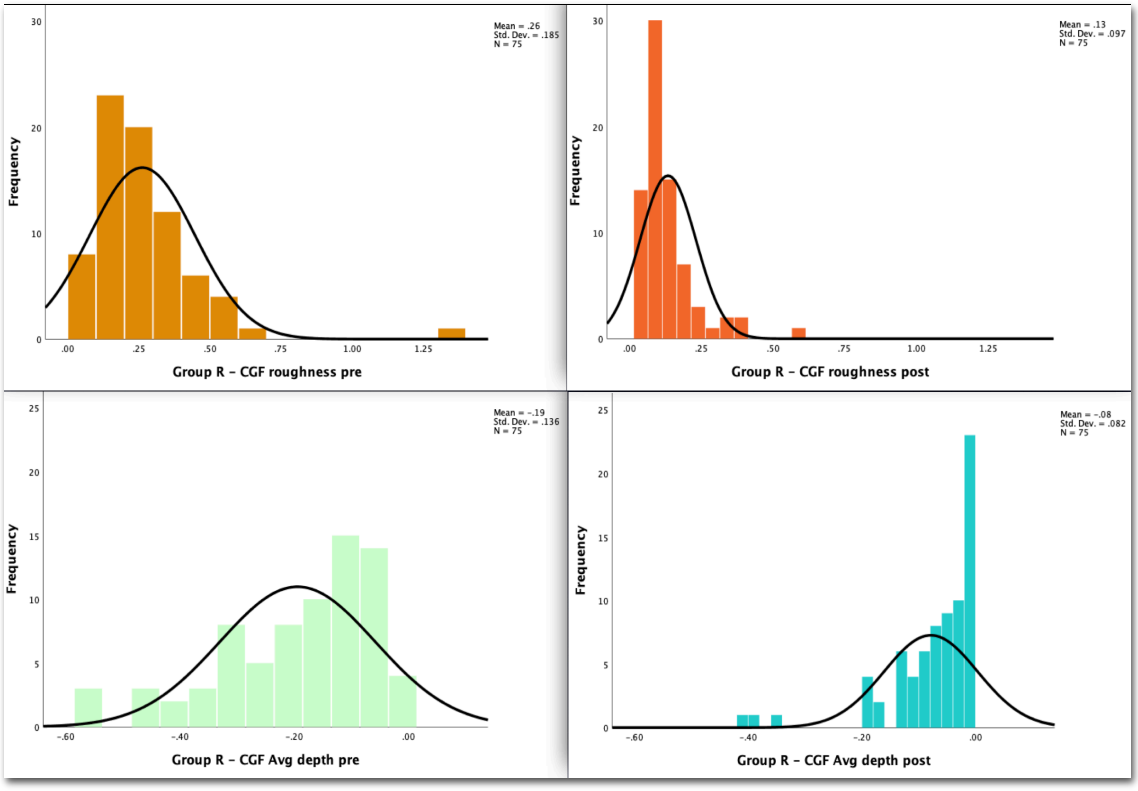

Figure 4.2: Histograms representing the population distribution related to the skin roughness and wrinkle average depth of group R-CGF. Data distribution were skewed and non-parametric tests were applied.

Table 4.2 presents the descriptive analysis of the variables roughness and average depth of the analysed wrinkles in group R-CGF.

Table 4.2 - Descriptive analysis of the variables roughness ($Rgh_{R\text{-}CGF}$) and average depth ($AD_{R\text{-}CGF}$) in group R-CGF (n= 75)

	Pre-procedure					Post-procedure					WRT
Variable	**Mean ±SD**	**Median**	**IQR**	**Min**	**Max**	**Mean ±SD**	**Median**	**IQR**	**Min**	**Max**	***p*-value**
Age (years)	58.1 ± 6.8	57.0	53.0 – 63.0	43.0	70.0	n/a	n/a	n/a	n/a	n/a	n/a
Rgh	0.26 ± 0.18	0.22	0.15 – 0.34	0.06	1.31	0.13 ± 0.1	0.11	0.08 – 0.16	0.04	0.61	**<0.01**
AD	-0.19 ± 0.14	-0.15	-0.29 – -0.09	-0.56	-0.01	-0.08 ± 0.08	-0.06	-0.11 – -0.02	-0.41	-0.01	**<0.01**
Rgh ∂ reduction						45.8 ± 17.4	45.0	34.4 – 58.3	4.7	79.0	n/a
AD ∂ reduction						57. 2 ± 27.3	62.5	34.5 – 81.8	-2.6	95.8	n/a
Simultaneous computation of AD and Rgh ∂ reduction						103 ± 37.4	105.5	74.6 – 134.3	2.1	165	n/a

IQR: interquartile range (25^{th} - 75^{th} percentiles); Min: Minimum: Max: Maximum; n/a : not applicable; WRT: Wilcoxon rank test; ∂ reduction is in percentage; AD is measured in mm

The non-parametric Wilcoxon sign-rank test (with a corresponding 95% prediction interval and alpha error set to 0.05) confirmed that the mean difference of the pre- and post-procedure data was very significant with a $p < 0.01$ for both variables. Pre-procedure, the median of RghR-CGF was 0.22 (IQR 0.15 – 0.34) compared to 0.11 post-procedure (IQR 0.08 – 0.16). ADR-CGF presented a median of -0.15 mm pre-procedure (IQR -0.29 – -0.09 mm), whereas the post-procedure ADR-CGF showed a median of -0.06 mm and IQR of -0.11 – -0.02 mm.

4.4.3 Clinical cases

Some clinical cases are presented as examples of the results of LAM according to the of the study group.

4.4.3.1 Group R-C

Figures 4.3 and 4.4 are two- and three-dimensional pictures of patients submitted to LAM with vitamin C. The simultaneous computation of ∂ reduction of the parameters Rgh_R and AD_R concerning the highlighted wrinkle in Figure 4.3 showed a ∂ reduction of 50% of these parameters. Despite the visual amelioration of the wrinkle highlighted in Figure 4.4, the 3D SPM system detected that the simultaneous ∂ reduction of Rgh_R + AD_R was not so expressive (22.7%).

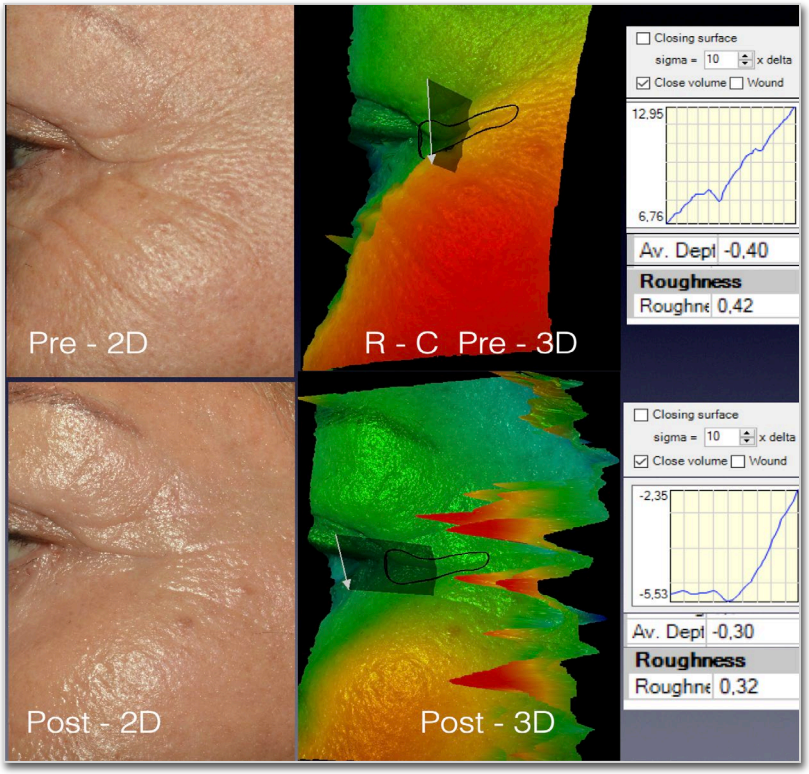

Figure 4.3: A 69-year-old patient from group R-C. The post-procedure images were obtained on the 94th day. The $Rgh_{R\text{-}CGF}$ of the delimited wrinkle decreased by 25%, and the $AD_{R\text{-}CGF}$ also decreased by 25%. The 3D images were rotated so that graphics on the right could show the variation of skin roughness in the area below the white arrow.

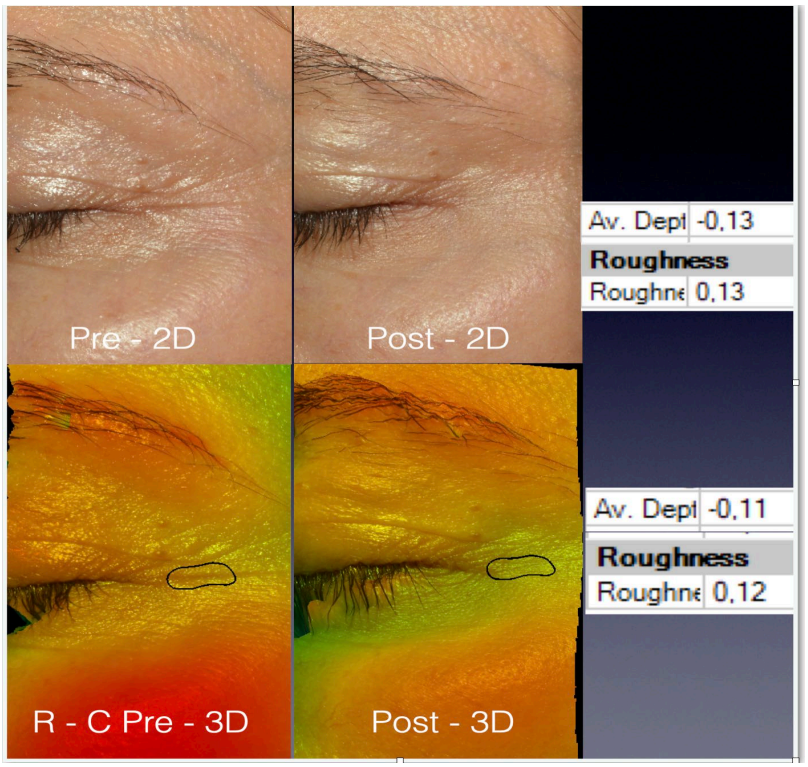

Figure 4.4: A 51-year-old patient from group R-C. Images post-procedure were obtained at three months. The software readouts are displayed on the right. The $Rgh_{R\text{-}C}$ of the designed wrinkle decreased by 7.7 % and the $AD_{R\text{-}C}$ decreased by 15%.

4.4.3.2 Group R-CGF

Figures 4.5 and 4.6 exhibit the two- and three-dimensional pictures of patients subjected to LAM with vitamin C and the cosmeceutical containing GFs.

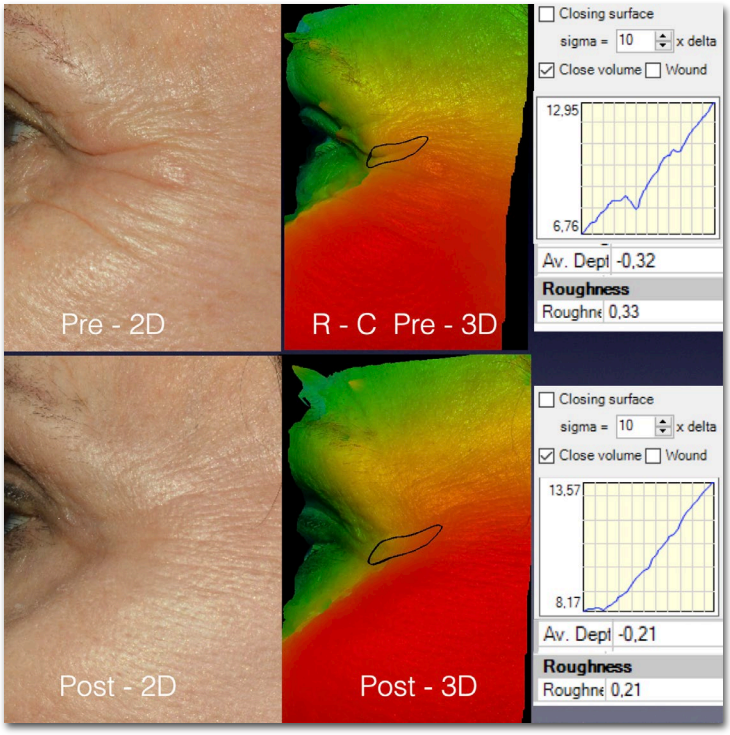

Figure 4.5: A 68-year-old patient from group R-CGF. Post-procedure pictures were obtained on the 92nd day. The graphics and data on the right were provided by the 3D SPM software and confirm the visual improvement of the periorbital wrinkles. $Rgh_{R\text{-}CGF}$ decreased by 36%, and $AD_{R\text{-}CGF}$ decreased by 34%.

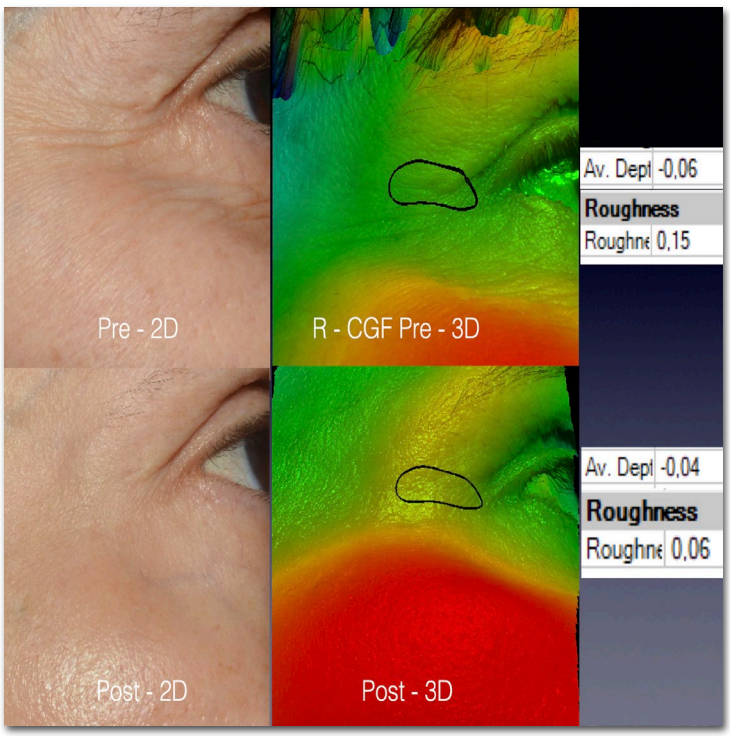

Figure 4.6: The pictures of a 57-year-old patient from group R-CGF. Post-procedure pictures were obtained on the 90th day. The visual skin improvement was confirmed by the data delivered by the 3D SPM system (on the right). $Rgh_{R\text{-}CGF}$ decreased by 60% and $AD_{R\text{-}CGF}$ decreased by 33.33%.

The wrinkle depicted in Figure 4.5 showed a simultaneous reduction of the parameters Rgh_R and AD_R of 70%, whereas the wrinkle depicted in Figure 4.6 exhibited a simultaneous ∂ reduction of Rgh_R + AD_R of 93.33 %.

4.4.4 Comparison between group R-C and group R-CGF

The correlation between both variables under consideration was performed through the Spearman's correlation coefficient (Sig 2-tailed) and is represented by scatterplots in Figure 4.7. The negative correlation between the RghR and ADR was significant in both groups. In group R-C, rho was -0.808 pre-procedure and became -0.780 post-procedure ($p < 0.01$). The negative correlation also became weaker in group R-CGF, with a rho = -0.770 pre-procedure and rho = -0.680 post-procedure ($p < 0.01$). This correlation represents the tendency to skin flattening and suggests that LAM was able to interfere with both variables at the same time.

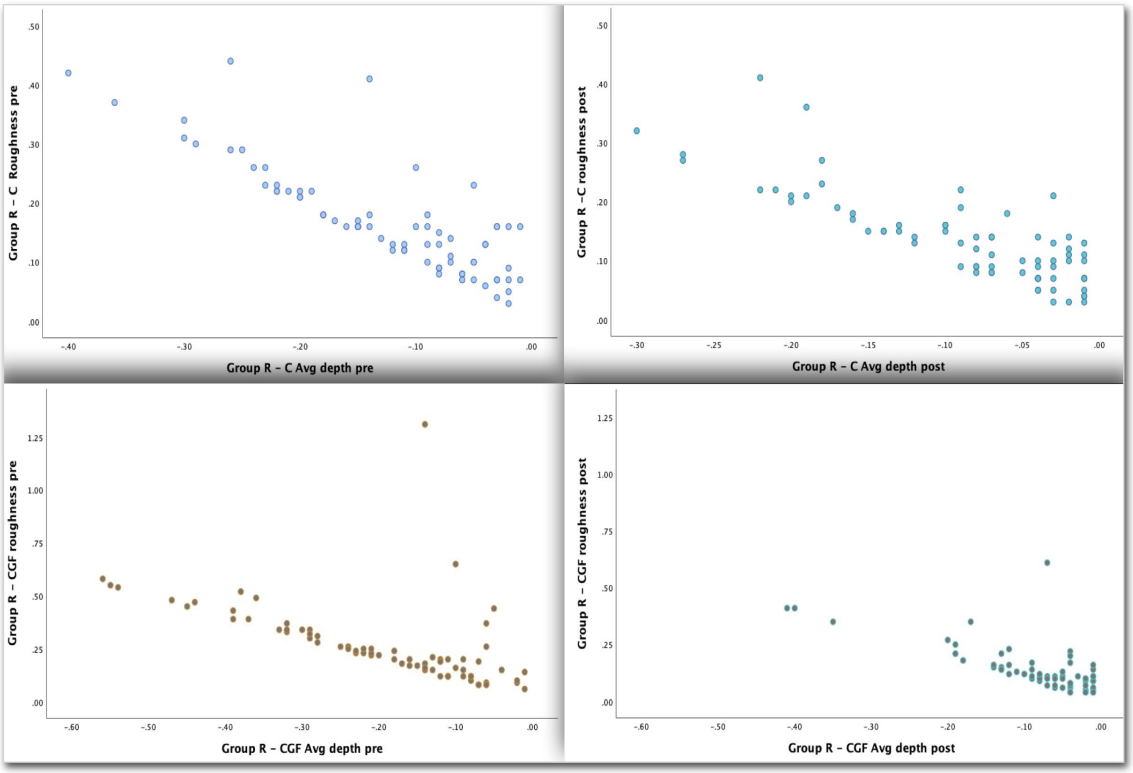

Figure 4.7: Scatterplots representing the negative correlation between the two variables under analysis in both groups. The correlation between Rgh_R and AD_R was strong in both groups.

Figure 4.8 is a boxplot representing the AD_R and Rgh_R ∂ reduction in patients of group R treated with vitamin C (R-C) and vitamin C plus the cosmeceutical containing GFs (R-CGF). The statistical analysis showed that the periorbital wrinkles presented an overall improvement in both groups.

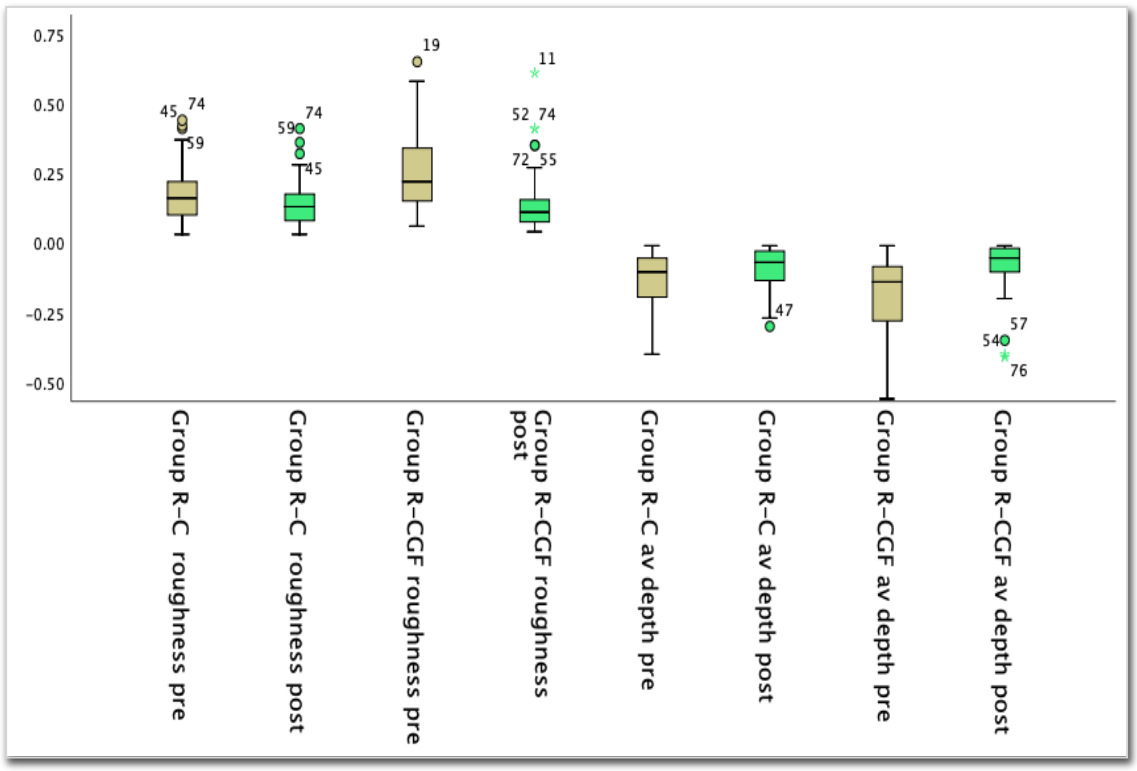

Figure 4.8: Boxplot representing the AD_R and Rgh_R ∂ reduction according to the treatment regimen in group R. The difference between patients treated with vitamin C and vitamin C plus the cosmeceutical was statistically significant (p<0.01) according to the Mann-Whitney test. The outliers are represented by circles and their correspondent case number.

No bias resulted from gender variation or age heterogeneity (Table 4.3). All patients were female, and the age variation between both groups was not significant (p = 0.39) according to Mann-Whitney test.

Table 4.3 - Descriptive analysis of the variables (roughness and average depth) according to the two treatment regimens

Variable	Group R-C (n = 74)		Group R-CGF (n = 75)		Mann-Whitney test p-value
	Median	IQR	Median	IQR	
Age (years)	57.1	52.0 – 62.3	58.1	53.0 – 63.0	0.39
Rgh_R – Pre-procedure	0.16	0.10 – 0.22	0.22	0.15 – 0.34	**<0.01**
Rgh_R – Post-procedure	0.13	0.08 – 0.17	0.11	0.08 – 0.16	0.5
AD_R - Pre-procedure	-0.11	-0.19 – 0.05	-0.15	-0.29 – -0.09	**0.01**
AD_R – Post-procedure	-0.07	-0.13 – -0.03	-0.06	-0.11 – -0.02	0.27
Rgh_R ∂ reduction	18.8	7.5 –29.1	45.0	34.4 –58.3	**<0.01**
AD_R ∂ reduction	33.3	8.5 –50.0	62.5	34.5 – 81.8	**<0.01**
Simultaneous computation of AD_R and Rgh_R ∂ reduction	50.1	18.8 –72.3	105.5	74.6 – 134.3	**<0.01**

According to the Mann-Whitney test, the AD_{R-CGF} ∂ reduction, Rgh_{R-CGF} ∂ reduction and the simultaneous reduction of both parameters (AD_R + Rgh_R) in group R-CGF were significantly higher than in group R-C ($p < 0.01$). Group R-C presented Rgh_{R-C} median ∂ reduction of 18.8% (IQR 7.5 – 29.1%) compared to Rgh_{R-CGF} ∂ reduction of 45% (IQR of 34.4 –58.3%) in group R-CGF.

The parameter AD_{R-C} underwent a median ∂ reduction of 33.3% (IQR 8.5 – 50.0%) in group R-C and the median of the AD_{R-CGF} ∂ reduction was 62.5% in group R-CGF (IQR of 34.5 – 81.8%). The median of the simultaneous computation of the ∂ reduction concerning both parameters (Rgh_R + AD_R) in patients subjected to LAM with vitamin C was 50.1% (IQR 18.8 –72.3) in group R-C against 105.5% (IQR 74.6 – 134.3%) in patients submitted to LAM with vitamin C associated with the cosmeceutical containing GFs.

These findings confirmed that patients subjected to LAM, using vitamin C plus GFs blended into a cosmeceutical, produced statistically significantly better results than those treated with LAM followed by vitamin C alone.

The ∂ reduction of Rgh_R and AD_R was transformed into a categorical variable according to the degree of change in the parameter being measured which was either as a reduction in skin creases in mm, neutral (no change) or augmentation of skin creases. The Fisher exact test was applied to the categorical variables to compare the two treatment regimens (C and CGF) to establish if their distribution was equivalent in both populations (Table 4.4). The tests confirmed that the group treated with vitamin C plus the cosmeceutical containing GF (R-CGF) presented very significant Rgh_R and AD_R ∂ reduction ($p < 0.01$) compared to the group treated with vitamin C alone.

Table 4.4 - Categorical variables according to the treatment regimen in group R: Fisher's exact test

Variable alteration	Group R-C (n=74)		Group R-CGF (*n* = 75)		*p*-value
	n	%	*n*	%	
Roughness (Rgh_R)					
reduction	65	87.8	75	100	**0.001**
neutral	5	6.8	0	0.0	
augmentation	4	5.4	0	0.0	
Average depth (AD_R)					
reduction	59	79.7	71	94.7	**0.009**
neutral	10	13.5	4	5.3	
augmentation	5	6.8	0	0.0	

Figure 4.9 shows one patient from group R-C who did not undergo skin thickening enough to make the presence of the veins more inconspicuous. However, the present study detected enhancement of the thickness of the periorbital skin in patients treated with the cosmeceutical containing GFs. Objective measurements and clinical examination confirmed this secondary outcome. The $Rgh_{R\text{-}C}$ ∂ reduction was 8.3%, and the ∂ reduction of $AD_{R\text{-}CGF}$ was 5%.

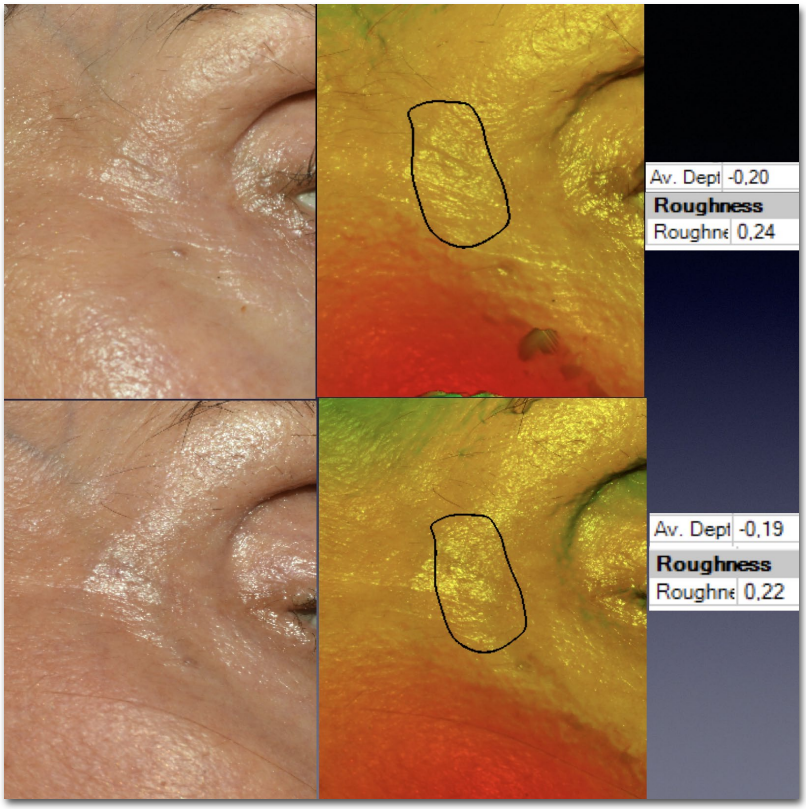

Figure 4.9: The two- and three-dimensional pictures of a 68-year-old patient subjected to LAM with vitamin C. Data on the right were collected by the 3D SPM on the 90th day post-procedure and concern the relief of the periorbital vein.

The significant improvement of the skin quality in patients treated with GFs (group R-CGF) is exemplified by Figures 4.10 and 4.11. The after-laser skin resurfacing neocollagenesis was enhanced in the group receiving GFs. In contrast with the patients in group R-C, Figure 4.10 shows the concealment of protuberant vessels in a patient from group R-CGF. The roughness of the area containing the prominent, temporal superficial veins reduced from 0.35 to 0.1, which corresponded to Rgh_R ∂ reduction of 71.4%. The wrinkle selected for analysis showed a simultaneous reduction of AD_R (from -0.11 to -0.06) and Rgh_R (from 0.2 to 0.11) of 90%. Patient in Figure 4.11 was treated with GFs (group R-CGF). The data displayed on the right support the clinical observation of the improvement of the skin surface of the periorbital area of a 70-year-old patient. The ∂ reduction of the $Rgh_{R\text{-}CGF}$ was 22.22%, and the ∂ reduction of $AD_{R\text{-}CGF}$ was 93.75%.

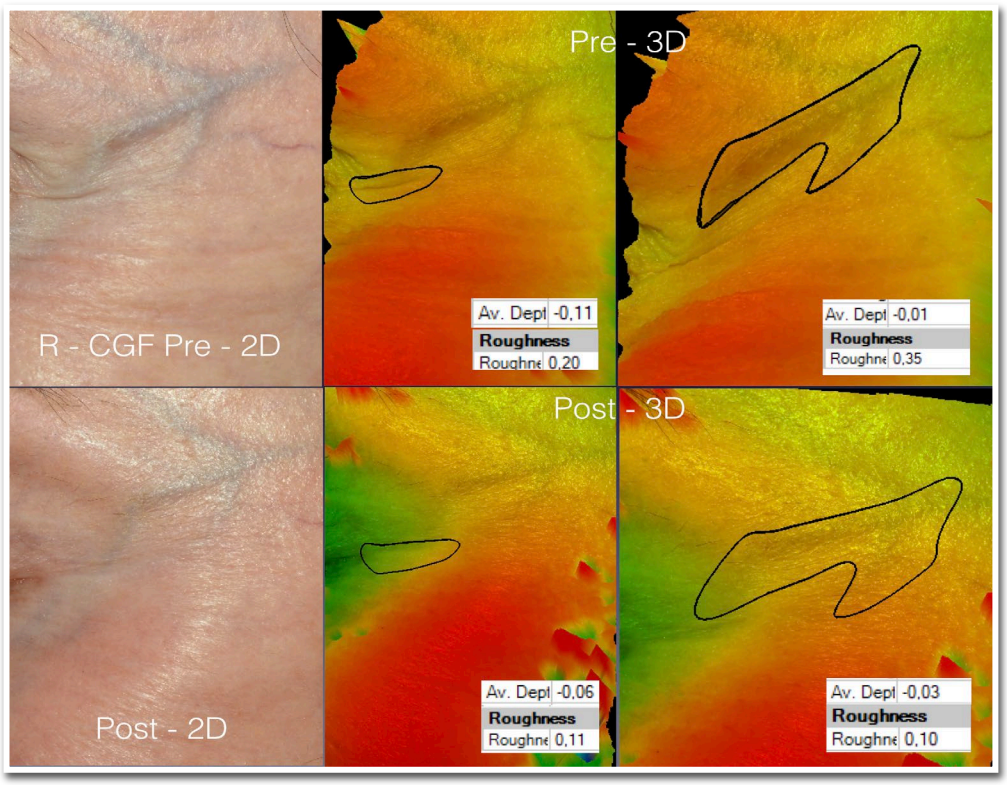

Figure 4.10: Pictures of a 66-year-old patient subjected to LAM with vitamin C and the cosmeceutical containing GFs. The post-procedure images were obtained on the 93rd day. The centre photographs display the measurements concerning the periorbital wrinkle. On the right, the prominent, temporal superficial veins became less visible after the treatment.

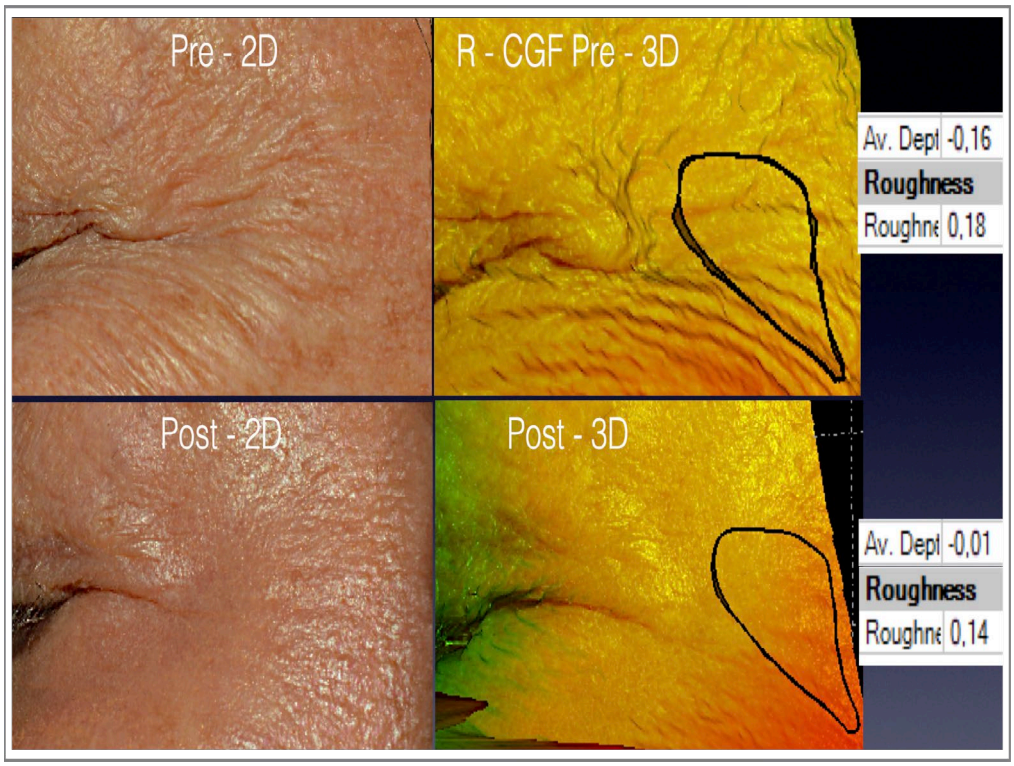

Figure 4.11: The pictures of a 70-year-old patient subjected to LAM with vitamin C plus the cosmeceutical containing GFs. The images were obtained on the 95th day post-procedure. A contour was drawn to illustrate the modification of skin roughness inside the design.

4.5 Discussion

As the cutaneous blood flow receives up to one-third of the circulating blood volume, this is a major concern related to LAM's theoretical risk of inducing systemic toxicity (Tsakovska et al., 2017), especially when the drug is applied over larger skin areas (Haedersdal et al., 2016). Clinical trials are of paramount importance to confirm the efficacy and safety of LAM (Aldag et al., 2016; Wenande et al., 2019), because *ex vivo* studies neglect the dynamic, dermal blood flow (Sklar et al., 2014), whereas the tissue vascularisation may be responsible for the absence of drug saturation *in vivo*. Furthermore, *in vitro* experiments do not replicate the ideal conditions for investigating skin drug penetration and do not provide information on treatment outcomes.

Although no adverse toxicity has ever actually been linked to LAM (Ibrahim et al., 2018), these possible occurrences generated apprehensiveness and restrictions of regulatory approval which limited the research and the commercialisation of active delivery products (Murphy & Carmichael, 2000; Watkinson 2013).

To investigate the possible drug absorption into the circulation via the laser-induced microchannels, Wenande et al. (2018) performed a 30–60-minute application of cisplatin and 5-fluouracil over a large skin surface area (112 cm^2) after CO_2 laser treatment. Neither substance was detected in the plasma samples taken hourly from 0 to 5 h, or at 48 and 120 h (Wenande et al., 2018). In this research, patients in both study groups, R-C and R-CGF, have been subjected to LAM in an area relatively bigger (full-face skin resurfacing), the findings coincided with that paper, and no adverse cutaneous reaction or systemic toxicity was registered.

The direct exposure of the underlying dermis and its vasculature to the outside environment carries some risk of bacterial infection, and this risk increases when drugs are applied (Ibrahim et al., 2018). Under ideal conditions, sterile products should be preferred. Although vitamin C used in this study was sterile, the cosmeceutical applied was not available as such. Even so, both study groups, R-C and R-CGF, did not exhibit local infection, whether bacterial or fungal. This may be explained by the high immunological proficiency of the skin because the cutaneous immune system elicits well-coordinated cell-mediated and humoral immune reactions after recognising potentially harmful agents (Basler et al., 2016; Sklar et al., 2014; Haedersdal et al., 2016).

On the other hand, these immunological reactions may include drugs enclosed in targeted delivery vehicles, and this responsiveness can lead to skin sensitisation (irritant dermatitis) and allergic contact reaction (Wiedersberg & Guy, 2014; Alves et al., 2015). Skin sensitisation to a drug is an adverse toxicological endpoint that is influenced by the

drug permeability, molecular weight (MW), frequency of exposure, and individual variation. In regular pharmaceutical formulations, the most common allergens have MW under 500 Dalton, and contact dermatitis may occur after previous single exposure, or even years of continuous exposure (Alves et al., 2015; Murphy & Carmichael, 2000; Ibrahim et al., 2018). Although skin sensitisation and granuloma formation have been reported after topical application of a serum containing vitamin C (Alegre-Sanchez et al., 2018; Soltani-Arabshahi et al., 2014), the present study detected high tolerability to the topically applied substances. The absence of cutaneous reactions may have accrued from the absence of toxicity related to vitamin C and the high MW of the GFs contained in the cosmeceutical. Furthermore, the cutaneous exposition to the topical medication was restricted to one session.

In 2018, Badawi & Osman published one of the few reports involving human subjects to confirm the efficacy of LAM. They performed a comparative study involving six sessions of laser-assisted transcutaneous delivery of hydroquinone in 30 female patients with bilateral melasma. One hemiface received hydroquinone only, and the other underwent laser-assisted delivery of hydroquinone. The interval between the Er: YAG laser sessions was 15 days and the hemiface treated with LAM exhibited a significant decrease in the degree of pigmentation ($p < 0.005$) compared to the side treated with the hydroquinone only, according to a 4-point clinical scale. Despite the quality of that report, the multiple laser sessions may have impaired a proper analysis of the results. To avoid this important source of bias, the present research involved one laser treatment session only, and the same protocol was applied to all patients. The laser protocol proved efficient and promoted drug penetration of macromolecules (GFs and cytokines). This inference has been supported by statistical analysis owing to the fact that the group receiving growth factors presented better results than the control group, which was medicated with vitamin C only. The ∂ reduction of the skin roughness was 18.8% in group R-C compared to 45% in group R-CGF. The ∂ reduction of the average depth of the wrinkles in group R-CGF was significantly higher (62.5%) than in group R-C (33.3%) ($p < 0.01$) (Table 4.3).

Laser fluence (energy output), density setting, pulse repetition (the number of times that the laser hits the target tissue) and the pulse duration influence the laser-tissue-drug interaction and consequent drug delivery and biodistribution. Comprehensive reviews on the fundamentals of fractional LADD reinforced the importance of establishing reproducible laser settings (Alegre-Sanchez et al., 2018; Wenande et al., 2019). This has been reported by Jacques et al. since the inception of LADD and several authors thereafter (Jacques et al., 1987; Banzhaf et al., 2019; Haedersdal et al. 2016; Disphanurat et al., 2020; Sklar et al., 2014; Hsiao et al., 2012).

The laser employed in this study (Er:YAG laser Starlux® Palomar 500; wavelength 2.940nm) provides dual pulse mode, a short one (0.25 ms) that targets cutaneous ablation and a long pulse (5 ms) that leads to tissue coagulation and skin contraction (Mattos et al., 2009). The blue optics scans with a spot size of 6 x 6 mm^2 and produces densities of 169 vertical microperforations (microbeam size: 100 –140 μm) per pass (Mattos et al., 2009; Genina et al., 2013), or yet, 469 microperforations per cm^2. Considering that 1 cm^2 has 100,000,000 μm^2, one laser pass with the blue optics performs a total area of 56,280 μm^2 of microperforations or a density of approximately 5.6%.

Several publications demonstrated that drug accumulation in skin stabilized when low densities up to 5% were reached and that the use of higher densities led to significant reductions in both intra- and transcutaneous delivery per single MTZ (Haak et al., 2012; Banzhaf et al., 2019; Ibrahim et al., 2018; Sklar et al., 2014). Although a comparison between different treatment densities was not the goal of this research, the positive results obtained with the average density of 5.6% corroborate that this density is also linked to improved clinical outcome.

In addition, by setting the laser to 250μs and 9 mJ/cm^2 (mJ/μb) for the short pulse and the long pulse to 8mJ/μb with a duration of 5 ms, a single laser pass yielded a skin surface ablation of 20 to 160 μm and produced vertical coagulation microchannels of 70 – 300 μm depth (on average, 70 – 100 μm) (Alexiades-Armenakas et al., 2012; Bay et al., 2017; Ganceviciene et al., 2012; Genina et al., 2013).

Despite the fact that the thickness of the skin and the age of the patient can interfere with the microchannel depth (Wenande et al., 2019), the laser action was restricted to four passes (four pulse repetitions) over the same skin surface area because the target chromophore (water) is increasingly reduced after each pass. This decision was supported by previous research, which confirmed that performing more than four laser passes on the skin surface increases the risk of thermal injury and enhances neither the drug uptake nor the effectiveness of the treatment (Sklar et al., 2014; Taudorf et al., 2014; Hsiao et al., 2012).

To establish LAM standards, researchers must consider not only the laser settings but ultimately the final microchannel morphology, because this variable can be transferred to any patient and will not be restricted to a specific laser device (Wenande et al., 2019). The high ultrapulsed energy delivered by the Er: YAG laser used in this research produced a lateral RTD of 20–35 μm. The small RTD may have been responsible for the increase in drug penetration because the laser-mediated thermal effect permits for

accentuated molecular motion and consequent cutaneous permeation of the topical medication towards the MTZs (Lee et al., 2014; Munch et al., 2017; Bay et al., 2017; Alegre-Sanchez et al., 2018; Ibrahim et al., 2018). In addition, the heat produced by the laser can reduce the epidermal enzymatic activity (Pyo & Maibach, 2019).

The laser settings can be correlated with other lasers to produce similar MTZs, and support professionals to perform equivalent treatments or to extend research towards the investigation of suitable medications and their ideal concentration in formulae.

As nano and microparticles have been reported to efficiently penetrate the skin up to depths of 230 μm after AFLX treatment, and have remained in the dermis for longer than one month (Genina et al., 2013), the time-lapse concerning the drug bioavailability must also be evaluated in future studies to establish if the therapeutic window for the topical delivery of medication can be extended. As vitamin C undergoes dietary influences and GFs are endogenously produced, tests to confirm the length of the bioavailability of these substances over the time are subjected to critical bias.

The time lag before applying the medication is an important aspect to be observed because the spatiotemporal closure of AFXL-induced channels occurs within 24 - 48 hours after laser exposure (Banzhaf et al., 2015; Banzhaf et al., 2017). Group R-C and R-CGF underwent transcutaneous medication during the first 30 minutes post-procedure, after gentle skin cleansing. Even though any residual disruption of cutaneous layers can still be observed three weeks after LSR (Haedersdal et al., 2016; Shashi et al., 2012; Amini-Nik et al., 2018), this standardised 30-minute period was recently confirmed as the optimal interval for LAM (Alegre-Sanchez et al., 2018; Wenande et al., 2017) because the dermis can quickly become inaccessible owing to the accumulation of debris, fibrin, inflammatory mediators, and keratinocytes inside the microchannels (Ibrahim et al., 2018). Furthermore, progressive swelling in the treated areas was observed from minutes to one hour after laser application (Figure 3.1), and this oedema can act as a mechanical limiting to the additional drug uptake as it compromises the lumen of the microchannels.

The increase in the skin thickness observed in the present research corroborates the study of Ono, who reported the cover-up of some superficial blood vessels in the dorsum of the hands of human subjects after an intradermal injection of GF (βFGF) (Ono, 2011).

The positive results obtained with this study confirm the efficiency of the protocol concerning laser parameters and allowed for establishing some guidelines:

- Performing more than four laser passes over the target increases risks and do not provide better results;
- To reduce the risk of infection, the vehicle should be sterile because the drug will be put into direct contact with inner layers of the skin and can eventually reach the bloodstream;
- Drugs approved for intravenous use are usually water-soluble, which makes them suitable to be part of a LAM.
- LAM enhances the uptake of hydrophilic compounds more efficiently than lipophilic agents; the use of higher densities while lasing the skin do not enhance the bioavailability of hydrophilic and lipophilic substances;
- To limit bioabsorption, the concentration and safe therapeutic dosage of the drug must be observed, and the size of the treatment area must be restricted;
- It is advisable to clean the skin before applying the substance so that debris, corneocytes and serosanguineous collection will not prevent the drug from penetrating the microchannels;
- Because of (i) the quick spatiotemporal closure of AFXL-induced channels, (ii) the decline of drug uptake in a short time frame, and (iii) the increased swelling in the treated area, the delivery of transcutaneous medication should ideally occur during the first 30 minutes post-procedure.

4.6 Conclusion

Laser skin resurfacing is a therapeutic modality that can deliver thermal energy to a skin surface to reduce wrinkles, and improve skin tone, texture and pigmentation. The collimation of the laser light on the surface of skin produces microchannels into the dermis at a homogeneous depth, irrespective of the irregularity of the wrinkles. By interrupting the integrity of the SC, AFXLs reduce the diffusional path length (membrane thickness) and the superficially applied drug fills the laser channels and penetrates towards the dermis. However, there is a theoretical risk of inducing systemic toxicity because an unknown amount can reach the bloodstream.

Analytical techniques and mathematical models do not provide accurate data concerning the drug bioavailability and penetration with respect to LAM because (i) the laser-tissue interaction, (ii) the blood flow, (iii) dietary intake and/or endogenous production of substances, and (iv) the complex, new surface area and geometry of the laser-induced microchannels impair these calculations.

The findings obtained in this study confirm that LAM consisting of the application of vitamin C and a cosmeceutical containing GFs provided significantly better results in

reducing skin wrinkles and dermal thickening than vitamin C alone. LAM with vitamin C and GFs has proved to be safe and effective, and there were no cutaneous reactions or adverse systemic reactions to either of the LAM substances.

The considerably higher positive therapeutic response of patients in the group treated with GFs indicates that (i) these substances were directly delivered to the dermis to exert their bioactive effect, (ii) bypassing the epidermis protected the GFs from enzymatic action.

Chapter 5

A Prospective, Randomised, Double-Blind, Comparative Clinical Study on the Effect of Laser-Assisted Medication (LAM) on Scars

5.1 Introduction

Alterations or disruptions affecting the molecular, intercellular communication signalled by GFs and cytokines pathways can result in permanent, and often unsightly, scars (Figure 5.1). The scar tissue is composed of thin collagen fibres and inelastic fibrous tissue lacking skin appendages (hair follicles and sebaceous glands). The scar does not exhibit the flexibility or strength of the original tissue (Boateng et al., 2008).

Figure 5.1: Unaesthetic scars on the left temporal area and the left hand of a 26-year-old female patient who underwent severe burn injuries.

Patients usually seek scar treatment to achieve aesthetic improvement and to relieve pain, itching or functional restriction. Apart from a wide variety of over-the-counter products that claim to improve scarring, the therapeutic armamentarium includes creams and massage therapy, cosmetic camouflage, compression therapy, topical silicone gel, dermabrasion, microneedling, early surgical intervention possibly followed by immediate radiation therapy, injection of fat into the scar tissue and cryotherapy (Amini-Nik et al., 2018). Current approaches have shown moderate efficacy in reducing or preventing scar formation. Ideally, treatments should prevent scarring as opposed to simply managing scar symptoms.

Laser therapy has become the standard of care in many burn centres because it is safe and effective in treating scars (Qu et al., 2012). The advantages of using laser therapy include increasing the pliability of the scar, decreasing scar volume and height, reduced pain, and improvement of colour and textural properties (Haak et al., 2012; Braun et al., 2016). The collagen fibres reorganise into a relatively normal, more orderly and parallel arrangement after laser treatment (Amini-Nik et al., 2018). Histologic findings post-laser treatment of scars show changes in the upper dermis with newly formed dermal papilla. Functionally, this improvement was represented by amelioration of skin surface roughness and skin tension (Lee et al., 2016 b).

AFXLs produce uniform microperforations into the dermis, irrespective of the scar contour and reproduce both a physical and thermal trauma on the skin surface in a controlled, very superficial manner. The response of the skin to the aggression will be minimal but will involve the same signalling pathways (GFs) described earlier in the phases of wound healing (Amini-Nik et al., 2018) (Chapter 1, item 1.3.2- Scars).

Pharmacological interventions that influence the molecular and biochemical activity of GFs have proved to exert a therapeutic benefit to scarring and skin senescence (Erlich et., 2006; Ono, 2011; Aldag et al., 2016; An et al., 2013; Park & Kyobum, 2017). However, GFs poorly penetrate the skin because they are hydrophilic proteins composed of hundreds of amino acids with a molecular size larger than 15000 Da. The direct introduction of GFs inside the dermis can enhance their bioavailability because these molecules can be quickly nullified inside the human skin due to epidermal proteolytic cleavage (Gainza et al., 2015; Koria, 2012).

The present clinical study performed in human volunteers investigates the use of laser-induced microchannels to effectively deliver GFs and/or vitamin C to scars and measure any therapeutic effect.

5.2 Study objectives

The objectives of this double-blind, randomised clinical trial were:

- To obtain scar inconspicuousness by reducing its roughness and/or volume;
- To quantify and compare the impact of using vitamin C (Vitasantina®) alone or associated with growth factors contained within a cosmeceutical (TNS Recovery Complex®), on a scar after Er:YAG laser resurfacing.

5.3 Material and methods

This prospective, double-blind, randomised study was approved by the Brazilian Ethics Committee and by the FREP at Anglia Ruskin University. Participants received a comprehensive explanatory information sheet about the research and signed a consent form to engage in the study.

5.3.1 Patients' demographics

All suitable patients requesting scar improvement were invited to participate in the study:

- Fitzpatrick skin types I to IV patients;
- 18 to 70 years old.

The following patients were excluded:

- patients who were not available for the follow-up visits;
- patients with unrealistic expectations;
- patients with a history of recent cutaneous allergies, chronic dermatitis or those taking anti-inflammatories or any other drug known to interfere with the healing processes;
- patients subjected to topical application or intradermal injections of corticosteroid within 6 months pre-treatment in the area to be treated.

5.3.2 Randomisation and treatment

The recruitment of participants took place between September 2018 and September 2019. A total of 132 patients met the inclusion criteria and were included in this study.

On the day of the treatment, all enrolled patients signed the consent form. They were screened with the 3D camera and the anaesthetic ointment was applied on the skin surface for 30 minutes. As mentioned in Chapter 1 (section 1.10.1), before entering the treatment room, each patient picked a paper from a container indicating the description of the treatment to be delivered by the researcher's assistant. Therefore, the participants were randomised either into a GFs plus vitamin C treatment group (group DS-CGF) or a no-GFs vitamin C only control group (group DS-C). Both the researcher and the patient were unaware of the randomised treatment given (double-blind study). Both study groups had one session of fractional ablative laser treatment. The medications were chosen according to the criteria described in Chapter 4 (section 4.1.5). Patients were followed-up at 3 months between January 2019 and January 2020.

5.3.3 Study design

All patients were photographed with the same 3D-SPM system (LifeViz^{TM} Micro) validated in Chapter 2. A laser tape measure was used to define selected and consistent anatomical landmarks across the topography of the scar. After photographic documentation, an anaesthetic ointment composed of lidocaine 7% and tetracaine 7% was topically applied to the targeted areas for 30 minutes.

After skin cleansing, all patients were subjected to one-session of fractional ablative laser treatment by the researcher (Starlux® 500 Palomar Inc., Burlington, MA). Standardised laser parameters were used for all patients, as presented in Table 3.1 (Chapter 3 section 3.2.2.1) regardless of the scar elevation.

After the laser treatment, the scar was cleaned to remove any blood clots and debris. The researcher's assistant applied the chemical substances according to the branch of the study. The doses applied were 200 mg of vitamin C in patients from group DS-C, in the form of a 2 ml aqueous, sterile solution plus 1 ml of the cosmeceutical containing

growth factors (serum solution) in patients from group DS-CGF. The medications were kept on the scar surface under occlusion for 30 minutes.

No anti-herpetic viral prophylaxis was prescribed. Both patient groups were instructed to clean the treated area with a saline solution once a day, and to cover the scar with dexpanthenol (Bepantol® - Bayer) four times a day until the cutaneous debris have entirely disappeared. Dexpanthenol is a derivative of pantothenic acid, which is a component of the B complex vitamins. Dexpanthenol was applied to all patients as a sole adjuvant as it acts as a skin protectant and moisturiser.

Photographs of the scar post-treatment were taken at a consistent angle, position and background lighting as the pre-treatment images. As described in Chapter 2 (section 2.3.4.1), the images were then transferred to the software, Dermapix® and synchronised to compare the same cicatricial area pre- and post-procedure. A contour comprising the scar area exhibiting significant surface irregularity was drawn in the pre-procedure image and replicated to the post-procedure image. Next, the 3D reconstruction was executed. The contour designed in the 2D photographs was transposed to the 3D images. The reference value, sigma, was displayed and constrained to value 10 in all patients. The software automatically calculated the measurements related to scar volume (V_{DS}) and scar roughness (Rgh_{DS}) contained within the limits of the marked area being investigated. Data from individual patients were transferred to a spreadsheet.

5.3.4 Statistical analysis

Data obtained via the Dermapix® software were analysed by the program SPSS IBM (Version 26.0 IBM Corp© for Mac, Armonk, New York, USA). Tests were applied to compare and correlate scar volume (V_{DS}) and scar roughness (Rgh_{DS}), pre and post-procedure. The objectives were to compare the efficacy of each treatment regimen and to confirm if there was a significant difference in the Rgh_{DS} and V_{DS} measurements between the two groups, DS-C and DS-CGF. The criterion for determining significance was set at 5% to all statistical tests; findings were considered significant with a *p*-value < 0.05 and very significant with a *p*-value <0.01. The descriptive analysis presented the data in the form of tables and illustrative graphics. The histograms concerning the population distribution in each group were displayed ahead.

The Shapiro-Wilk test showed that data were not normally distributed and were summarised by quartiles (median, IQR, minimum and maximum). The interquartile range (IQR) is a measure of dispersion that contains 50% of the observations (interquartile range) between the limits that correspond to the 1st quartile (25th percentile) and the 3rd quartile (25th percentile). The non-parametric Wilcoxon signed-rank test evaluated the

difference between the pre- and post-procedure data to measure the parameter variability and Spearman *rho* was used for correlation between scar volume (V_{DS}) and roughness (Rgh_{DS})in each study group. Additionally, the Mann-Whitney U test and the corresponding descriptive level (*p*-value) were calculated by comparing both study groups.

5.4 Results

In both groups, crusting lasted around 18 days, and complications, such as post-treatment hypochromia and cutaneous reactions were not verified. As with the literature, no adverse reactions related to cutaneous use of vitamin C, GFs and the cosmeceutical medium used in this research was documented.

5.4.1 Group DS-C

Statistical tests compared the pre- and post-procedure measurements regarding V_{DS} and Rgh_{DS} comprising the cicatricial tissue. The histograms in Figure 5.2 demonstrate that the data were not normally distributed.

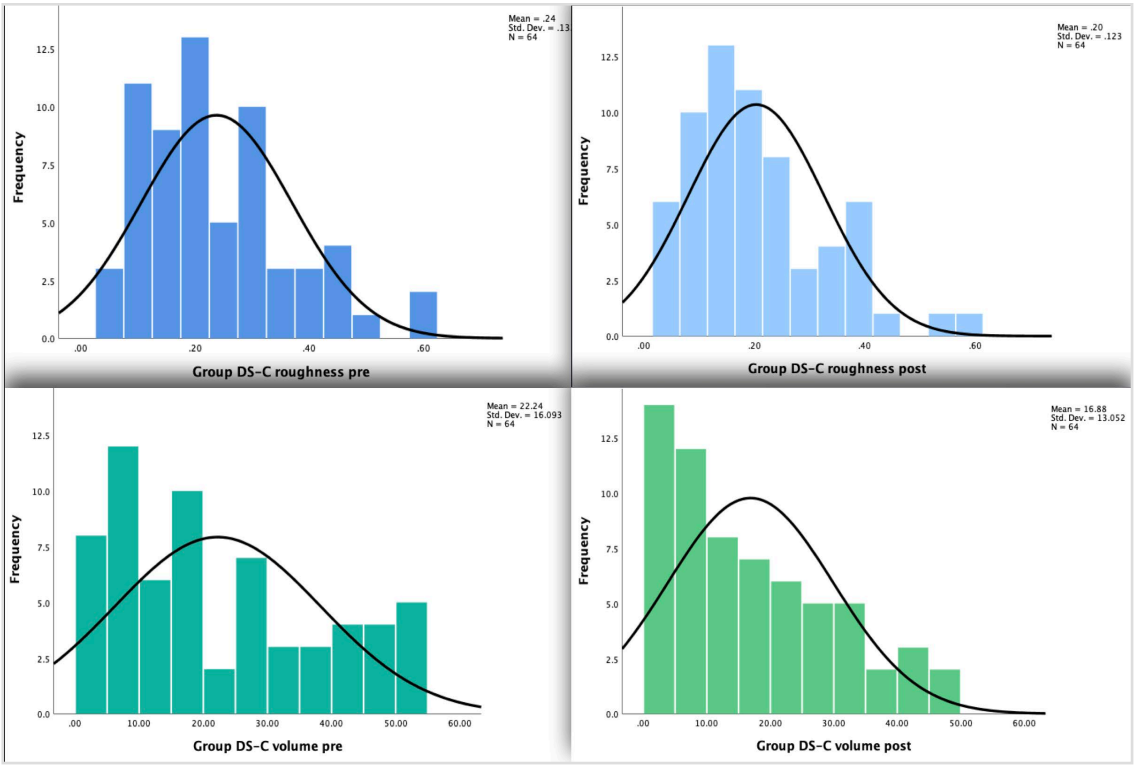

Figure 5.2: Histograms representing the population distribution related to the variables scar roughness and volume in group DS-C. Data distribution were skewed and non-parametric tests were used.

Of the 132 patients enrolled in group DS, 64 patients composing group DS-C were treated with LAM followed by topical application of vitamin C. A total of 62 patients were properly followed up and two patients were documented on day 118. Participants were aged from 19 to 62 years (median 39 years and IQR 29.5 – 44.8 years-old); 53 patients

(82.8% of the cases) were female. The median scar age pre-study was 6 months (IQR 4 – 11.8 months).

In group DS-C, Rgh_{DS} decreased in 81.3% of the patients, whereas 92.2% of the patients presented V_{DS} reduction. The Wilcoxon signed-rank test has shown statistical significance for both variables ($p < 0.01$). The pre-procedure Rgh_{DS} median was 0.21 (IQR: 0.13 – 0.32) compared to 0.18 (IQR: 0.1 – 0.28) post-procedure. The median V_{DS} was 17.3 mm^3 (IQR: 8.3 – 35.1 mm^3) pre-procedure compared to 14.4 mm^3 (IQR: 6 – 27.8 mm^3) post-procedure. The variation between the pre- and post-procedure (∂ reduction) concerning the scar volume (V_{DS}) and scar roughness (Rgh_{DS}) was calculated by the formula:

$$\text{Percentage of parameter modification } (\partial \text{ reduction}) = \frac{(\text{pre - post measure})}{\text{pre-measure}} \times 100$$

The median concerning Rgh_{DS} reduction was 13.3% (IQR: 3.5 – 25%) and the median concerning V_{DS} reduction was 20.5% (IQR:11.4 – 36.4%). Mean and SD are also displayed in Table 5.1.

Table 5.1 - Descriptive analysis of the variables (roughness and volume) in group DS-C (control group, treated with vitamin C) (n= 64)

	Pre-procedure					Post-procedure					WRT
Variable	**Mean ±SD**	**Median**	**IQR**	**Min**	**Max**	**Mean ±SD**	**Median**	**IQR**	**Min**	**Max**	***p*-value**
Rgh_{DS}	0.24 ± 0.13	0.21	0.13 – 0.32	0.05	0.62	0.2 ± 0.12	0.18	0.1 – 0.28	0.04	0.57	**<0.01**
V_{DS}	22.2 ± 16.1	17.3	8.3 – 35.1	0.4	53.1	16.9 ± 13.1	14.4	6.0 – 27.8	0.4	48.6	**<0.01**
Rgh_{DS} ∂ reduction						14.5 ± 20.6	13.3	3.5 – 25.0	-78.3	57.6	n/a
V_{DS} ∂ reduction						23.3 ± 22.0	20.5	11.4 – 36.4	62.1	71.3	n/a
Simultaneous computation of V_{DS} and Rgh_{DS} ∂ reduction						35.0 ± 37.4	37.8	18.9 – 59.6	-90.9	115	n/a

IQR: interquartile range (25^{th} - 75^{th} percentiles); Min: Minimum: Max: Maximum; n/a : not applicable; WRT: Wilcoxon rank test; ; ∂ reduction is in percentage; V_{DS} is measured in mm^3

5.4.2 Group DS-CGF

Of the 132 patients enrolled in group DS, 68 patients comprising group DS-CGF were reviewed at follow-up. Participants were aged from 19 to 68 years, with a median of 52 years-old (IQR 39.0 – 58.0 years-old). Fifty-seven patients (83.8% of the cases) were female. The median age of scars pre-study was 7.0 months (IQR 5 – 10.8 months). Figure 5.3 illustrates data distribution in group DS-CGF.

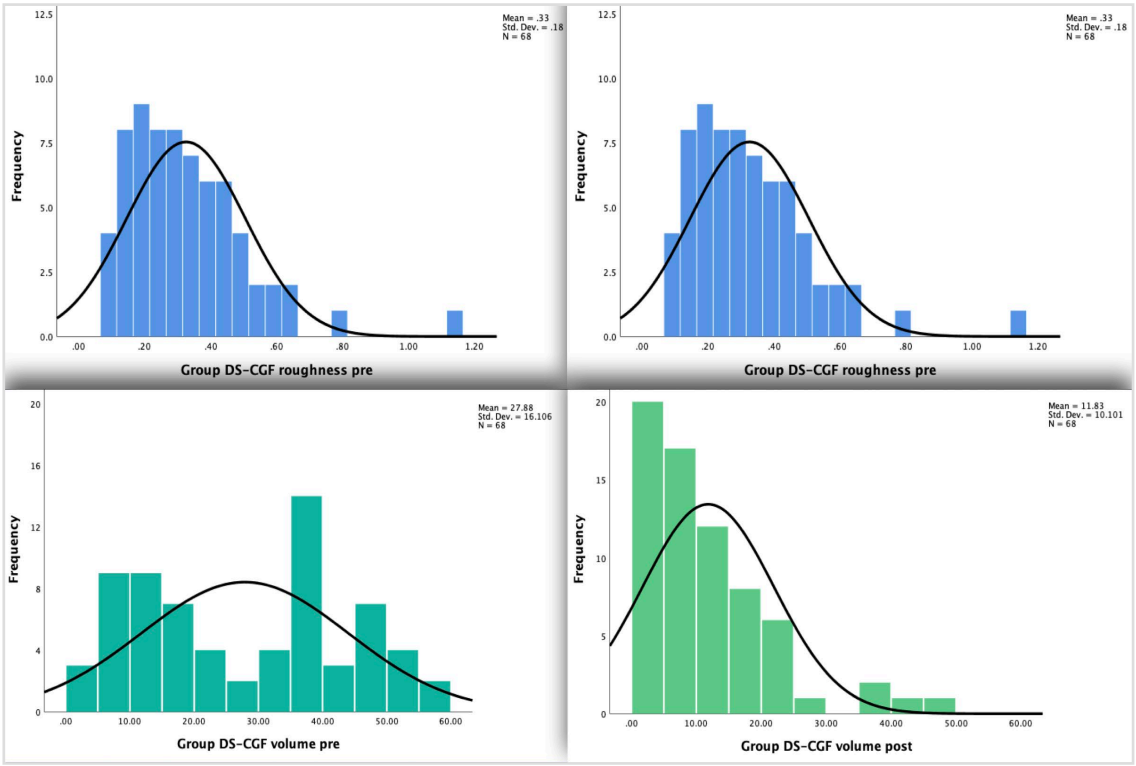

Figure 5.3: Histograms representing the data distribution concerning the variables scar roughness and volume in group DS-CGF. Data were skewed and non-parametric tests were applied.

Both $Rgh_{DS\text{-}CGF}$ and $V_{DS\text{-}CGF}$ decreased in 98.5% of the cases. The Wilcoxon signed-rank test confirmed statistical significance for the reduction concerning both parameters ($p < 0.01$). The pre-procedure Rgh_{DS} median was 0.3, with an IQR of 0.19 – 0.42 compared to 0.17 with an IQR of 0.12 – 0.23 post-procedure. The V_{DS} median was 28.8 mm^3 with an IQR of 11.8 – 39.9 mm^3 pre-procedure compared to 8.3 mm^3 with an IQR of 4.5 – 17.1 mm^3 post-procedure (Table 5.2).

Table 5.2 - Descriptive analysis of the variables roughness ($Rgh_{DS\text{-}CGF}$) and volume ($V_{DS\text{-}CGF}$) in group DS-CGF (n= 68)

	Pre-procedure					Post-procedure					WRT
Variable	**Mean ±SD**	**Median**	**IQR**	**Min**	**Max**	**Mean ±SD**	**Median**	**IQR**	**Min**	**Max**	***p*-value**
Rgh_{DS}	0.33 ± 0.18	0.30	0.19 – 0.42	0.09	1.12	0.19 ± 0.11	0.17	0.18 – 0.23	0.06	0.60	**<0.01**
V_{DS}	27.9 ± 16.1	28.8	11.8 – 39.9	2.90	58.3	11.8 ± 10.1	8.30	4.5 – 17.1	0.4	47.4	**<0.01**
Rgh_{DS} ∂ reduction						37.5 ± 18.8	36.0	24.4 – 53.8	-3.6	75.5	n/a
V_{DS} ∂ reduction						56. 2 ± 23.4	54.9	40.7 – 74.0	-8.9	98.8	n/a
Simultaneous computation of V_{DS} and Rgh_{DS} ∂ reduction						93.7 ± 35.5	89.0	71.8 – 118.4	12.4	157	n/a

IQR: interquartile range (25^{th} - 75^{th} percentiles); Min: Minimum: Max: Maximum; n/a : not applicable; WRT: Wilcoxon rank test; ∂ reduction is in percentage; V_{DS} is measured in mm^3

The mean of $Rgh_{DS\text{-}CGF}$ ∂ reduction was 37.5 ± 18.8% and of $V_{DS\text{-}CGF}$ ∂ reduction was 56.2 ± 23.4%. The mean of 93.7 ± 35.5% related to the simultaneous computation of ∂ reduction of the parameters Rgh_{DS} and V_{DS} represented the visual scar relief improvement.

5.4.3 Clinical case examples

5.4.3.1 Group DS-C

Figures 5.4 and 5.5 illustrate clinical cases pertaining to group DS-C, treated with LSR followed by topical application of vitamin C.

The scars in Figure 5.4 resulted from trauma on the right hemiface occurred 8 months before the treatment with LAM with vitamin C. Patient in Figure 5.5 underwent an abdominoplasty 13 months before the LAM.

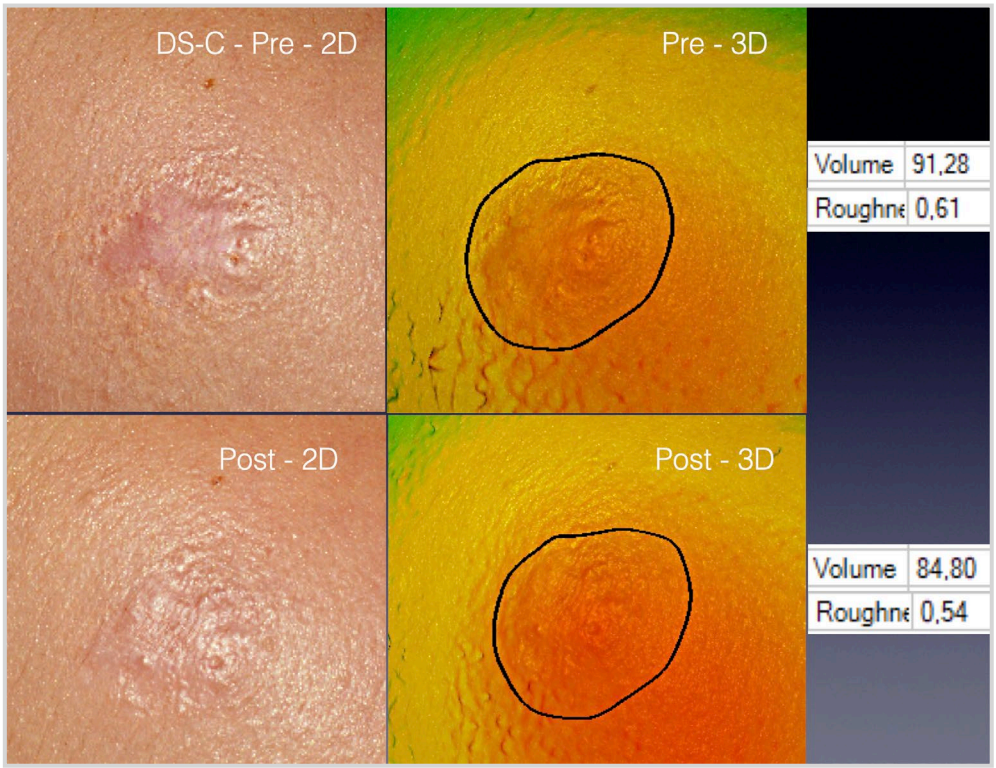

Figure 5.4: Two- and three-dimensional pictures of a 22-year-old patient. The readouts were provided by the 3D SPM system on the 90th day after the procedure. The ∂ reduction was 11.5% for $Rgh_{DS\text{-}C}$ (from 0.61 pre-procedure to 0.54 post-procedure) and 7% for $V_{DS\text{-}C}$ (from 91.29 mm^3 to 84.8 mm^3).

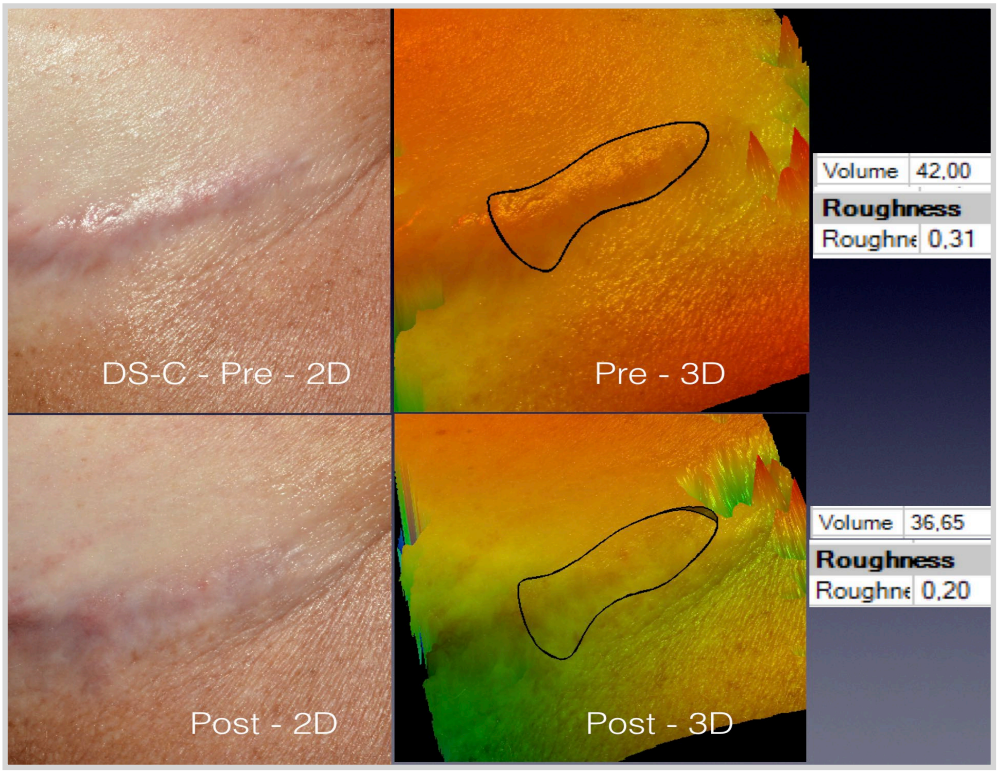

Figure 5.5: Pictures of a 32-year-old patient subjected to LAM with vitamin C. Data displayed on the right were obtained on the 94th day. The ∂ reduction of $Rgh_{DS\text{-}C}$ was 35%, whereas $V_{DS\text{-}C}$ decreased by 12.7%.

5.4.3.2 Group DS-CGF

Figures 5.6 and 5.7 illustrate clinical cases pertaining to group DS-CGF.

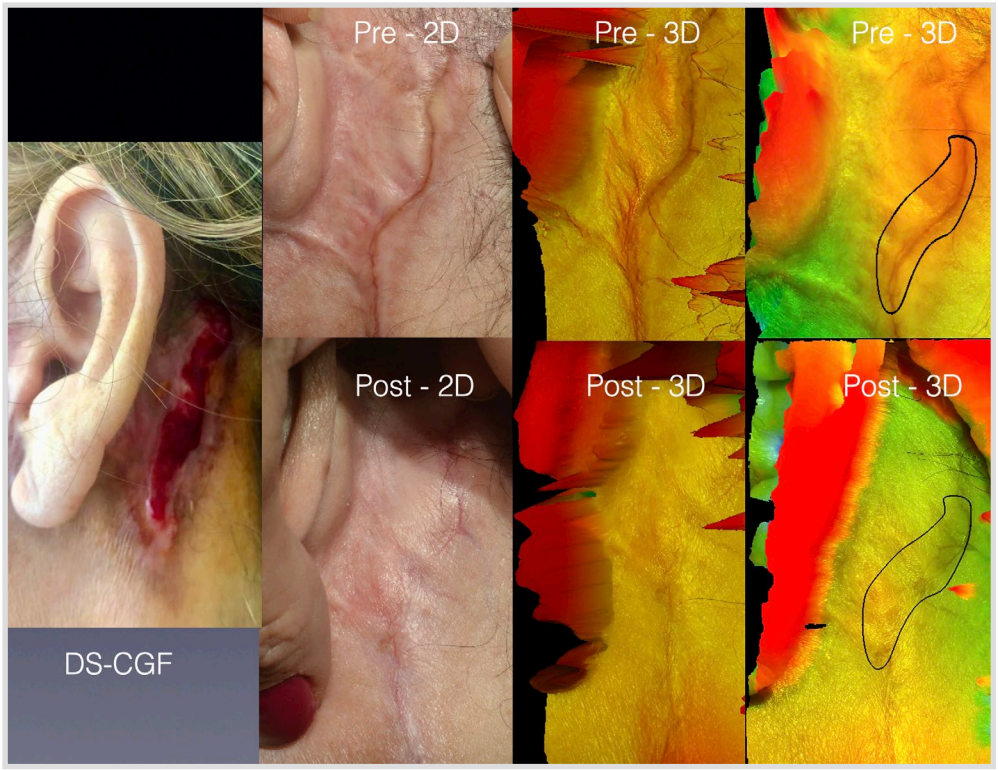

Figure 5.6: The pictures of a 63-year-old patient exhibiting a scar resulting from a retroauricular flap necrosis post-facelift 6 months before. The scar improvement was confirmed by the photographs on the centre and

the data provided by the 3D SPM system on the 97th day post-procedure. The drawn contour in the pictures on the right showed that the ∂ reduction of VDS-CGF was 61% and RghDS-CGF decreased by 42.5%.

Figure 5.6 demonstrates improvement in the appearance of a sinuous vessel, which was also seen in other patients of group R-CGF, as described in Chapter 4 (section 4.3.3.3).

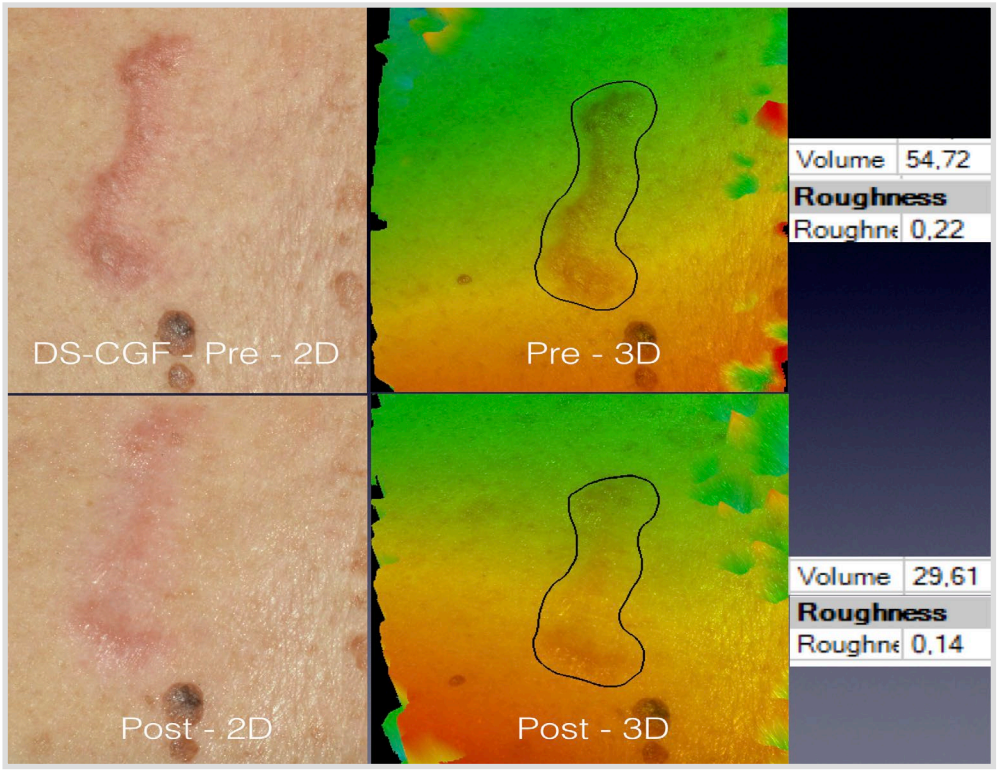

Figure 5.7: A 53-year-old patient presenting a hypertrophic scar after lumpectomy (removal of breast nodulation) performed 16 months before LAM. Data obtained on the 90th day showed that the ∂ reduction of VDS-CGF was 46% and the RghDS-CGF decreased by 36%.

5.4.3.3 Comparison between groups DS-C and DS-CGF and correlation of the research findings with published studies

Table 5.3 shows the population distribution in terms of scar classification, aetiology, skin type according to Fitzpatrick classification and the treated scar area. The area of treatment of the scars varied from 4 to 35 cm^2. The smallest scars were located mainly on the face while the largest ones were verified on the abdomen.

Table 5.3 - Distribution of study groups concerning scar classification, scar aetiology, Fitzpatrick skin type and scar area

	Group DS-C		Group DS-CGF	
Scar Classification				
	n	%	*n*	%
keloid	2	3.1	5	7.4
hypertrophic	60	93.8	57	83.8
Atrophic	2	3.1	6	8.8
Aetiology				
	n	%	*n*	%
Burn	2	3.1	5	7.4
Surgical incision	61	95.3	59	86.7
Trauma (car accident)	1	1.6	3	4.4
Healing by secondary intention	0	0	1	1.5
Fitzpatrick Skin Type				
	n	%	*n*	%
I	4	6.2	2	2.9
II	17	26.6	10	14.8
III	41	64.1	47	69.1
IV	2	3.1	9	13.2
Scar area in cm^2				
	n	%	*n*	%
4 - 15	12	18.7	10	14.7
15 - 30	39	61.0	49	72.1
30 - 35	13	20.3	9	13.2

A Mann-Whitney test established a comparison between groups DS-C and DS-CGF. The differences concerning the age of the scars (p = 0.53) and the age of the patients (p = 0.57) were not significant (Table 5.4).

Table 5.4 - Age of the patients and age of the scars: differences between groups DS-C and DS-CGF - Mann-Whitney test

	Group DS-C					Group DS-CGF					MWT
Variable	**Mean ±SD**	**Median**	**IQR**	**Min**	**Max**	**Mean ±SD**	**Median**	**IQR**	**Min**	**Max**	***p*-value**
Age (years)	38.9 ± 11.2	39.0	29.5 – 44.8	19	62	48.5 ± 13.9	52	39.0 – 58.0	20	68	**0.57**
Age of the scars (months)	7.9 ± 5.5	6.0	4.0 – 11.8	2.0	28	7.8 ± 4.1	7.0	5.0 – 10.8	2	17	**0.53**

IQR: interquartile range (25th - 75th percentiles); Min: Minimum: Max: Maximum; MWT: Mann-Whitney U test

Fisher's exact test analysed the categorical variables of gender distribution and anatomical location of the scars to determine any heterogeneity between both study groups (DS-C and DS-CGF) that could have accrued from the randomisation (Table 5.5). The differences between the two groups were not statistically significant. These data added to the results of the Mann-Whitney test confirm that similar conditions were being compared and could have prevented bias accruing from possible heterogeneity between both groups.

Table 5.5 - Group DS - Fisher's exact test

Variable	**Group C** (*n* = 64)		**Group CGF** (*n* = 68)		***p*-value**
Gender	*n*	%	*n*	%	
male	11	17.2	11	16.2	0.87
female	53	82.8	57	83.8	
Anatomical site	*n*	%	*n*	%	
face/neck	20	31.3	23	33.8	0.94
abdomen/flanks	23	35.9	24	35.3	
breast/thorax	21	32.8	21	30.9	

The boxplots in Figure 5.8 illustrate the variation of scar volume and scar roughness in both study groups.

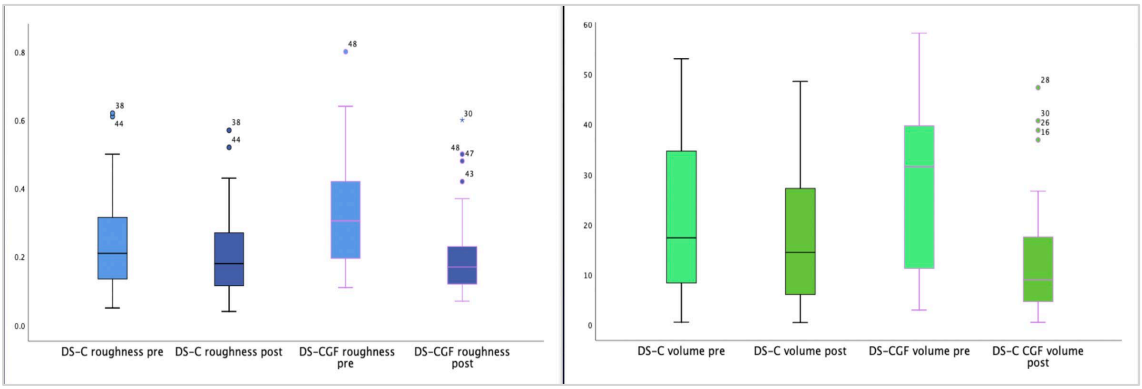

Figure 5.8: Boxplots representing the modification of the variables scar roughness (blue) and scar volume (green) in group DS-C and DS-CGF. Outliers are represented by circles and their correspondent case number. The scar modification was statistically significant according to Wilcoxon signed-rank test ($p < 0.01$).

According to the Mann-Whitney U test, the patients in group DS-CGF presented scars with more roughness and more volume than patients in group DS-C ($p < 0.05$) (Table 5.6). In addition, the Rgh_{DS} ∂ reduction and the VDS ∂ reduction was higher in the group treated with GFs. This finding was also statistically significant.

Table 5.6 - Mann-Whitney test regarding the variables in groups DS-C and DS-CGF

	Group C (n = 64)		**Group CGF** (n = 68)		
Variable	Median	**IQR (25^{th} – 75^{th} percentiles)**	Median	**IQR (25^{th} – 75^{th} percentiles)**	***p*-value**
Rgh_{DS} pre-procedure	0.21	0.13 – 0.32	0.3	0.19 – 0.42	**0.002**
Rgh_{DS} post-procedure	0.18	0.11 – 0.28	0.17	0.12 – 0.23	0.77
V_{DS} pre-procedure	17.3	8.3 – 35.1	28.8	11.8 – 39.9	**0.04**
V_{DS} post-procedure	14.4	6 – 27.8	8.3	4.5 – 17.1	**0.03**
Rgh_{DS} ∂ reduction	13.3	3.5 – 25.0	36.0	24.4 – 53.8	**< 0.01**
V_{DS} ∂ reduction	20.5	11.4 – 36.4	54.9	40.7 – 74.0	**< 0.01**
Simultaneous computation of Rgh_{DS} + V_{DS} ∂ reduction	35.0	18.9 – 59.6	89.0	71.8 – 118.4	**< 0.01**

IQR: interquartile range (Q1-Q3). Mann-Whitney test; ∂ reduction is in percentage; V_{DS} is measured in mm^3

Group DS-CGF presented more volume reduction ($p < 0.05$), Rgh_{DS} ∂ reduction ($p < 0.01$) and V_{DS} ∂ reduction ($p < 0.01$) and the simultaneous computation of ∂ reduction of V_{DS} + Rgh_{DS} ($p < 0.01$) than group DS-C. These results complement the findings described in Chapter 4, which demonstrated that periorbital wrinkles treated with vitamin C plus GFs presented statistically significant better results than controls. This finding confirms the thesis hypothesis that a scar or facial wrinkle treated with a cosmeceutical

containing a combination of growth factors (GFs) and vitamin C after superficial LSR gives a favourable outcome over controls.

Spearman correlation coefficient (Sig 2-tailed) established the correlation between scar roughness and volume. In group DS-C, *rho* was 0.417 pre-procedure and 0.387 post-procedure (p <0.01), whereas in group DS-CGF, *rho* was 0.306 pre-procedure and 0.280 post-procedure (p <0.01). In contrast to the clinical study described in Chapter 4, the correlation between the variables was not strong (Figure 5.9). This finding suggests that (i) the disarrangement of the architecture of skin structure of scars is more complex, and (ii) that Rgh_{DS} and V_{DS} did not respond to LAM with the same intensity.

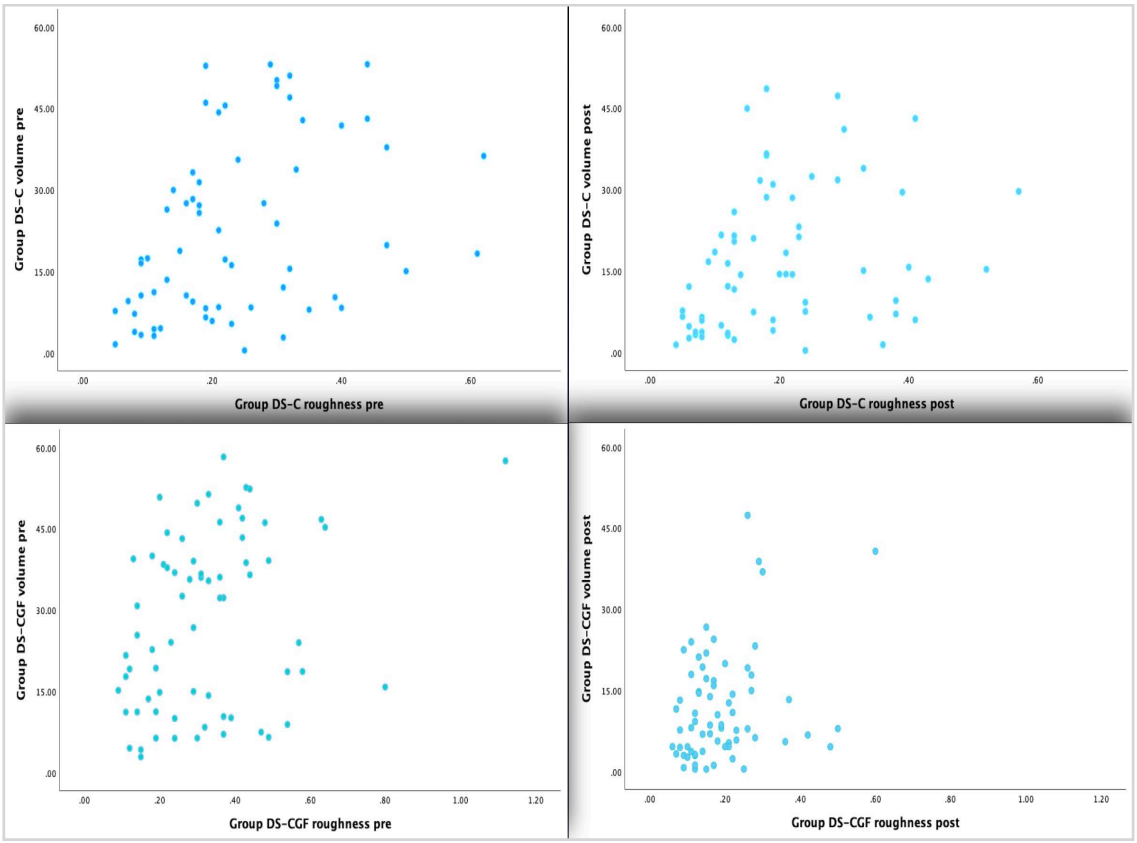

Figure 5.9: The scatterplots comparing both groups demonstrate that the correlation between Rgh_{DS} and V_{DS} was not strong in the two groups, in spite of the fact that the parameters decreased and converged towards zero. In group DS-C, *rho* was 0.417 pre-procedure and 0.387 post-procedure (p < 0.01). In group DS-CGF, *rho* was 0.306 pre-procedure and 0.280 post-procedure (p < 0.01).

To conclude the statistical analysis, the scars were grouped and stratified by anatomical location (face/neck, abdomen/flanks and breast/thorax). A Mann-Whitney test was run to compare groups DS-C and DS-CGF. The correspondent *p*-value related to each variable showed that all findings were statistically significant, which represents that the scars responded to treatment regardless of the anatomical location (Table 5.7). However, the data confirmed that group DS-CGF presented ∂ reduction of Rgh_{DS} and V_{DS} that was significantly higher than the control group (DS-C).

Table 5.7 - Mann-Whitney test regarding the anatomical location of scars in groups DS-C and DS-CGF

Variable	Group DS-C			Group DS-CGF			*p*-value
	n	Median	IQR	*n*	Median	IQR	
Site: face/neck							
Rgh_{DS} ∂ reduction	20	16.0	9.5 – 27.7	23	37.5	23.3 – 50.0	0.002
V_{DS} ∂ reduction	20	22.3	17.8 – 33.8	23	59.3	39.6 – 72.8	0.01
Site: abdomen/flanks							
Rgh_{DS} ∂ reduction	23	11.1	0 – 27.8	24	35.2	18.9 – 57.0	< 0.01
V_{DS} ∂ reduction	23	16.2	6.0 – 44.3	24	58.7	38.7 – 80.6	0.0003
Site: breast/thorax							
Rgh_{DS} ∂ reduction	21	11.1	3.6 - 25.0	21	35.5	27.9 - 52.9	< 0.01
V_{DS} ∂ reduction	21	18.4	10.8 - 36.3	21	53.0	41.3 - 70.5	< 0.01

IQR: interquartile range (25^{th} – 75^{th} percentiles); ; ∂ reduction is in percentage

Finally, the majority of the scars were hypertrophic (95.3% of the cases in group DS-C and 91.2% in group DS-CGF). Three patients in group DS-C and six patients in group DS-CGF presented atrophic scars. The treatment of atrophic scars is challenging because it is difficult to rebuild the complex skin architecture composed of collagen fibres and ECM. A recent study has shown that the use of LAM (laser skin resurfacing immediately followed by topical application of poly-L-lactic acid has shown improvement of scar atrophy (Rein et al., 2014). In the present study, patients in group DS-CGF showed more significant visual improvement of atrophic scars compared to those in group DS-C. Figures 5.10 and 5.11 are examples of pre and post-procedure pictures of atrophic scars in each study group.

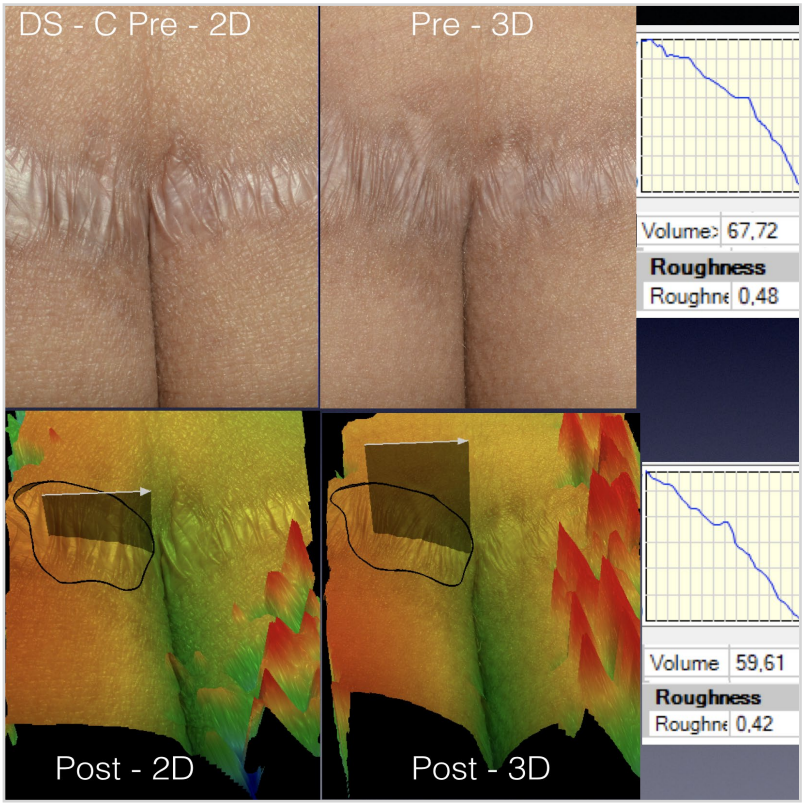

Figure 5.10: Pictures of a 42-year-old patient from group DS-C subjected to a flankplasty. 3D SPM data were collected on the 93rd day post-procedure. The graphics on the right show the variation under the area highlighted under the white arrow. Rgh_{DS} ∂ reduction was 4%.

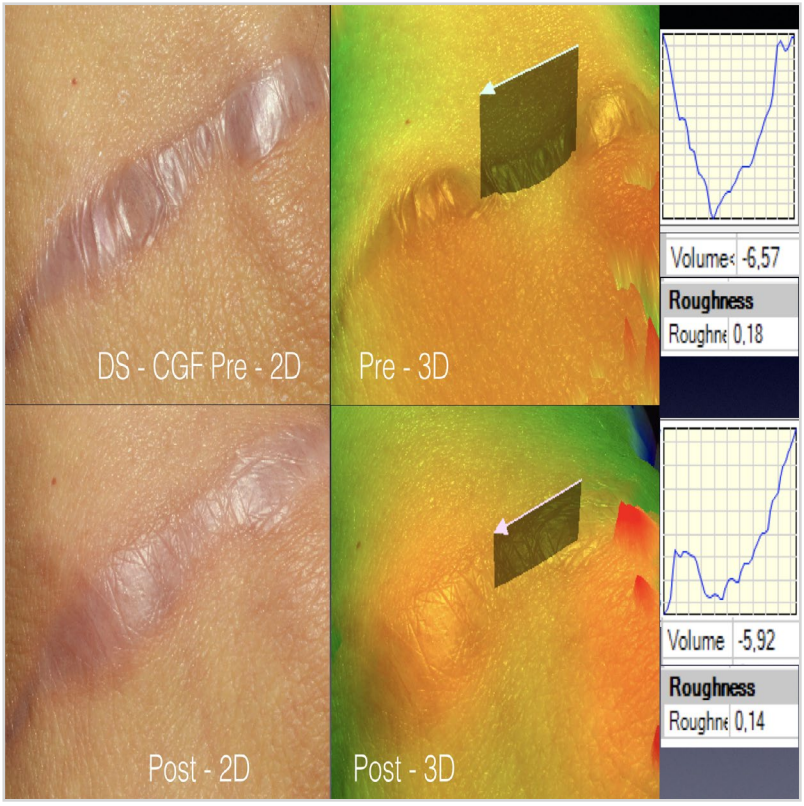

Figure 5.11: Pictures of a 51-year-old patient from group DS-CGF with scar located on the flank. The post-procedure images were obtained the 90th after the treatment. The graphics on the right show the roughness variation in the area highlighted under the white arrow. The Rgh_{DS} ∂ reduction was 22%.

5.5 Discussion

The microthermal injury caused by AFXLs is supposed to reduce the expression of TGF-β and FGF-β, suppress collagen (I and III) deposition and break down the disorganised collagen fibrils that create the scar contracture (Qu et al., 2012). The LSR followed by topical application of GFs has been recently reported as an effective alternative to reduce healing time of partial-thickness burns, improve scarring pigmentation, pliability, height and vascularity, and treat other skin conditions by delivering therapeutic doses of GFs (Zhang et al., 2016; Bertin et al., 2018).

As for the substances to be applied on the skin surface, safety and potential beneficial effects were carefully considered during the design of the present study. Dexpanthenol was applied to the lasered skin surface of all patients treated under the same regimen as an adjuvant only. Further studies can investigate whether dexpanthenol has additional roles in laser-assisted drug delivery.

For safety measures, the treatment was restricted to the face of patients in group R and to scars of up to 35 cm in width and 6 cm in height, that is 210 cm^2, at most (e.g. scars post-abdominoplasty or mammaplasty) in group DS.

The option for using vitamin C as the medication to be used in the control group was based on its benefits on skin ageing and wound healing (Masaki, 2010; Ganceviciene et al., 2012; Humbert et al., 2012). Vitamin C is necessary for wound re-epithelialisation and wound contraction (Qing, 2017). Vitamin C presents an inhibitory action on the tyrosinase enzyme, and also decreases melanin production due to its anti-inflammatory effect (Sobhi et al., 2018). Furthermore, ascorbic acid inhibits the oxidative damage to the skin that eventually may be induced by laser irradiation (Fujimoto et al., 2017). Finally, its use after fractional lasers increases its transepidermal penetration several times (Sobhi et al., 2018; Huang et al., 2013). As mentioned before, the vitamin C employed in this research was approved for intravenous use and no toxicity has been reported when this water-soluble vitamin was applied as part of LAM (Hsiao et al., 2012).

Any artificial supplementation of GFs is supposed to mimic the physiological, molecular biology process to promote skin rejuvenation and enhance the self-healing capacity (Erlich et., 2006; Ono, 2011; Aldag et al., 2016; An et al., 2013; Park & Kyobum, 2017). Initially, the experiments showing the efficacy of GFs were performed on animals using intracoronary injection of βFGF. However, there has been evidence in the literature to support the effectiveness of intravenous application of growth factors in humans as early as 1999 (Laham et al., 1999). In addition, Ono (2011) has demonstrated that the intradermal injection of βFGF in the hands of human subjects has resulted in skin

rejuvenation (Ono, 2011). Although a recent metanalysis found no significant adverse events when applying GFs after laser resurfacing (Zhang et al., 2016), investigation of the supplementation of GFs on human subjects are scarce, and some studies involved a low number of patients to permit further conclusions (Bertin et al., 2018).

Bertoncelj et al. (2014) and Park et al. (2017) considered that the bolus injections of a blend of GFs (PDGF, TGF-β, VEGF, IGF and HGF) obtained from Platelet-rich plasma (PRP) is more effective compared to the administration of a single GF because a single GF cannot counteract all the deficiencies related to the ageing process. Nonetheless, PRP is an off-label method and leads to a decreased relative metabolic activity of cells related to iron release from erythrocyte degradation, which contributes to cell destruction (Bertoncelj et al., 2014). As PRP probably would not be ethically permitted as a source of GFs, this research used the cosmeceutical containing GFs in order to obtain a constant concentration of actives.

The cosmeceutical used in the present clinical study contains a high concentration of patented human growth factor blend GFs (93.6%). The mixture of GFs includes VEGF, PDGF, HGF, and TGF-β1 obtained from cell fibroblast cultures of newborns (Husein el Hadmed & Castillo, 2016). These substances can promote angiogenesis (VEGF and HGF), modulate inflammation (interleukin-6 and interleukin-8), and enhance ECM deposition (TGF-β1 and PDGF) (Source: SkinMedica TNS Recovery Complex Leaflet; document 8.1, available on Chapter 8: Appendices). Some authors have investigated this cosmeceutical, and no irritation or adverse reactions have been detected (Erlich et al., 2006; Aldag et al., 2016).

One comparative study on 12 healthy females with facial wrinkles from 42 to 74 years old (mean 50 years old) compared two cosmeceuticals. The patients elected one hemiface to apply one cosmeceutical containing TGF-β1, ascorbic acid, and *Cimicifuga racemosa* extract and the other side received the cosmeceutical used in this research (Erlich et al., 2006). Both products provided significant improvement in facial rhytids, which was credited to the incorporation of GFs. Similarly to the present study, the skin was also treated with ascorbic acid, which may have been essential in proportioning skin improvement (Aldag et al., 2016).

Disphanurat et al. (2020) investigated 24 participants treated for striae alba (stretch marks) with ablative fractional carbon dioxide (CO_2) laser followed by topical application of recombinant human epidermal growth factor (rhEGF) or Aloe Vera gel. Three sessions of fractional laser treatment at 4-week intervals were applied in areas containing stretch marks. After the laser resurfacing, each side of the body received either rhEGF or Aloe

Vera gel treatment. Patients were required to apply the medication twice daily up to 1 month after the last laser treatment session. Despite both sides of the body has presented a statistically significant improvement of the striae surface texture, no statistical significance was found between the rhEGF- and Aloe Vera-treated sides. Nonetheless, some criticism of the paper published by Disphanurat et al. (2020) include:

- Although the laser pulse energy was specified, the number of passes was not stated;
- The authors have left untreated areas for comparison. However, this may have been a hindrance because it is difficult to establish landmarks that delimitate which stretch marks have been treated and which have not;
- Their sample may have been insufficient for providing proper power to the statistical analysis;
- Those authors stated as a study limitation that GF being applied just after the procedure may have some systemic absorption and also been responsible for the skin improvement observed on the side treated with Aloe Vera;
- Aloe Vera can increase (i) the proliferation of fibroblasts, (ii) type I collagen formation (iii) the secretion of the KGF, VEGF, which contributes to skin regeneration and (iv) stimulate tissue re-epithelisation. These effects may have made the comparison between Aloe Vera and rh-EGF not appropriate;
- Three laser sessions with no information on the pulse repetition in each patient made it difficult to establish whether the improvement resulted from the laser treatment itself or the intradermal delivery of medication;
- The one-month interval between laser sessions was not enough to achieve the best result concerning the neoformation of collagen fibres;
- The additional topical application of the substances on the skin surface for one month, twice a day, after the last laser session may have hydrated the SC and interfered with the analysis of results. Furthermore, patients may not have uniformly complied with this treatment step;
- The 3D SPM system was a scanner, which required contact and slight pressure on the skin surface to obtain skin analysis.

By contrast, the present clinical study:

- Consisted of one treatment session, which prevented the laser interference from overpassing and stifling the action of the medication;
- All patients received the same laser protocol so that the laser treatment could not be a variable interfering with the comparison of the outcomes;

- The application of vitamin C in both groups turned the DS-C group into the control group which reduced the possibility of bias. Besides, no area was left without treatment;
- Each patient received only one treatment regime to avoid that any eventual systemic absorption of GFs could interfere with the collagen stimulation in areas treated with vitamin C only;
- The 3D SPM system chosen for this research was contactless to avoid interference with the readouts.

Comparing with studies by Erlich et al. (2006) and Ono (2011) and the metanalysis performed by Zhang et al. (2016), the present study has confirmed the safety and the efficiency of using GFs as part of LAM in the clinical setting in a high number of participants. These results encourage further investigation on GFs pharmacokinetics and the possible combination of these compounds in formulations aiming at skin rejuvenation and scar improvement.

As some authors have reported the inefficiency of the application of one GF only (Bertoncelj et al., 2014; Park et al., 2017), the combination of GFs may have permitted for satisfactory intercellular communication and resulted in the overall satisfactory result. If the degradation is excessive, the biomolecules may not exist in sufficient concentrations to exert their functions. Consequently, a supraphysiologic dose of GFs must be incorporated into the products to ensure a sufficient active concentration, which then restricts their regulatory approval, and causes the medication to be very costly. Furthermore, higher absorbed doses of GFs may decrease the cellular metabolic activity and cause undesirable side effects such as inflammation, ectopic tissue growth or tumorigenesis (Koria, 2012; Bertoncelj et al., 2014). The future challenge is to determine a formulation containing an optimum combination of GFs, and to establish the concentration necessary to maintain their bioactivity and therapeutic functionality within the skin layers for a specific moment of skin needs.

5.6 Conclusion

After skin trauma, the body launches a series of dynamic and physiological events that result in wound healing. These phenomena involve molecular mechanisms that are mediated by GFs, which control vital inflammatory responses, neoangiogenesis, ECM deposition and the formation of granulation tissue. In recent years, considerable progress has been made in the understanding of controlling normal wound healing and these mediators.

The transcutaneous delivery of a synergistic combination of multiple exogenous GFs can (i) exert a positive effect on skin rejuvenation, (ii) enhance skin repair, (iii) optimise the morphology of regenerative tissues, (iv) accelerate the cellular activities during the healing process and (v) produce less noticeable scars. The challenge is to engineer a delivery system that can protect the bioactive and labile GFs from the cutaneous proteolytic enzyme's rich environment.

The findings of this study addressed the research primary objective, which consisted of evaluating the efficiency of using growth factors (GFs) as part of LAM to improve skin relief. The groups treated with vitamin C only were established as control groups, which has precluded the necessity of an additional control arm investigating the laser action alone.

Although the results obtained in this study could be somewhat weakened by the significant physical involvement of the laser treatment, LAM provided an opportunity to demonstrate the effect of applying GF directly into the superficial dermal target area. The positive therapeutic response of the patients whose scars were treated with vitamin C and GFs was statistically significant in comparison with the control group, which was treated with laser and vitamin C only. This finding confirms the efficacy of adding GFs to scar treatment as part of LAM.

LAM using vitamin C and GFs has proved to be safe as the treatment did not cause local adverse events or systemic reactions. It is advisable to use sterile drugs suitable for intravenous application and with a potential contribution to the pathways involved in wound healing and skin regeneration. This choice can minimise the risk of infection and inadvertent systemic absorption of drugs applied on the skin surface after laser resurfacing. However, most actives are not available as such.

Despite the satisfactory results seen in the studies described in this thesis, scars presented a challenging architecture to work with. The low correlation between the analysed variables (scar volume and scar roughness) contrasts with the correlation between the two variables analysed in group R (skin roughness and average depth of a wrinkle) as described in Chapter 4 (section 4.3.3.3). This confirms that it is easier for LAM to reduce skin roughness and average depth of a wrinkle than to reduce the scar roughness and the scar volume, at the same time. This finding seems to be related to the disarranged structure of the skin post-trauma.

Chapter 6

Conclusion

6.1 Research contribution

The lipid bilayer of the *stratum corneum* repels outside insults and is impermeable to water-soluble and large molecules. Therefore, the direct introduction of a drug into skin deep layers can lower the concentration of the active agents applied on the skin surface and potentially obviate their side effects. Fractional ablative lasers disrupt the *stratum corneum* barrier and fabricate microchannels large enough to admit macromolecules, particles, and cells into dermal layers. The laser-induced trauma replicates the microenvironment involved in the wound healing process, including the activation of signalling pathways provided by growth factors. Furthermore, the heat produced by the laser action is relevant for drug diffusion.

In vitro and *ex vivo* experiments involving laser-assisted medication cannot mimic the laser-tissue interaction and the drug diffusion by the dermal vasculature. Despite the superiority of *in vivo* research, the scarcity of robust studies involving human subjects is a hindrance to establishing standards for this therapeutic modality which has the potential to impact several fields of medicine. This research represents an important advance in translational medicine.

This is the first prospective, randomised, double-blind, comparative clinical trial that:

- establishes 3D SPM as a valid and accurate tool to measure the impact of a laser-assisted medication on wrinkle and scar improvement;
- investigates laser-assisted medication on a significant number of patients comparing two different medication regimes applied to two different skin conditions (scars and wrinkles);
- has evaluated the therapeutic outcome of patients subjected to LAM and confirmed the efficacy of the method as opposed to the trivial demonstration of enhanced delivery of substances;
- suggests that the laser-assisted medication on damaged or hypertrophic/scarred skin is more challenging and may be less efficient than on normally ageing skin.

Reaching its objective, this thesis quantified the LAM impact on the skin surface. The statistical superiority of the results obtained in the groups treated with growth factors over the control groups confirmed that the laser enhanced the medication bioavailability. The microchannels produced by the fractional laser increased the transcutaneous absorption of the exogenous GFs, which otherwise could have demonstrated nullified or reduced efficacy because of (i) degradation by epidermal proteolytic enzymes or (ii) the high MW (15000 Da). The statistical findings were ratified by the clinical evidence of the improvement of wrinkles and scars. As a secondary outcome, the concealment of the

protuberant vessels under the skin surface confirms the efficiency of the treatment in recovering the skin thickness.

The laser protocol included four, high-energy, laser passages and relatively low densities and these settings were enough to achieve therapeutic benefits. These parameters can be converted into a framework that can be transferred to other laser devices to produce the same penetration depth and the same limited residual thermal zone in every patient. By standardising laser parameters, the most important variable under investigation in future studies involving LAM will be the drug's pharmacokinetics.

This research permitted for suggesting some safety guidelines for researchers investigating laser-assisted medication:

- The medication should ideally be applied in the first 30 minutes after the laser treatment because the tissue heat is still high and the laser microchannels are wide open;
- It is prudent to use laser-assisted medication to treat localised body surface areas, and to avoid substances with potential toxicity;
- It is safer to use medications suitable for intradermal and intravenous injection, or topical medications in pure formulations, on condition that the dosage is calculated based on the corporal weight, as with any injectable medication, because the drug may eventually reach the bloodstream;
- The vehicle containing the active compound should be sterile to reduce the risk of infection because the drug will be put into direct contact with inner layers of the skin;
- As skin sensitisation is usually related to chronic exposure and the application of chemicals with low molecular weight, laser-assisted medication should consist of few treatment sessions if followed by the topical application of the same substance and this should present high molecular weight.

6.2 Research limitations and strengths

This research has been subject to challenges and limitations:

- The 3D SPM system required training to yield reliability and avoid the loss of data;
- The follow-up of the patients during the clinical study (phase 3) was strenuous and rigorous to avoid missing data;
- Although the post-procedure crusting and spontaneous skin exfoliation occur in a relatively short period, dexpanthenol was applied to all patients on the treated surface. Although this substance has been applied in all patients, this may have increased local skin hydration and exerted some interference, to a certain extent.

- For ethical reasons, the growth factors applied composed a duly CE-approved cosmeceutical. Although fabricants stated that the GFs' concentration was 93.6%, the formula is protected by a patent and did not permit the identification of the main GFs exerting the beneficial effect on the skin surface;
- Even under the scope of pharmaceutical investigations, it is not possible to determine the drug permeation after laser resurfacing based solely on molecular peculiarities. The mathematical models that take into account the temporal bio-distribution of the drugs inside the complex and new geometry of the laser-induced microchannels are not available yet. Furthermore, clinical trials are essential to investigate if the enhanced drug bioavailability is followed by an enhanced effect.

The major strengths of this study were:

- The research was supported by a validation study that confirmed that the methodology was adequate and accurate;
- A pilot study was conducted to confirm the research feasibility and provide the sample size calculation for each study group to ensure power and statistical significance;
- On phase 3, the interventions were randomised and double-blind;
- By standardising the laser settings on all study groups, the variance of the results concerning LAM effectiveness relied on the applied medications only.

Finally, two different skin conditions were evaluated, and both confirmed the thesis hypothesis that medicating the skin with growth factors after laser resurfacing enhances the treatment result.

6.3 Future work

Future research will focus on determining suitable drugs and formulae for this route of delivery and which vehicles are best for permeation. Formulae for LAM will probably be aqueous, aseptic and include biocompatible active compounds, such as nanoparticles and liposomes, to enhance the efficacy of the treatment. Once suitable formulations are identified and the efficacy is clinically demonstrated, mathematical predictions will permit estimating the ideal chemical concentration, which must neither underestimate nor overestimate the tissue needs.

Chapter 7

Bibliographic references

Bibliographic references

Aldag, C., Nogueira Teixeira, D., Leventhal, P.S., 2016. Skin rejuvenation using cosmetic products containing growth factors, cytokines, and matrikines: a review of the literature. *Clinical, cosmetic and investigational dermatology*, 9, 411-419.

Alegre-Sanchez, A., Jimenez-Gomez, N., Boixeda, P., 2018. Laser-Assisted Drug Delivery. *Actas Dermo-Sifiliograficas* (English Edition), 109(10), 858-867.

Alexiades-Armenakas, M., Dover, J., Arndt, K., 2012. Fractional Laser Skin Resurfacing. *Journal of drugs in dermatology,* JDD: 11, 1274-87.

Ali, F.R., Al-Niaimi, F., 2016. Laser-assisted drug delivery in dermatology: from animal models to clinical practice. *Lasers in Medical Science*, 31(2), 373-381.

Al-Niaimi, F., Chiang N.Y.Z., 2017. Topical vitamin C and the skin: mechanisms of action and Clinical applications. *J Clin Aesthet Dermatol*.;10(7): 14-17.

Alves, V. M., Muratov, E., Fourches, D., Strickland, J., Kleinstreuer, N., Andrade, C. H., Tropsha, A., 2015. Predicting chemically-induced skin reactions. Part II: QSAR models of skin permeability and the relationships between skin permeability and skin sensitization. *Toxicology and applied pharmacology*, 284(2), 273-280.

Amini-Nik S, Yousuf Y, Jeschke MG., 2018. Scar management in burn injuries using drug delivery and molecular signaling: current treatments and future directions. *Advanced drug delivery reviews*. Jan 1; 123:135-54.

An, J. J., Eum, W. S., Kwon, H. S., Koh, J. S., Lee, S. Y., Baek, J. H., ... & Jang, S. H., 2013. Protective effects of skin permeable epidermal and fibroblast growth factor against ultraviolet-induced skin damage and human skin wrinkles. *Journal of cosmetic dermatology*, 12(4), 287-295.

Anderson, R., 1981. Ascorbate-mediated stimulation of neutrophil motility and lymphocyte transformation by inhibition of the peroxidase/H_2O_2/halide system in vitro and in vivo. *The American journal of clinical nutrition*, *34*(9), 1906-1911.

Anissimov, Y.G. and Roberts, M.S., 2011. Modelling dermal drug distribution after topical application in human. *Pharmaceutical research*, 28(9), p.2119.

Ardehali, B., Nouraei, S.A.R., Van Dam, H., Dex, E., Wood, S., Nduka, C., 2007. Objective assessment of keloid scars with three-dimensional imaging: quantifying response to intralesional steroid therapy. *Plastic and reconstructive surgery*, 119(2), pp. 556-561.

Badawi, A. M., & Osman, M. A., 2018. Fractional erbium-doped yttrium aluminum garnet laser-assisted drug delivery of hydroquinone in the treatment of melasma. *Clinical, cosmetic and investigational dermatology*, 11, 13.

Banzhaf, C.A., Wind, B.S., Mogensen, M., Meesters, A.A., Paasch, U., Wolkerstorfer, A., Haedersdal, M., 2015. Spatiotemporal closure of fractional laser- ablated channels imaged by optical coherence tomography and reflectance confocal microscopy. *Lasers in surgery and medicine*, 48(2), pp. 157-165.

Banzhaf, C. A., Thaysen-Petersen, D., Bay, C., Philipsen, P. A., Mogensen, M., Prow, T., Haedersdal, M., 2017. Fractional laser-assisted drug uptake: Impact of time-related

topical application to achieve enhanced delivery. *Lasers in surgery and medicine*, *49*(4), 348-354.

Banzhaf, C.A., Ortner, V.K., Philipsen, P.A., Haedersdal, M. 2019. The ablative fractional coagulation zone influences skin fluorescence intensities of topically applied test molecules—An in vitro study with fluorescence microscopy and fluorescence confocal microscopy. *Lasers in surgery and medicine*, 51(1), pp.68-78.

Bao, P., Kodra, A., Tomic-Canic, M., Golinko, M.S., Ehrlich, H.P., Brem, H., 2009. The role of vascular endothelial growth factor in wound healing. *Journal of Surgical Research*, 153, 347- 358.

Bay, C., Lerche, C.M., Ferrick, B., Philipsen, P.A., Togsverd-Bo, K. and Haedersdal, M., 2017. Comparison of physical pretreatment regimens to enhance protoporphyrin IX uptake in photodynamic therapy: a randomized clinical trial. *JAMA dermatology*, *153*(4), pp.270-278.

Barrientos, S., Stojadinovic, O., Golinko, M.S., Brem, H., Tomic Canic, M., 2008. Growth factors and cytokines in wound healing. *Wound Repair and Regeneration*, 16, 585-601.

Bartko, J.J., Carpenter, W.T., 1976. On the Methods and Theory of Reliability. *The Journal of Nervous and Mental Disease*, **163**(5):307-316.

Basler, K., Bergmann, S., Heisig, M., Naegel, A., Zorn-Kruppa, M., Brandner, J. M., 2016. The role of tight junctions in skin barrier function and dermal absorption. *Journal of Controlled Release*, 242, 105-118.

Behm, B., Babilas, P., Landthaler, M. and Schreml, S., 2012. Cytokines, chemokines and growth factors in wound healing. *Journal of the European Academy of Dermatology and Venereology*, 26(7), 812-820.

Bertin, A.C.J., Vilarinho, A., Junqueira, A.L.A., 2018. Fractional non-ablative laser-assisted drug delivery leads to improvement in male and female pattern hair loss. *Journal of Cosmetic and Laser Therapy*, *20*(7-8), pp.391-394.

Bertoncelj, V., Pelipenko, J., Kristl, J., Jeras, M., Cukjati, M., Kockbek, P., 2014. Development and bioevaluation of nanofibers with blood-derived growth factors for dermal wound healing. *European journal of pharmaceutics and biopharmaceutics*, 88(1), pp. 64.

Bloemen, M. C., van Gerven, M. S., van der Wal, M. B., Verhaegen, P. D., Middelkoop, E., 2011. An objective device for measuring surface roughness of skin and scars. *Journal of the American Academy of Dermatology*, 64(4): 706-715.

Boateng, J., Matthews, K., Stevens, H., Eccleston, G., 2008. Wound healing dressings and drug delivery systems: A review. *Journal of pharmaceutical sciences*, 97(8), 2892-2923.

Braun, S. A., Schrumpf, H., Buhren, B. A., Homey, B., Gerber, P. A., 2016. Laser-assisted drug delivery: mode of action and use in daily clinical practice. JDDG: *Journal der Deutschen Dermatologischen Gesellschaf*t, 14: 480–488. doi:10.1111/ddg.12963.

Breitkreutz, D., Koxholt, I., Thiemann, K., & Nischt, R., 2013. Skin basement membrane: the foundation of epidermal integrity—BM functions and diverse roles of bridging molecules nidogen and perlecan. *BioMed research international,* Jan 1.

Catorze, M.G., 2009. Laser: fundamentos e indicações em dermatologia. *Med Cutan Iber Lat Am*;37(1):5-27.

Cavallini M., Papagni M.F., 2016. New Evaluation Method to Assess the Improvement of Glabellar Lines and Crow's Feet Lines with Onabotulinum Toxin A. *J Clin Exp Dermatol Res* 7: 351.

Daniell H.W., 1971. Smoker's wrinkles. A study in the epidemiology of 'crow's feet'. *Ann Intern Med.*; **75**:873–80.

Dayan, N., 2005. Pathways for skin penetration. *Cosmetics and toiletries*, *120*(6), 67-76.

Demidova-Rice, T. N., Hamblin, M. R., & Herman, I. M., 2012. Acute and impaired wound healing: pathophysiology and current methods for drug delivery, part 2: role of growth factors in normal and pathological wound healing: therapeutic potential and methods of delivery. *Advances in skin & wound care*, 25(8), 349.

Dieamant, G., Costa, A., Bechelli, L., Tiberio, J., Pereira, C., 2012. In vitro evaluation of the safety profile of cosmeceuticals containing growth factors and their analogues. *Surgical and Cosmetic Dermatology*, v. 4, n. 3, p. 229-236. Available at: <http://hdl.handle.net/11449/74031>.

Disphanurat, W., Kaewkes, A., & Suthiwartnarueput, W., 2020. Comparison between topical recombinant human epidermal growth factor and Aloe vera gel in combination with ablative fractional carbon dioxide laser as treatment for striae alba: A randomized double-blind trial. *Lasers in surgery and medicine*, 52, n. 2, p. 166-175 https://doi.org/10.1002/lsm.23052.

Dobos, G. , Lichterfeld, A. , Blume-Peytavi, U. , Kottner, J., 2015. Evaluation of skin ageing: a systematic review of clinical scales. *Br J Dermatol*, 172: 1249-1261.

Dominguez-Delgado, C. L., Rodríguez-Cruz, I. M., López-Cervantes, M., Escobar-Chávez, J., Merino, V., 2010. The skin a valuable route for administration of drugs. *Current Technologies To Increase The Transdermal Delivery Of Drugs*. The Netherlands: Bentham Science Publishers Ltd, 1-22.

Edwards J., 2011. Scar therapy. *Journal of Community Nursing*, 25 (2), 17-24 March/April.

Ehrlich, M., Rao, J., Pabby, A. and Goldman, M.P., 2006. Improvement in the Appearance of Wrinkles with Topical Transforming Growth Factor β1 and l-Ascorbic Acid. *Dermatologic surgery*, *32*(5), pp.618-625.

Flynn, T.C., Carruthers, A., Carruthers, J., Geister, T.L., Gortelmeyer, R., Hardas, B., Narins, R.S., 2012. Validated assessment scales for the upper face. *Dermatologic Surgery*; **38**(2ptII), 309-319. DOI: 10.1111/j.1524-4725.2011.02248. PMID: 22316187.

Fujimoto, T., Wang, J., Baba, K., Oki, Y., Hiruta, Y., Ito, M., Ito, S., Kanazawa, H., 2017. Transcutaneous drug delivery by liposomes using fractional laser technology. *Lasers in surgery and medicine*, *49*(5), 525-532.

Gainza, G., Villullas, S., Pedraz, J.L., Hernandez, R.M., Igartua, M., 2015. Advances in drug delivery systems (DDSs) to release growth factors for wound healing and skin regeneration. *Nanomedicine: Nanotechnology, Biology and Medicine*, *11*(6), 1551-1573.

Ganceviciene R., Liakou A.I., Theodoris A., Makrantonaki E., Zoubolis C.C., 2012. Skin anti-aging strategies. *Dermato-endocrinology* 4:3, 308–319; July–December

Gauglitz, G.G., Korting, H.C., Pavicic, T., Ruzicka, T., Jeschke, M.G., 2011. Hypertrophic scarring and keloids: pathomechanisms and current and emerging treatment strategies. *Molecular medicine*, 17(1-2), pp.113-125.

Genina E.A., Bashkatov A.N., Dolotov L.E., Maslyakova G.N., Kochubey V.I., Yaroslavsky, I., Altshuler G.B., Tuchin, V. V., 2013. Transcutaneous delivery of micro- and nanoparticles with laser microporation. *J Biomed Opt* 18: 111406.

Ghoddousi, H., Edler, R., Haers, P., Wertheim, D., Greenhill, D., 2007. Comparison of three methods of facial measurement. *International Journal of Oral & Maxillofacial Surgery*, 36(3):250-258.

Groenwold, R. H., Moons, K. G., Vandenbroucke, J. P., 2014. Randomized trials with missing outcome data: how to analyze and what to report. *Cmaj*, *186*(15), 1153-1157.

Haak, C.S., Bhayana, B., Farinelli, W.A., Anderson, R.R., Haedersdal, M., 2012. The impact of treatment density and molecular weight for fractional laser-assisted drug delivery. *Journal of controlled release*, 163(3), 335-341.

Haak, C. S., Hannibal, J., Paasch, U., Anderson, R. R., & Haedersdal, M., 2017. Laser-induced thermal coagulation enhances skin uptake of topically applied compounds. *Lasers in Surgery and Medicine*, *49*(6), 582-591.

Haedersdal, M., Erlendsson, A.M., Paasch, U. and Anderson, R.R., 2016. Translational medicine in the field of ablative fractional laser (AFXL)-assisted drug delivery: a critical review from basics to current clinical status. *Journal of the American Academy of Dermatology*, 74(5), pp.981-1004.

Hameeteman, M., Verhulst, A.C., Vreeken, R.D., Maal, T.J.J., Ulrich, D.J.O., 2016. 3D stereophotogrammetry in upper-extremity lymphedema: An accurate diagnostic method. *Journal of plastic, reconstructive & aesthetic surgery*: JPRAS, 69(2): 241-247.

Hendel, K. K., Bagger, C., Olesen, U. H., Janfelt, C., Hansen, S. H., Haedersdal, M., Lerche, C. M., 2019. Fractional laser-assisted topical delivery of bleomycin quantified by LC-MS and visualized by MALDI mass spectrometry imaging. *Drug delivery*, 26(1), 244-251.

Hermans, D.J.J., Maal, T.J.J., Berge, S.J. and Vleuten, C. J. M. Van Der, 2014. Three-dimensional stereophotogrammetry: a novel method in volumetric measurement of infantile hemangioma. *Pediatric Dermatology*, 31(1):118-122.

Hoevenaren, I.A., Maal, T.J.J., Krikken, E., Haan, A. F. J., Berge, S.J., Ulrich, D.J.O., 2015. Development of a three-dimensional hand model using 3D stereophotogrammetry: Evaluation of landmark reproducibility. *Journal of Plastic Reconstructive and Aesthetic Surgery*, 68(5): 709-716.

Honeybrook A., Bloom J. D., Woodard C., Bernstein E. F., 2018. Three-Dimensional Photography for Measuring Volumetric Changes After Submental Cryolipolysis. *The American Journal of Cosmetic Surgery*, 35(3): 135-142.

Hsiao, C.Y., Huang, C.H., Hu, S., Ko, Y.S., Sung, H.C., Chen, C.C., Huang, S.Y., 2012. Fractional Carbon Dioxide Laser Treatment to Enhance Skin Permeation of Ascorbic

Acid 2-Glucoside with Minimal Skin Disruption. *Dermatologic surgery*, *38*(8), pp.1284-1293

Huang, C. H., Sung, H. C., Hsiao, C. Y., Hu, S., & Ko, Y. S., 2013. Transdermal delivery of three vitamin C derivatives by Er: YAG and carbon dioxide laser pretreatment. *Lasers in medical science*, *28*(3), 807-814.

Humbert, P., Viennet, C., Legagneux, K., Grandmottet, F., Robin, S., Oddos, T., Muret, P., 2012. In the shadow of the wrinkle: theories. *Journal of cosmetic dermatology*, 11(1), 72-78.

Husein el Hadmed, H., Castillo, R. F., 2016. Peptides, proteins, and growth factors. *Journal of Cosmetic Dermatology*, 15, 514-519.

Ibrahim, O., Wenande, E., Hogan, S., Arndt, K. A., Haedersdal, M., Dover, J. S., 2018. Challenges to laser-assisted drug delivery: Applying theory to clinical practice. *Lasers in surgery and medicine*, 50(1), 20-27.

Jabbour, S.F., Kechichian, E.G., Awaida, C.J., Tomb, R.R., Nasr, M.W., 2017. Botulinum toxin for neck rejuvenation: Assessing efficacy and redefining patient selection. *Plastic and reconstructive surgery*, 140(1), pp.9-17.

Jacques, S. L., McAuliffe, D. J., Blank, I. H., & Parrish, J. A.,1987. Controlled removal of human stratum corneum by pulsed laser. *Journal of investigative dermatology*, *88*(1), 88-93.

Jacobi, U., Chen, M., Frankowski, G., Sinkgraven, R., Hund, M., Rzany, B., Lademann, J., 2004. In vivo determination of skin surface topography using an optical 3D device. *Skin Research and Technology*, 10(4):207-214.

Kalil C.L.P.V., Frainer R.H., Dexheimer L.S., Tonoli R.E., Boff A.L., 2015. Treatment of acne scars using the microneedling and drug delivery technique. *Surg Cosmet Dermatol,* 7(2):144-8.

Kamel, D., Frame, J., Frame, J. D., & Harle, T., 2016. Histological Findings from Controlled Application of a Thermal Plasma to Human Skin. *Clin Surg,* 1, 1176.

Kauvar A., Hruza G. 2005. Principles and Practices in Cutaneous Laser Surgery. 1st edition. CRC Press. ISBN-13: 978-0824758332.

Khavkin, J., & Ellis, D. A., 2011. Aging skin: histology, physiology, and pathology. *Facial Plastic Surgery Clinics*, 19(2), 229-234.

Ko, E.J., Hong, J.Y., Kwon, T.R., Choi, E.J.… & Kim, B.J., 2017. Efficacy and safety of non-invasive body tightening with high-intensity focused ultrasound (HIFU). *Skin Research and Technology,* Nov; 23(4):558-62.

Kohl, E., Meierhofer, J., Koller, M., Zeman, F., Klein, A., Hohenleutner, U., Landthaler A, M., Hohenleutner, S., 2014. Fractional carbon dioxide laser resurfacing of rhytides and photoageing: a prospective study using profilometric analysis. *British Journal of Dermatology*, 170(4), 858-865.

Kohl E., Meierhöfer J., Koller M., Zeman F., Groesser L., Karrer S., Hohenleutner U., Landthaler M., Hohenleutner S., 2015. Fractional carbon dioxide laser resurfacing of rhytides and photoaged skin–a prospective clinical study on patient expectation and satisfaction. *Lasers in surgery and medicine*, Feb;47(2): 111-119.

Koria, P., 2012. Delivery of Growth Factors for Tissue Regeneration and Wound Healing. *BioDrugs*, 26(3), 163-175.

Kottner, J., Schario, M., Bartels, N. G., Pantchechnikova, E., Hillmann, K., Blume-Peytavi, U., 2013. Comparison of two in vivo measurements for skin surface topography. *Skin Research and Technology*, 19(2), 84-90.

Kwon, Y., Kim, H., Roh, D., Yoon, S., Baek, R., Kim, J., Kweon, H., Lee, K., Park, Y., Lee, J., 2006. Topical application of epidermal growth factor accelerates wound healing by myofibroblast proliferation and collagen synthesis in rat. *Journal of veterinary science*, 7, 105- 109.

Laham, R. J., Rezaee, M., Post, M., Sellke, F. W., Braeckman, R. A., Hung, D., Simons, M., 1999. Intracoronary and intravenous administration of basic fibroblast growth factor: myocardial and tissue distribution. *Drug Metabolism and Disposition*, 27(7), 821-826.

Landis J.R., Koch G.G., 1977. The measurement of observer agreement for categorical data. *Biometrics*, 159-174.

Lee, W. R., Shen, S. C., Aljuffali, I. A., Li, Y. C., & Fang, J. Y., 2014. Impact of different vehicles for laser-assisted drug permeation via skin: full-surface versus fractional ablation. *Pharmaceutical research*, *31*(2), 382-393.

Lee, W. R., Shen, S. C., Aljuffali, I. A., Lin, Y. K., Huang, C. W., & Fang, J. Y., 2016 (a). Non-ablative fractional laser assists cutaneous delivery of small-and macro-molecules with minimal bacterial infection risk. *European Journal of Pharmaceutical Sciences*, *92*, 1-10.

Lee, K.C., Dretzke, J., Grover, L., Logan, A., Moiemen, N., 2016 (b). A systematic review of objective burn scar measurements. *Burns & trauma*, 4:14.

Lee, H., Song, C., Baik, S., Kim, D., Hyeon, T., Kim, D. H., 2018. Device-assisted transdermal drug delivery. *Advanced drug delivery reviews*, *127*, 35-45.

Levy, J. L., Pons, F., Agopian, L., Besson, R., 2004. Subjective Evaluation and Objective Measurement Methods in Cosmetic Dermatology. *Medical Laser Application*, 19(4), 223.

Manstein D., Herron G.H., Sink R.K., Tanner H., Anderson R.R., 2004. Fractional Photothermolysis: A New Concept for Cutaneous Remodelling Using Microscopic Patterns of Thermal Injury. *Lasers in Surgery and Medicine* 34:426–438.

Martin, N.A.J., Lundy, J.B., Rickard, R.F., 2014. Lack of precision of burn surface area calculation by UK Armed Forces medical personnel. *Burns: Journal of the International Society for Burn Injuries*, 40(2):246.

Masaki, H., 2010. Role of antioxidants in the skin: anti-aging effects. *Journal of dermatological science*, 58(2), 85-90.

Mattos, R. A., Valente, N. Y., Senise, M., Campos, V. B., 2009. Erbium laser 2940 nm, fractionated with double pulse, for photorejuvenation: clinical and histopathological study of the effects on skin tissue. *Surgical & Cosmetic Dermatology*, *1*(4), 163-167.

Mbah CJ, Uzor PF., 2011. Perspectives on Transdermal Drug Delivery. *J. Chem. Pharm. Res*., 3(3):680-700.

Metcalfe, A., Ferguson, M., 2007. Tissue engineering of replacement skin: the crossroads of biomaterials, wound healing, embryonic development, stem cells and regeneration. *Journal of The Royal Society Interface* 4, 413-437.

Miranda, R., Matayoshi, S., Brabo, J., Miyoshi, L., 2018. Use of stereophotogrammetry for measuring the volume of external facial anatomy: a systematic review. *Rev. Bras. Cir. Plast*. 33(4):572-579. DOI: 10.5935/2177-1235.2018RBCP0180

Morgado, P.I.C., 2011. Development of different drug delivery systems for skin regeneration. Thesis presented to obtain the master's degree in biomedical sciences. Universidade da Beira Interior. Covilhã.

Münch, S., Wohlrab, J., Neubert, R. H. H., 2017. Dermal and transdermal delivery of pharmaceutically relevant macromolecules. *European Journal of Pharmaceutics and Biopharmaceutics*, 119, 235-242.

Murphy, M., Carmichael, A. J., 2000. Transdermal drug delivery systems and skin sensitivity reactions. *American journal of clinical dermatology*, 1(6), 361-368.

Nedelec, B., Shankowsky, H.A., Tredget, E.E., 2000. Rating the resolving hypertrophic scar: comparison of the Vancouver Scar Scale and scar volume. *The Journal of burn care & rehabilitation*, 21(3), pp. 205-212.

Noordzij, M., Tripepi, G., Dekker, F.W., Zoccali, C., Tanck, M.W., Jager, K.J., 2010. Sample size calculations: basic principles and common pitfalls. *Nephrology dialysis transplantation*, 25(5), pp.1388-1393.

Ohtsuki, R., Sakamaki, T., Tominaga, S., 2013. Analysis of skin surface roughness by visual assessment and surface measurement. *Optical review*, *20*(2), 94-101.

Ono I., 2011. Viscoelasticity alterations after growth factor administration. *Journal of Cutaneous and Aesthetic Surgery*, May-Aug 2011, Volume 4, Issue 2.

Park, J. W., Hwang, S. R., Yoon, I. S., 2017. Advanced growth factor delivery systems in wound management and skin regeneration. *Molecules*, 22(8), 1259.

Park U., Kyobum K., 2017. Multiple Growth Factor Delivery for Skin Tissue Engineering Applications. *Biotechnology and Bioprocess Engineering* 22: 659-670 DOI 10.1007/s12257-017-0436-1.

Piérard, G. E., Uhoda, I., & Piérard-Franchimont, C., 2003. From skin microrelief to wrinkles. An area ripe for investigation. *Journal of cosmetic dermatology*, *2*(1), 21-28.

Plooij, J.M., Swennen, G.R.J., Rangel, F.A., Maal, T.J.J., Schutyser, F.A.C., Bronkhorst, E.M., Kuijpers-, A.M., Berge, S.J., 2009. Evaluation of reproducibility and reliability of 3D soft tissue analysis using 3D stereophotogrammetry. *International Journal of Oral & Maxillofacial Surgery*, 38(3), pp. 267-273.

Prausnitz, M. R., Langer, R., 2008. Transdermal drug delivery. *Nature biotechnology*, 26(11), 1261.

Preissig, J., Hamilton, K., Markus, R., 2012. Current laser resurfacing technologies: a review that delves beneath the surface. *Seminars in plastic surgery*, vol. 26, No. 03, 109-116.

Puviani, M., Milani, M., 2015. A pilot, prospective, open-label study on the effects of a topical photorepair and photoprotection film-forming medical device in patients with actinic keratoses evaluated by means of skin analysis camera Antera 3D. *J Clinical Exp Dermatol Res*, 6:263. http://dx.doi.org/ 10.4172/2155-9554.1000263

Pyo S.M., Maibach H.I, 2019. Skin Metabolism: Relevance of Skin Enzymes for Rational Drug Design. *Skin Pharmacol Physiol,* 4:283-294. doi: 10.1159/000501732

Qing, C., 2017. The molecular biology in wound healing & non-healing wound. *Chinese Journal of Traumatology*, 20(4), 189-193.

Qu, L., Liu, A., Zhou, L., He, C., Grossman, P. H., Moy, R. L., ... Ozog, D., 2012. Clinical and molecular effects on mature burn scars after treatment with a fractional CO_2 laser. *Lasers in surgery and medicine*, 44(7), 517-524.

Rhee, J. S., & McMullin, B. T., 2008. Measuring outcomes in facial plastic surgery: a decade of progress. *Current opinion in otolaryngology & head and neck surgery*, 16(4), 387-393.

Rijsbergen M, Pagan L, Niemeyer-van der Kolk T., … van Poelgeest MI., 2019. Stereophotogrammetric three-dimensional photography is an accurate and precise planimetric method for the clinical visualization and quantification of human papilloma virus-induced skin lesions. *Journal of the European Academy of Dermatology and Venereology*, Aug;33(8):1506-12.

Rkein, A., Ozog, D., Waibel, J. S., 2014. Treatment of atrophic scars with fractionated CO_2 laser facilitating delivery of topically applied poly-L-lactic acid. *Dermatologic Surgery*, 40(6), 624-631.

Sasaki, G. H., Abelev, N., Papadopoulos, L., 2017. A split face study to determine the significance of adding increased energy and treatment levels at the marionette folds. *Aesthetic surgery journal*, *37*(8), 947-960.

Seidel R, Moy RL., 2015. Improvement in atrophic acne scars using topical synthetic epidermal growth factor (EGF) serum: a pilot study. *J Drug Dermatol*., 14:1005–1010. [PubMed]

Shashi P., Anroop N., Vipin S., Neelam S., 2012. Skin Kinetics and Dermal Clearance. *International Research Journal of Pharmacy* 3 (8), 14-15.

Sinno, S., Lee, D. S., Khachemoune, A., 2011. Vitamins and cutaneous wound healing. *Journal of wound care*, 20(6), 287-293.

Sklar, L. R., Burnett, C. T., Waibel, J. S., Moy, R. L., Ozog, D. M., 2014. Laser assisted drug delivery: A review of an evolving technology. *Lasers Surg. Med*., 46: 249–262. doi:10.1002/lsm.22227.

Skvara, H., Burnett, P., Jones, J., Duschek, N., Plassmann, P., Thirion, J., 2013. Quantification of skin lesions with a 3D stereovision camera system: validation and clinical applications. *Skin Research and Technology*, 19(1), 190.

Sobhi, R.M., Sharaoui, I., El Nabarawy, E.A., Esmail, R.S.E.N., Hegazy, R.A., Aref, D.H.F., 2018. Comparative study of fractional CO_2 laser and fractional CO_2 laser-assisted drug delivery of topical steroid and topical vitamin C in macular amyloidosis. *Lasers in medical science*, *33*(4), 909-916.

Soltani-Arabshahi, R., Wong, J. W., Duffy, K. L., Powell, D. L., 2014. Facial allergic granulomatous reaction and systemic hypersensitivity associated with microneedle therapy for skin rejuvenation. *JAMA dermatology*, *150*(1), 68-72.

Stekelenburg, C. M, Jaspers, M. E.H., Niessen F. B., Knol D. L., Van Der Wal M. B. A., De Vet H. C. W., Van Zuijlen P.P.M., 2015. In a clinimetric analysis, 3D stereophotogrammetry was found to be reliable and valid for measuring scar volume in clinical research. *Journal of Clinical Epidemiology*, 68(7), 782-787.

Stewart, N., Lim, A. C., Lowe, P. M., Goodman, G., 2013. Lasers and laser-like devices: Part one. *Australasian Journal of Dermatology*, *54*(3), 173-183.

Stockton, K.A., McMillan, C.M., Storey, K.J., David, M.C., Kimble, R.M., 2015. 3D photography is as accurate as digital planimetry tracing in determining burn wound area. *Burns*, 41(1), 80-84.

Taudorf, E.H., Haak, C.S., Erlendsson, A.M., Philipsen, P.A., Anderson, R.R., Paasch, U., Haedersdal, M., 2014. Fractional ablative erbium YAG laser: histological characterization of relationships between laser settings and micropore dimensions. *Lasers in surgery and medicine*, 46(4), 281-289.

Tchvialeva, L., Zeng, H., and Markhvida, I., 2010. Skin Roughness Assessment. *New Developments in Biomedical Engineering*. Domenico Campolo (Ed.), ISBN: 978- 953-7619-57-2, InTech, Available from http://www.intechopen.com/books/new-developments-in-biomedicalengineering/skin-roughness-assessment.

Tobin, D. J., 2017. Introduction to skin aging. *Journal of tissue viability*, 26(1), 37-46.

Trojahn, C., Dobos, G., Schario, M., Ludriksone, L., Blume-Peytavi, U., Kottner, J., 2015. Relation between skin micro-topography, roughness, and skin age. *Skin Research and Technology*, 21(1), 69-75.

Tsakovska, I., Pajeva, I., Al Sharif, M., Alov, P., Fioravanzo, E., Kovarich, S., ... Cronin, M. T., 2017. Quantitative structure-skin permeability relationships. *Toxicology*, 387, 27-42.

Tzou, C.J., Artner, N.M., Pona, I., Hold, A., Placheta, E., Kropatsch, W.G., Frey, M., 2014. Comparison of three-dimensional surface-imaging systems. *Journal of plastic, reconstructive & aesthetic surgery*: JPRAS, 67(4):489.

Ud-Din, S., Greaves, N.S., Sebastian, A., Baguneid, M., Bayat, A., 2015. Non-invasive device readouts validated by immunohistochemical analysis enable objective quantitative assessment of acute wound healing in human skin. *Wound Repair and Regeneration*, 23(6):901-914.

Valet, F., Ezzedine, K., Malvy, D., Mary, J. Y., Guinot, C., 2009. Assessing the reliability of four severity scales depicting skin ageing features. *British Journal of Dermatology*, 161(1), 153-158.

Van der Loon, B., Maal, T.J., Plooij, J.M., Ingels, K.J., Borstlap, W.A., Kuijpers-Jagtman, A.M., Spauwen, P.H., Berge, S.J., 2010. 3D Stereophotogrammetric assessment of pre- and postoperative volumetric changes in the cleft lip and palate nose. *International Journal of Oral & Maxillofacial Surgery*, 39(6):534-540.

Verhaegen, P.D., Van Zuijlen, P.P., Pennings, N.M., Van Marle, J., Niessen, F.B., Van Der Horst, C.M. Middelkoop, E., 2009. Differences in collagen architecture between

keloid, hypertrophic scar, normotrophic scar, and normal skin: an objective histopathological analysis. *Wound Repair and Regeneration*, 17(5), pp.649-656.

Watkinson A., 2013. Clinical Trials and Translational Medicine. Transdermal Drug Delivery Systems in Clinical Trials. *Journal of Pharmaceutical Sciences*, Vol. 102, 3082–3088.

Wenande, E., Tam, J., Bhayana, B., Schlosser, S. K., Ishak, E., Farinelli, W. A., ... Anderson, R. R., 2018. Laser-assisted delivery of synergistic combination chemotherapy in in vivo skin. *Journal of Controlled Release*, 275, 242-253.

Wenande, E., Anderson, R. R., Haedersdal, M., 2019. Fundamentals of fractional laser-assisted drug delivery: An in-depth guide to experimental methodology and data interpretation. *Advanced Drug Delivery Reviews*, Jan 1; 153:169-184 https://doi.org/10.1016/j.addr.2019.10.003.

Wiedersberg, S., Guy, R. H., 2014. Transdermal drug delivery: 30+ years of war and still fighting! *Journal of Controlled Release*, 190, 150-156.

Wilbur R.L., 2019. The Difference Between Topical and Transdermal Medications. Available at https://genscopharma.com/difference-topical-transdermal-medications/ July 24th.

Zapletalova, A., Pata, V., Janis, R., Kejlova, K., Stoklasek, P., 2017. Objective measurements of skin surface roughness after microdermabrasion treatment. *Skin Research and Technology*, 23(3), 346-353.

Zhang, Y., Wang, T., He, J., Dong, J., 2016. Growth factor therapy in patients with partial-thickness burns: a systematic review and meta-analysis. *International wound journal*, *13*(3), pp.354-366.

Zorec, B., Preat, V., Miklavcic, D., Pavselj, N., 2013. Active enhancement methods for intra-and transdermal drug delivery: a review. *Slovenian Medical Journal*, 82(5)

Chapter 8

Appendices

8.1 Information on the cosmeceutical and the 3D stereophotogrammetric system used in the research

8.1.1 Leaflet of TNS Recovery Complex® (SkinMedica)

SkinMedica TNS Recovery Complex FAQ

TNS Recovery Complex® has a high concentration of a patented growth factor blend, 93.6% Tissue Nutrient Solution (TNS®) with over 380 growth factors and cytokines identified. TNS® is the main ingredient in TNS Recovery Complex which is formulated from naturally occurring growth factors, antioxidants, soluble collagen, cytokines, and matrix proteins.

Ingredients

Human Fibroblast Conditioned Media, Isoceteth-20, Ethoxydiglycol, Acrylates/C10-30 Alkyl Acrylate Crosspolymer, Aminomethyl Propanol, Disodium EDTA, Ethylhexylglycerin, Glycerin, Caprylyl Glycol, Caprylhydroxamic Acid, Phenoxyethanol, Parfum/Fragrance, Hydroxycitronellal, Linalool, Coumarin, Alpha-Isomethyl Ionone, Geraniol, Isoeugenol

What is TNS Recovery Complex?

TNS Recovery Complex with NouriCel-MD is a patented formulation, designed to give your skin the natural growth factors, antioxidants, matrix proteins, and collagens it needs for optimal health. This product works by stimulating the skin's own natural rejuvenating processes and assists in improving the health and appearance of sun-damaged and aging skin.

How does TNS Essential Serum® stand out from other growth factor products on the market?

TNS Recovery Complex® is the first topical cosmetic made almost entirely of stabilized human growth factor (93.6%). The growth factors are harvested using a patented process that ensures their stability and activity. Furthermore, TNS Recovery Complex® formulation and manufacturing process maintains the stability of active growth factors. Multiple published studies in scientific journals and conferences have verified the presence of active growth factors in TNS Recovery Complex®. Carefully selected antioxidants and peptides present in TNS Essential Serum® complement the benefits of growth factors.

How long must I use this product?

A minimum of 3 months is recommended, but in general the longer it is used the better the results.

What is the science behind this product?

Growth factors are naturally occurring proteins that play important roles in the regulation of cell division and tissue proliferation. Each growth factor has specific cell-surface receptors. These natural proteins result in new collagen formation, new elastic tissue, new blood vessel formation, as well as elimination of abnormal cells and structures in the skin. Our growth factors are natural products of bio-engineered tissue collagen of human skin developed by Advanced Tissue Sciences. These growth factors have been studied extensively and are known to have a complete compliment of naturally occurring growth factors.

What is the difference between growth hormones and growth factors?

Growth hormones are hormones that your body secretes to control growth of your entire body, as well as muscle growth and various other endocrine or internal factors. Growth factors are not hormones. They are wound healing regulatory proteins that control natural wound healing of the skin.

What is the active ingredient in TNS Recovery Complex?

TNS Recovery Complex contains NouriCel-MDä. NouriCel-MD is a professional strength concentration of Advanced Tissue Science's enriched nutrient solution by-product of growing tissue-engineered skin. NouriCel-MD is the only product on the market that contains the same natural chemicals that newborn baby skin has including a unique combination of growth factors, soluble collagens, proteins, hyaluronic acid, amino acids and powerful natural antioxidants.

Are growth factors safe?

There have been more than 8000 procedures to date utilizing Advanced Tissue Sciences burn and wound healing products, TransCyte® and Dermagraft® with not one reported adverse reaction or rejection. NouriCel-MD does not contain Epidermal Growth Factor (EGF) because it is made from dermal fibroblast cells. EGF is the only growth factor that has been linked to cancerous cell growth and division when tested on laboratory mice. All safety testing on NouriCel-MD has resulted in no experimental irritation or adverse reaction.

What are dermal fibroblasts?

The skin loses about 1% of its fibroblasts and thickness per year. Dermal fibroblasts are the “architects” or framework of the dermis. Fibroblasts produce new collagen fibers, which plump the skin from underneath. Collagen keeps skin strong and dense. The loss of collagen and elastin causes a breakdown of resiliency and skin thickness, which causes lines and wrinkles to result. Upon reaching adulthood, the dermis becomes thinner and the fibroblasts fewer, which translates into aging skin.

Where do the dermal fibroblast cells come from?

Selected neonatal foreskins have been donated by parents to help burn and wound victims. Normally, this tissue would be disposed of in the surgical process. The epidermal layer of skin is separated from the dermal layer and the cells from the dermal layer, dermal fibroblasts, are used for growing human tissue. This tissue helps burn victims to heal faster, with less scarring and reduced pain. It also heals chronic diabetic foot ulcers helping patients avoid infection and possible amputation.

What testing procedures are used to test the dermal fibroblast cells?

Advanced Tissue Sciences’ master cell bank has been safety tested and approved by the United States Food and Drug Administration. Cells undergo testing for all know antigens and pathogens including HIV.

What growth factors are contained in NouriCel-MD and what are the functions?

The NouriCel-MD ingredient contains Transforming Growth Factor-Beta(TGF-b), which is responsible for collagen secretion. Increased collagen fills in the depression under the wrinkles and restores the support structure of the skin. Vascular Endothelial Growth Factor (VEGF) and Hepatocyte Growth Factor (HGF) are responsible for new blood vessel formation. New blood vessels deliver nutrients to the tissue. Keratinocyte Growth Factor (KGF) is responsible for epithelial cell growth. Interleukins (IL3 and IL6) are responsible for reduced inflammation.

Are there other products on the market containing NouriCel-MD?

No, SkinMedica has the exclusive rights to NouriCel-MD in the medical market. NouriCel-MD is available only through physician offices and physician directed medical spas.

Are there any side effects?

No side effects have been detected in the use of these products. In fact, in more than 8,000 procedures using Advanced Tissue Sciences' burn and wound healing products (TransCyte® and Dermagraft®), there has not been a single adverse reaction nor rejection. These products contain the same growth factors as NouriCel-MD.

Can anyone use this product?

Yes. The presence of sun damage is a primary suggestion for the use of this product. Sun damage is an accumulative event and requires as little as six or seven minutes of sun exposure a day to result in sun damage that will progress and accumulate.

Can younger people use NouriCel-containing products?

Many factors influence the skin's tendency to wrinkle only one of which is age. Our environment, sun, stress, diet, even our emotions all affect how our skin holds up, as we get older. Products containing NouriCel-MD are for people of any age who would like to maintain healthy skin.

Will this product help with hyperpigmentation?

It is thought that this product will result in more normal pigmentation, but studies have not been performed yet to prove or disprove this potential benefit.

Will NouriCel increase my sensitivity to the sun?

No, NouriCel will not increase sensitivity to the sun.

What are the benefits of using this product? Specifically, what types of improvement will I be able to see in the skin?

The use of this product will result in making the skin texture appear smoother and make fine lines less visible. With continued use, it may help the skin achieve a more healthy appearance and much better elasticity and resilience.

How is the performance of TNS Recovery Complex optimized?

Improved results have been noted when used in combination with regular exfoliation and products containing Vitamin C. Exfoliation eliminates dead cells, opens the pores and allows TNS Recovery Complex to penetrate the skin. Vitamin C is known to stimulate the production of collagen.

8.1.2 Email in response to the inquiry regarding the cosmeceutical TNS Recovery Complex

From: barbara@barbaramachado.com.br <barbara@barbaramachado.com.br>
Sent: Thursday, August 27, 2020 6:02 AM
To: medinfo.brazil@allergan.com
Cc: IR-Medcom@allergan.com; Bhb105 <bhb105@pgr.aru.ac.uk>; clinica <clinica@barbaramachado.com.br>
Subject: urgent inquiry concerning TNS recovery complex - paper publication

Dear sir/madam

I am a PhD researcher and a plastic surgeon working in Brazil. My PhD studies have been developed on drug delivery involving growth factors. I have bought TNS recovery complex to perform the clinical study. I have had positive results with the use of the cosmeceutical and now I am sending the papers for publications. However, some papers have been refused because they request for additional information concerning active concentrations and penetration profile.
Would it be possible to contact someone from SkinMedica and get a piece of minimal information on any growth factor concentration to satisfy the journal's request?
I appreciate any help or guidance that you can give me.
Kind regards,

Barbara Helena Barcaro Machado
Plastic surgeon
Rio de Janeiro - Brazil

CS-Product_Questions
28/08/2020 15:50
Para barbara@barbaramachado.com.br, medinfo.brazil; IR-Medcom; Bhb105

Dear Dr. Machado,

Thank you for contacting SkinMedica® with your inquiry.
SkinMedica® Tissue Nutrient Solution (TNS®) is a physiologically balanced and naturally secreted human growth factor solution containing amino acids, vitamins, antioxidants, and several cytokines/growth factors. TNS Recovery Complex® is a cosmetic product formulated with a high concentration of this patented growth factor blend at 93.6%

TNS® is obtained from the growth medium of cultured neonatal foreskin fibroblasts. Originally developed by Advanced Tissue Sciences (La Jolla, CA), a three-dimensional artificial matrix is used to grow neonatal foreskin fibroblasts into what ultimately becomes an artificial dermis. The artificial skin is grown for its fibroblast cells in a controlled environment (temperature and air controlled) and, as the fibroblasts grow and proliferate on the matrix, they generate extracellular substances such as naturally produced collagen, growth factors, and cytokines. With earlier research, we identified 110 growth factors and cytokines in TNS®[1,2]. Since that time, we have been able to identify over 380 growth factors and other naturally-occurring proteins in TNS®[3].

In clinical studies conducted with SkinMedica cosmetic products, we look at cosmetic endpoints (ie; improvement in the appearance of skin, improvement in the appearance of fine lines, improvement in the appearance of skin tone evenness).

With regards to penetrating capacity of key ingredients, we do not conduct penetration (or absorption) studies with our cosmetic products. These types of studies are typically done with topical drug products only.

Our theory is that topical application of growth factors work via communication signalling cascade resulting in supportive benefits of extracellular matrix proteins (i.e. collagen and elastin) that are important for skin rejuvenation.

References:

1. Mehta RC, Smith SR, Grove GL, et al. Reduction in facial photodamage by a topical growth factor product. J Drugs Dermatol. 2008;7864-871.

2. Sundaram H, Mehta RC, Norine JA, Kircik L, Cook-Bolden FE, Atkins DH, Wershler WP, Fitzpatrick RE. Topically applied physiologically balanced growth factors: a new paradigm of skin rejuvenation. J Drugs Dermatol. 2009;8s:4-13.

3. Kadoya K, Makino ET, Jiang LI, Bachelor M, Chung R, Tan P, Cheng T, Naughton GK, Mehta RC. Upregulation of Extracellular Matrix Genes Corroborates Clinical Efficacy of Human Fibroblast-Derived Growth Factors in Skin Rejuvenation. J Drugs Dermatol. 2017 Dec 1;16(12):1190-1196.

Best Regards,

TIMOTHY SIAW
Senior Safety Analyst
Safety, Regulatory & Medical Affairs - Skincare
2525 Dupont Drive
Irvine, CA 92612
OFFICE +1 714 246 4979
CELL +1 949 537 8670
Email SIAW_TIMOTHY@ALLERGAN.COM
allerganaesthetics.com

8.1.3 Leaflet of the 3D stereophotogrammetric system LifeViz™ Micro provided by the manufacturer Quantificare S.A. (Sophia Antipolis, June 2009)

QuantifiCare's LifeViz™ Micro: a new breakthrough in 3D devices

With its new "LifeViz™ Micro", QuantifiCare is launching a breakthrough system for macro-views of skin surfaces using stereo-vision.

LifeViz™ Micro is a validated system complementing the 60cm distance 3D LifeViz™ developed by QuantifiCare which is used for the face and other body areas. With a shortrange (~20cm distance), LifeViz™ Micro enables visualization and quantitative measurement of fine wrinkles, skin texture, acne lesions and acne scars, moles, basal cell carcinoma, etc.

LifeViz™ Micro's field of view is approximately 5.25cm x 3.75cm, with a pixel resolution of 0.02mm x 0.02mm (20µm x 20µm). LifeViz™ Micro is able to reliably evaluate the depth of a paper sheet of 0.1mm (100µm). Noise measurements on a flat surface of 4cm2 lead to a variation of less than 10µm on average relative to a flat area. Validation experiments on relative volume variation are exhibiting an average depth precision of 0.008mm (8µm).

LifeViz™ Micro's regular package includes the camera, DermaPix® "Pro" or higher version software, DermaPix® 3D module, polar flash system (enabling cross polarization, i.e. very reduced specular "spot-light" reflection) and dual beam pointers to enable exact repositioning of the 3D camera relative to distance and image center.

LifeViz™ Micro is also used in QuantifiCare's services for clinical development and specifically for clinical studies where objective 3D quantification and accurate 3D photodocumentation are needed.

The design of the LifeViz™ Micro makes it the most compact system developed for stereovisualization. Dual beam pointers enable exact repositioning relative to distance and central focus point. A specific and patented flash design (iXp technology) enables increased accuracy in surface reconstruction.

LifeViz™ "Micro" is a validated system for the quantitative assessment of 3D shapes, 3D perimeter, 3D surface, 3D volume and 3D volume variation.

Relying upon the LifeViz™ technology development and improvements, LifeViz™ "Micro" is concentrating upon a restricted field of view and a closer range, capable of even higher accuracy and precision than with the conventional 60cm distance LifeViz™. It enables reaching fine wrinkles and under some conditions allows skin texture information.

LifeViz™ "Micro" validation has been conducted by using two approaches. The first one is the absolute measurement of the 3D perimeter, surface and volume of a physical phantom where the actual geometrical parameters are known ("Absolute measurements

validation"). The second set of experiments are based on the computation of relative volume variations of known physically injected quantities of material. Measured parameters with correspond to an error of:

- 2.5% (21mm^3, that is, 0.021cc^3) for the volume
- 5.5% (22mm^2) for the surface
- 0.4% (0.27mm) for the perimeter
- Average depth error is 0.066mm, that is, 66 microns.

Whenever possible, the relative measurement methods of volume variations are always far better and more accurate than the difference of absolute measurements. In addition, endpoints in studies are generally relative to volume variations or absence of variations. The LifeViz™ technology enables such relative volume variation computation. To validate these measurements, we have used a device similar to the "3D Validator" system developed and used to validate the regular LifeViz™ , but with a much lower level of injected volume. Measurements are remarkably linear, with a correlation of 0.9999 between injected quantities and measured quantities. A drift in the measurement is observed (systematic bias). It was not possible to assess if this drift was due to a mechanical property of the system, such as the elasticity of the syringe piston, or due to the measurement method. This systematic bias is reducing the accuracy of the measurement to: Accuracy (RMS)= 9.8mm^3.

As the measurement surface is 178mm^2, it leads to an average depth accuracy of 0.055mm (55 microns), close to observed accuracy for absolute measurements. Note that measured volume variation accuracy (9.8mm^3) is also close to the accuracy of injected material (5mm^3), therefore, part of the volume variation errors can be due to the inaccuracy of the validation system.

The precision of the system can also be evaluated (corrected for systematic bias). In clinical studies, the precision is the most important, as populations are compared using the same system, which enables to pinpoint very subtle differences. The precision is very high. For a measurement surface of 178mm^2, the average depth precision is 0.008mm, that is 8 microns.

Examples of 3D surface reconstruction using LifeViz™ Micro.

Acne lesions volumes can be easily detected and accurately quantified with LifeViz™ Micro. The size of these acne lesions are approximately 3.5mm in diameter.

Details as small as pores, very fine wrinkles or chickenpox scars can be detected and quantified. The chickenpox scar diameter illustrated above is approximately 3mm in diameter and less than a 1 mm deep. The fine wrinkle width is approximately 1mm.

Nasolabial fold volume variations can be accurately quantified using 3D LifeViz, but other parameters are also made accessible such as surface principal curvatures.

Very fine wrinkles (forehead) of less than 1mm width, which are still detectable and

quantifiable using LifeViz™ Micro, make this system the ideal tool to quantitatively study the effects of treatment like botulinum toxin.

Large wrinkles (forehead) of more than 2mm width and 1mm deep are accurately captured.

3D LifeViz™ Micro QC-2009-0512-1.4. QuantifiCare S.A.
http://www.quantificare.com
Headquarters: QuantifiCare S.A, 1180 routes des Dolines, Bât. Athéna B, 06560 Valbonne, France
Tel.: +33 (0) 4 92 91 54 20 – Fax.: +33 (0) 4 92 91 95 00 - E-mail: info@quantificare.com

8.2 Presentations in Congresses

8.2.1 37th Jornada Carioca of Plastic Surgery

Period: 1 – 4 August 2018

Location: Rio de Janeiro, Brasil

Theme: Measuring the impact of laser-assisted drug delivery on skin surface through three-dimensional stereophotogrammetry (oral presentation)

8.2.2 24th ISAPS Global Congress

Period: 31 October 4 November 2018

Location: Miami Beach, Florida, USA

Theme: Measuring skin improvement with a three-dimensional stereophotogrammetry imaging system (lecture)

ISAPS
Global Congress

Barbara Helena BARCARO MACHADO, MD

presented

MEASURING SKIN IMPROVEMENT WITH 3D STEREOPHOTOGRAMMETRY IMAGING-SYSTEM

during the 24th Congress of ISAPS
Miami Beach, Florida • October 31 - November 4, 2018

Vakis Kontoes, MD, PhD
Chair, ISAPS Education Council

Renato Saltz, MD, FACS
President, ISAPS

8.2.3 57th Brazilian Congress of Plastic Surgery

Period: 20 – 24 November 2019

Location: Brasilia, Brazil

Theme: Three-dimensional stereophotogrammetric analysis of scar improvement after laser-assisted medication (lecture)

SOCIEDADE BRASILEIRA DE
CIRURGIA PLÁSTICA

Sociedade Brasileira de Cirurgia Plástica
Comissão de Concursos e Concessão de Prêmios
A Sociedade Brasileira de Cirurgia Plástica
certifica que

Barbara Helena Barcaro Machado

Recebeu menção honrosa do Prêmio Jussara Personelle, pelo trabalho apresentado durante o 56º Congresso Brasileiro de Cirurgia Plástica, na cidade de Brasília/DF, intitulado "Análise estereofotogramétrica tridimensional da melhoria de cicatrizes após medicação assistida por laser", tendo como co-autores: Ivy Dantas de Melo e Silva e Mohammad Najlah

Brasília, 22 de novembro de 2019.

Dr. Nivyo Steffen
Presidente SBCP

Dr. Denis Calazans
Secretário Geral SBCP

Dra. Lydia Masako Ferreira
Coordenadora Comissão de Prêmios

8.2.4 20th Scientific Meeting of ICAPS (International Consortium of Aesthetic Plastic Surgeons)

Period: 31 May – 2 June 2019

Location: Naples, Italy

Theme: Laser-assisted drug delivery (lecture)

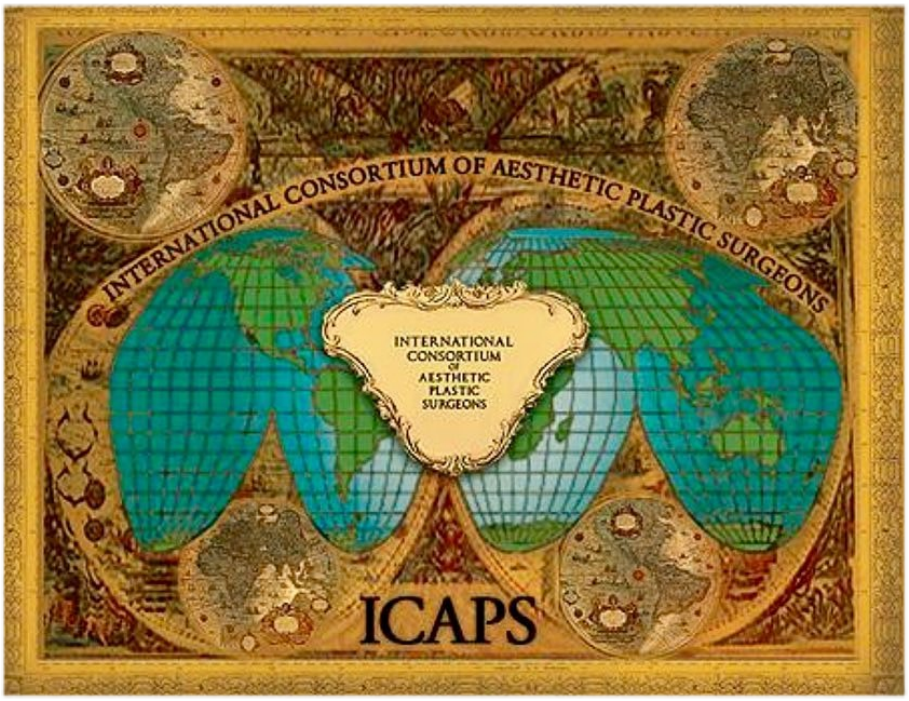

Scientific Program — **FRIDAY 31th MAY**

3. minutes of previous meeting	Stephen Gilbert
4. president's report	Hans-Leo Nathrath
5. financial report	Alfonso Barrera
6. election of officers	Hans-Leo Nathrath
7. membership (list of proposed new member)	Hans-Leo Nathrath
8. Survery	Clayton Moliver
9. Website	Clayton Moliver
10. Annual Dues	Alfonso Barrera
11. South Africa 2020	Russell Walton
12. Financing meetings	Russell Walton
13. Meeting 2021	Russell Walton
14. General Business	Nathrath & Walton

** end of 2nd day **

Scientific Program — **SATURDAY 1st JUNE**

Regina Isabella CONFERENCE ROOM

Moderator: Alfonso Barrera

GENERAL TOPICS

15.00	**Harry Fok** My otoplasty technique	15 min
15.15	**Russell Walton** Skew you: our asymmetrical bodies	15 min

Scientific Program — **SATURDAY 1st JUNE**

15.30	**Ana Zulmira Diniz Badin** Immunological Revolution	15 min
15.45	**Bárbara Machado** Laser assisted drug delivery	15min
16.00	**Clayton Moliver** Non-opioid analgesia	15 min
16.15	**tea / coffee break**	

FINAL PAPERS

16.20	**Pier Luigi Canta** Enchantment Forehead Lift	15 min
16.35	**Alfonso Barrera** An uncommon complication of a facelift and how to correct it	10 min
15.45	**Darryl Hodgkinson** 12 years ORH Charity Support of the Philippine Medical Centre Craniofacial Unit	10min

*** end of Scientific Meeting ***

SUNDAY 2nd JUNE — **Official Goodbye to ICAPS NAPOLI**

8.2.5 All About Face II

Period: 16 and 17 August 2019

Location: Curitiba, Brazil

Theme: Drug delivery in wrinkles and scars (lecture)

8.3 Award

Prize Jussara Personelle for the best paper on non-invasive laser surgery granted on 22 November 2019 during the 57th Brazilian Congress of Plastic Surgery, in Brasilia, Brazil.

Theme: Three-dimensional stereophotogrammetric analysis of scar improvement after laser-assisted medication (oral presentation)

8.4 Publications

8.4.1 Journal: Aesthetic Plastic Surgery (open access)

Title: Comparative study on the outcome of periorbital wrinkles treated with laser-assisted delivery of vitamin C or vitamin C plus growth factors: a randomized double-blind clinical trial

Aesth Plast Surg; https://doi.org/10.1007/s00266-020-02035-z

Aesth Plast Surg
https://doi.org/10.1007/s00266-020-02035-z

Comparative Study on the Outcome of Periorbital Wrinkles Treated with Laser-Assisted Delivery of Vitamin C or Vitamin C Plus Growth Factors: A Randomized, Double-blind, Clinical Trial

Barbara Helena Barcaro Machado[1,5] · James Frame[2] · Jufen Zhang[3] · Mohammad Najlah[4]

Received: 8 September 2020 / Accepted: 24 October 2020

Abstract

Background Despite promising results, laser-assisted drug delivery (LADD) is not yet considered as standard therapies and published data rely mainly on laboratory tests, animal experiments or cadaver skin.

Objectives This double-blind, prospective, randomized clinical trial investigates the impact in topical application of vitamin C and a cosmeceutical containing growth factors (GFs) on periorbital wrinkles primarily treated with laser skin resurfacing.

Material and Methods In total, 149 female patients with average depth of the wrinkles between the two groups after treatment.

Results There was a significant reduction in both skin roughness and average depth of the wrinkles in the group treated with vitamin C and growth factors ($p < 0.01$) than those treated with LADD followed by topical application of vitamin C alone. There were no cutaneous reactions or adverse systemic reactions observed in this study related to LAM with vitamin C and GFs.

Conclusion Controlled laser application might have a great potential to facilitate the absorption of exogenous macro-

8.4.2 Journal: Scientific Reports

Title: Scientific Validation of Three-Dimensional Stereophotogrammetry Compared to the IGAIS Clinical Scale for Assessing Wrinkles and Scars after Laser Treatment

Preprint from Research Square, 03 Jan 202. DOI: 10.21203/rs.3.rs-126281/v1 PPR: PPR261148

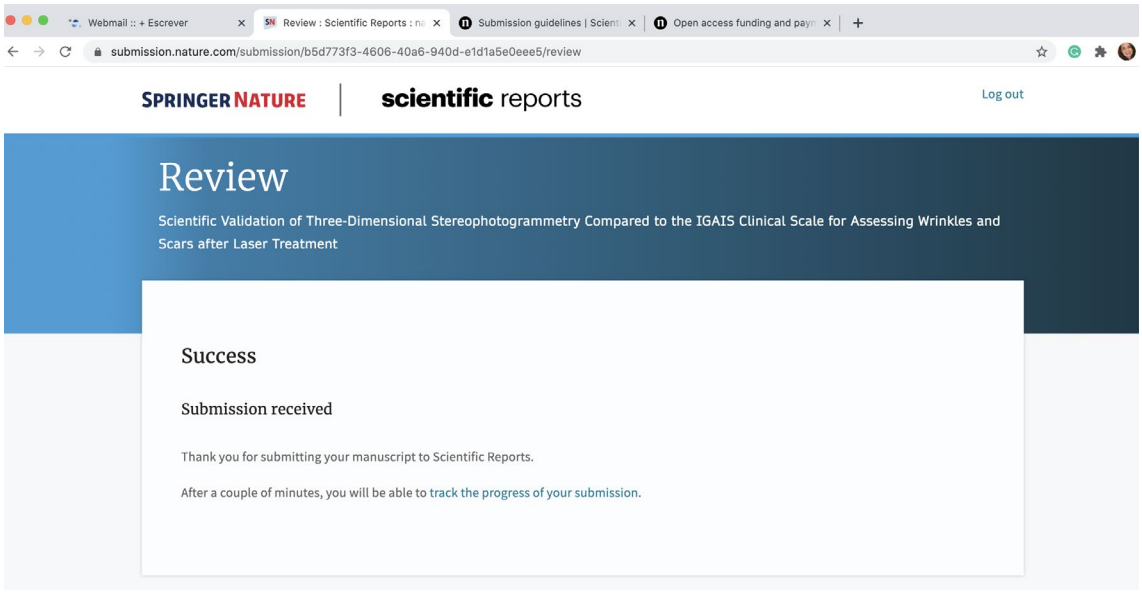

8.4.3 Journal: Aesthetic Plastic Surgery

Title: Treatment of Scars with Laser-Assisted Delivery of Growth Factors and Vitamin C – A Comparative, Randomised, Double-Blind, Early Clinical Trial

Accepted for publication. Waiting for DOI number and publication.